Synthesis, binding and threading properties of double porphyrin cage compounds

Kathleen Stout

Synthesis, binding and threading properties of double porphyrin cage compounds

Kathleen Stout

Synthesis, binding and threading properties of double porphyrin cage compounds

Proefschrift

ter verkrijging van de graad van doctor
aan de Radboud Universiteit Nijmegen
op gezag van de rector magnificus prof. dr. J.H.J.M. van Krieken,
volgens besluit van het college van decanen
in het openbaar te verdedigen op vrijdag 27 september 2019
om 12.30 uur precies

door

Kathleen Stout
geboren op 1 augustus 1988
te Ede

The studies described in this thesis were financed by the Netherlands Research School Combination Catalysis (project number 620013227) and the European Research Council (ERC Advanced grants ALPROS, number 290886 and ENCOPOL, number 740295)

ISBN
978-94-0000-000-0

Design/lay-out
Promotie In Zicht, Arnhem

Print
Ipskamp Printing, Enschede

Promotoren
Prof. dr. Roeland J.M. Nolte
Dr. Hans A.A.W. Elemans

Manuscriptcommissie
Prof. dr. Floris P.J.T. Rutjes
Prof. dr. Joost N.H. Reek (Universiteit van Amsterdam)
Dr. Peter A. Korevaar

Voor onvoorwaardelijke steun en liefde

Voor Oma en Snuf

Paranimfen
Theo Peters
Dianne van Dulmen

Table of contents

List of abbreviations

$(EtOH)_2V$	*N,N'*-Diethanol viologen dihexafluorophosphate
[H]	Concentration of free host
$[H]_0$	Total concentration of host
[HL]	Concentration of host-ligand complex
$[HL_2]$	Concentration host-ligand$_2$ complex
2σ	Error of the measurement (2 times the standard deviation)
3D	Three-dimensional
A	Absorption
Å	Angstrom
A	Adenine
A_0	Initial absorption
A_{max}	Maximum absorbance
ArH	Aromatic hydrogen
BBr_3	Boron tribromide
bipy	4,4'-Bipyridine
bs	Broad singlet
C	Cytosine
$CDCl_3$	Deuterated chloroform
COSY	Correlation spectroscopy
CuAAC	Copper-catalyzed azide-alkyne cycloaddition reaction
δ	Chemical shift
d	Doublet
DABCO	1,4-Diazabicyclo[2.2.2]octane
dbV	Double blocked viologen
DCM	Dichloromethane
DMSO-d_6	Deuterated dimethylsulfoxide
DNA	Deoxyribonucleic acid
EM	Effective molarity
Eq	Equivalents
FRET	Fluorescence resonance energy transfer
G	Guanine
GMO	Genetically modified organism
$H_2(OH)_4SC$	Free base tetrahydroxy single porphyrin cage
$H_2(U)_4SC$	Free base tetraethylureapropoxy single porphyrin cage
H_2SC	Free base single porphyrin cage
$H_4C_{11}DC$	Free base double porphyrin cage linked via a bistriazole-undecamethylene spacer
H_4C_3DC	Free base double porphyrin cage linked via a bistriazole-trimethylene spacer
H_4C_5DC	Free base double porphyrin cage linked via a bistriazole-pentamethylene spacer
H_4C_xDC	Free base double porphyrin cage
HMBC	Heteronuclear multiple bond correlation
HSQC	Heteronuclear single quantum correlation
Hz	Hertz

J	Coupling constant
K	Kelvin
$K_{1:1}$	Binding constant of the 1:1 complex
$K_{1:2}$	Binding constant of the 1:2 complex
k_{on}	Apparent rate constant for threading
L_n	Polymer length
m	Multiplet and/or multiple resonances
M	Molar
MALDI-TOF	Matrix-assisted laser desorption/ionization time of flight
Me_2V	*N,N'*-dimethylviologen dihexafluorophosphate
MeCN	Acetonitrile
MeCN-d_3	Deuterated acetonitrile
MMP^+	1-Methyl-4-phenylpyridinium
M_n	Number average weight
$Mn(OMe)_4TPP$	Manganese tetra(methoxyphenyl) porphyrin
$Mn(U)_4SC$	Manganese tetraethylureapropoxy single porphyrin cage
Mn_2C_xDC	Manganese double porphyrin cage compounds
MnSC	Manganese single porphyrin cage
MnTPP	Manganese tetra(phenyl) porphyrin
M_w	Molecular weight
n	Degree of polymerization
P#	Polymer compounds
P1	Viologen-blocked polyTHF chain of 41 repeating units
P2	Viologen-blocked polyTHF chain of 80 repeating units
P3	Viologen-blocked polyTHF chain of 111 repeating units
PCR	Polymerase chain reaction
PDI	Polydispersity index
polyB	Poly(1,4-butadiene)
polyTHF	Polytetrahydrofuran
ppm	Parts per million
q	Quartet
RNA	Ribonucleic acid
ROESY	Rotating-frame overhauser spectroscopy
s	Singlet
SC	Single porphyrin cage
ssDNA	Dingle stranded DNA
T	Thymine
t	Triplet
tbpy	*Tert*-butyl pyridine
td	Triplet of doublets
TIPSA BF_3K	Potassium triisopropylsilylacetylene trifluoroborate
TMS	Trimethylsilyl
TMSA	Trimethylsilylalkynyl
V	Viologen
$Zn(OH)_4SC$	Zinc tetrahydroxy single porphyrin cage

$Zn(U)_4SC$	Zinc tetraethylureapropoxy single porphyrin cage
Zn_2BisP	Zinc bis-porphyrin
$Zn_2C_{11}DC$	Zinc double porphyrin cage linked via a bistriazole-undecamethylene spacer
$Zn_2C_{11}TTBP$	Zinc double tri-tolyl porphyrin linked via a bistriazole-undecamethylene spacer
Zn_2C_3DC	Zinc double porphyrin cage linked via a bistriazole-trimethylene spacer
Zn_2C_5DC	Zinc double porphyrin cage linked via a bistriazole-pentamethylene spacer
Zn_2C_xDC	Zinc double porphyrin cage
$ZnMnC_xDC$	Zinc manganese double porphyrin cage
ZnSC	Zinc single porphyrin cage
α	Cooperativity factor
$\Delta G^{\ddagger}_{on}$	Gibbs free energy of activation
$\Delta\varepsilon_{HL}$	Molar absorption coefficient of the 1:1 host-ligand complex
$\Delta\varepsilon_{HL2}$	Molar absorption coefficient of the 1:2 host-ligand complex
ε	Molar absorption coefficient
λ	Wavelength

1

Introduction

1.1. Data storage

Nowadays, finding new methods to store digital data is an emerging research field given the expectation that the global digital archive will contain 3×10^{24} bits by 2040 and this amount of data cannot be sustained by the use of traditional silicon memory chips.[1] At the same time, Moore's law predicts that the performance of chips devices will double every 18 months, but also that this growth cannot be sustained due to limitations in miniaturization.[2–4] Due to these two constraints, new methods are needed to store and process data. This problem was already envisioned by Jean-Marie Lehn in his Nobel lecture in the late 80s.[5] Here, Lehn stated that the processing and transferring of information in the future will be done by 'linking processes of artificial intelligence and molecular behavior'. Although this goal has not yet been achieved, it has inspired scientists to develop new molecular systems that can store data on a molecular scale. It inspired our group to design an enzyme mimic based on DNA polymerase, which might enable the storage of binary data in synthetic polymers in the future. Synthetic polymers are preferred over biological polymers such as DNA because they are often easier to handle, more robust, and they enable more easily the use of a binary code by assigning two different chemical functions to the 0 and 1 bits.[6] An enzyme mimic designed to enable data storage in synthetic polymers has to possess several characteristics, such as a cavity to bind to a polymer chain and thread over it, a catalyst to modify this chain by 'writing' chemical functionalities on it, and an information transfer mechanism to control this writing. In this chapter, the relevant background information and current state of research on the topics of data storage in natural and artificial polymers and information transfer using different model systems are presented.

1.2. Data storage in nature: DNA polymerase

Nature's way to store data is to encode it into DNA.[7–9] This information storage is enabled by a special class of enzymes, such as DNA and RNA polymerases and λ- endo and exonucleases.[7–9] These enzymes served as the inspiration and basis for our research on the encoding of polymers with information and are therefore discussed in some depth in this section.

Enzymes are mostly based on proteins, except for some catalytically active RNA molecules, and are involved in almost every biological process ranging from the extraction of nutrients and energy by degrading food to its basic components, to the transcription of genetic information by the duplication of the genome.[10] The high catalytic activity of an enzyme is closely related to its three-dimensional (3D) structure into which the long chain of amino-acids is folded.[10,11] Within this 3D structure, an active site with a distinctive shape is present; it can induce a high substrate and

product selectivity, as well as a high stereospecificity in its reactions by using non-covalent interactions with the substrate or product. Examples of such interactions are hydrogen bonding, metal-ligand coordination interactions, pi-pi-stacking, and/or ion pairing.[10,11] This active site may contain a catalytic center in the form of a (binding) site, in which amino-acids are lined up in such a way that they can exert the above described specific non-covalent interactions with a substrate. In addition, the active site may impose a certain geometry on the substrate as a result of which the transition state of the catalyzed reaction is stabilized and lowered in energy.[11] The exclusion of water from the active site upon binding of the substrate often increases the strength of the non-covalent interactions.

The classes of enzymes to which the DNA and RNA polymerases, and the λ- endo and exonucleases belong, are found in all cellular organisms. They perform the replication and transcription of the genetic information, which is stored in the DNA molecules (Figure 1).[7–9] The copying of genetic information is carried out by the replisome, which consists of several different enzymes and proteins that all have a specific function.[7,12,13] While a myriad of different replisomes are known of which the exact structure differs between organisms, all of them ensure that the information encoded in the pattern of the nucleotides is maintained during the replication of DNA.[14,15] The initiation of DNA replication starts at a defined region called the origin, which is rich in adenine (A) and thymine (T) nucleotides.[16] At this region, the assembly of the replisome starts by the binding of initiator proteins that are recognized by the protein complexes that recruit the replisome.[17–19] Here, the double helix of DNA is unwound by helicases to ensure access to the nucleotides on the single stranded DNA (ssDNA) chain, after which replication on the leading (3' to 5' direction) and the lagging strand (5' to 3' direction) begins.[12,16,20–22] At the leading strand, the genetic information is duplicated in a rapid unidirectional and sequentially processive fashion.[7] This means that while the replisome is attached to the ssDNA, it preforms several consecutive reactions while it moves one nucleotide at the time in one direction (from the 3' to the 5' end).[23–25] This replication process is ensured and greatly enhanced by the fact that a sliding clamp is present, which encircles the DNA and tethers proteins or enzymes to the ssDNA chain with specific binding interactions without itself having a catalytic function.[7,13,15,23,26–29] The initiation of the synthesis of the new (daughter) strand is accomplished by the binding of a short RNA primer, which is synthesized by primases.[20] Only one primer is needed for the duplication of the leading strand, because of the unidirectional processive movement of the replisome. The lagging strand, however, is oriented antiparallel with respect to the leading strand and because replication has to occur in 3' to 5' direction, this strand is replicated in a discontinuous fashion, meaning that only small, so-called 'Okazaki fragments' of ~250 base pairs can be synthesized in the 3' to 5' direction.[12,30–33] After the synthesis of each Okazaki fragment, the polymerase and clamp release the ssDNA and attach again at another primer site, until at the end of the replication

process, the separate Okazaki fragments are ligated together by the enzyme ligase. Eventually, the encoding mother strand and the newly synthesized daughter strand are indistinguishable from those in the original parent DNA double strand. RNA synthesis follows the same process as DNA replication, yielding a complementary RNA strand that dissociates from its template and often undergoes further modification by other enzymes.

The duplication of the ssDNA strand occurs with a high fidelity.[20] A mistake in nucleotide insertion is made in less than one per 10^9 nucleotides, resulting in an error frequency of one per every 1000 replications of a bacterial genome such as *E. Coli*. This high fidelity can be attributed to different factors.[11,16,20,31,35] When Watson and Crick eluded the structure of the double stranded helix of DNA, they suggested that the specific pairing of the bases can imply a copying mechanism for the genetic material and that this specific base pairing can contribute to the specificity of DNA replication.[31,36] The nucleotides A (adenosine), T (thymidine), C (cytosine) and G (guanine) form specific hydrogen bonds with complementary nucleobases. As a result, correct base pairing (A&T and G&C) occurs and the stacking of base pairs on top of each other further stabilizes the DNA chain.[8,14,16,20] However, when only the energy difference between correct and incorrect base pairing is taken into account (0.2-4 kJ/mol), high fidelity cannot be assured.[20,31] Therefore, it is believed that upon the binding of a nucleotide in the active site of a DNA polymerase, water that surrounds the nucleotide is released, decreasing the entropy of the system and hence increasing the fidelity of the DNA replication.[20,31] Another contributing factor

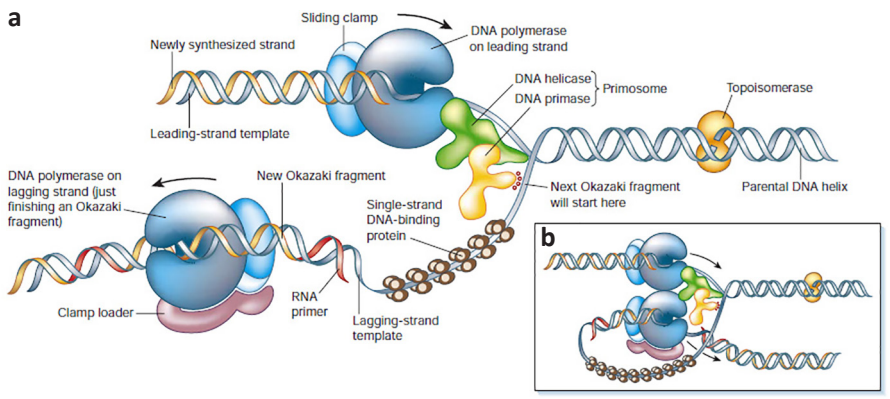

Figure 1 *Schematic representation of DNA replication. At the leading strand, the sliding clamp and the DNA polymerase proceed in the 3' to 5' direction, while the helicase unwinds the parental strand. The lagging strand is replicated by the synthesis of small Okazaki fragments in a discontinuous fashion. Both of the DNA polymerases are anchored to the mother strand via clamp proteins, while the topoisomerase facilitates the unwinding of the parental strand.*[34]

is that when the bases are paired correctly, they fit tightly into the binding pocket of the active site without any steric clashes. In contrast, when a wrong base pairing occurs, the resulting geometry of the pair leads to steric problems, which reduce the binding affinity of the base pair in the active site, causing conformational changes that disrupt the most favorable geometry for catalysis and reduce the rate of phosphodiester bond formation.[16,20,31] Another important contribution to the high fidelity of DNA polymerases is the proofreading exercised by exonucleases.[11,14,16,20,35] Once a mismatched nucleotide is incorporated, the mismatched primer terminus is more difficult to extend than a properly paired primer terminus.[14,20] As a result of this delay, the wrongly inserted nucleotide can be checked, removed and replaced with a correctly matched nucleotide before the next base is attended.[20] Furthermore, there are several enzymatic systems that can correct mismatched nucleotides after the replication of DNA which also increases the fidelity.[7,37]

1.3. Models for binary data storage

The highly efficient storage of information in DNA does not resemble the storage of digital information in the form of 0 and 1 bits in silicon transistors. In this section, several methods and models for binary data storage are discussed. First, the concept of modern computing is presented, followed by a discussion how chemical information can be stored in physical carriers or sequence-controlled polymers. Lastly, interactions found in nature that can be employed to direct data storage by mimicking characteristics of enzymes are reported.

1.3.1 The Turing machine as a blueprint for nowadays computing

Nowadays computing is not based on methodologies that nature employs, but on a thought-experiment, which was reported by Alan Turing in 1936.[38] Turing proposed a mathematical model in which he envisioned a machine that has become the fundamental basis of current computers, and which is known as the 'Turing machine'.[38] It has unlimited memory capacity in the form of an infinitely long tape, which is divided into square sites in which a symbol (0 or 1 in nowadays computing) can be printed (Figure 2).[39] The tape-head of the Turing machine can scan (read) the symbol, write a new symbol onto the tape and move along the tape (a square to the right or to the left), or show no movement at all. The tape-head is connected to or contains a state-register, which stores the state of the Turing machine. The combination of the symbol on the tape and the state of the tape-head results in a certain action that is stored in the instruction table. In a certain state and upon reading a symbol on the tape, the tape-head can erase or write a symbol, can move to the right, left, or not at all, and can remain in the same state or alter to another state. This process can in principle continue for an infinitely long time, until the tape-head enters an accepted

state (task is complete) or a rejected state (task is impossible to complete). Therefore, the Turing machine can in theory perform any computational task.

Since the thought-experiment of Alan Turing, major steps have been taken in computer development, starting with the design of Von Neumann, which is based on silicon chips.[41] However, computations carried out by a computer are based on a finite number of states, because it has a finite memory and it can therefore not fully simulate a Turing machine. Programming languages do not necessarily have this limitation, and therefore, if a programming language can fully model a Turing machine, it is called 'Turing Complete'.

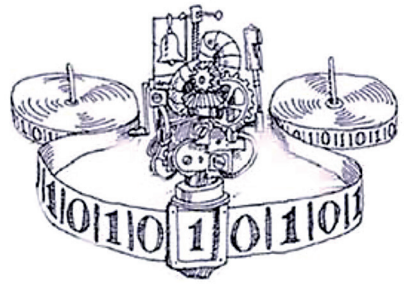

Figure 2 *Artist impression of a Turing machine with a tape-head that can read, write and move along an infinite long tape, which is divided into squares on which 0s and 1s are read and written.*[40]

1.3.2 Infochemistry and sequence-controlled polymers

Since it is the expectation that, within a couple of decades, computation based on silicon chips is reaching its limitations, scientists are searching for new methods to store data.[1–4] One of the pioneers in this field is the group of Whitesides, who coined the term 'infochemistry' in two papers that describe the chemical storage of data in or onto physical carriers.[42,43] One of these carriers was a nitrocellulose strap, named 'infofuse', onto which several patches of alkali metal coatings were applied (Figure 3). These patches were spatially separated and differed in sequence of alkali metal coatings.[42] When the infofuse strap was ignited at one end, the consecutively burning of the alkali metal coatings led to the emission of photons of a well-defined wavelength. When the combination and order of the different alkali metal coatings were encoded as characters, messages could be read out. A severe limitation of this method is that it can only be read out once, because during reading the infofuse is destroyed.

Another information carrier that Whitesides *et al.* employed, was based on the use of microdroplets in a microfluidic reactor.[43] The microdroplets were generated at specific time intervals and could be loaded with chemicals that respond to light.

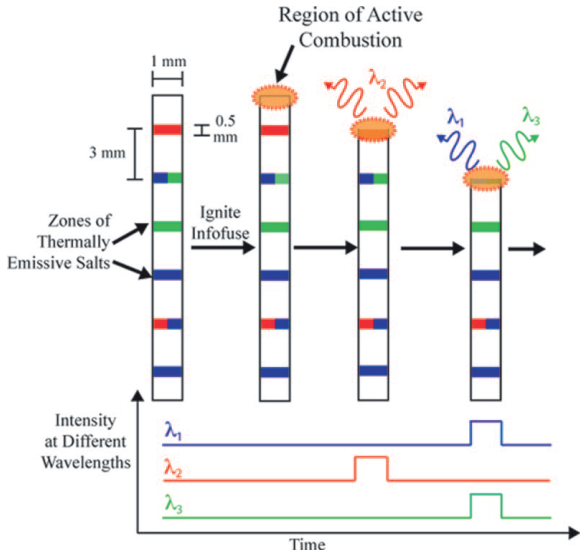

Figure 3 *Schematic representation of the operation of an infofuse. Ignition of the tape creates a burning front and when it passes a region loaded with alkali-metal coating, light of a characteristic wavelength is emitted. The sequence and composition of the alkali metal coatings encode information.*[42]

When the droplets are generated in such a way that they all end up in the semicircular turns of a wave-shaped channel, selective illumination with a photomask yielded dark and light spots that represent 0 and 1 bits. In this way data can be stored and read, but it cannot be copied, which is a limitation of this system.

The ability to copy data has been implemented in a micro-array system based on genetically modified organisms (GMO's).[44] In this system, bacteria can express one of three fluorescent proteins, and by placing the GMO's on the micro-array, the information can be read by detecting the fluorophores. The copying of information is subsequently attained by the multiplication of the bacteria.

Chemical storage of data at the molecular level was accomplished by Ratner *et al.*, who stored information by using the relative intensities of methylene singlets of compounds in an NMR spectrum (Figure 4). They employed a set of aromatic molecules containing isolated methylene functionalities (Figure 4b).[45] When these compounds were mixed, their methylene protons all generate singlets at specific chemical shifts, resulting in specific intensity profiles if the NMR spectrum is plotted from low to high field. In such profiles, singlets can be grouped. And if the chemical shifts and integrals of these groups are compared to a predetermined encoding table, where is reported which integral of a singlet at a chemical shift represents which letter of the alphabet,

the data can be decrypted. However, this system also lacks the ability to copy the information.

a)

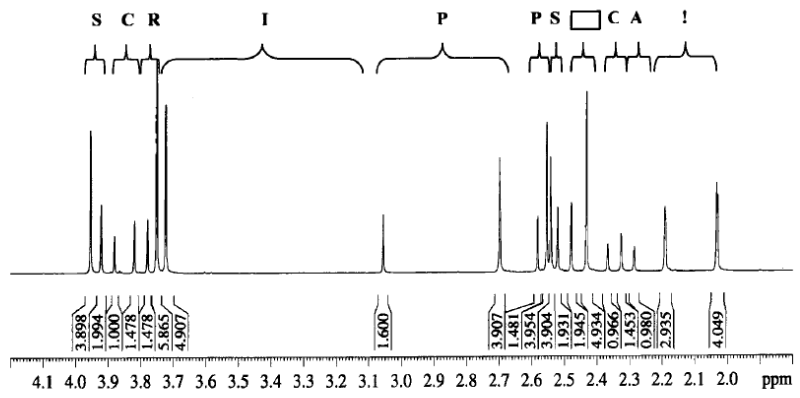

b)

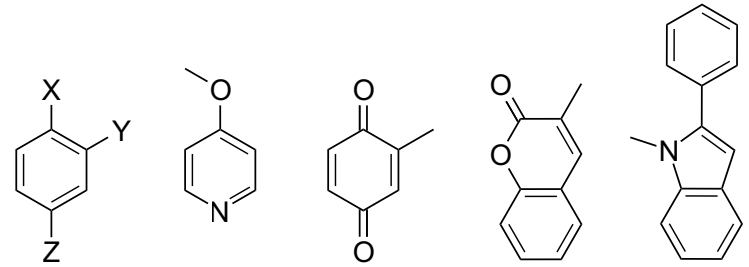

X = Me, OMe, NMe_2, SMe, COMe or CO_2Me

Y = H, Br or NO_2

Z = H, Cl, Br, I, NO, NO_2, CN or CHO

Figure 4 *a) Example of an encoded message (Scrips CA!) in a ^{1}H-NMR sample. The relative integrals read from low to high field can be converted to symbols by using a predetermined encoding table. b) Chemical structures of the aromatic molecules employed to give a methylene singlet in the ^{1}H-NMR spectrum.*[45]

Inspired by nature, data storage on single molecules was accomplished by Goldman *et al.* and Church *et al.,* by employing DNA as the information carrier.[46,47] They stored non-biological data such as the 154 sonnets of Shakespeare on DNA. An algorithm was developed that converted the binary code of the text into a quaternary code corresponding to the four nucleotides of DNA. The DNA was then synthesized using

conventional techniques, and the stored information could be read with high fidelity. This system allows the storage, reading and replication of data at the single molecule level. The drawbacks of this approach are that the conversion of the two-bit digital code to the four nucleotides can lead to instabilities in the DNA molecule. Furthermore, DNA strands are known to be fragile and unstable; hence, the preservation and reading of data is only possible under controlled conditions, such as in aqueous media and in a rather narrow temperature range.

To overcome these drawbacks, synthetic polymers might be more suitable for the storage of data, since they are often easier to handle and are more robust. Furthermore, they enable the use of a binary code by assigning two different chemical functions to the 0 and 1 bits.[6] In addition, such polymers can be produced on large scales and at lower costs than their natural equivalents, and a much broader range of chemical structures is available.[48] When more than two different chemical functionalities can be used as different bits, creating e.g. a quaternary code, information-storage capacities may be significantly enlarged.[49] The storage of data on synthetic polymers that are composed of more than one type of monomer was already envisioned some time ago and provides nowadays an interesting research topic focusing on sequence-controlled polymers.[50] The simplest method to prepare such polymers is by the on-by-one addition of the monomers, using solid-phase synthesis.[51–55] A bi-functional monomer, of which one reactive functionality is protected, is employed. After coupling to another monomer, deprotection and purification of the product, the same process can be repeated until a complete polymer chain is obtained. Although in recent publications more efficient methods circumventing the need of protecting groups have been reported, the process remains very time consuming.[54,55] Sequence-controlled polymers can also be obtained via chain-growth polymerization methods, in which the sequence is dependent on the relative reactivity of the monomers. Lutz *et al.* employed the protocol of controlled/living chain-growth polymerization, in which they locally functionalized the polymer and hence controlled its primary structure.[53,56–61] They used the time-controlled addition of small amounts of a functional acceptor e.g. an ultra-reactive N-substituted maleimide to the reaction mixture for the polymerization of styrene. This functional acceptor favors co-polymerization over homo-polymerization and is therefore consumed ultrafast upon its addition to the polymerization reaction mixture. Because it is more favorable to incorporate the functional acceptor than a styrene monomer, incorporation of the small amount of functional acceptor occurs in narrow regions of the growing polymer and the location and size of these regions can be controlled by the addition time of the functional acceptor. This method could be employed for a variety of functional acceptors, e.g. N-substituted maleimides.[58] Another route to synthesize information-carrying polymers involved a multistep synthesis protocol, which employs two phosphoramidite monomers containing either a propyl or a 2,2-dimethylpropyl group as the 0 and 1 bits,

respectively.[62] This method uses a three-step cycle per monomer addition, involving deprotection, coupling, and oxidation. Nevertheless, polymers with long encoded sequences could be synthesized. Post modification of the polymers was achieved by incorporation of a 2,2-dipropargylprophyl monomer, which can be further modified via a copper-catalyzed azide-alkyne cycloaddition reaction (CuAAC). In order to bypass the elaborate deprotection and oxidation steps, Lutz *et al.* also developed an 'AB + CD' concept, which uses two building blocks that can be coupled selectively (Figure 5a).[53,54,63–65] Because the functional group of monomer A only reacts with

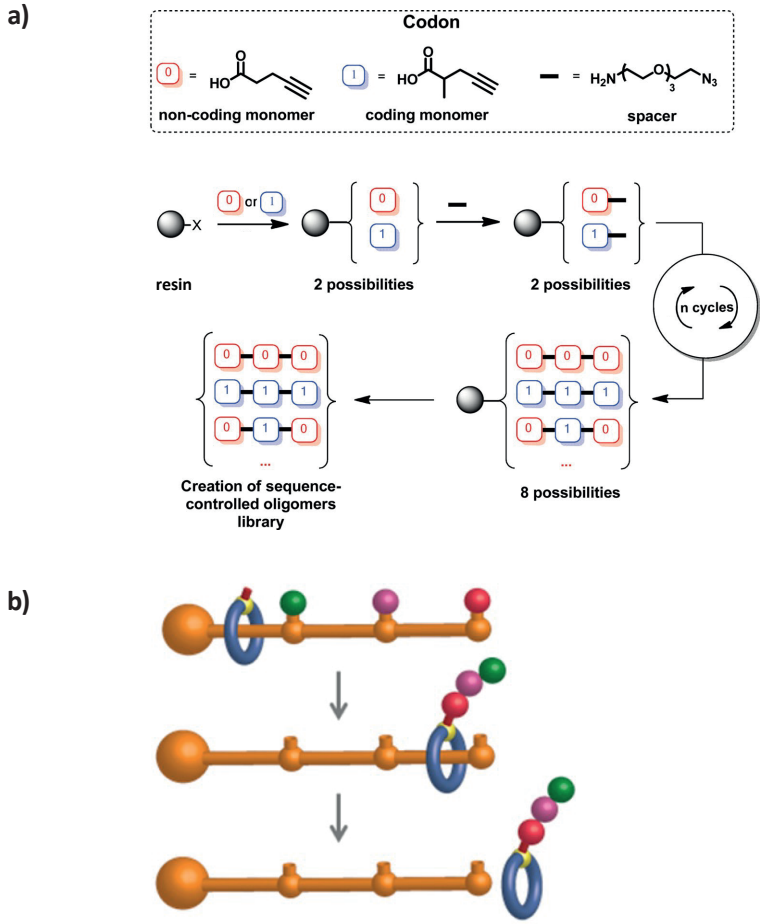

Figure 5 *a) General strategy for synthesizing sequence-defined polymers via an "AB + CD" concept.[63] b) Schematic representation of a rotaxane-based nanomachine. The molecular ring (blue) moves along a thread (brown) and when it passes a station equipped with an amino acid (green, purple and red spheres), it is attached to the molecular ring until no more stations are present and the ring detaches from the thread.[66]*

the functional group of monomer C, and the same holds for those of monomers B and D, protecting groups are not required and selective coupling can be obtained. Diverse building blocks can be employed and the sequence-encoded polymers could be easily analyzed with tandem mass spectrometry.

Leigh *et al.* reported another method to synthesize sequence-controlled polymers, which made use of a rotaxane-based nanomachine (Figure 5b).[66–70] This rotaxane machine mimics the function of a ribosome and synthesizes oligopeptides in a sequence-controlled manner. A molecular ring equipped with a thiolate function moves along a thread to which stations equipped with amino acids are attached. When the ring reaches a station, the amino acid is incorporated into the oligopeptide chain. The movement of the ring is not unidirectional but a station can only be surpassed when the amino acid is incorporated, ensuring sequence-controlled polymerization. The drawbacks of this method are that the synthesis of the thread with the stations is elaborate, and that the thread can be used only in one cycle.

1.3.3 Enzyme mimics suitable for information storage

As mentioned above, nature makes use of catalytic machines, e.g. the DNA polymerases, to write and store information. To store data by chemical means, the processes occurring in nature can be employed as a blueprint to control the writing and storing of information on synthetic polymers. Nature often employs cooperativity to regulate the activity and function of proteins and enzymes.[71] Cooperativity arises when two or more simultaneously occurring interactions within a system result in a different behavior of the system as would be expected for the behavior based on the properties of the individual interactions.[71] When binding of a substrate at the same or a remote site of an enzyme influences the binding properties of another substrate within the same enzyme, the system shows cooperative binding behavior. When the first binding event enhances the second binding event, the cooperativity is positive, whereas if a diminishing effect takes place, the cooperativity is negative. An allosteric effect is present when the binding of an effector in the first binding event triggers a conformational change in a protein or enzyme, which is reversible.[72] When the effector and the substrate are identical or different molecules, the allosteric effect is named homotropic or heterotropic, respectively. The best known example of an allosteric protein is hemoglobin, which has four binding sites for molecular oxygen and the affinity for molecular oxygen increases with every oxygen molecule that is bound.[72–74]

Because cooperativity is a powerful and versatile tool to regulate the binding properties and catalytic activity of molecules, it is no surprise that it has been a focus of research in the past in order to gain a better understanding of the interactions that enable cooperativity and the corresponding effects.[75] Cooperative effects may also be employed to control the writing of information onto synthetic polymers. The earliest work in which cooperative interactions were employed in artificial systems

has been reported by Rebek Jr. *et al.,* who described multiple heterotropic cooperative substrate binding processes in crown ether derivatives functionalized with a 3,3'-disubstituted 2,2'-bipyridine moiety. In this system, negative cooperativity occurred upon the binding of alkali metal ions in the crown ether rings and simultaneous coordination of transition metals to the bipyridine ligand.[76–78] Homotropic positive allosteric binding of substrates was reported by Shinkai *et al.* for crown ether-functionalized porphyrin double decker complexes (Figure 6a).[79–82] The binding of a potassium ion in one of the crown ether ligands is hindered by the rotation of the two

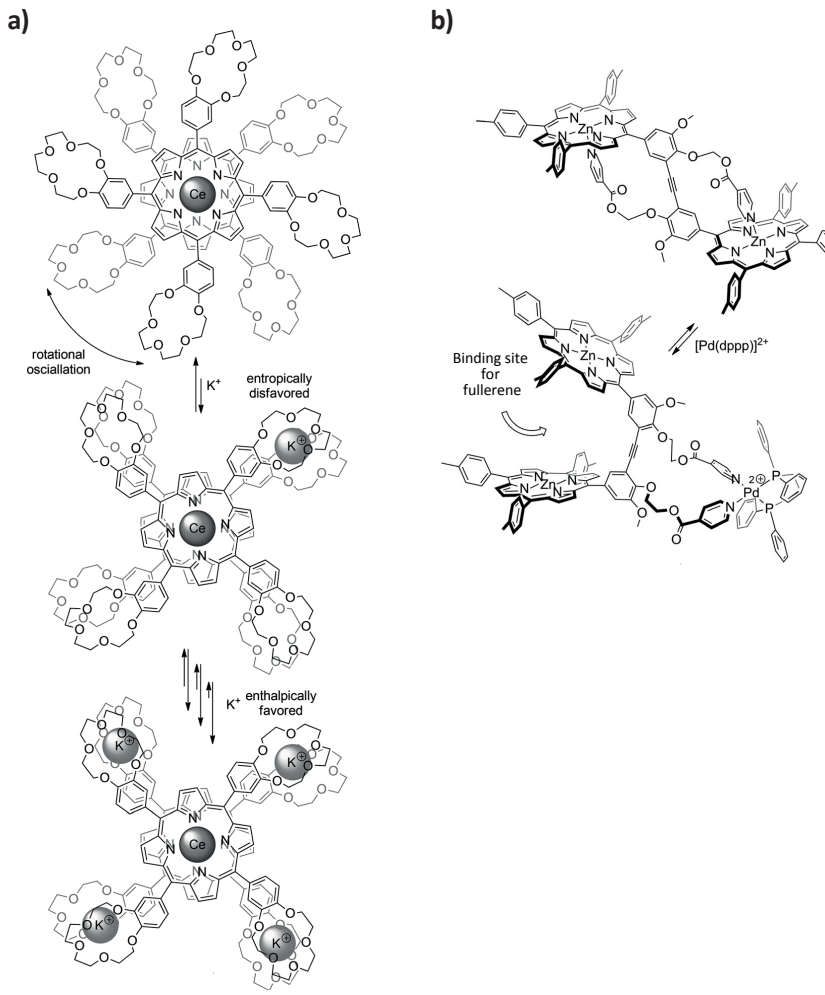

Figure 6 *a) Cerium (IV) porphyrin double decker complex displaying positive allosteric binding of potassium ions. b) Zinc porphyrin tweezer that can bind fullerenes upon the coordination to a palladium complex.[72]*

porphyrins around the cerium metal center, but once the first ion is bound, this rotation is suppressed and therefore the binding of the other three ions is enhanced. However, upon the addition of silver ions, the opposite effect was observed and rotation was accelerated. It was demonstrated that the binding of a large silver ion pushes the porphyrin planes apart, creating space for the binding of additional silver ions. At the same time, however, the rotational movement around the cerium center was accelerated, which made binding of the additional silver ions less favorable.

Another example of a system in which allosteric binding of a substrate occurs has also been reported by the group of Shinkai, and involves a porphyrin tweezer in which the two porphyrin planes are linked together via a palladium(II) diphosphane complex (Figure 6b).[83] Upon the binding of the palladium complex, the tweezer switches from an *anti*- to a *syn*-conformation, arranging the porphyrin planes into a geometry that enables the binding of fullerenes. Several variations on tweezers that are activated for binding by the complexation of an ion have been reported.[82,84–89] Aida *et al.* reported an artificial receptor that displays negative homotropic or positive heterotropic allosteric binding, depending on the molecule that is bound (Figure 7).[90,91] The receptor consists of two fused zinc porphyrins that are connected via two flexible linkers. When two identical guests (fullerene or 4,4'-bipyridine) are bound in between the zinc porphyrins, the binding of the first guest lowers the binding constant of the second guest and thus the system displays negative cooperativity. However, binding of two different guests resulted in positive cooperativity, because when first a 4,4'-bipyridine guest was bound, the binding of fullerene to this complex was 8.5 times stronger than in the absence of 4,4'-bipyridine. It was suggested that the positive allosteric effect originates from electronic communication between the two guests, enabled by the conjugated porphyrins. The formation of a 1:2 complex between the porphyrin host and fullerene was not observed due to strongly negative cooperative effects.

Cooperative interactions also guide the folding process of proteins and other biomolecules such that it can be completed within milliseconds. Similar cooperative interactions were employed to construct complex assemblies of multiple molecules.[92] The porphyrin ladders and the porphyrin nanorings described by Anderson *et al.* are well-known examples of this strategy.[93–95] The porphyrin ladders are constructed by the assembly of linear zinc porphyrin oligomers into double stranded structures by the coordination of ditopic ligands, e.g. 4,4'-bipyridine or DABCO (1,4-diazabicyclo[2.2.2]octane) (Figure 8a). It was found that ladder formation is an 'all or nothing process', because upon the addition of a small amount of DABCO to the linear zinc porphyrin oligomers, only free porphyrin strands and fully complexed ladders were detected, while no signals for porphyrins with mono-coordinated DABCO ligands were present in the NMR spectra. The binding of the DABCO ligands in the ladders was found to be a strongly cooperative process: binding of the first ligand between two zinc porphyrins pre-organizes the porphyrin planes in the rest of

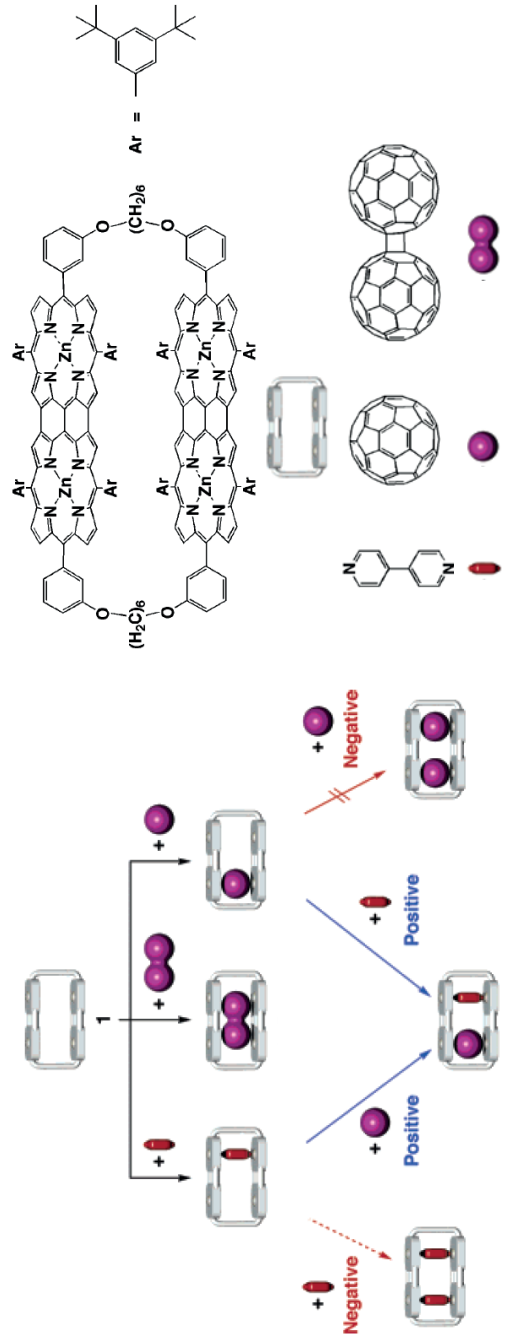

Figure 7 *Allosteric binding of guests within a fused porphyrin receptor.*[90]

the strand, making the binding of additional DABCO ligands favorable. Instead of linear ladder structures, also cyclic assemblies could be formed by means of pre-organization.[96–100] By using templates containing multiple nitrogen-containing ligands, porphyrin nanorings of various sizes could be synthesized.[100–102] These nanorings could subsequently be assembled into double nanorings by using the same strategy as for the construction of porphyrin ladders, i.e. via the coordination of ditopic ligands (Figure 8b).[96] Also for the formation of these double rings, strong positive cooperative effects were observed for the coordination of DABCO, resulting in an 'all or nothing' formation process.

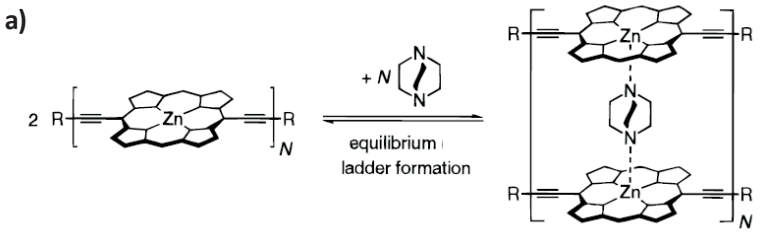

Figure 8 *a) Porphyrin ladder formation upon the addition of DABCO to rigid linear zinc porphyrin oligomers.[95] b) Formation of a double nano-ring from two monomeric zinc nano-rings upon the addition of DABCO.[96]*

1.3.3.1. Porphyrin cage compounds as mimics of DNA polymerase

The cooperative effects that were described in the previous section resulted in the formation of large, self-assembled molecular architectures. However, these architectures were not further used as functional systems for e.g. catalysis or information storage. So far, only a few examples of information storage in synthetic polymers have been reported, and all of these are based on a step-by-step synthesis of a polymer chain.[53,62,64,65] The aim of the work described in this thesis is to develop an enzyme mimic, based on DNA polymerase that will be able to write a binary code on an already existing synthetic polymer, instead of synthesizing the polymer in a step-by-step fashion. Previously, the Nolte group had already developed an enzyme mimic that is based on the key features of DNA polymerases, i.e. a molecule that contains a catalytic site connected to a ring-shaped cavity that can bind to a polymer chain and keep the catalyst attached to this chain. This so-called 'porphyrin cage' (**H_2SC**, Figure 9) consists of a rigid molecular cage based on diphenylglycoluril, which is covalently attached to a porphyrin 'roof'.[103] When a catalytically active metal is coordinated in the porphyrin, the porphyrin cage can mimic the active site of an enzyme, since it contains a cavity in close proximity to a catalyst.[104] The idea was that this porphyrin cage compound could be modified to serve as the main component in a system that will be able to write a binary code onto a synthetic polymer chain via information transfer.

Initially, **H_2SC** was synthesized by equipping a diphenylglycoluril-based cavity molecule with four aldehyde functionalities, which yielded a porphyrin roof upon cyclization with pyrrole.[103] Since this method came with a very low yield (6%) in the final step, an alternative synthesis route was developed in which a tetrahydroxy porphyrin was pre-synthesized and directly connected to a tetratosyl-functionalized diphenylglycoluril-based cavity molecule.[104] **H_2SC** has a rigid and symmetric cavity of 9 Å in which small aromatic guest molecules such as dihydroxbenzene and viologen derivatives can be complexed.[103] With the aim to vary the flexibility and size of the system, two additional porphyrin cage molecules were synthesized in which the four spacers between the cage molecule and the porphyrin contain an extra ethyleneoxy group (**H_2BSC-1** and **H_2BSC-2**, Figure 9).[103,105] NMR studies revealed that the porphyrin planes in these compounds were no longer situated symmetrically above the cavity, but adopted an offset orientation to its side. To protect the exposed face of the porphyrin, **H_2SC** was also functionalized at the outer *ortho*-positions of the porphyrin *meso*-phenyl groups.[106–108] Four ethylureapropoxy tails were attached (**$H_2(U)_4$SC**, **$Zn(U)_4$SC**, and **$Mn(U)_4$SC**, Figure 9), which folded over the porphyrin in the case of the free base compound and coordinated to the zinc or the manganese center in the case of the metallo-porphyrin cages.[106] A porphyrin cage with four hydroxy groups (**$H_2(OH)_4$SC**, Figure 9) on the outer meso-phenyl *ortho*-positions was found to dimerize in solution via the formation of hydrogen bonds between the hydroxy groups.[107,108]

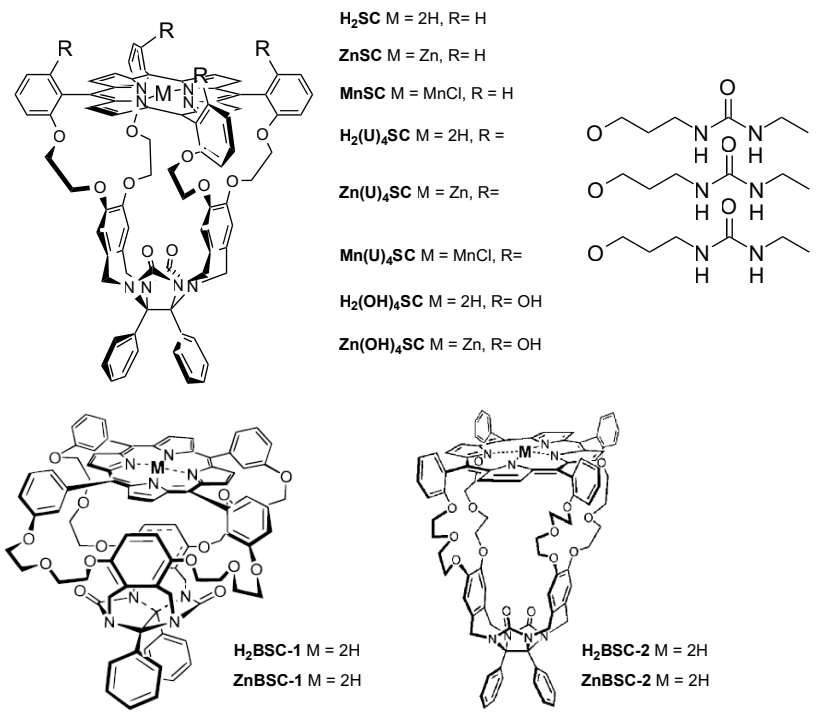

Figure 9 *Chemical structures of porphyrin cage molecules.*[103,105–108]

The porphyrin cage molecules could all bind a variety of guests in their cavities, via non-covalent interactions such as π-π stacking with the aromatic side walls, hydrogen bonding and electrostatic interactions with the carbonyl and crown ether functionalities, and axial metal-ligand coordination in the case a metal center was complexed in the porphyrin.[103,109]

1.4. Characteristics of porphyrin cage compounds

The following sections will focus on the guest binding, polymer threading, and catalytic properties of the porphyrin cage compounds that were described in the previous section. These properties are essential when the porphyrin cages will be employed as catalysts to write digital information on synthetic polymer chains via information transfer. In order to enable this information transfer ability, the porphyrin cage compounds need to be modified in such a way that a cofactor molecule can bind and influence their catalytic activity. This information transfer should occur by means of allosteric interactions. In the following first the allosteric behavior of

porphyrin cage compounds will be discussed, followed by the binding of guests that can function as cofactor molecules. Finally, the threading of polymeric chains through their cavities and their performance as processive catalysts will be highlighted.

1.4.1. Binding of ligands to zinc porphyrin cages

In order to influence the selectivity and/or reactivity of the catalytic center in the porphyrin cage compounds one may make use of conformational changes. Additionally, if communication between one part of the molecule and another part is required, allosteric interactions should be built in. For the porphyrin glycoluril cages mentioned in the above sections, allosteric interactions have been reported between ligands coordinated to the porphyrin metal center and guest molecules that are complexed in the cavities of the molecules. The nitrogen-containing ligand pyridine was found to exclusively bind inside the cavity of **ZnSC**, with a binding constant of K_a = 7.5 x 10^4 M^{-1} in a solvent mixture of chloroform and MeCN (1:1, (v/v)).[110] This binding constant is almost two orders of magnitude higher than that found for the binding of pyridine to Zn(II)-tetra(*meso*-phenyl)-porphyrin and is a result of the presence of additional π-π stacking interactions between the ligand and the cavity side walls of the porphyrin cage, and a cavity-filling effect. When the cavity of the porphyrin cage is more pre-organized for binding of the ligand, a higher binding constant is observed. Previous research also showed that coordination of a bulky ligand that does not fit in the cavity of **ZnSC**, such as *tert*-butyl pyridine (tbpy, Figure 10), occurs on the outside of porphyrin plane with a binding constant K_a = 1.3 x 10^2 M^{-1} in a solvent mixture of chloroform and MeCN (1:1, (v/v)).[110] For larger porphyrin cages, such as **ZnBSC-2**, more bulky axial ligands, such as Si-tpby (Figure 10), are needed if exclusive coordination to the outside of the cage molecule is required.

By using a ditopic ligand such as 1,4-diazabicyclo[2.2.2]octane (DABCO, Figure 10) dimeric structures can be generated from zinc porphyrin cage molecules. When DABCO was added to **ZnSC**, a complex containing two cage molecules and one DABCO ligand was formed with binding constants of K_a = 5 x 10^4 M^{-1} and 6 x 10^2 M^{-1} for the first and second binding event of the cage compound to the ligand, respectively.[107] At a concentration of 1 mM **ZnSC** and 0.5 mM DABCO, 22 % of the 2:1 **ZnSC**:DABCO complex was present in solution. To increase the abundance of this 2:1 complex, **ZnSC** was equipped with hydroxyl substituents on its *meso* phenyl rings (**Zn(OH)$_4$SC**, Figure 9).[107] Molecular modeling indicated that these substituents are 3 Å apart when two **Zn(OH)$_4$SC** molecules are coordinated to a DABCO ligand, hence, it was expected that these hydroxyl functions would form hydrogen bonds, further stabilizing the 2:1 complex.[107] This expectation was found to be correct: the first and second binding constants were now measured to be K_a = 1 x 10^4 M^{-1} and 6 x 10^6 M^{-1}, respectively.[108] A similar dimeric complex could not be formed when the hydroxy functionalities were changed into urea functions, i.e. ethylureapropoxy tails (**Zn(U)$_4$SC**, Figure 9), because of steric effects. Instead of facilitating dimer formation

between two **Zn(U)$_4$SC** molecules, the urea moieties coordinated intramolecularly to the zinc center, thereby hindering coordination of an external axial ditopic ligand to the outer face of the porphyrin cage.[106] This intramolecular coordination of the urea functions could be prevented by binding a pyridine molecule inside the cavity of the porphyrin cage compound.[106]

1.4.2. Binding of viologen guests and their allosteric effects on porphyrin cage compounds

In previous studies it was found that *N,N'*-disubstituted 4,4-dipyridinium (viologen) compounds bind within porphyrin cage molecules with high binding constants, making them promising candidates to act as promotor molecules in combination with other guest or ligand molecules.[103,105,109] Dimethyl viologen dihexafluorophosphate (**Me$_2$V**, Figure 10) binds inside the cavity of **H$_2$SC**, with a binding constant of K_a = 6.0 x 10^5 M^{-1} in a solvent mixture of chloroform and MeCN (1:1, (v/v)).[103] The viologen is orientated perpendicular to the porphyrin plane (Figure 11a), and its binding is stabilized by various interactions: (*i*) parallel and T-shaped π-π stacking interactions with the cavity side walls and the porphyrin aromatic system, (*ii*) electrostatic interactions with the ethyleneoxy spacers, and (*iii*) weak hydrogen bonding interactions of its 3,3'-protons with the carbonyl groups of the glycoluril framework.[103] When the methyl groups of the viologen were substituted for ethanol groups (**(EtOH)$_2$V**, Figure 10), the hydroxy functions were found to form hydrogen bonds with the carbonyls of the glycoluril group, resulting in a binding constant of K_a = 7.4 x 10^6 M^{-1} in a solvent mixture of chloroform and MeCN (1:1, (v/v)).[103] As a result of these additional hydrogen bonding interactions the aromatic surface of **(EtOH)$_2$V** orients itself parallel to the porphyrin plane (Figure 11b). Binding of viologen derivatives in **H$_2$BSC-1** occurred via an induced-fit mechanism, involving a conformational change in which the porphyrin plane was lifted from the side walls.[103] Due to this reorganization, and to weaker interactions between host and guest, the binding constant between **H$_2$BSC-1** and **Me$_2$V** was much lower (K_a = 1100 M^{-1} in a solvent mixture of chloroform and MeCN (1:1, (v/v))).[103] When (**EtOH)$_2$V** was bound in **H$_2$BSC-1**, the porphyrin was located more centrally above the cavity than when **Me$_2$V** was bound, resulting in a somewhat higher binding constant K_a = 3500 M^{-1}.[103] The binding between **Me$_2$V** and **H$_2$BSC-2** also occurred via an induced-fit mechanism and the guest was bound in a 'pseudosuit(2)ane' geometry, in which the aromatic plane of the guest is oriented parallel to the porphyrin plane and in a traversed direction over the cavity, with the positive charges of the guest located inbetween the crown ether spacers.[105] The binding constant between **Me$_2$V** and **H$_2$BSC-2** (K_a = 6.4 x 10^5 M^{-1} in a solvent mixture of chloroform and MeCN (1:1, (v/v))) is about the same as the binding constant between this guest and **H$_2$SC**.[105]

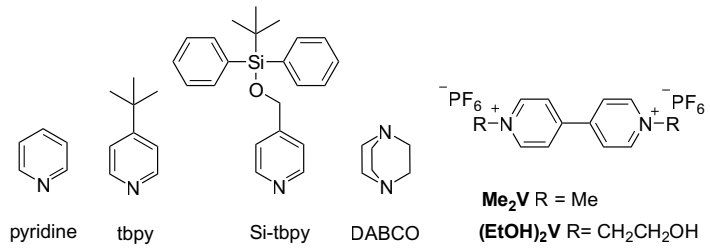

Figure 10 *Chemical structures of several guests and ligands that can bind to or inside porphyrin cage compounds.*

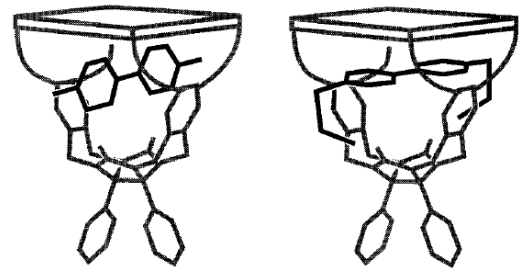

Figure 11 *Schematic representation of the orientation of **Me$_2$V** (a) and **(EtOH)$_2$V** (b) in **H$_2$SC**.*

Previous studies have reported allosteric behavior when nitrogen-containing axial nitrogen ligands and **Me$_2$V** are combined in the binding to **ZnSC**, making these combinations of molecules promising candidates for realizing information transfer in porphyrin cage compounds. When *tert*-butyl pyridine (tbpy) was coordinated to the porphyrin at the outside of the cavity of **ZnSC**, and one equivalent of **Me$_2$V** was subsequently added, the amount of **ZnSC** with tbpy coordinated to its zinc center increased from 17% to >98% at a concentration of 10^{-6} M.[107] The binding of tbpy and **Me$_2$V** to **ZnSC** occurs via an allosteric process because the binding of **Me$_2$V** in the cavity of **ZnSC** results in pinching of the cavity which 'pushes' the zinc center further out of the porphyrin plane, making it more available for the binding of tbpy. The reverse effect also takes place, i.e. the binding of tbpy leads to a pinching of the cavity leading to a higher binding of the viologen molecule and since both processes involve a reversible structural change in **ZnSC**, the phenomenon is considered to be allosteric. Experiments showed that the allosteric magnification (equation 4) is 250 for the binding of tbpy in the presence of **Me$_2$V**, whereas it is 3 for the binding of **Me$_2$V** in the presence of tbpy. Hess's law, however, states that both effects should be the same in magnitude, and therefore it was hypothesized that solvent molecules

that are coordinated to the zinc center first need to dissociate.[107] However, in a complete cycle, also the coordination of solvent molecules should be balanced out if all the measurements are carried out at the same concentration. Since the difference in binding constants of tbpy and **Me_2V** leads to measurements at different concentrations, the combination of the solvent effect and the different concentrations account for the discrepancy in the observed allosteric magnification.[107] A similar but smaller allosteric magnification was observed for the binding of **Me_2V** when pyridine was used as the axial ligand.[110] Since both molecules can bind inside the cavity of **ZnSC** they compete with each other, but nonetheless a positive allosteric effect was observed, which depended on the concentration of pyridine.

$$\textit{Allosteric magnification} = \frac{K_{\textit{for ligand in the presence of guest}}}{K_{\textit{for ligand in the absence of guest}}} \qquad (4)$$

When DABCO was employed as nitrogen containing ligand, 1:2 ligand:**ZnSC** complexes can be formed. In the presence of 10 equivalents of **Me_2V** the binding constant of DABCO increased from 5 x 10^4 M^{-1} to 4 x 10^5 M^{-1}, which leads to a cooperativity factor (α, equation 5) of 0.05 for **ZnSC**.[107] The cooperative binding had a profound effect on the distribution of species. When **Me_2V** was added, 57% of **ZnSC** was present in the form of a complex with DABCO (1:1:1 or 2:2:1 **Me_2V**:**ZnSC**:DABCO complex) compared to only 22% in the absence of **Me_2V** (at concentrations of 1 mM **ZnSC** and 0.5 mM DABCO).[107] When hydroxy substituents were present on the top of the cage compound (**$Zn(OH)_4SC$**) the amount of the 2:2:1 **Me_2V**:**$Zn(OH)_4SC$**:DABCO complex increased to 98.5% at the same concentrations. The binding constant of DABCO to **$Zn(OH)_4SC$** increased from 2 x 10^6 M^{-1} to 9 x 10^6 M^{-1} upon the addition of 10 equivalents of **Me_2V**, leading to a cooperativity factor of 17.[107]

$$\alpha = \frac{4K_{1:2}}{K_{1:1}} \qquad (5)$$

1.4.3. Threading of polymer chains through the cavities of porphyrin cage compounds

The translocation of the DNA polymerase along the DNA strand is vital for the functioning of the enzyme. The aim of the research described in this thesis is to employ porphyrin cage compounds for the writing of data onto synthetic polymers. In this connection translocation of the cage compounds along a polymers chain is vital as well. To investigate this possibility, the threading and translocation of porphyrin glycoluril cage compounds onto polytetrahydrofuran (polyTHF) and poly(1,4-butadiene) (polyB) chains connected to a thermodynamic trap (viologen (**V**) moiety) with a high affinity for the cavity of **SC** was investigated. This **V**-moiety was located at one end of the polymer chain, close to a 3,5-di-tert-butylphenyl blocking group, i.e. a group that is too large to be traversed by the cavity of the **SC** compounds (Figure 12a). As a result, the cage molecule has to thread onto the polymer chain at the open end and

has to translocate along the chain before complexation to the **V**-moiety can occur. This complexation was recorded by following the fluorescence of the porphyrin, which became quenched as soon as this molecule had reached the viologen trap (Figure 12b).[111] MALDI-TOF spectrometry and NMR spectroscopy was used to confirm the formation of the 1:1 **SC**:polymer complex.[111] These fluorescence studies revealed that the threading of the cage compounds on the above mentioned polymers occurred via a second order process, and that **H_2SC** is able to traverse polyTHF chains lengths of up to at least 54 nm.[111] The reverse process (dethreading) could also be studied, i.e. by diluting a milimolar solution of the 1:1 **H_2SC**:polyTHF complex 1000 times. The dethreading was monitored by following the increase in fluorescence signal over time and this process was found to be first order.[111] The threading processes were subsequently measured at different temperatures, providing Eyring plots from which positive $\Delta H^{\ddagger}_{on}$-values, which were equal for all polymer lengths could be derived and strongly negative $\Delta S^{\ddagger}_{on}$-values that increased with increasing polymer length. It can be concluded, therefore, that an entropic barrier is present for the threading of the cage onto the polymer, which was ascribed

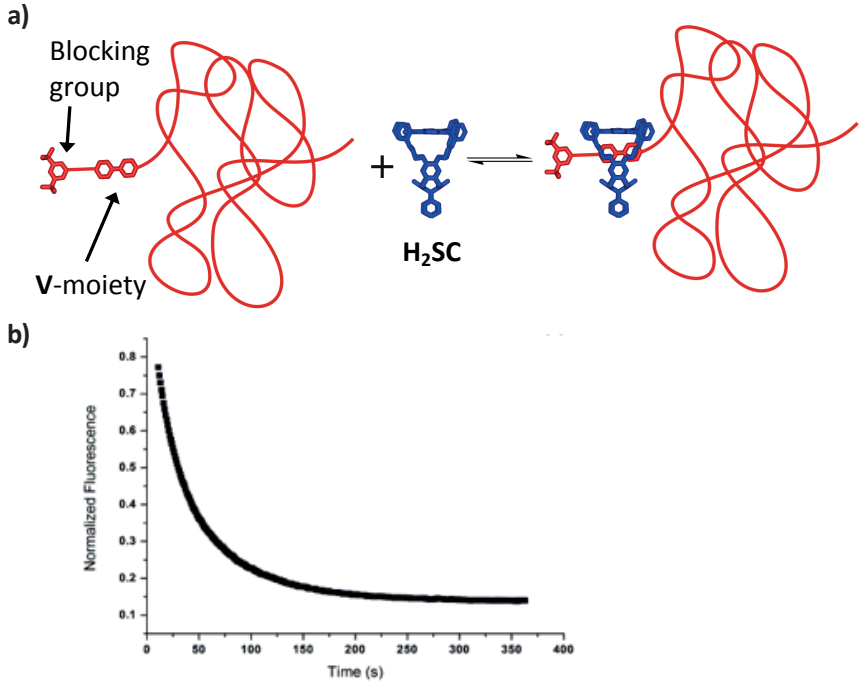

Figure 12 *a) Schematic representation of the threading of* ***H_2SC*** *(blue) onto polymers equipped with a viologen trap (red). b) Decay of the normalized fluorescence intensity over time upon the threading of* ***H_2SC*** *onto a polyTHF chain functionalized with a viologen trap and a blocking group.*[111]

to the stretching of the chain and the conformational adjustment of the components.[111] It was calculated that, on average, the movement of **H_2SC** occurs with a rate of 750 and 14 pm/s along a polyTHF and a polybutadiene chain, respectively.[111] **ZnSC** was found to traverse more slowly along a polyTHF chain than its free base analogue, although it has almost no additional interactions with the polymer chain.[112] When tbpy was coordinated to the zinc center, threading occurred faster, and when pyridine was used to block the cavities by coordinating to the zinc center from the inside, almost no threading was observed. Therefore, it was concluded that the lower threading rate observed for **ZnSC** originates from a partial blocking of the cavity by the coordination of solvent molecules, e.g. MeCN, to the zinc center.[112]

To investigate the mechanism of the threading process in more detail, blocked viologen derivatives functionalized with alkane chains and polymer chains of various lengths were threaded through **SC**.[113] When the length of the chain exceeded 22 atoms, the threading rate decreased with increasing polymer chain length. It was concluded that, after an initial binding event in which **SC** binds onto the polymer, a consecutive hopping mechanism occurs in which the cage compound moves stepwise along the polymer chain to eventually reach the **V**-moiety (Figure 13a).[113] During each hopping step, **SC** moves randomly from one energy minimum to the next, and the number of energy minima is linearly dependent on the length of the polymer chain. However, in the case of short chains it was observed that when the chain length exceeds eight atoms, the threading rates remain more or less constant up to a chain length of 22 atoms. It was concluded that in this case another pathway of threading must be operative, in which the cage compound first associates on its outside with the **V**-moiety, allowing the open end of the polymer chain to loop into the cavity (Figure 13b, middle).[113] Effective molarity effects favor such a threading mechanism for chain lengths of 8 to 40 atoms, but not for the longer polymer chains. At the moment that the last 8 atoms of the chain need to be traversed by the cage in order to form the complex between the cage and the **V**-moiety, dissociation of the latter molecule from the outside of the cage occurs. An alternative mechanism, in which the cage compound threads over a folded polymer, was discarded after control experiments with model compounds (Figure 13b, right).[114] When the cavity of the cage compound was enlarged (**H_2BSC-1**, Figure 9), the threading rate decreased due to a higher affinity of the cage compound for the chain, which wrapped itself around it as a result of induced-fit binding effects.[115] When one-side blocked polyTHF chains provided with a viologen group were added to a 2:1 **Zn(OH)$_4$SC**:DABCO complex, 2:1:1 and 2:1:2 **Zn(OH)$_4$SC**:DABCO:polymer complexes were formed simultaneously.[108] Because of the presence of DABCO, the association constant of the viologen moiety in the cavities of the complexes was three times larger than in the absence of the ligand. Also the reverse effect, i.e. the fact that the binding of the viologen moiety increases the binding constant of DABCO, was observed. These allosteric interactions

ensured that the 2:1:2 **Zn(OH)$_4$SC**:DABCO:polymer was formed as the major species in solution. As a result of the allosteric interactions, the dethreading rate of the polymers was slowed down considerably. In the case of the 2:1:1 **Zn(OH)$_4$SC**:DABCO:polymer complex, the slow dethreading may originate from the fact that the second cavity is occupied by the open end of the polyTHF chain that already has threaded through the first cavity of the dimeric complex (Figure 13c).[108]

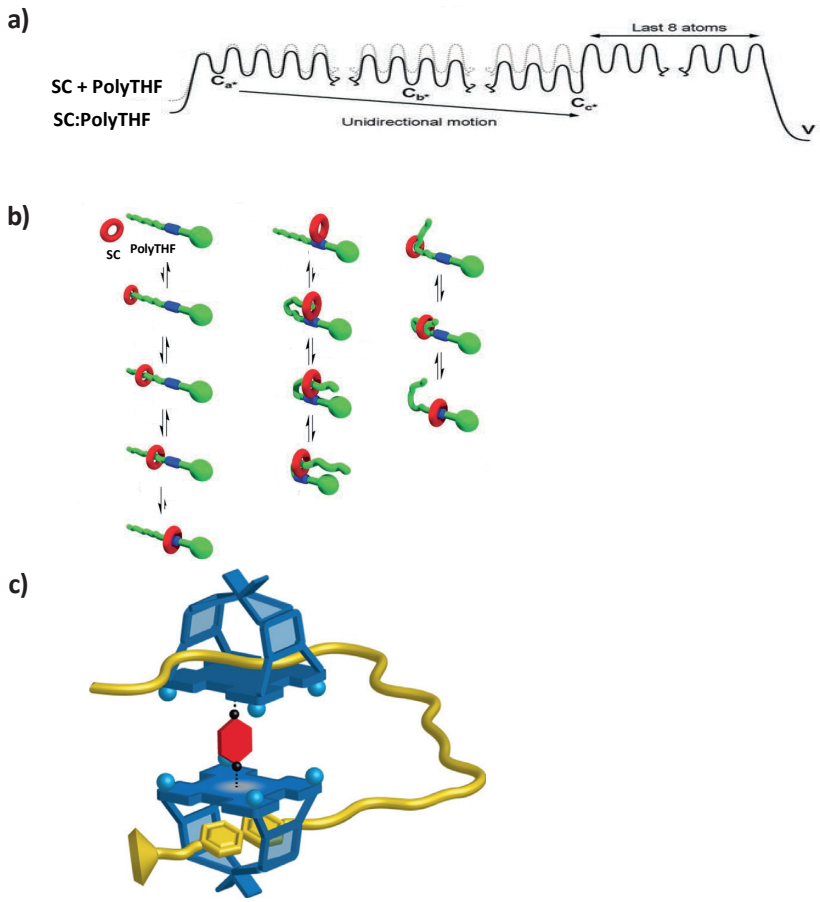

Figure 13 *Schematic representation of the energy landscapes and mechanisms of the threading process of blocked viologen derivatives functionalized with alkyl or polymer chains. In (a) the consecutive hopping mechanism is depicted, in (b) the possible threading mechanisms: intermolecular threading (left), threading in which the viologen moiety is first complexed to the outside of the cage compound (middle) and the alternative path involving a folded polymer chain (right).[113] In (c) the complexation of polyTHF to a **Zn(OH)$_4$SC** dimer (blue), coordinated to DABCO (red) in which the second cavity is blocked by the end of the polymer chain (yellow) bound in the first cavity, is depicted.[108]*

1.4.4. Catalysis by porphyrin cage compounds

The ability of porphyrin cage compounds to form epoxides from alkenes may be used to store digital data onto synthetic polymers that contain alkene functions and can be seen as a form of writing. When a manganese center is inserted into **SC** the resulting cage **MnSC** (Figure 9) becomes catalytically active in the epoxidation of alkenes.[116] When a pyridine ligand was coordinated to the manganese center at the inside of the cavity of **MnSC**, the epoxidation of α-pinene was completed within two hours, while the reaction under the same conditions but using the reference porphyrin **MnTPP** (Figure 14) as the catalyst required over 10 hours.[104,116] The significant rate enhancement observed for catalyst **MnSC** is a direct result of the activation of the manganese center by the strong binding of pyridine inside its cavity. *Cis*-stilbene was epoxidized by the 1:1 **MnSC**:pyridine complex with a much higher *cis*-selectivity than by the **MnTPP** reference catalyst, because the strong binding of pyridine inside the cavity of the first mentioned compound pulls the manganese center more into the plane of the porphyrin, preventing rotation around the C-C-bond of the substrate in the transition state of the reaction.[104] A drawback of porphyrins such as **MnTPP** is that decomposition of the catalyst may occur because μ-oxo bridged manganese porphyrin dimers can be formed, which subsequently decompose due to self-oxidation.[104,116] The cavity of **MnSC** protects one side of the porphyrin plane for formation of such dimeric species, and when additionally tbpy is coordinated to the manganese center at the outside of the cage compound, both sides of the porphyrin are protected and decomposition of the catalyst is prevented. As a result of the coordination of tbpy, conversion of substrates has to occur inside the cavity of **MnSC**. While the epoxidation rate of α-pinene was not affected, the epoxidation rate of *cis*-stilbene was significantly slower when **MnSC** was used as the catalyst compared to **MnTPP**. The high *cis*-selectivity of the conversion of *cis*-stilbene could be explained by the steric bulk imposed by the cavity, which limits the rotation around the C-C bond of the substrate in the transition state. To investigate whether **MnSC** could also mimic the processive catalytic function of a DNA polymerase enzyme, a polymer (polybutadiene) was used as the substrate in the epoxidation reaction with **MnSC** and tbpy as the catalytic system (Figure 15).[117] It turned out that **MnSC** could epoxidize all the double bonds of polybutadiene with a different stereoselectivity (80% *trans*-, 20% *cis*-epoxide) than the reaction catalyzed by a reference catalyst without a cavity. The preference for forming the *trans*-epoxide originates again from the sterically demanding cavity, and is opposite to the product selectivity obtained when **Mn(OMe)$_4$TPP** is used as the catalyst (22% *trans*-, 78% *cis*-epoxide, Figure 14).[117] When using **MnSC**, the catalytic process was proposed to be random instead of sequentially processive, because the speed of catalysis was (on average) ~1 pm/s, which is considerably slower than the movement of the cage compound along the polybutadiene chain (14 pm/s).[111] When **Mn(U)$_4$SC** (Figure 9) was used as the catalyst, the presence of tbpy as a bulky ligand was not necessary to increase

the stability of the catalyst, because of the intramolecular protection by the urea-containing substituents.[118]

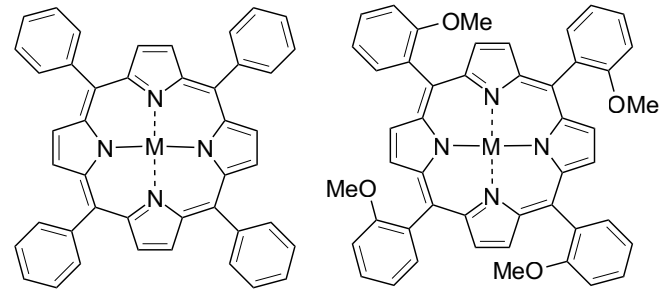

MnTPP M = MnCl **Mn(OMe)$_4$TPP** M = MnCl

Figure 14 *Chemical structures of reference porphyrin catalysts **MnTPP** and **Mn(OMe)$_4$TPP** employed.[104,116,117]*

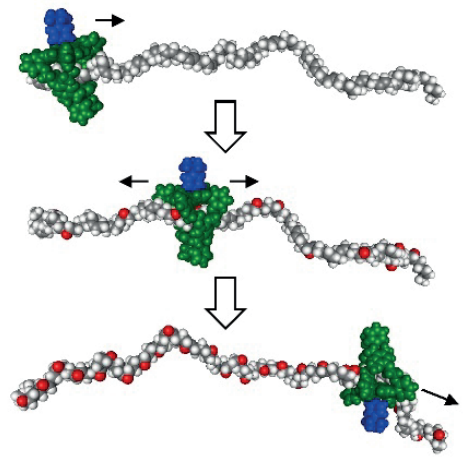

Figure 15 *Molecular modelling representations of the manganese porphyrin cage with tert-butyl pyridine as axial ligand, which epoxidizes all the double bounds in a polybutadiene chain in a randomly processive fashion.*

1.5. Aim and outline of the thesis

The storage of data on natural or synthetic polymers is appealing, because it allows for a much higher information density than conventional silicon-based storage media, at least in principle.[49] Currently there is no method to directly modify synthetic polymers for use as binary data storage materials. Therefore, the aim of the work described in this thesis is to synthesize an enzyme mimic that is capable of writing a binary code onto an already existing synthetic polymer, instead of writing this code by the step-by-step synthesis of two monomers that represent the 0 and 1 bits. The design of the enzyme mimic is based on the porphyrin cage compounds that have already proven themselves to function as processive catalysts in the epoxidation of polybutadiene (**MnSC**, Figure 9).[117] The writing of oxygen atoms on a polymer chain can be considered as the writing of binary data in a chemical fashion, in which case an epoxide moiety is defined as a digit 1 and an unreacted double bond as a digit 0. In the previously developed catalytic system epoxidation occurs via a randomly processive mechanism in which **MnSC** moves in both directions along the polymer chain, meaning that no well-defined and controlled sequential encoding

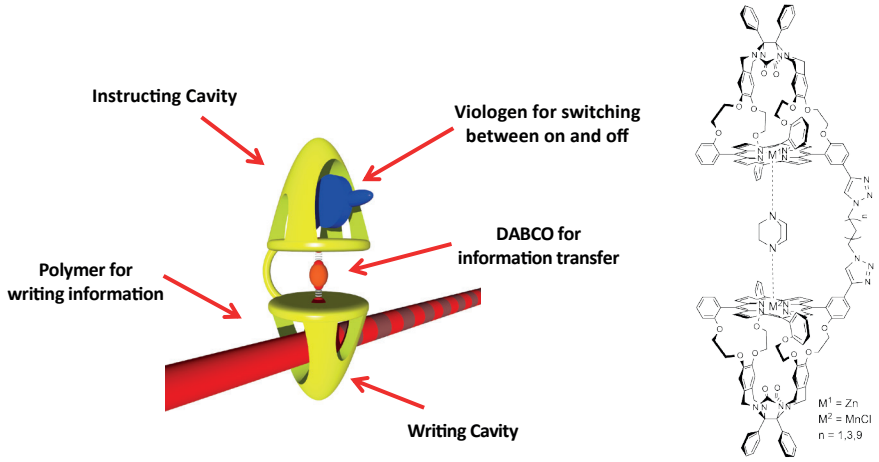

Figure 16 *a) Schematic representation of a double porphyrin cage (yellow) consisting of two receptor molecules capped with a porphyrin roof that are covalently linked. The instructing cavity contains a zinc center and the writing cavity a manganese center. The coordination of a ditopic ligand such as DABCO (orange) in between the two porphyrins might allow the transfer of information from the instructing cavity to the writing cavity, thus enabling the possibility of influencing the catalytic reaction. The binding of a viologen guest (blue) inside the instructing cavity may influence the coordination of DABCO to the manganese center, which can perform a catalytic reaction on, for example, a polymer substrate (red), via a series of allosteric interactions. b) Chemical structure of the zinc-manganese double porphyrin cages with alkyl spacer lengths of 3, 5, and 11 carbon atoms, binding DABCO as a ditopic axial ligand.*

can be accomplished. Therefore, it was decided to extend **MnSC** with a second, 'instructing' zinc-containing cage, leading to a 'double porphyrin cage' (**ZnMnC$_x$DC**, Figure 1). The idea is that by binding so-called 'promotor' molecules in the zinc-containing cage, which is attached to the manganese-containing cage via a covalent linker and a coordinating ditopic bridging ligand, the catalytic reaction in the manganese-containing cage can be influenced. Via cooperative and/or allosteric interactions between the two porphyrin cages, the promotor molecule may switch the catalytic reaction from an 'off' to an 'on'-state, or *vice versa*. In principle, in the instructing cavity a number of different promotor molecules can be bound, and this binding of different guests create different "catalytic states" of the tape head, as proposed by Turing in his theoretical machine. This will in principle enable the double porphyrin compounds to function as a Turing machine that can read and write epoxides at specific spots onto a polymer substrate.

It has previously been shown that the coordination of axial ligands such as DABCO to the metal center in the porphyrin cage is influenced, via allosteric interactions, by the binding of a **Me$_2$V** guest inside the cavity.[110,119] Therefore, DABCO is selected as the axial ligand to facilitate the coordination bonds, and **Me$_2$V** as the promotor to influence the catalytic reaction. The aim of this thesis is the development of these double porphyrin cage compounds for binary data storage on synthetic polymers and to investigate their binding properties. In a stepwise fashion, the synthesis and characterization of the new double porphyrin cages, their binding properties, and their polymer threading behavior will be investigated.

In Chapter 1, the relevant background information to describe the state-of-the-art in biological and chemical data storage, and the binding and catalytic properties of porphyrin cage compounds based on diphenylglycoluril, is described. In Chapter 2, as a first step in the development of double porphyrin cage compounds for information storage, the design, synthesis, and characterization of three double porphyrin cages is presented. These new compounds differ with respect to the length of the spacer between the two cage moieties, i.e. these are alkyl chains with 3, 5, and 11 carbon atoms, respectively.

As the second step, Chapter 3 describes the binding of a ditopic ligand (DABCO) to the zinc derivatives of the new double porphyrin cage compounds (**Zn$_2$C$_x$DC**). The formation of the complexes is investigated with the help of UV-Vis and NMR studies in various solvents.

Chapter 4 reports on the third step in the development of catalytic systems based on double porphyrin cage compounds and discusses the influence of the binding of **Me$_2$V** in the cavities of **Zn$_2$C$_x$DC** compounds on the coordination of DABCO, via allosteric interactions.

The threading of polytetrahydrofuran chains, which on one side contain a blocking group and a nearby viologen binding station, through the cavities of complexes between DABCO and **Zn$_2$C$_x$DC** compounds is investigated in Chapter 5. It represents

the fourth step in the development of catalytic double porphyrin cage compounds for information storage purposes.

The final Chapter 6 provides a detailed discussion of the results reported in the previous chapters and gives a perspective on the future of double porphyrin cage molecules for use as possible information storage systems. Summaries in English and Dutch conclude this thesis.

1.6 References

(1) Zhirnov, V.; Zadegan, R. M.; Sandhu, G. S.; Church, G. M.; Hughes, W. L. Nucleic Acid Memory. *Nat. Mater.* **2016**, *15* (4), 366–370.
(2) Moore, G. E. Cramming More Components onto Integrated Circuits. *Electronics* **1965**, *38* (8), 114–117.
(3) R. W. Keyes. Fundamental Limits of Silicon Technology. *Proc. IEEE* **2001**, *89* (3), 227–239.
(4) Markov, I. L. Limits on Fundamental Limits to Computation. *Nature* **2014**, *512*, 147.
(5) Lehn J. M. Supramolecular Chemistry—Scope and Perspectives Molecules, Supermolecules, and Molecular Devices (Nobel Lecture). *Angew. Chem. Int. Ed. Engl.* **1988**, *27* (1), 89–112.
(6) Colquhoun, H.; Lutz, J.-F. Information-Containing Macromolecules. *Nat. Chem.* **2014**, *6* (6), 455–456.
(7) Kelman, Z.; Hurwitz, J.; O'Donnell, M. Processivity of DNA Polymerases: Two Mechanisms, One Goal. *Structure* **1998**, *6* (2), 121–125.
(8) Kool, E. T.; Morales, J. C.; Guckian, K. M. Mimicking the Structure and Function of DNA: Insights into DNA Stability and Replication. *Angew. Chem. Int. Ed.* **2000**, *39* (6), 990–1009.
(9) Hübscher, U.; Maga, G.; Spadari, S. Eukaryotic DNA Polymerases. *Annu. Rev. Biochem.* **2002**, *71* (1), 133–163.
(10) Bugg, T. D. Enzymes: General Properties. In *eLS*; American Cancer Society, 2001.
(11) Hedstrom, L. Enzyme Specificity and Selectivity. In *eLS*; John Wiley & Sons, Ltd, 2001.
(12) Pellegrini, L.; Costa, A. New Insights into the Mechanism of DNA Duplication by the Eukaryotic Replisome. *Trends Biochem. Sci.* **2016**, *41* (10), 859–871.
(13) Johnson, A.; O'Donnell, M. Cellular DNA Replicases: Components and Dynamics at the Replication Fork. *Annu. Rev. Biochem.* **2005**, *74* (1), 283–315.
(14) Steitz, T. A. DNA Polymerases: Structural Diversity and Common Mechanisms. *J. Biol. Chem.* **1999**, *274* (25), 17395–17398.
(15) Indiani, C.; O'Donnell, M. The Replication Clamp-Loading Machine at Work in the Three Domains of Life. *Nat. Rev. Mol. Cell Biol.* **2006**, *7*, 751.
(16) Nelson, D. L.; Lehninger, A. L.; Cox, M. M. *Lehninger Principles of Biochemistry, Fourth Edition*; W.H.Freeman & Co Ltd: New York.
(17) Benkovic, S. J.; Valentine, A. M.; Salinas, F. Replisome-Mediated DNA Replication. *Annu. Rev. Biochem.* **2001**, *70*, 181–208.
(18) Frick, D. N.; Richardson, C. C. DNA Primases. *Annu. Rev. Biochem.* **2001**, *70* (1), 39–80.
(19) Sclafani, R. A.; Holzen, T. M. Cell Cycle Regulation of DNA Replication. *Annu. Rev. Genet.* **2007**, *41* (1), 237–280.
(20) McCulloch, S. D.; Kunkel, T. A. The Fidelity of DNA Synthesis by Eukaryotic Replicative and Translesion Synthesis Polymerases. *Cell Res.* **2008**, *18*, 148.
(21) Tuteja, N.; Tuteja, R. Unraveling DNA Helicases. *Eur. J. Biochem.* **2004**, *271* (10), 1849–1863.
(22) Tuteja, N.; Tuteja, R. Prokaryotic and Eukaryotic DNA Helicases. *Eur. J. Biochem.* **2004**, *271* (10), 1835–1848.
(23) van Dongen, S. F. M.; Clerx, J.; Nørgaard, K.; Bloemberg, T. G.; Cornelissen, J. J. L. M.; Trakselis, M. A.; Nelson, S. W.; Benkovic, S. J.; Rowan, A. E.; Nolte, R. J. M. A Clamp-like Biohybrid Catalyst for DNA Oxidation. *Nat. Chem.* **2013**, *5* (11), 945–951.
(24) Dongen, S. F. M. van; Elemans, J. A. A. W.; Rowan, A. E.; Nolte, R. J. M. Processive Catalysis. *Angew. Chem. Int. Ed. 53* (43), 11420–11428.
(25) Steitz, T. A. Visualizing Polynucleotide Polymerase Machines at Work. *EMBO J.* **2006**, *25* (15), 3458.
(26) Stillman, B. Smart Machines at the DNA Replication Fork. *Cell 78* (5), 725–728.
(27) Kovall, R.; Matthews, B. W. Toroidal Structure of λ-Exonuclease. *Science* **1997**, *277* (5333), 1824–1827.
(28) Anson, B.; Handayani, R.; Williams, C. R.; Bertram, J. G.; Hingorani, M. M.; O'Donnell, M.; Goodman, M. F.; Bloom, L. B. Mechanism of Loading the Escherichia Coli DNA Polymerase III Beta Sliding Clamp on DNA. *J. Biol. Chem.* **2003**, *287* (12), 10033–10040.
(29) O'Donnell, M.; Kuriyan, J. Clamp Loaders and Replication Initiation. *Protein-Nucleic Acid Interactions-Folding Bind.* **2006**, *16* (1), 35–41.
(30) Ogawa, T.; Okazaki, T. Discontinuous DNA Replication. *Annu. Rev. Biochem.* **1980**, *49* (1), 421–457.
(31) Kunkel, T. A. DNA Replication Fidelity. *J. Biol. Chem.* **2004**, *279* (17), 16895–16898.

(32) Hamdan, S. M.; Loparo, J. J.; Takahashi, M.; Richardson, C. C.; van Oijen, A. M. Dynamics of DNA Replication Loops Reveal Temporal Control of Lagging-Strand Synthesis. *Nature* **2008**, *457*, 336.
(33) Langston, L. D.; O'Donnell, M. DNA Replication: Keep Moving and Don't Mind the Gap. *Mol. Cell 23* (2), 155–160.
(34) Alberts, B.; Johnson, A.; Lewis, J.; Raff, M.; Roberts, K.; Walter, P. *Molecular Biology of the Cell*; New York, 2002.
(35) Albertson, T. M.; Preston, B. D. DNA Replication Fidelity: Proofreading in Trans. *Curr. Biol. 16* (6), R209–R211.
(36) Watson, J. D.; Crick, F. H. C. Molecular Structure of Nucleic Acids: A Structure for Deoxyribose Nucleic Acid. *Nature* **1953**, *171*, 737.
(37) Friedberg, E. C.; Wagner, R.; Radman, M. Specialized DNA Polymerases, Cellular Survival, and the Genesis of Mutations. *Science* **2002**, *296* (5573), 1627.
(38) Turing A. M. On Computable Numbers, with an Application to the Entscheidungsproblem. *Proc. Lond. Math. Soc.* **1936**, *s2-42* (1), 230–265.
(39) Turing, A. M. Intelligent Machinery, a Heretical Theory. *Philos. Math.* **1948**, *4* (3).
(40) Varghese, S.; Elemans, J. A. A. W.; Rowan, A. E.; Nolte, R. J. M. Molecular Computing: Paths to Chemical Turing Machines. *Chem. Sci.* **2015**, *6* (11), 6050–6058.
(41) M. D. Godfrey; D. F. Hendry. The Computer as von Neumann Planned It. *IEEE Ann. Hist. Comput.* **1993**, *15* (1), 11–21.
(42) Thomas, S. W.; Chiechi, R. C.; LaFratta, C. N.; Webb, M. R.; Lee, A.; Wiley, B. J.; Zakin, M. R.; Walt, D. R.; Whitesides, G. M. Infochemistry and Infofuses for the Chemical Storage and Transmission of Coded Information. *Proc. Natl. Acad. Sci.* **2009**, *106* (23), 9147.
(43) Hashimoto, M.; Feng, J.; York, R. L.; Ellerbee, A. K.; Morrison, G.; Thomas III, S. W.; Mahadevan, L.; Whitesides, G. M. Infochemistry: Encoding Information as Optical Pulses Using Droplets in a Microfluidic Device. *J. Am. Chem. Soc.* **2009**, *131* (34), 12420–12429.
(44) Palacios, M. A.; Benito-Peña, E.; Manesse, M.; Mazzeo, A. D.; LaFratta, C. N.; Whitesides, G. M.; Walt, D. R. InfoBiology by Printed Arrays of Microorganism Colonies for Timed and on-Demand Release of Messages. *Proc. Natl. Acad. Sci.* **2011**, *108* (40), 16510.
(45) Ratner, T; Reany, O; Keinan, E. Encoding and Processing of Alphanumeric Information by Chemical Mixtures. *ChemPhysChem* **2009**, *10* (18), 3303–3309.
(46) Goldman, N.; Bertone, P.; Chen, S.; Dessimoz, C.; LeProust, E. M.; Sipos, B.; Birney, E. Towards Practical, High-Capacity, Low-Maintenance Information Storage in Synthesized DNA. *Nature* **2013**, *494* (7435), 77–80.
(47) Church, G. M.; Gao, Y.; Kosuri, S. Next-Generation Digital Information Storage in DNA. *Science* **2012**, *337* (6102), 1628.
(48) Lutz, J.-F.; Ouchi, M.; Liu, D. R.; Sawamoto, M. Sequence-Controlled Polymers. *Science* **2013**, *341* (6146).
(49) Lutz, J.-F. Coding Macromolecules: Inputting Information in Polymers Using Monomer-Based Alphabets. *Macromolecules* **2015**, *48* (14), 4759–4767.
(50) Dawkins, R. *The Blind Watchmaker*; W. W. Norton & Company, Inc.: New York, 1986.
(51) Badi, N.; Lutz, J.-F. Sequence Control in Polymer Synthesis. *Chem. Soc. Rev.* **2009**, *38* (12), 3383–3390.
(52) Merrifield, R. B. Solid Phase Peptide Synthesis. I. The Synthesis of a Tetrapeptide. *J. Am. Chem. Soc.* **1963**, *85* (14), 2149–2154.
(53) Pfeifer, S.; Zarafshani, Z.; Badi, N.; Lutz, J.-F. Liquid-Phase Synthesis of Block Copolymers Containing Sequence-Ordered Segments. *J. Am. Chem. Soc.* **2009**, *131* (26), 9195–9197.
(54) Hartmann L.; Börner H. G. Precision Polymers: Monodisperse, Monomer-Sequence-Defined Segments to Target Future Demands of Polymers in Medicine. *Adv. Mater.* **2009**, *21* (32-33), 3425–3431.
(55) Hartmann Laura. Polymers for Control Freaks: Sequence-Defined Poly(amidoamine)s and Their Biomedical Applications. *Macromol. Chem. Phys.* **2010**, *212* (1), 8–13.
(56) Lutz Jean-François; Schmidt Bernhard V. K .J.; Pfeifer Sebastian. Tailored Polymer Microstructures Prepared by Atom Transfer Radical Copolymerization of Styrene and N-substituted Maleimides. *Macromol. Rapid Commun.* **2011**, *32* (2), 127–135.

(57) Pfeifer, S.; Lutz, J.-F. A Facile Procedure for Controlling Monomer Sequence Distribution in Radical Chain Polymerizations. *J. Am. Chem. Soc.* **2007**, *129* (31), 9542–9543.
(58) Pfeifer Sebastian; Lutz Jean-François. Development of a Library of N-Substituted Maleimides for the Local Functionalization of Linear Polymer Chains. *Chem. – Eur. J.* **2008**, *14* (35), 10949–10957.
(59) Berthet, M.-A.; Zarafshani, Z.; Pfeifer, S.; Lutz, J.-F. Facile Synthesis of Functional Periodic Copolymers: A Step toward Polymer-Based Molecular Arrays. *Macromolecules* **2010**, *43* (1), 44–50.
(60) Chan-Seng Delphine; Zamfir Mirela; Lutz Jean-François. Polymer-Chain Encoding: Synthesis of Highly Complex Monomer Sequence Patterns by Using Automated Protocols. *Angew. Chem. Int. Ed.* **2012**, *51* (49), 12254–12257.
(61) Schmidt, B. V. K. J.; Fechler, N.; Falkenhagen, J.; Lutz, J.-F. Controlled Folding of Synthetic Polymer Chains through the Formation of Positionable Covalent Bridges. *Nat. Chem.* **2011**, *3*, 234.
(62) Al Ouahabi, A.; Charles, L.; Lutz, J.-F. Synthesis of Non-Natural Sequence-Encoded Polymers Using Phosphoramidite Chemistry. *J. Am. Chem. Soc.* **2015**, *137* (16), 5629–5635.
(63) Trinh Thanh Tam; Oswald Laurence; Chan-Seng Delphine; Lutz Jean-François. Synthesis of Molecularly Encoded Oligomers Using a Chemoselective "AB + CD" Iterative Approach. *Macromol. Rapid Commun.* **2014**, *35* (2), 141–145.
(64) Trinh, T. T.; Oswald, L.; Chan-Seng, D.; Charles, L.; Lutz, J.-F. Preparation of Information-Containing Macromolecules by Ligation of Dyad-Encoded Oligomers. *Chem. – Eur. J.* **2015**, *21* (34), 11961–11965.
(65) Roy, R. K.; Meszynska, A.; Laure, C.; Charles, L.; Verchin, C.; Lutz, J.-F. Design and Synthesis of Digitally Encoded Polymers That Can Be Decoded and Erased. *Nat. Commun.* **2015**, *6*, 7237.
(66) Erbas-Cakmak, S.; Leigh, D. A.; McTernan, C. T.; Nussbaumer, A. L. Artificial Molecular Machines. *Chem. Rev.* **2015**, *115* (18), 10081–10206.
(67) Lewandowski, B.; De Bo, G.; Ward, J. W.; Papmeyer, M.; Kuschel, S.; Aldegunde, M. J.; Gramlich, P. M. E.; Heckmann, D.; Goldup, S. M.; D'Souza, D. M.; et al. Sequence-Specific Peptide Synthesis by an Artificial Small-Molecule Machine. *Science* **2013**, *339* (6116), 189.
(68) De Bo, G.; Kuschel, S.; Leigh, D. A.; Lewandowski, B.; Papmeyer, M.; Ward, J. W. Efficient Assembly of Threaded Molecular Machines for Sequence-Specific Synthesis. *J. Am. Chem. Soc.* **2014**, *136* (15), 5811–5814.
(69) Wilson Claire Margaret; Gualandi Andrea; Cozzi Pier Giorgio. A Rotaxane Turing Machine for Peptides. *ChemBioChem* **2013**, *14* (10), 1185–1187.
(70) De Bo, G.; Gall, M. A. Y.; Kitching, M. O.; Kuschel, S.; Leigh, D. A.; Tetlow, D. J.; Ward, J. W. Sequence-Specific β-Peptide Synthesis by a Rotaxane-Based Molecular Machine. *J. Am. Chem. Soc.* **2017**, *139* (31), 10875–10879.
(71) Hunter Christopher A.; Anderson Harry L. What Is Cooperativity? *Angew. Chem. Int. Ed.* **2009**, *48* (41), 7488–7499.
(72) Kremer, C.; Lützen, A. Artificial Allosteric Receptors. *Chem. – Eur. J.* **2013**, *19* (20), 6162–6196.
(73) Perutz, M. F.; Fermi, G.; Luisi, B.; Shaanan, B.; Liddington, R. C. Stereochemistry of Cooperative Mechanisms in Hemoglobin. *Acc. Chem. Res.* **1987**, *20* (9), 309–321.
(74) Ackers, G.; Doyle, M.; Myers, D.; Daugherty, M. Molecular Code for Cooperativity in Hemoglobin. *Science* **1992**, *255* (5040), 54.
(75) Raynal, M.; Ballester, P.; Vidal-Ferran, A.; van Leeuwen, P. W. N. M. Supramolecular Catalysis. Part 2: Artificial Enzyme Mimics. *Chem. Soc. Rev.* **2014**, *43* (5), 1734–1787.
(76) Rebek, J.; Trend, J. E.; Wattley, R. V.; Chakravorti, S. Allosteric Effects in Organic Chemistry. Site-Specific Binding. *J. Am. Chem. Soc.* **1979**, *101* (15), 4333–4337.
(77) Rebek, J.; Wattley, R. V. Allosteric Effects. Remote Control of Ion Transport Selectivity. *J. Am. Chem. Soc.* **1980**, *102* (14), 4853–4854.
(78) Rebek, J.; Marshall, L. Allosteric Effects: An on-off Switch. *J. Am. Chem. Soc.* **1983**, *105* (22), 6668–6670.
(79) Ikeda Masato; Kubo Yohei; Yamashita Kousei; Ikeda Tomohiro; Takeuchi Masayuki; Shinkai Seiji. Dynamic Rotational Oscillation of Cerium(IV) Bis(porphyrinate) and Its Control by Diamine Guest Binding with Positive Homotropic Allosterism. *Eur. J. Org. Chem.* **2007**, *2007* (12), 1883–1886.
(80) Ikeda Masato; Takeuchi Masayuki; Shinkai Seiji; Tani Fumito; Naruta Yoshinori; Sakamoto Shigeru; Yamaguchi Kentaro. Allosteric Binding of an Ag+ Ion to Cerium(IV) Bis-porphyrinates Enhances the Rotational Activity of Porphyrin Ligands. *Chem. – Eur. J.* **2002**, *8* (24), 5541–5550.

(81) Sugasaki, A.; Ikeda, M.; Takeuchi, M.; Robertson, A.; Shinkai, S. Efficient Chirality Transcription Utilizing a cerium(IV) Double Decker Porphyrin: A Prototype for Development of a Molecular Memory System. *J. Chem. Soc. [Perkin 1]* **1999**, No. 22, 3259–3264.
(82) Takeuchi, M.; Imada, T.; Shinkai, S. Highly Selective and Sensitive "Sugar Tweezer" Designed from a Boronic-Acid-Appended μ-Oxobis[porphinatoiron(III)]. *J. Am. Chem. Soc.* **1996**, *118* (43), 10658–10659.
(83) Ayabe, M.; Ikeda, A.; Shinkai, S.; Sakamoto, S.; Yamaguchi, K. A Novel [60]fullerene Receptor with a Pd(ii)-Switched Bisporphyrin Cleft. *Chem. Commun.* **2002**, No. 10, 1032–1033.
(84) Monti, D.; La Monica, L.; Scipioni, A.; Mancini, G. Effect of the Inclusion of Sodium Cations on the Binding Properties of a Switchable Diporphyrin Receptor. *New J. Chem.* **2001**, *25* (6), 780–782.
(85) Tomohiro, Y.; Satake, A.; Kobuke, Y. Synthesis of Bipyridylene-Bridged Bisporphyrin by Nickel-Mediated Coupling Reaction: ON–OFF Control of Cofacial Porphyrin Unit by Reversible Complexation. *J. Org. Chem.* **2001**, *66* (25), 8442–8446.
(86) Blom, M.; Norrehed, S.; Andersson, C.-H.; Huang, H.; Light, E. M.; Bergquist, J.; Grennberg, H.; Gogoll, A. Synthesis and Properties of Bis-Porphyrin Molecular Tweezers: Effects of Spacer Flexibility on Binding and Supramolecular Chirogenesis. *Molecules* **2016**, *21* (1).
(87) Lee Chi-Hwa; Yoon Hongsik; Jang Woo-Dong. Biindole-Bridged Porphyrin Dimer as Allosteric Molecular Tweezers. *Chem. – Eur. J.* **2009**, *15* (39), 9972–9976.
(88) Murphy, R. B.; Pham, D.-T.; Lincoln, S. F.; Johnston, M. R. Molecular Tweezers with Freely Rotating Linker and Porphyrin Moieties. *Eur. J. Org. Chem.* **2013**, *15*, 2985–2993.
(89) Valderrey, V.; Aragay, G.; Ballester, P. Porphyrin Tweezer Receptors: Binding Studies, Conformational Properties and Applications. *Coord. Chem. Rev.* **2014**, *258*, 137–156.
(90) Sato, H.; Tashiro, K.; Shinmori, H.; Osuka, A.; Murata, Y.; Komatsu, K.; Aida, T. Positive Heterotropic Cooperativity for Selective Guest Binding via Electronic Communications through a Fused Zinc Porphyrin Array. *J. Am. Chem. Soc.* **2005**, *127* (38), 13086–13087.
(91) Sato, H.; Tashiro, K.; Shinmori, H.; Osuka, A.; Aida, T. Cyclic Dimer of a Fused Porphyrin Zinc Complex as a Novel Host with Two [Small Pi]-Electronically Coupled Binding Sites. *Chem. Commun.* **2005**, No. 18, 2324–2326.
(92) von Krbek, L. K. S.; Schalley, C. A.; Thordarson, P. Assessing Cooperativity in Supramolecular Systems. *Chem. Soc. Rev.* **2017**, *46* (9), 2622–2637.
(93) Anderson, H. L. Conjugated Porphyrin Ladders. *Inorg. Chem.* **1994**, *33* (5), 972–981.
(94) Camara-Campos, A.; Hunter, C. A.; Tomas, S. Cooperativity in the Self-Assembly of Porphyrin Ladders. *Proc. Natl. Acad. Sci. U. S. A.* **2006**, *103* (9), 3034.
(95) Taylor, P. N.; Anderson, H. L. Cooperative Self-Assembly of Double-Strand Conjugated Porphyrin Ladders. *J. Am. Chem. Soc.* **1999**, *121* (49), 11538–11545.
(96) Sprafke Johannes K.; Odell Barbara; Claridge Timothy D. W.; Anderson Harry L. All-or-Nothing Cooperative Self-Assembly of an Annulene Sandwich. *Angew. Chem. Int. Ed.* **2011**, *50* (24), 5572–5575.
(97) Anderson Harry L.; Sanders Jeremy K. M. Amine-Template-Directed Synthesis of Cyclic Porphyrin Oligomers. *Angew. Chem. Int. Ed. Engl.* **2003**, *29* (12), 1400–1403.
(98) Anderson, S.; Anderson, H. L.; Sanders, J. K. M. The Roles of Templates in the Syntheses of Porphyrin Oligomers. *J. Chem. Soc. [Perkin 1]* **1995**, No. 18, 2255–2267.
(99) Anderson Sally; Anderson Harry L.; Sanders Jeremy K. M. Scavenger Templates: Synthesis and Electrospray Mass Spectrometry of a Linear Porphyrin Octamer. *Angew. Chem. Int. Ed. Engl.* **2003**, *31* (7), 907–910.
(100) Kondratuk Dmitry V.; Perdigao Luis M. A.; O'Sullivan Melanie C.; Svatek Simon; Smith Gareth; O'Shea James N.; Beton Peter H.; Anderson Harry L. Two Vernier-Templated Routes to a 24-Porphyrin Nanoring. *Angew. Chem. Int. Ed.* **2012**, *51* (27), 6696–6699.
(101) O'Sullivan, M. C.; Sprafke, J. K.; Kondratuk, D. V.; Rinfray, C.; Claridge, T. D. W.; Saywell, A.; Blunt, M. O.; O'Shea, J. N.; Beton, P. H.; Malfois, M.; et al. Vernier Templating and Synthesis of a 12-Porphyrin Nano-Ring. *Nature* **2011**, *469*, 72.
(102) Kondratuk, D. V.; Perdigão, L. M. A.; Esmail, A. M. S.; O'Shea, J. N.; Beton, P. H.; Anderson, H. L. Supramolecular Nesting of Cyclic Polymers. *Nat. Chem.* **2015**, *7*, 317.

(103) Elemans, J. A. A. W.; Claase, M. B.; Aarts, P. P. M.; Rowan, A. E.; Schenning, A. P. H. J.; Nolte, R. J. M. Porphyrin Clips Derived from Diphenylglycoluril. Synthesis, Conformational Analysis, and Binding Properties. *J. Org. Chem.* **1999**, *64* (19), 7009–7016.
(104) Elemans, J. A. A. W.; Bijsterveld, E. J. A.; Rowan, A. E.; Nolte, R. J. M. Manganese Porphyrin Hosts as Epoxidation Catalysts – Activity and Stability Control by Axial Ligand Effects. *Eur. J. Org. Chem.* **2007**, *5*, 751–757.
(105) Deutman, A. B. C.; Smits, J. M. M.; de Gelder, R.; Elemans, J. A. A. W.; Nolte, R. J. M.; Rowan, A. E. Strong Induced-Fit Binding of Viologen and Pyridine Derivatives in Adjustable Porphyrin Cavities. *Chem. – Eur. J.* **2014**, *20* (36), 11574–11583.
(106) Hidalgo Ramos, P.; Saisaha, P.; Elemans, J. A. A. W.; Rowan, A. E.; Nolte, R. J. M. Conformational Analysis and Binding Properties of a Cavity Containing Porphyrin Catalyst Provided with Urea Functions. *Eur. J. Org. Chem.* **2016**, *26*, 4487–4495.
(107) Thordarson, P.; Coumans, R. G. E.; Elemans, J. A. A. W.; Thomassen, P. J.; Visser, J.; Rowan, A. E.; Nolte, R. J. M. Allosterically Driven Multicomponent Assembly. *Angew. Chem. Int. Ed.* **2004**, *43* (36), 4755–4759.
(108) Cantekin, S.; Markvoort, A. J.; Elemans, J. A. A. W.; Rowan, A. E.; Nolte, R. J. M. Allosterically Controlled Threading of Polymers through Macrocyclic Dimers. *J. Am. Chem. Soc.* **2015**, *137* (11), 3915–3923.
(109) Rowan, A. E.; Aarts, P. P. M.; Koutstaal, K. W. M. Novel Porphyrin–viologen Rotaxanes. *Chem. Commun.* **1998**, *5*, 611–612.
(110) Deutman, A. B. C.; Monnereau, C.; Moalin, M.; Coumans, R. G. E.; Veling, N.; Coenen, M.; Smits, J. M. M.; de Gelder, R.; Elemans, J. A. A. W.; Ercolani, G.; et al. Squaring Cooperative Binding Circles. *Proc. Natl. Acad. Sci. U. S. A.* **2009**, *106* (26), 10471–10476.
(111) Coumans, R. G. E.; Elemans, J. A. A. W.; Nolte, R. J. M.; Rowan, A. E. Processive Enzyme Mimic: Kinetics and Thermodynamics of the Threading and Sliding Process. *Proc. Natl. Acad. Sci. U. S. A.* **2006**, *103* (52), 19647–19651.
(112) Hidalgo Ramos, P.; Coumans, R. G. E.; Deutman, A. B. C.; Smits, J. M. M.; de Gelder, R.; Elemans, J. A. A. W.; Nolte, R. J. M.; Rowan, A. E. Processive Rotaxane Systems. Studies on the Mechanism and Control of the Threading Process. *J. Am. Chem. Soc.* **2007**, *129* (17), 5699–5702.
(113) Deutman, A. B. C.; Monnereau, C.; Elemans, J. A. A. W.; Ercolani, G.; Nolte, R. J. M.; Rowan, A. E. Mechanism of Threading a Polymer Through a Macrocyclic Ring. *Science* **2008**, *322* (5908), 1668–1671.
(114) Deutman, A. B. C.; Varghese, S.; Moalin, M.; Elemans, J. A. A. W.; Rowan, A. E.; Nolte, R. J. M. Slippage of a Porphyrin Macrocycle over Threads of Varying Bulkiness: Implications for the Mechanism of Threading Polymers through a Macrocyclic Ring. *Chem. – Eur. J.* **2015**, *21* (1), 360–370.
(115) Deutman, A. B. C.; Cantekin, S.; Elemans, J. A. A. W.; Rowan, A. E.; Nolte, R. J. M. Designing Processive Catalytic Systems. Threading Polymers through a Flexible Macrocycle Ring. *J. Am. Chem. Soc.* **2014**, *136* (25), 9165–9172.
(116) Elemans, J. A. A. W.; Bijsterveld, E. J. A.; Rowan, A. E.; Nolte, R. J. M. A Host–guest Epoxidation Catalyst with Enhanced Activity and Stability. *Chem. Commun.* **2000**, *24*, 2443–2444.
(117) Thordarson, P.; Bijsterveld, E. J. A.; Rowan, A. E.; Nolte, R. J. M. Epoxidation of Polybutadiene by a Topologically Linked Catalyst. *Nature* **2003**, *424* (6951), 915–918.
(118) Monnereau, C.; Ramos, P. H.; Deutman, A. B. C.; Elemans, J. A. A. W.; Nolte, R. J. M.; Rowan, A. E. Porphyrin Macrocyclic Catalysts for the Processive Oxidation of Polymer Substrates. *J. Am. Chem. Soc.* **2010**, *132* (5), 1529–1531.
(119) Thordarson, P.; Bijsterveld, E. J. A.; Elemans, J. A. A. W.; Kasák, P.; Nolte, R. J. M.; Rowan, A. E. Highly Negative Homotropic Allosteric Binding of Viologens in a Double-Cavity Porphyrin. *J. Am. Chem. Soc.* **2003**, *125* (5), 1186–1187.

2

Synthesis of double porphyrin cage compounds

Part of this chapter will be published:

Synthesis of double porphyrin cage compounds and the formation of sandwich complexes with a ditopic ligand - *Manuscript in preparation*

K. Stout, T. Peters, M. F. J. Mabesoone, F. Visschers, E. M. Meijer, J. van den Berg, J-R. Klop, S. Cantekin, P. B. White, P. T. Tinnemans, J. A. A. W Elemans, A. E. Rowan, and R. J. M Nolte

Abstract

In this chapter double porphyrin cage compounds, which were designed as part of a program aimed at writing information on a synthetic polymer chain in the form of a binary code, are described. Naturally occurring processive enzyme systems, i.e. DNA polymerases, served as a source of inspiration for this work. The present double cage compounds consist of two porphyrins that are each attached to a diphenylglycoluril clip via four spacers. The two compounds are linked together by a single alkyl chain of different length using 'click'-chemistry. In a newly developed multistep synthesis procedure three of these double porphyrin cages were synthesized, each characterized by a spacer of different length, i.e. 3, 5, and 11 carbon atoms, between the two porphyrin compounds. The structures of the double porphyrin cages were fully characterized by NMR, which revealed that they consist of mixtures of two diastereo-isomers.

2.1. Introduction

In the past decades, nature has served as a source of inspiration for scientists working on the design of new molecular systems capable of mimicking the action of enzymes, e.g. with respect to rate and substrate selectivity. A class of the enzymes that stands at the basis of life are the DNA-polymerases, which together with exonucleases, replicate and break down the DNA present in organisms.[1,2] During DNA replication, the information stored in the pattern of nucleotides on the encoding (mother) strand is transferred to the new daughter strand. One of the factors contributing to the high replication fidelity of DNA-polymerases is the fact that they make use of sequentially processive catalysis, meaning that the enzyme stays bound to the substrate while performing multiple rounds of consecutive reactions. The movement of the DNA polymerase during these consecutive reactions is discrete and unidirectional, as it repeatedly moves one nucleotide further to carry out the next reaction. In this way, information is stored and copied by making use of the four nucleobases present in the DNA. Recently, Goldman *et al.* and Church *et al.* have reported that it is possible to store information in the form of non-biological data, e.g. the 154 sonnets of Shakespeare, on DNA, and they were able to successfully retrieve this information with high fidelity.[3,4] In order to be able to store information on DNA the binary code consisting of zeros and ones, which is nowadays used in computing, had to be converted into a code using the four nucleotides and this code was subsequently synthesized using conventional DNA synthesis techniques. The storage of data on natural or synthetic polymers is appealing, because they allow high-density information storage, which is vital given the fact that the global digital archive is enormous and is expected to contain some 3×10^{24} bits by 2040.[5] Around 10^9 kg of silicon wafers would be needed to store such a large amount of data in a conventional way. This very much contrasts with the projected total silicon wafer supply, which is estimated to be 10^7–10^8 kg. Hence, the global digital archive will exceed the available silicon supply. Other ways of storing information are, therefore, clearly needed. Storage of information on biopolymers, such as DNA may be an option. A disadvantage of natural polymers, such as DNA, is that they are less robust to environmental changes than synthetic polymers and that they operate only in aqueous media and in a narrow temperature range.[6] For this reason, the storage of information on synthetic polymers is more desirable, since they are often easier to handle, more robust, and more easily enable the use of a binary code by assigning two different chemical functions to the 0 and 1 bits.[7,8] Until now only a few examples of information storage on synthetic polymers have been reported.[9–14] By using DNA as a template molecule, Liu *et al.* were able to form sequence-selective synthetic polymers in vitro.[10] Lutz and coworkers have described the storage of information onto a synthetic polymer chain by using the protocol of controlled/living chain-growth polymerization, in which the primary structure of the polymer was tuned by using time-controlled additions of

two different monomers.[9] A synthesis route that consists of repeating a multistep synthesis protocol, which resulted in an information carrying polymer, was also described by Lutz. This route employed two phosphoramidite monomers containing either a propyl or a 2,2-dimethylpropyl group as the 0 and 1 bit, respectively. Although in this approach a three-step cycle per monomer coupling was used, long encoded sequences could be synthesized.[11–14]

As mentioned above nature makes use of catalytic machines, i.e. the DNA polymerases, to write and store information. The overall goal of the present study is to synthesize an enzyme mimic that would be capable of writing a binary code onto an already available synthetic polymer, instead of writing this code in a step-by-step fashion from two monomers representing the 0 and 1 bits. The design of such an enzyme mimic is based on the key features exhibited by the DNA-polymerases, i.e. a catalytic part (polymerase enzyme) and a ring that keeps this catalyst attached to the polymer chain. In our case this natural design was translated into a ring-shaped cage compound that is located in close proximity to a catalytically active metal complex. The former cage may thread onto a polymer chain and the encoding reactions may take place at the catalyst center. Ideally, the writing of the code is controlled in such a way that an external condition, e.g. a promotor molecule, can help write a 1 (promotor present, catalysis) or a 0 (promotor absent, no catalysis). A cage molecule that fulfills these characteristics is the so-called 'porphyrin clip' (**H_2SC**, Figure 1a).[15] It consists of a concave framework based on diphenylglycoluril to which a porphyrin 'roof' is attached. When a catalytically active metal is coordinated inside the porphyrin plane, the porphyrin cage compound can function as an active site and the cage as a ring that can thread onto a polymer chain. In a previous study it has been shown that the manganese porphyrin cage compound (**MnSC**) can thread onto a polybutadiene substrate and convert all its double bonds into epoxide functions in a randomly processive fashion (Figure 1c).[16–18]

If a formed epoxide is defined as a 1 and an unreacted double bond as a 0, then binary information can in principle be written and stored with the help of this system. However, since the catalytic epoxidation reaction occurs via a randomly processive mechanism, eventually leading to full epoxidation of the polymer, the porphyrin cage compound should also harbor structural characteristics, enabling it to control the location at which the catalytic epoxidation reaction takes place thus enabling the storage of information on a synthetic polymer. In the previous studies the speed of movement of **MnSC** along the polymer chain was faster than the catalytic epoxidation reaction, making that no control over the writing process was possible. More recently it was reported that by enlarging the cavity of the porphyrin cage compound, i.e. in such a way that the cage wraps itself around the polymer, the movement along the polymer chain could be slowed down to the extent that it matches the rate of the catalytic conversion, making it a promising candidate for sequential processive catalysis.[19] In order to be able to control the writing process and hence achieve data

storage, it was decided to extend the porphyrin cage compound **MnSC** with a second, so-called 'instructing' cage in which a promotor molecule can be bound, leading to the 'double porphyrin cage' (**H_4C_xDC**, Figure 2). The idea was that this second porphyrin cage, which is attached to the first one via a covalent linker and a coordination bond, can influence the catalytic reaction that takes place in the latter one via allosteric interactions. This might be possible, at least in principle, if a guest molecule (promotor, e.g. N,N'-dimethylviologen dihexafluorophosphate, **Me_2V**) binds in the instructing cavity shown in Figure 2 and switches the catalytic process from the "off"- to the "on" state or *vice versa*.

In this chapter we will describe our synthetic efforts to covalently link two porphyrin cage compounds in a geometry that ensures close proximity of the metal centers in the two porphyrin planes (Figure 2). It has previously been shown that the binding of axial ligands such as 1,4-diazabicyclo[2.2.2]octane (DABCO) to the metal center in the porphyrin cage is influenced, via allosteric interactions, by the binding of a N,N'-dimethylviologen dihexafluorophosphate (**Me_2V**) guest inside the cavity.[20,21] It is hoped that when the additional porphyrin cage contains a zinc center, an 'instructing cavity' can be created that influences the catalytic activity of the manganese center in the other porphyrin cage, i.e. by means of an allosteric effect via the DABCO ligand (Figure 2a). When DABCO is bound between the two porphyrin cages, the binding of **Me_2V** in the instructing cavity might turn on the catalytic reaction by an allosteric effect and hence start the writing of epoxide functions on a polymer.

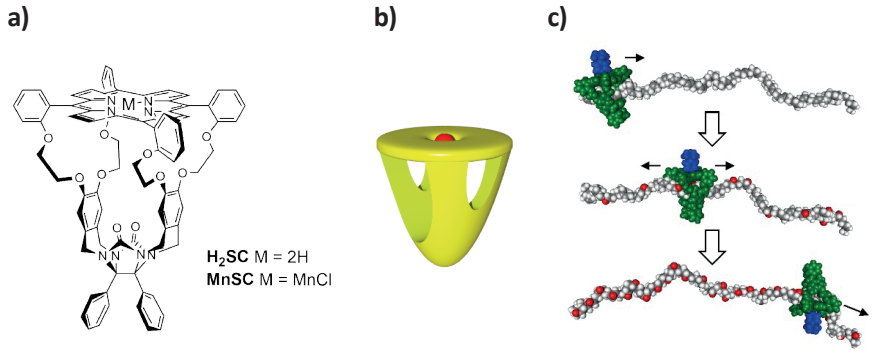

Figure 1 *a) Chemical structure of porphyrin cage compound (**H_2SC**) and its catalytically active manganese derivative (**MnSC**). b) Schematic representation of the porphyrin cage (yellow) with a metal center (M, red) bound inside the porphyrin. c) Molecular modeling representations of the manganese porphyrin cage compound with tert-butyl pyridine as axial ligand, which converts the double bounds in a polybutadiene chain into epoxide functions (red balls) in a randomly processive fashion.[16]*

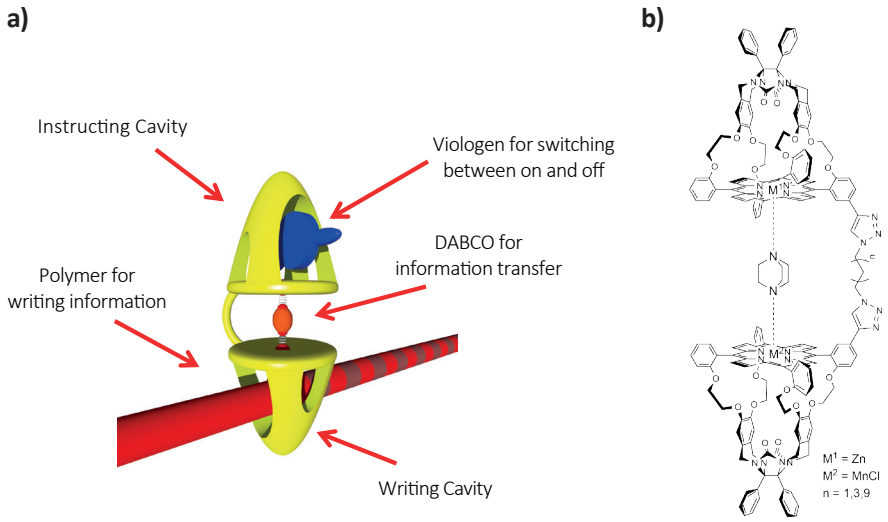

Figure 2 *a) Schematic representation of a double porphyrin cage compound consisting of two molecular cages capped with a porphyrin roof that are covalently linked (yellow). The instructing cavity contains a zinc center and the writing cavity a manganese center. The binding of a ditopic ligand such as DABCO (orange) in between the two porphyrins might allow the transfer of information from the instructing cavity to the writing cavity, thus enabling the possibility of performing a catalytic reaction. The binding of a viologen guest (promotor molecule, blue) inside the instructing cavity may influence the binding of DABCO to the manganese center that performs the catalytic reaction on a polymer (red), via a series of allosteric interactions. b) Chemical structure of the zinc-manganese double porphyrin cage with spacer lengths of 3, 5 and 11 carbon atoms, binding DABCO as a ditopic axial ligand.*

2.2. Results and discussion

2.2.1 Synthetic pathways to a mono-functionalized porphyrin cage compound

As outlined in the Introduction section, for the construction of a porphyrin-based polymerase mimic that can perform binary data storage on a polymer chain, a covalently linked dimer of two porphyrin cages is required. For the synthesis of such a dimer, the previously reported porphyrin cage **H_2SC** needs to be equipped with a functional handle. Coupling of two porphyrin cages via such a handle will generate the desired double porphyrin cage compound. It was reasoned that this functional handle would be best located at the *meta*-position of the *meso*-phenyl ring of the porphyrin ring, because this would ensure that the two porphyrin rings within the double porphyrin cage will be in close proximity. Such a handle is synthetically accessible because the hydroxy substituents on the porphyrin ring are ortho/para

directing groups for the electrophilic aromatic substitution reaction that is required to introduce the handle. The desired mono-functionalized porphyrin cage may be synthesized by connecting a mono-functionalized tetrahydroxy porphyrin to a tetra-tosyl-functionalized cage based on diphenylglycoluril (**7**, for numbering see Figure 8), or by substituting the tosyl-groups of the afore-mentioned cage with one functionalized and three unfunctionalized hydroxybenzaldehydes prior to the cyclization reaction generating the porphyrin (Figure 3, Route 2).[15,22] Both routes are characterized by the fact that they have statistical steps, i.e. the required mono-substituted compounds are formed together with other compounds and these compounds have to be separated.

2.2.1.1. Attempted synthesis of a mono-functionalized porphyrin cage compound via a mono-functionalized porphyrin formed by a statistical route

Several routes for the synthesis of a mono-functionalized tetrahydroxyphenyl porphyrin that can be connected to the diphenylglycoluril cage were investigated. The first attempts to synthesize a mono-functionalized porphyrin started with the synthesis of 5-(5-bromo-2-methoxyphenyl)-10,15,20-tris-(2-methoxyphenyl)porphyrin via the direct condensation of pyrrole with *o*-methoxy-benzaldehyde and 5-bromo-2-methoxybenzaldehyde (Figure 4, left) or via a stepwise condensation route, in which an intermediate a,c-bilane compound is formed (Figure 4, right).

In both procedures, pyrrole, 2-methoxybenzaldehyde and 5-bromo-2-methoxy-benzaldehyde were employed as the starting compounds (see appendix A1, Table 1, entry 1a,b).[23,24] Mass spectrometry and NMR spectroscopy showed that each of the two reactions yielded mixtures of atropisomers of porphyrins substituted with up to four bromine atoms. These atropisomers are present because the methoxy-protecting groups hinder the free rotation of the *meso*-phenyl-porphyrin bond. The atropisomeric mixtures of both reaction routes could not be separated by column chromatography. By inserting a zinc center into the porphyrin and by adding pyridine to the eluent used during the column chromatography, it was attempted to disentangle possible aggregates of the differently substituted porphyrins in the mixture (see appendix A1, Table 1, entry 2).[15] Although now fractions of partly separated porphyrins were isolated, it was concluded, based on mass spectrometry, that all fractions still contained a mixture of differently substituted porphyrins. In order to increase the difference in polarity of these different porphyrin components, the bromine groups in the unseparated reaction mixture were reacted with 2-methyl-3-butyn-2-ol via a Sonogashira cross coupling reaction to provide porphyrins with acetone-protected acetylenes (see appendix A1, Table 1, entry 3).[25] However, still no separation of the compounds could be achieved by column chromatography. Since the presence of atropisomers was thought to complicate the separation of the differently substituted porphyrins, the mixture of bromo-functionalized tetramethoxy porphyrins was deprotected to yield the corresponding mixture of bromo-tetra-hydroxy porphyrins, in which the *meso*-phenyl-porphyrin bonds can freely rotate

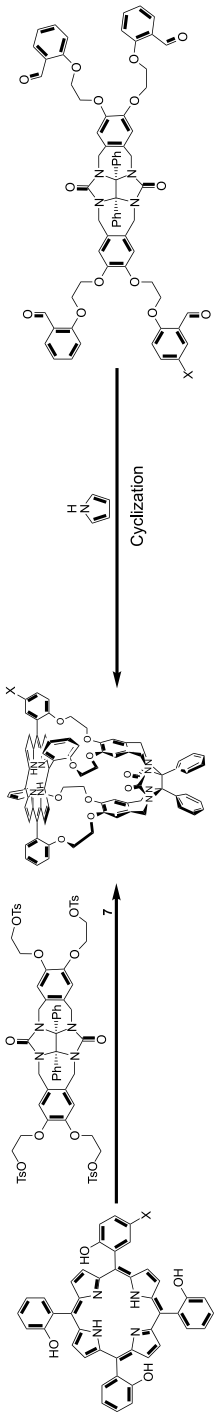

Figure 3 Two possible synthetic pathways to form a mono-substituted porphyrin cage compound, with X indicating the desired functional handle. The synthetic routes include statistical steps.

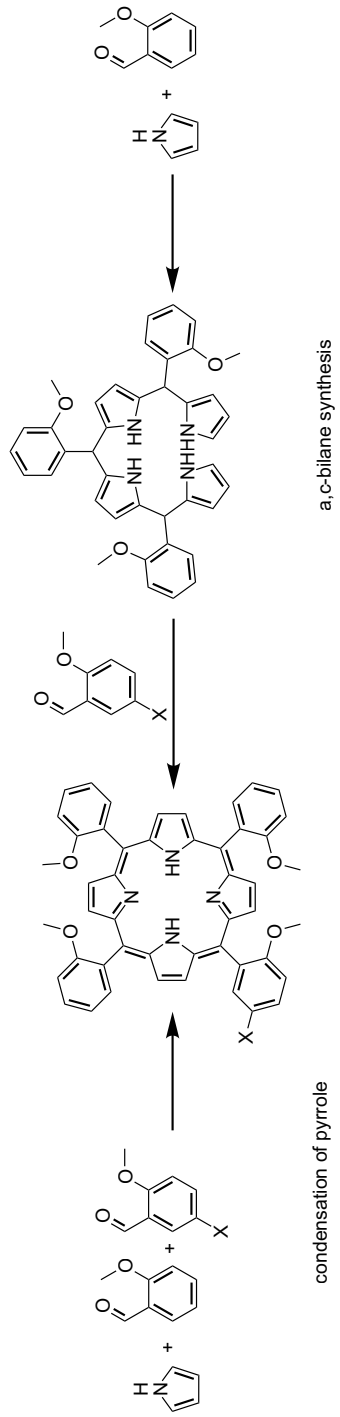

Figure 4 Two possible synthetic pathways to form a mono-substituted porphyrin with X indicating the desired functional handle. (Left) Direct cyclization of pyrrole and two different benzaldehydes and (right) stepwise condensation of pyrrole, o-methoxybenzaldehyde, and 5-bromo-2-methoxybenzaldehydeleading to the formation of an intermediate a,c-bilane.

(see appendix A1, Table 1, entry 4).[22] Although a gradient from non-substituted to tetra-substituted tetrahydroxy porphyrins was observed by mass spectrometry carried out on the fractions that eluted during the column chromatography, no pure mono-bromo-functionalized porphyrin could be obtained. In order to change the difference in polarity, the hydroxy groups were subsequently protected with acetyl groups during an acetylation reaction (see appendix A1, Table 1, entry 5).[26] Again no pure mono-bromo-substituted tetra-acetoxy porphyrin could be isolated by column chromatography. We envisaged that substituting the bromine for a nitro function might help increase the polarity difference between the products formed in the statistical mixture. Hence, 5-nitro -2-methoxybenzaldehyde instead of 5-bromo-2-methoxybenzaldehyde was employed as a starting material (see appendix A1, Table 1, entry 6).[23] In this case a partial separation of the products was obtained, resulting in a mixture of non-functionalized and mono-nitro-functionalized porphyrins as was indicated by mass spectrometry. However, during the subsequent deprotection of the methoxy groups with boron tribromide (BBr_3), mass spectrometric and NMR analysis revealed that a random substitution of β-pyrrolic protons for bromine atoms from the BBr_3 had occurred. For this reason, also this synthesis route was not suitable to obtain a mono-functionalized tetrahydroxyporphyin.[22]

2.2.1.2. Attempted synthesis of a mono-functionalized porphyrin cage compound via a diphenylglycoluril clip with different aldehyde substituents

Given the fact that the synthesis of sufficiently pure amounts of a mono-functionalized porphyrin was unsuccessful, a second strategy was attempted. It involves the substitution of the tosyl-groups of compound **7** by various benzaldehydes, followed by their condensation with pyrrole to give a mono-functionalized porphyrin cage compound (Figure 3, right route). In the different strategies to synthesize a mono-functionalized porphyrin clip discussed below, the functionality is either a bromine or a carboxylic acid group. The first attempts involved the synthesis of a mono-functionalized porphyrin clip with a bromine function. Two routes were followed, i.e. the stepwise and the one pot substitution of the tosyl-groups of compound **7** (see appendix A2, Table 2, entry 1 a,b)**.**[15] In the stepwise substitution procedure, first one equivalent of 5-bromo-2-methoxybenzaldehyde was reacted with **7**. Mass spectrometry showed that substitution of the tosyl-groups of **7** with up to four aldehydes had occurred and that the differently substituted compounds could not be separated by column chromatography. Nevertheless, the obtained mixture was further reacted with 3 equivalents of 2-methoxybenzaldehyde, yielding a mixture in which all the tosyl-groups had been substituted by aldehydes. Analysis by mass spectrometry revealed that various compounds were present, containing up to four bromine substituents, which could not be separated by column chromatography. The mixture was condensed with four equivalents of pyrrole to give diphenylglycoluril cages with a porphyrin roof, however, the polarity differences between the

differently substituted porphyrin cages proved to be too small to achieve separation by column chromatography. Subsequently, the one pot synthesis procedure was tried. To this end a mixture of 5-bromo-2-methoxybenzaldehyde and 2-methoxybenzaldehyde, in a ratio of 1:3, was reacted with **7** under basic conditions. Mass spectrometry showed that a mixture of aldehyde products with up to four bromine substituents was formed, which unfortunately, turned out to be inseparable by column chromatography.

In a next attempt we tried to differentiate the reactive arms present on compound **7** by employing a solid phase synthesis route (Figure 5). This might prevent stochastic substitutions of the tosyl-groups on **7**, at least in principle.[27]

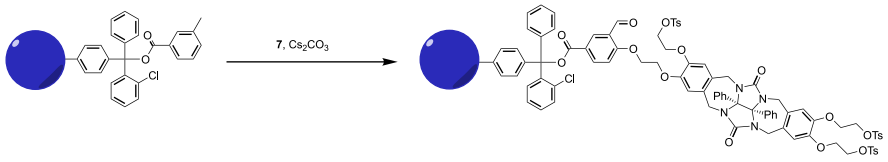

Figure 5 *Differentiation of the reactive arms of **7** by attaching one arm to a solid state resin (blue circle).*

A 2-chlorotrityl chloride resin was applied, which is susceptible to nucleophilic attack and the product can be cleaved from the resin with mild acid after the substitution reaction. 3-Formyl-4-hydroxybenzoic acid was attached to the resin, which would eventually result in the attachment of one carboxylic acid-functionalized aldehyde to the diphenylglycoluril clip and hence after reaction with pyrrole to a porphyrin cage functionalized with a carboxyl group. Compound **7** was coupled to the anchored 3-formyl-4-hydroxybenzoic acid in DMF using cesium carbonate as a base. Unfortunately, after cleavage of the resin, no product was obtained, possibly because compound **7** is too sterically demanding to reach the reactive sites located inside the resin and because low temperatures had to be applied (at maximum 40 ˚C) in order to remain below the glass transition temperature of the resin.[28]

2.2.1.3. Successful synthesis of a mono-functionalized porphyrin cage compound via a mono-substituted porphyrin formed by a non-statistical, stepwise route

As turned out in the previous sections a mono-functionalized porphyrin cage compound could not be synthesized because the required mono-substituted tetrahydroxyporphyrin or a diphenylglycoluril clip containing one aldehyde arm that is different from the other aldehyde arms were not accessible by employing statistical procedures. Therefore, a non-statistical, step-by-step route was designed (Figure 6).

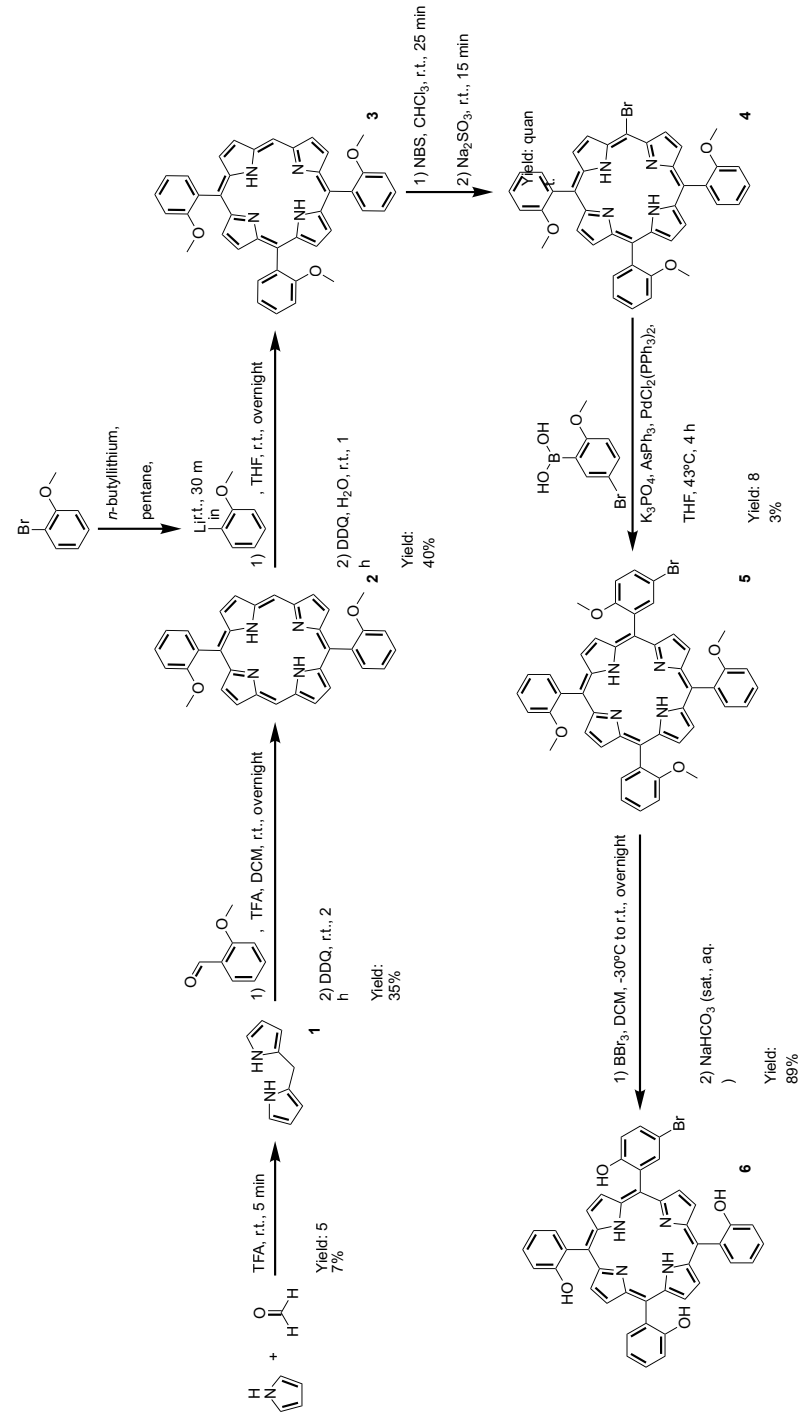

Figure 6 *Step-wise synthesis route to a mono-functionalized porphyrin*

It started with the condensation of paraformaldehyde with pyrrole in the presence of TFA to yield dipyrromethane (**1**) in 57% yield.[29,30]

A MacDonald [2+2] condensation of this compound with 2-methoxybenzaldehyde gave 5,15-bis(2-methoxyphenyl)porphyrin (**2**) in 35% yield after oxidation with DDQ.[31,32] The attachment of the third *meso*-substituent was accomplished by nucleophilic addition of *o*-methoxyphenyllithium (synthesized by reacting 2-bromoanisole with *n*-butyllithium) to one of the available *meso*-positions of **2**.[31,33] After oxidation with DDQ, compound **3** was obtained in 40% yield.[34] A side product in which a CH_2 group was present between the porphyrin and one of the *o*-methoxyphenyl rings was obtained, as was confirmed by mass spectrometry and NMR spectroscopy (Figure 7). When, the excess of *o*-methoxyphenyllithium was removed from the reaction mixture, the formation of this side product was reduced. It is unknown where this additional CH_2 group originates from.

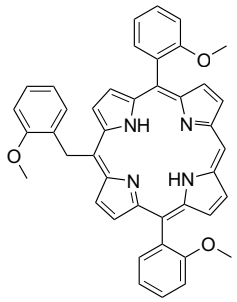

Figure 7 *Chemical structure of the side product formed during the reaction of* o*-methoxyphenyllithium with* ***2****.*

In compound **3**, one free *meso*-position remains and therefore a reaction with a suitable lithium compound to prepare a mono-functional porphyrin is less favorable. The reason is that during the reaction of the lithium salt with the free *meso*-position of porphyrin **2**, a Meisenheimer-type complex is formed. The negative charge of this complex is located and stabilized at the opposite *meso*-position, which therefore should also be a free position.[35] Since compound **3** has not such an extra free *meso*-position and since the preparation of the required reagent, i.e. a 5-bromo-2-methoxyphenyl lithium salt is troublesome, a Suzuki cross-coupling reaction was selected. To this end first a functional group was introduced in a regio-selective fashion at the free *meso*-position of **3**, i.e. by brominating this compound with NBS, giving compound **4** in quantitative yield.[36] Subsequent reaction of **4** with 5-bromo-2-methoxyphenyl boronic acid in the presence of a palladium catalyst gave porphyrin **5** in 83% yield.[37] To prevent a second Suzuki cross-coupling reaction to occur at the bromo-functionalized *meso*-phenyl ring of **5**, product formation was

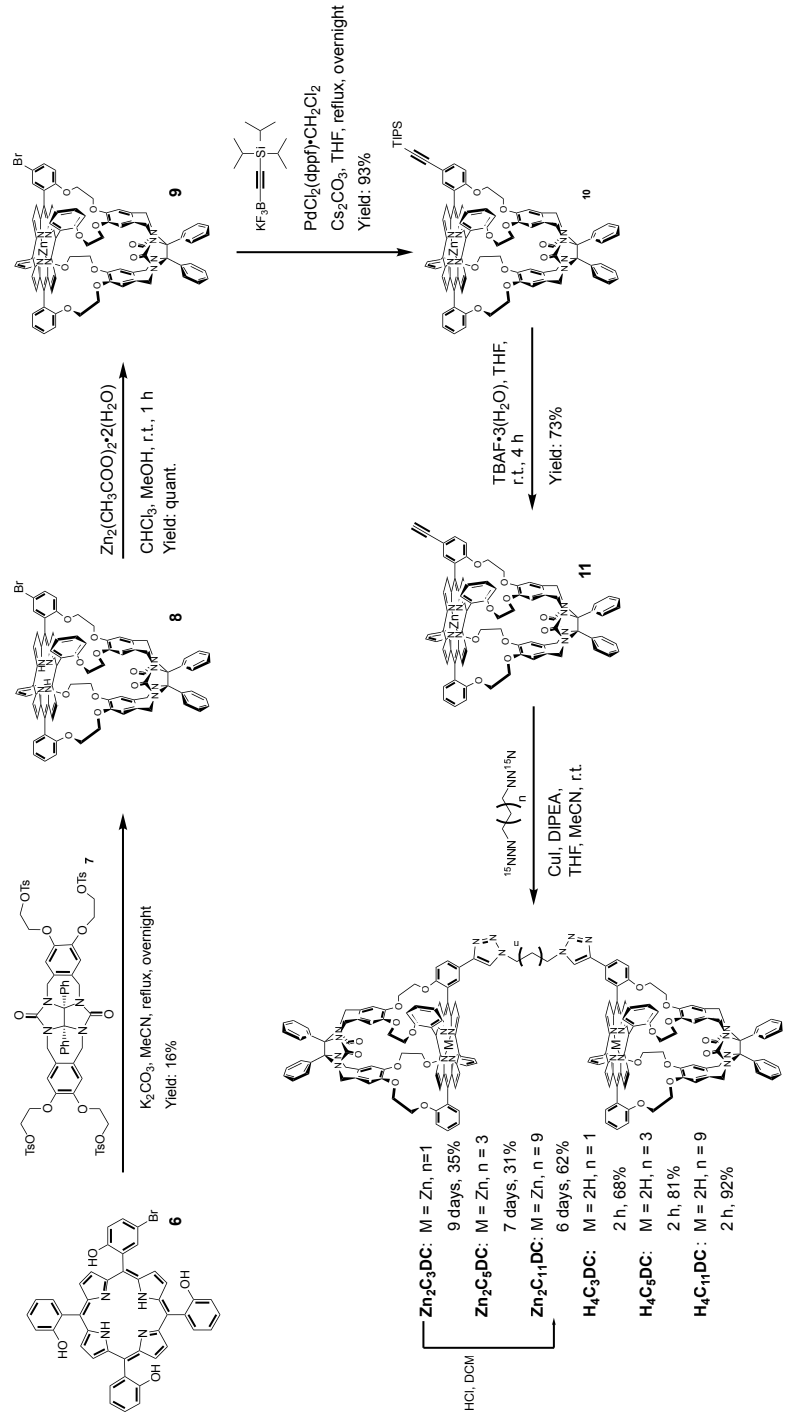

Figure 8 *Synthesis route of* ***H_4C_xDC*** *with x being 3, 5 or 11 methylene groups.*

followed over time with the help of mass spectrometry, and the reaction was carried out at a moderate temperature. When mass spectrometry had shown that almost all starting material had disappeared, the reaction was stopped. Subsequently, the methoxy groups of **5** were deprotected using boron tribromide to give the desired mono-bromo-functionalized tetrahdroxyporphyrin **6** in 89% yield.[22]

Finally, to prepare the desired mono-functionalized porphyrin cage porphyrin **6** was coupled to compound **7** following a literature procedure, giving the mono-bromo-substituted porphyrin clip (**8**) in 16% yield (Figure 8).[22] In order to protect the pyrrole NH-protons of **8** from undesired metal insertion in following synthesis steps (see next section), a zinc center was inserted into the porphyrin, giving compound **9** in quantitative yield.[15]

2.2.2. Synthesis of the double porphyrin cage compounds

2.2.2.1. Substitution of the bromine substituent of the mono-bromo-porphyrin cage compound 9

It was envisaged that a double porphyrin cage compound could be obtained by the coupling of two mono-functionalized porphyrin cages. For this coupling reaction a copper-catalyzed azide-alkyne 1,3-dipolar cycloaddition (CuAAC) was selected, because of its known high efficiency.[38–41] In order to be able to employ a CuAAC reaction, an alkyne functionality that can react with a diazidoalkane spacer needs to be present on the porphyrin clip. Several attempts to convert the bromine atom of compound **9** into an alkyne function were tried (see appendix A3, Table 3). The first attempt involved a Sonogashira cross coupling reaction using trimethylsilyl (TMS) protected acetylene (see appendix A3, Table 3, entry 1).[42] However, no full conversion was achieved and the separation of compound **9** from the trimethylsilylalkynyl (TMSA)-substituted porphyrin cage compound by column chromatography turned out to be impossible due to the low difference in polarity between the two compounds. To enable easier separation by increasing the polarity difference, 2-methyl-3-butyn-2-ol was employed as the acetylene functionality (see appendix A3, Table 3, entry 2).[43] According to mass spectrometry and NMR spectroscopy the desired product was obtained, but a white contamination that could not be removed by column chromatography remained present. Hence, the mono-acetone-protected acetylene porphyrin cage compound could not be isolated in pure form. The observed contamination most likely consists of inorganic salts, as they were not observed by NMR spectroscopy. So far, the salts were not identified, but they may originate from the used palladium catalyst and be trapped in the cavity of the mono-functionalized porphyrin cage compound. In an attempt to enable their separation, the polarity of the cage compound was changed by deprotecting the acetylene moiety (see appendix A3, Table 3, entry 3).[44] Although full conversion to the mono-acetylene porphyrin clip **11** was observed, the separation of this compound from the salts remained troublesome and could not be realized. Therefore, a different method to

convert the bromine substituent to an alkyne functionality was employed. A Suzuki-Miyaura cross coupling reaction that uses potassium triisopropylsilylacetylene trifluoroborate (TIPSA BF_3K) proved to be successful to convert the bromine functionality of compound **9** into a triisopropylsilyl-protected acetylene (**10**), in 93% yield after purification by column chromatography (see appendix A3, Table 3, entry 4 and Figure 8).[45]

2.2.2.2. Synthesis of the double porphyrin cage compounds (H_4C_xDC)

Compound **11** was used as the starting material for the synthesis of a series of three double cage compounds, i.e. **H_4C_3DC**, **H_4C_5DC** and **$H_4C_{11}DC$**. First, the TIPS protecting group of the protected acetylene compound **10** was removed with tetrakis-*n*-butylammonium fluoride to give compound **11** in 73% yield. Subsequently, **11** was employed in CuAAC reactions with α,ω-diazidoalkanes of various lengths (C_3, C_5 and C_{11}) to generate the zinc double porphyrin cages (**Zn_2C_xDC**).[46] In order to facilitate the characterization of the new compounds by NMR ^{15}N-enriched α,ω-diazidoalkanes were used. They were synthesized using a procedure described in the literature. For this purpose ^{15}N-enriched sodium azide, in which the ^{15}N isotope is located at one of the two terminal positions, was used.[47] After the CuAAC reactions the zinc double porphyrin cage compounds with varying spacer length (**Zn_2C_xDC**) were obtained in yields of 35% (**Zn_2C_3DC**), 31% (**Zn_2C_5DC**), and 62% (**$Zn_2C_{11}DC$**), respectively.[48] These yields are relatively low, which is attributed to the steric hindrance between the two approaching porphyrin compounds during the 'click' reaction. During purification with column chromatography, it was possible to retrieve unreacted **11**, which could be employed in another 'click' reaction. After treatment of the **Zn_2C_xDC** compounds with aqueous hydrochloric acid (6 M), the free base double porphyrin cage compounds **H_4C_3DC**, **H_4C_5DC** and **$H_4C_{11}DC$** were obtained in yields of 68, 81, and 92%, respectively.

2.2.3. Structural characterization of the double cage compounds H_4C_xDC

The structures of the double porphyrin cage compounds in chloroform were investigated with the help of NMR spectroscopy (500 MHz, for an example see Figures 9 and 10). All proton and carbon resonances of the double porphyrin compounds could be assigned with the help of 2D techniques. The 1D ^{15}N spectrum of **H_4C_3DC** showed four singlets for the ^{15}N-labeled nitrogen atoms (Figure 11). The fact that two sets of two singlets are observed for the two different types of ^{15}N labeled nitrogen atoms present in the triazole rings of the linkers indicates that two different species of **H_4C_3DC** must be present (see below).

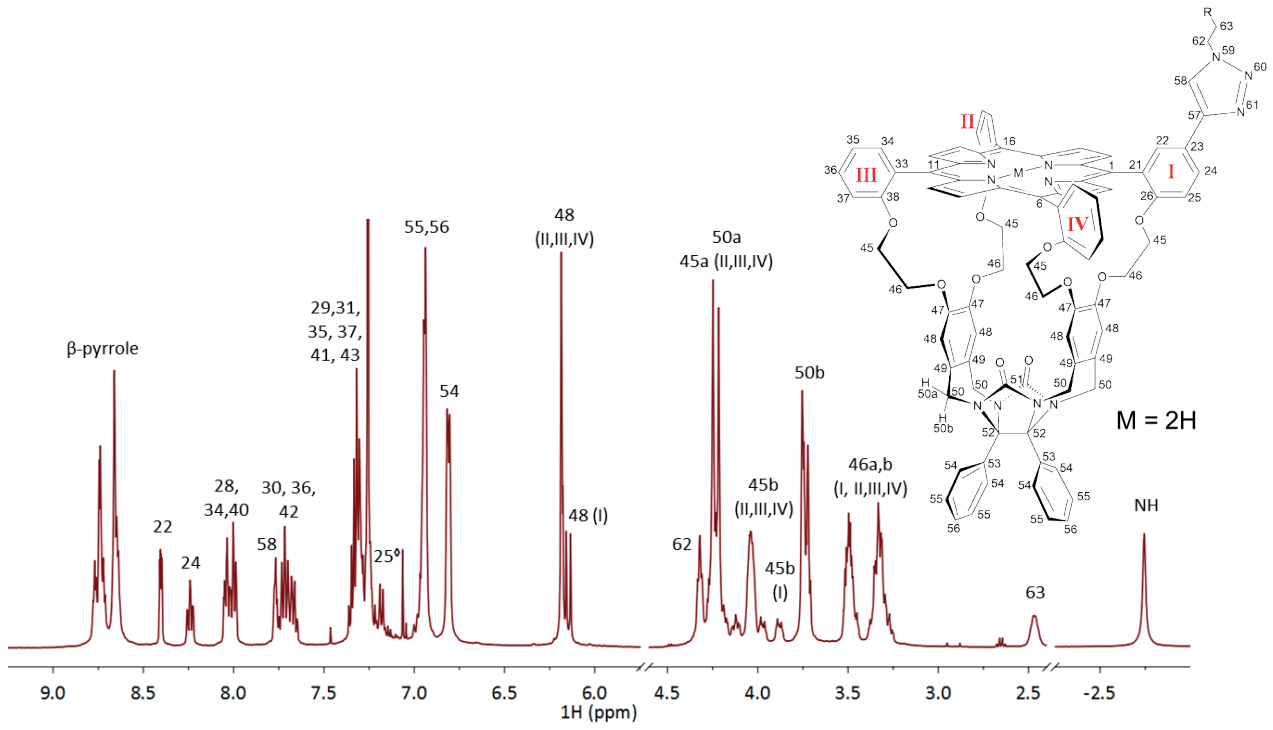

Figure 9 *^{1}H NMR spectrum and proton assignments of **H_4C_3DC** in $CDCl_3$ at 293.15 K. I-IV indicate the differently substituted phenyl rings of the porphyrin macrocycle in **H_4C_3DC**, as shown in the chemical structure.*

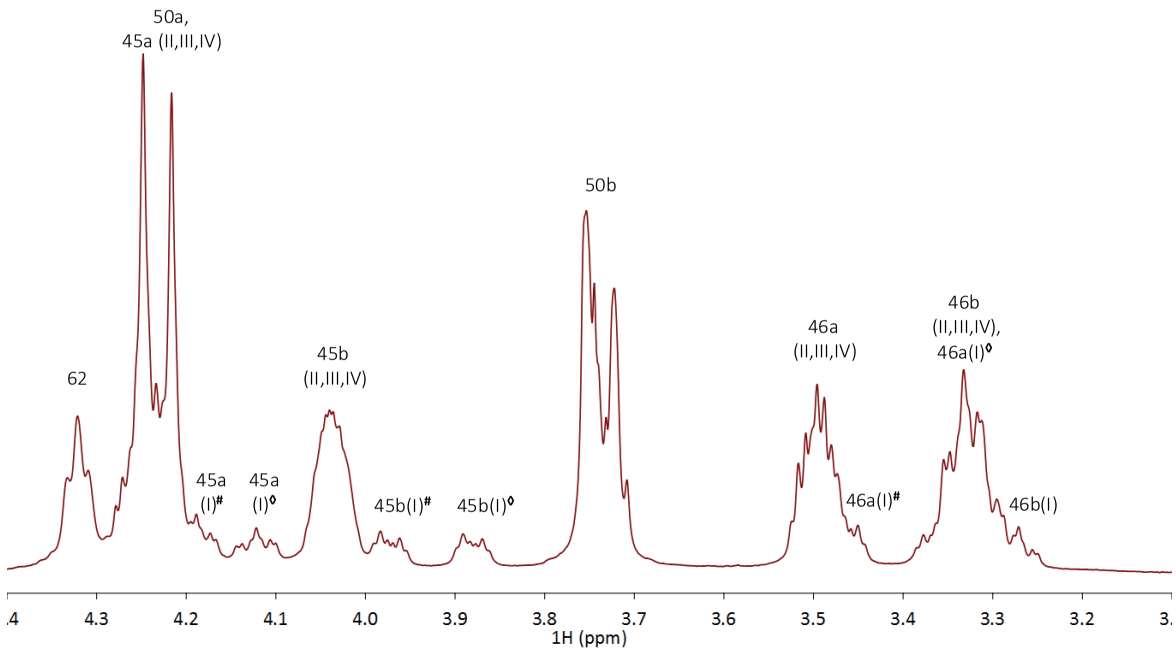

Figure 10 *^{1}H NMR spectrum and proton assignment of **H_4C_3DC** in CDCl3 at 293.15 K in the region of 4.4 to 3.1 ppm. I-IV represent the differently substituted phenyl rings of the porphyrin macrocycle in **H_4C_3DC** as is indicated in the chemical structure in Figure 9.*

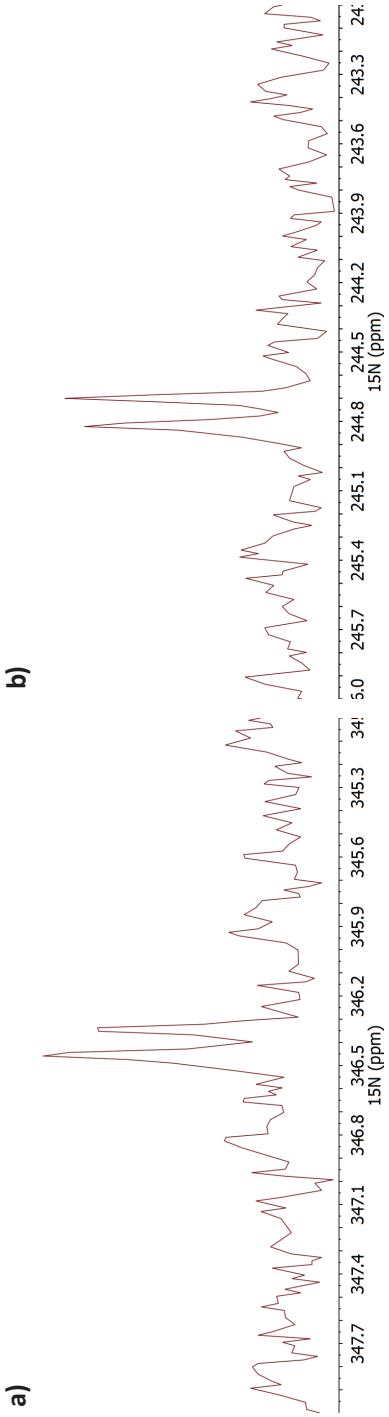

Figure 11 *a) ^{15}N NMR spectrum of **H_4C_3DC** in $CDCl_3$ at 298.15 K in the region from 347.7 to 345.3 ppm. Two signals for ^{15}N-**61** are present at 346.45 and 346.54 ppm, respectively. b) The same spectrum showing the region from 245.7 to 243.3 ppm where the two signals of ^{15}N-**59** are located at 244.89 and 244.77 ppm, respectively.*

A ^{1}H-^{15}N HBMC spectrum revealed that the peaks of ^{15}N-**61** at 346.45 and 346.54 ppm both coupled with the triazole proton signal belonging to H-**58** at 7.77 ppm. The peaks at 244.89 and 244.77 ppm of ^{15}N-**59** were found to couple with the triazole proton signal belonging to H-**58**. They coupled as well as to the proton signals at 4.32 and 2.47 ppm belonging to the linker CH_2 groups (CH_2-**62** and CH_2-**63**, respectively). Via a ROE contact between the triazole proton H-**58** and the phenyl proton ArH-**22** in the 2D ROESY spectrum, the resonance position of the latter proton in the ^{1}H NMR spectrum could be located (8.40 ppm). Proton ArH-**22** has a HMBC-coupling to proton ArH-**24** (8.28-8.21 ppm), which in turn has two COSY-cross coupling peaks with proton ArH-**25** (see Figure 12, at 7.20 and 7.26 ppm). The fact that for this proton two well-separated resonances are observed confirms the abovementioned existence of two different species.

The two signals for ArH-**25** integrate for 1 proton each, meaning that the two species are present in a 1:1 ratio. The related peaks in phenyl rings II, III, and IV of the molecule (ArH-**37**) integrate for 6 protons and are observed as a multiplet ranging from 7.22 to 7.38 ppm. The protons ArH-**25**, ArH-**45**, ArH-**46**, and ArH-**48** in phenyl ring I and the arm connected to this ring all give two distinct signals, originating from the two different species.

Although this is at first sight not easily recognizable, mono-porphyrin cage compound **11** is chiral: when inspecting its 3D structure, two non-superimposable

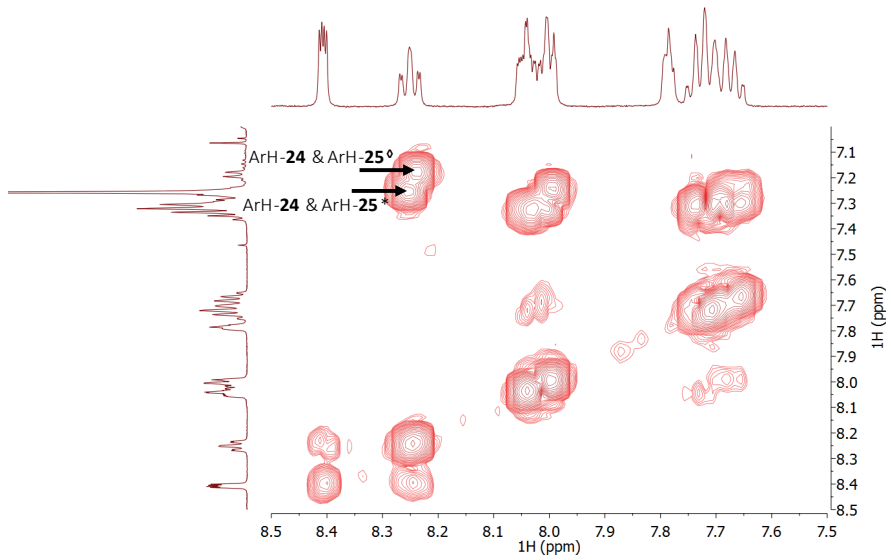

Figure 12 *COSY spectrum of **H_4C_3DC** showing the region of 8.5 to 7.0 ppm where the cross-coupling peaks of ArH-**24** (8.28-8.21) and ArH-**25#** (7.26 ppm) and ArH-**25⁰** (7.20 ppm) are located.*

mirror images exist and, hence, the compound exists as two enantiomers (Figure 13). This chirality can be recognized more clearly when the top view of **11** is inspected (Figure 13a).

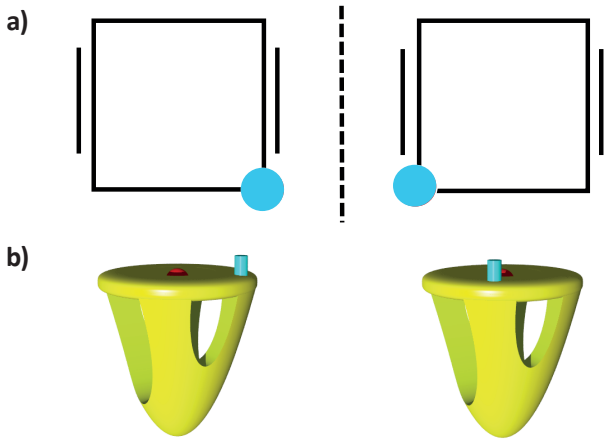

Figure 13 *Schematic drawing of the two enantiomeric forms of zinc mono-acetylene porphyrin clip **11**. (a) Top view of the porphyrin cage compound represented by the black square (the parallel lines denoting the sidewalls); (b) 3D view of **11** (yellow). The acetylene group in a) and b) is indicated in cyan.*

These enantiomers are, obviously, indistinguishable by NMR spectroscopy. The compound displays a plane of chirality and has two chiral centers which are the two carbon atoms **52** in the diphenylglycoluril framework (Figure 9). Two molecules of **11** can be covalently coupled to form a double cage compound by connecting either the same two enantiomers, or the two opposite enantiomers (Figure 14). Hence, the covalent coupling of **11** leads to the formation of two diastereoisomers (*RR*&*SS* and *RS*&*SR*), which are distinguishable by NMR spectroscopy. Since the integrals of the two proton signals observed for all the protons ArH-**25**, ArH-**45**, ArH-**46**, and ArH-**48** in phenyl ring I and its arm are in a 1:1 ratio, the diastereoisomers must be present in a 1:1 ratio as well. This result is to be expected, because **11** will not react enantioselectively with a diazido-spacer during the 'click'-reaction. Also for **H_4C_5DC**, two sets of proton signals were observed for ArH-**25**, ArH-**45**, ArH-**46**, and ArH-**48**. However, in the case of **H_4C_{11}DC**, these proton signals did not appear as double sets of resonances, which is proposed to be the result of the longer spacer length in this double cage compound. In **H_4C_{11}DC** the two cavities are further apart, and as a result they do not experience a significant enough difference in chemical environment, such that the two diastereoisomers give rise to double resonances for the same proton.

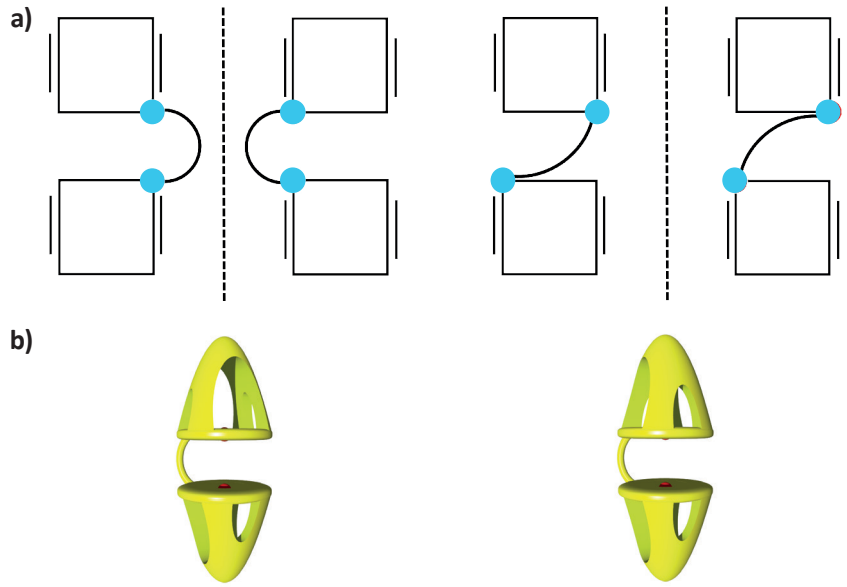

Figure 14 *Schematic representation of the two diastereomeric forms of the double porphyrin cage compound (RS&SR and RR&SS). (a) Top view of the diastereoisomers (black squares, the parallel lines indicate the sidewalls). The atoms of the connection points are indicated in cyan; (b) 3D view.*

The insertion of zinc centers into the porphyrins resulted in broadening of the proton signals of the resulting **Zn_2C_xDC** compounds in $CDCl_3$ (Figure 15). Upon the addition of deuterated pyridine to these solutions, all proton signals sharpened. It is therefore proposed that the broadening of the signals is caused by intermolecular or intramolecular coordination of the triazole nitrogen atoms to the porphyrin zinc centers. The added deuterated pyridine will coordinate to the zinc centers and prevent any internal coordination and break up any aggregates that are formed. In order to characterize the **Zn_2C_xDC** compounds, NMR-spectra were recorded at 60 ˚C in DMSO-d_6, a solvent that also prohibits such intramolecular or intermolecular coordination. The spectra of the **Zn_2C_xDC** compounds in DMSO-d_6 gave sharp resonances, which could be assigned completely to the two diastereoisomeric forms of the **H_4C_xDC** compounds.

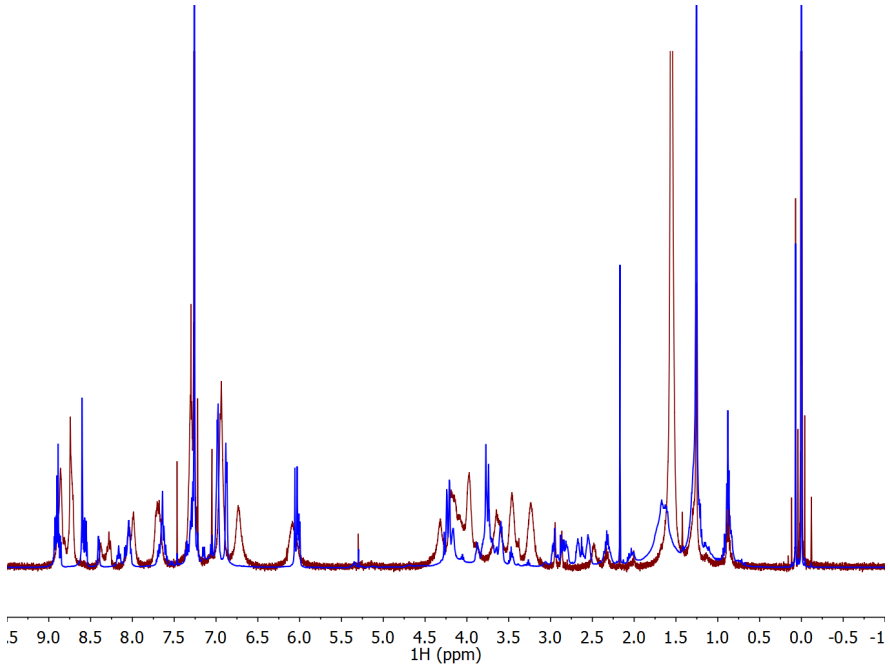

Figure 15 ^{1}H *NMR spectrum of* ***Zn$_2$C$_3$DC*** *in* $CDCl_3$ *(red) and in* $CDCl_3$ *with a drop of pyridine-*d_5 *(blue) at 293.15 K.*

2.3. Conclusion

In this chapter we report a multi-step route for the synthesis of covalently linked double porphyrin cage compounds (**H$_4$C$_x$DC**). For the synthesis of these compounds a mono-substituted porphyrin cage compound is required. Initial attempts to prepare this compound via statistical routes were unsuccessful. However, a non-statistical, step-wise route turned out to be successful. Starting from paraformaldehyde and pyrrole, a mono-bromo-functionalized tetrahydroxyporphyrin was obtained in 6 steps. This compound could be coupled to a diphenylglycoluril-based clip compound to yield a mono-bromo-substituted porphyrin cage compound, which was obtained as a racemate of two intrinsically chiral cage molecules. After converting the bromo-substituent of the mono-substituted cage compound into an acetylene function, double cage compounds **H$_4$C$_3$DC**, **H$_4$C$_5$DC**, and **H$_4$C$_{11}$DC** were obtained via 'click' reactions with α,ω-diazidoalkanes of different lengths. With the help of extensive NMR spectroscopy experiments all ^{1}H, ^{13}C, and ^{15}N signals of the double cage compounds could be assigned. The presence of multiple resonances for the same

protons in **H$_4$C$_3$DC** and **H$_4$C$_5$DC** proved the existence of two diastereoisomeric forms of these compounds. In the case of **H$_4$C$_{11}$DC** these multiple proton resonances were not observed, indicating that the two cavities are so remote that they no longer feel each other's chirality. Upon insertion of zinc centers in the porphyrin rings of the double cage compounds, the NMR proton signals significantly broadened, suggesting that intramolecular or intermolecular coordination of the nitrogen atoms in the triazole rings to the zinc centers in the porphyrin planes occurred.

2.4. Experimental

All chemicals were commercially obtained and used without further purification unless stated otherwise. Dry *n*-pentane was stored under argon in the glovebox, THF was distilled under nitrogen from potassium, DCM was distilled under nitrogen from calcium hydride, and MeCN was distilled under argon from calcium chloride. For TLC analysis, TLC Silicagel 60 F_{254} (Merck) and for column chromatography, Silica gel 0.035-0.070 mm 60A (Acros), SilicaFlash® P60 40-63 µm (SiliCycle) or Silicagel 60 H (Merck) was used. ^{1}H and ^{13}C-NMR spectra were recorded on Varian Inova 400 MHz or Bruker Avance III 400 or 500 MHz spectrometers at 25˚C unless stated otherwise. Chemical shifts are reported in parts per million (ppm) relative to tetramethylsilane (TMS) as the internal reference. NMR data are presented as follows: chemical shift (ð) in ppm, multiplicity (s = singlet, bs = broad singlet, d = doublet, t = triplet, q=quartet, td = triplet of doublets, m = multiplet and/or multiple resonances), integration, assignment and coupling constant (*J*) in hertz (Hz). All NMR signals were assigned on the basis of ^{1}H, ^{13}C-NMR, COSY, ROESY, HSQC, and HMBC experiments. The numbering of the proton, carbon, and nitrogen atoms used in the assignments is depicted in Figure 16. Phase and baseline correction was applied to all NMR spectra. As most porphyrin compounds were obtained as a mixture of several atropisomers that were inseparable by column chromatography, the reported chemical shifts represent the averaged shifts over all of these atropisomers. Assigning all inequivalent ^{13}C-signals was not possible due to the limited resolution of the 2D spectra and overlapping proton signals, therefore ranges are reported for several almost identical ^{13}C atoms. LCQ mass spectra were recorded in methanol on a Thermo Finnigan LCQ Advantage Max mass spectrometer, and MALDI-TOF mass spectra were measured in reflective mode with dithranol as matrix on a Bruker Microflex LRF MALDI-TOF mass spectrometer. Accurate MALDI-TOF mass spectra were obtained on a Brukerdaltonics autoflex (ST-A2130) MALDI-TOF mass spectrometer with cesium triiodide as matrix in reflective mode. Accurate masses were obtained from a solution of the compound in methanol on a JEOL AccuTOF CS JMS-T100CS. All reactions were carried out under an argon atmosphere. Compound **7** was synthesized according to a literature procedure.[15]

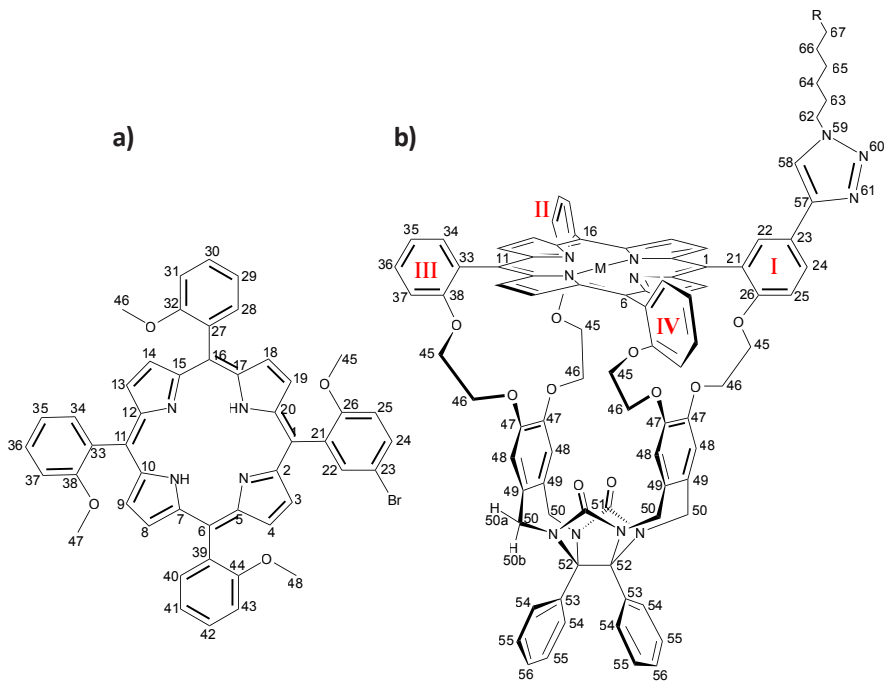

Figure 16 *Carbon, proton, and nitrogen numbering of 5-(5-bromo-2-methoxyphenyl)-10, 15, 20-tris(2-methoxyphenyl) porphyrin (**5**) and the **M_2C_xDC** molecule, as used for all NMR analyses, with M=2H or M=Zn. For the double cage compounds the same numbering is used. These double cage compounds are obtained by attaching at R the same molecule as is shown, with the restriction that for **Zn_2C_3DC** the attachment starts at carbon number 63, for **Zn_2C_5DC** at carbon atom 64, and for **$Zn_2C_{11}DC$** at carbon atom 67 (this compound is shown). The CH_2-groups of the diphenylglycoluril framework (carbon atoms 45, 46, and 50) all have two inequivalent protons, marked as a and b. The location of the signals of these protons could only be identified for CH_2-50 with the help of ROESY experiments.*

Synthesis of di(1*H*-pyrrol-2-yl)methane (1)[30]

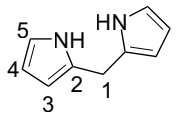

To distilled pyrrole (153 mL, 2.21 mol, 24.5 eq.) a 37% aq. formaldehyde solution (9 mL, 90.42 mmol, 1 eq.) was added. Argon was led through the solution for 15 min, after which TFA was added (0.82 mL, 10.21 mmol, 0.11 eq.). The reaction mixture was stirred at r.t. for 5 min. The orange solution was diluted with DCM (150 mL) and washed with sat. aq. Na_2CO_3 (3 x 100 mL) and water (100 mL). The organic layer was concentrated *in vacuo*. The excess of pyrrole was removed by vacuum distillation at 35˚C. Silicagel column chromatography using DCM/*n*-heptane (60/40 (v/v)) as the eluent afforded the product (**1**, 7.469 g, 51 mmol, 57%) as a white fluffy solid.

^{1}H-NMR ($CDCl_3$, 400 MHz): ∂ 7.91 (bs, 2H, N*H*), 6.68 (td, 2H, Ar*H*-**5**, *J* = 2.6, 1.5 Hz), 6.15 (q, 2H, Ar*H*-**4**, *J* = 2.9 Hz), 6.05-6.02 (m, 2H, Ar*H*-**3**), 3.99 (s, 2H, CH_2-**1**); ^{13}C{^{1}H}-NMR ($CDCl_3$, 100 MHz): ∂ 129.03 (Ar*C*-**2**), 117.24 (Ar*C*-**5**), 108.38 (Ar*C*-**4**), 106.36 (Ar*C*-**3**), 26.38 (CH_2-**1**).

Synthesis of 5,15-bis(2-methoxyphenyl)porphyrin (2)[32]

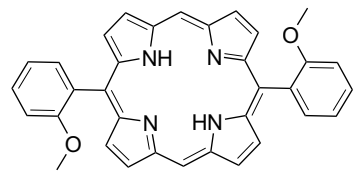

Argon was led through DCM (1.85 L) for 30 min before di(1*H*-pyrrol-2-yl)methane (**1**, 1.205 g, 8.24 mmol, 2 eq.), 2-methoxybenzaldehyde (1.122 g, 8.24 mmol, 2 eq.) and TFA (0.140 mL, 1.82 mmol, 0.44 eq.) were added. The reaction mixture was stirred in the dark at r.t. for 16 h. Then a solution of DDQ (2.685 g, 11.83 mmol, 2.88 eq.) in DCM (70 mL) was added. After stirring for 2 h the mixture was quenched with TEA (6 mL) and concentrated *in vacuo*. The residue was purified over a silicagel column using chloroform as the eluent. The crude product was dissolved in DCM, filtered, and precipitated in *n*-heptane. After washing the precipitate with *n*-pentane (4x), drying *in vacuo* yielded the product (**2**, 749.1 mg, 1.43 mmol, 35%) as a purple solid containing 2 atropisomers. ^{1}H-NMR ($CDCl_3$, 500 MHz): ∂ 10.23 (s, 2H, Ar*H*-**1,11**), 9.33 (d, 4H, ß-pyrrole-H-**3,9,13,19**, *J* = 4.5 Hz), 8.97 (d, 4H, ß-pyrrole-H-**4,8,14,18**, *J* = 4.5 Hz), 8.06 (d, 2H, Ar*H*-**28,40**, *J* = 7.2 Hz), 7.80 (t, 2H, Ar*H*-**30,42**, *J* = 7.9 Hz), 7.41 (t, 2H, Ar*H*-**29,41**, *J* = 7.5 Hz), 7.38 (d, 2H, Ar*H*-**31,43**, *J* = 8.0 Hz), 3.61 (s, 6H, O*Me*-**46,48**), -3.07 (s, 2H, N*H*); ^{13}C{^{1}H}-NMR ($CDCl_3$, 126 MHz): ∂ 159.45 (Ar*C*-**32,44**), 147.28 (Ar*C*-**5,7,15,17**), 145.18 (Ar*C*-**2,10,12,20**), 135.80 (Ar*C*-**28,40**), 131.33 (Ar*C*-**3,9,13,19**), 130.68 (Ar*C*-**4,8,14,18**), 130.29 (Ar*C*-**27,39**), 129.89 (Ar*C*-**30,42**), 119.61 (Ar*C*-**29,41**), 115.01 (Ar*C*-**6,16**), 111.07 (Ar*C*-**31,43**), 104.78 (Ar*C*-**1,11**), 55.81 (O*Me*-**46,48**); UV-Vis ($CHCl_3$) λ/nm (log(ε/M^{-1} cm^{-1})) 408 (5.53), 502 (4.21); Accurate mass; m/z: 523.21361 $(M+H)^+$; calculated for $C_{34}H_{27}N_4O_2$ 523.213040; Anal. Calcd for $C_{34}H_{26}N_4O_2$: C, 78.14; H, 5.01; N, 10.72. Found: C, 77.99; H, 4.92; N, 10.68.

Synthesis of 5,10,15-tris(2-methoxyphenyl)porphyrin (3)[36]

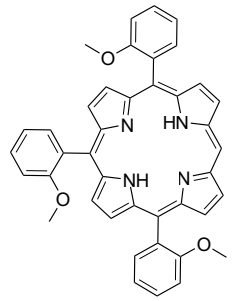

2-Bromoanisole (2.763 g, 14.77 mmol, 19.69 eq.) was added to dry *n*-pentane (50 mL). *n*-Butyllithium (1.6 M in hexanes, 8 mL, 12.79 mmol, 17.05 eq.) was added and the reaction mixture was stirred for 30 min at r.t. until a white precipitate was formed. The mixture was filtered under Schlenck conditions and the white residue was washed with dry *n*-pentane (4 x 40 mL), after which it was dissolved in distilled THF (150 mL). 5,15-Bis(2-methoxyphenyl)porphyrin (**2**, 390 mg, 0.75 mmol, 1 eq.) was added and the reaction mixture was stirred at r.t. for 16 h. Water (3.5 mL) was added, followed by DDQ

(761.32 mg, 3.35 mmol, 4.47 eq.). After stirring for 1 h at r.t. the reaction mixture was purified over a silicagel column using chloroform as the eluent. The crude product was subsequently purified by silicagel column chromatography using DCM/*n*-heptane (75/25, (v/v)) as the eluent to yield the product (**3**, 187.7 mg, 0.29 mmol, 40%) as a purple solid containing 3 atropisomers.

^{1}H-NMR ($CDCl_3$, 500 MHz): ∂ 10.11 (s, 1H, Ar*H*-**1**), 9.25 (d, 2H, ß-pyrrole-H-**3,19**, *J* = 4.6 Hz), 8.90 (d, 2H, ß-pyrrole-H-**4,18**, *J* = 4.4 Hz), 8.79-8.75 (m, 4H, ß-pyrrole-H-**8,9,13,14**), 8.04 (d, 1H, Ar*H*-**34**, *J* = 7.3 Hz), 8.02-7.92 (m, 2H, Ar*H*-**28,40**), 7.80-7.70 (m, 3H, Ar*H*-**30,36,42**), 7.39-7.35 (m, 3H, Ar*H*-**29,35,41**), 7.35-7.26 (m, 3H, Ar*H*-**31,37,43**), 3.61-3.51 (m, 9H, O*Me*-**46,47,48**), -2.89 (s, 2H, N*H*); ^{13}C{^{1}H}-NMR ($CDCl_3$, 126 MHz): ∂ 159.56-159.37 (Ar*C*-**32,38,44**), 149.00-144.00 (broad, Ar*C*-**2,5,7,10,12,15,17,20**), 135.78-135.50 (Ar*C*-**28,34,40**), 131.49-130.77 (Ar*C*-**27,33,39**), 131.20-130.10 (broad, Ar*C*-**3,4,8,9,13,14,18,19**), 129.76-129.68 (Ar*C*-**30,36,42**), 119.46-119.26 (Ar*C*-**29,35,41**), 115.87-115.19 (Ar*C*-**6,11,16**), 111.05-110.81 (Ar*C*-**31,37,43**), 104.40 (Ar*C*-**1**), 55.81 (O*Me*-**46,47,48**); UV-Vis ($CHCl_3$) *λ*/nm (log(*ε*/M^{-1} cm^{-1})) 413 (5.74), 508 (4.25); Accurate mass: m/z: 629.25449 $(M+H)^+$; calculated for $C_{41}H_{33}N_4O_3$ 629.25526.

Synthesis of 5-bromo-10,15,20-tris(2-methoxyphenyl)porphyrin (4)

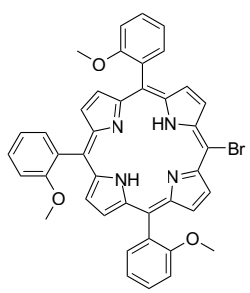

5,10,15-Tris(2-methoxyphenyl)porphyrin (**3**, 385.4 mg, 0.61 mmol, 1 eq.) was dissolved in chloroform (25 mL) and NBS (128.15 mg, 0.72 mmol, 1.18 eq.) was added. After stirring at r.t. for 25 min the reaction mixture was quenched by the addition a solution of Na_2SO_3 (177.33 mg, 1.41 mmol, 2.3 eq.) in water (10 mL). After 15 min the reaction mixture was diluted with chloroform (50 mL) and washed with water. The organic layer was dried over Na_2SO_4, filtered and evaporated to dryness. The crude product was purified by silicagel column chromatography using DCM/*n*-heptane (50/50 going to 75/25, (v/v)) as an eluent to yield the product (**4**, 467.7 mg, 0.66 mmol, 100%) as a purple solid containing 3 atropisomers.

^{1}H-NMR ($CDCl_3$, 500 MHz): ∂ 9.60 (d, 2H, ß-pyrrole-H-**3,19**, *J* = 4.8 Hz), 8.80 (bs, 2H, ß-pyrrole-H-**4,18**), 8.68 (bs, 4H, ß-pyrrole-H-**8,9,13,14**), 8.03-7.89 (m, 3H, Ar*H*-**28,34,40**), 7.79-7.70 (m, 3H, Ar*H*-**30,36,42**), 7.38-7.33 (m, 3H, Ar*H*-**29,35,41**), 7.33-7.26 (m, 3H, Ar*H*-**31,37,43**), 3.62-3.52 (m, 9H, O*Me*-**46,47,48**), -2.63 (s, 2H, N*H*); ^{13}C{^{1}H}-NMR ($CDCl_3$, 126 MHz): ∂ 159.50-159.20 (Ar*C*-**32,38,44**), 135.62-135.38 (Ar*C*-**28,34,40**), 130.74 (Ar*C*-**27,33,39**), 129.91-129.84 (Ar*C*-**30,36,42**), 119.41 (Ar*C*-**29,35,41**), 116.53-116.29 (Ar*C*-**6,11,16**), 110.97-110.77 (Ar*C*-**31,37,43**), 102.43 (Ar*C*-**1**), 55.79 (O*Me*-**46,47,48**); UV-Vis ($CHCl_3$) *λ*/nm (log(*ε*/M^{-1} cm^{-1})) 421 (5.54), 517 (4.21); Accurate mass; m/z: 707.16436 $(M(^{79}Br)+H)^+$, 709.16321 $(M(^{81}Br)+H)^+$; calculated for $C_{41}H_{32}BrN_4O_3$ 707.16578 (^{79}Br); 709.16373 (^{81}Br); Anal. Calcd for $C_{41}H_{31}BrN_4O_3$: C, 69.59; H, 4.42; N, 7.92; Found: C, 69.16; H, 4.34; N, 7.76.

Synthesis of 5-(5-bromo-2-methoxyphenyl)-10,15,20-tris(2-methoxyphenyl) porphyrin (5)

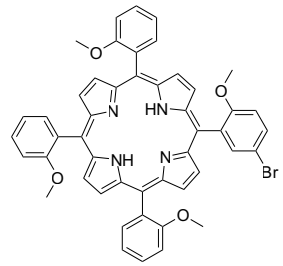

5-Bromo-10,15,20-tris(2-methoxyphenyl)porphyrin (**4**, 690 mg, 0.98 mmol, 1 eq.), (5-bromo-2-methoxyphenyl)boronic acid (1.125 g, 4.88 mmol, 5 eq.), triphenylarsine (119.9 mg, 0.39 mmol, 0.4 eq.), bis(triphenyl-phosphine)palladium (II) dichloride (137 mg, 0.20 mmol, 0.2 eq.), and tripotassium phosphate (1.035 g, 4.88 mmol, 5 eq.) were dissolved in distilled THF (175 mL). The reaction mixture was stirred at 42.5˚C for 4 h. After cooling to r.t., the reaction mixture was purified by a silicagel column using DCM as the eluent. Subsequently, the crude product was purified by silicagel column chromatography using DCM/*n*-heptane (60/40 going to 80/20 (v/v)) as the eluent to yield the product (**5**, 660.5 mg, 0.81 mmol, 83%) as a purple solid containing 8 atropisomers.

^{1}H-NMR ($CDCl_3$, 500 MHz): ∂ 8.78-8.68 (m, 8H, ß-pyrrole-H-**3,4,8,9,13,14,18,19**), 8.20-8.07 (m, 1H, Ar*H*-**22**), 8.06-7.91 (m, 3H, Ar*H*-**28,34,40**), 7.84 (d, 1H, Ar*H*-**24**, *J* = 9.0 Hz), 7.75 (t, 3H, Ar*H*-**30,36,42**, *J* = 7.9 Hz), 7.36-7.32 (m, 3H, Ar*H*-**29,35,41**), 7.32-7.28 (m, 3H, Ar*H*-**31,37,43**), 7.21-7.14 (m, 1H, Ar*H*-**25**), 3.63-3.50 (m, 12H, O*Me*-**45,46,47,48**), -2.65 (s, 2H, N*H*); ^{13}C{^{1}H}-NMR ($CDCl_3$, 126 MHz): ∂ 159.46 (Ar*C*-**32,38,44**), 158.73 (Ar*C*-**26**), 137.96-137.64 (Ar*C*-**22**), 135.83-135.40 (Ar*C*-**28,34,40**), 133.37 (Ar*C*-**21**), 132.38 (Ar*C*-**24**), 131.11 (Ar*C*-**27,33,39**), 129.72 (Ar*C*-**30,36,42**), 119.33 (Ar*C*-**29,35,41**), 115.71 (Ar*C*-**6,11,16**), 113.44 (Ar*C*-**1**), 112.51 (Ar*C*-**25**), 111.77 (Ar*C*-**23**), 110.91 (Ar*C*-**31,37,43**), 56.09 (O*Me*-**45,[46,47,48]**), 55.85 (O*Me*-**[45],46,47,48**); UV-Vis ($CHCl_3$) *λ*/nm (log(*ε*/M^{-1} cm^{-1})) 419 (5.62), 514 (4.28); Accurate mass; m/z: 813.20482 $(M(^{79}Br)+H)^+$, 815.20403 $(M(^{81}Br)+H)^+$; calculated for $C_{48}H_{38}BrN_4O_4$ 813.20764 (^{79}Br); 815.20560 (^{81}Br); Anal. Calcd for $C_{48}H_{37}BrN_4O_4$: C, 70.85; H, 4.58; N, 6.89. Found: C, 70.55; H, 4.45; N, 6.80.

Synthesis of 5-(5-bromo-2-hydroxyphenyl)-10,15,20-tris(2-hydroxyphenyl) porphyrin (6)

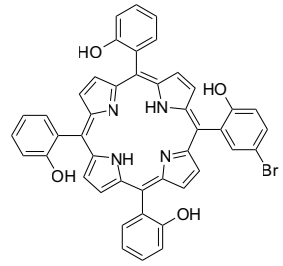

5-(5-Bromo-2-methoxyphenyl)-10,15,20-tris(2-methoxyphenyl)-porphyrin (**5**, 660.5 mg, 0.81 mmol, 1 eq.) was dissolved in distilled DCM (40 mL) and this solution was cooled to -30˚C. Then, BBr_3 (1.55 mL, 16.2 mmol, 20 eq.) was added. The reaction mixture was allowed to warm up to r.t. overnight before it was poured into an ice-water mixture (100 mL). Ethyl acetate (110 mL) and sat. aq. $NaHCO_3$ (250 mL) were added upon which the color of the mixture turned from green to red. The organic layer was washed with sat. aq. $NaHCO_3$ (2 x 70 mL) and dried over $MgSO_4$, filtered, and evaporated to

dryness. The crude product was purified by silicagel column chromatography using ethylacetate/chloroform (50/50 (v/v)) as an eluent, yielding the product (**6**, 549.4 mg, 0.73 mmol, 89%) as a purple solid containing 8 atropisomers.
^{1}H-NMR ($CDCl_3$, 500 MHz): ∂ 8.96-8.88 (m, 8H, ß-pyrrole-*H*-**3,4,8,9,13,14,18,19**), 8.13-8.08 (m, 1H, Ar*H*-**22**), 7.98-7.94 (m, 3H, Ar*H*-**28,34,40**), 7.83 (t, 1H, Ar*H*-**24**, *J* = 8.8 Hz), 7.73 (t, 3H, Ar*H*-**30,36,42**, *J* = 8.1 Hz), 7.37-7.32 (m, 6H, Ar*H*-**29,31,35,37,41,43**), 7.23 (d, 1H, Ar*H*-**25**, *J* = 2.5 Hz), 4.92 (bs, 4H, O*H*), -2.78 (s, 2H, N*H*); ^{13}C{^{1}H}-NMR ($CDCl_3$, 126 MHz): ∂ 155.40 (Ar*C*-**32,38,44**), 154.72 (Ar*C*-**26**), 137.07 (Ar*C*-**22**), 135.01 (Ar*C*-**28,34,40**), 133.57 (Ar*C*-**24**), 133.00-131.00 (broad Ar*C*-**3,4,8,9,13,14,18,19**), 130.76 (Ar*C*-**30,36,42**), 129.35 (Ar*C*-**21**), 127.22 (Ar*C*-**27,33,39**), 119.77-119.73 (Ar*C*-**29,35,41**), 117.36 (Ar*C*-**25**), 115.71-115.55 (Ar*C*-**31,37,43**), 114.01-113.73 (Ar*C*-**6,11,16**), 111.95-111.91 (Ar*C*-**23**), 111.53-111.30 (Ar*C*-**1**); UV-Vis ($CHCl_3$) *λ*/nm (log(*ε*/M^{-1} cm^{-1})) 419 (5.32), 513 (4.20); Accurate mass; m/z: 757.14343 (M(^{79}Br)+H)$^+$, 759.14233 (M(^{81}Br)+H)$^+$; calculated for $C_{44}H_{30}BrN_4O_4$ 757.14504 (^{79}Br); 759.14300 (^{81}Br); Anal. Calcd for $C_{44}H_{29}BrN_4O_4$: C, 69.75; H, 3.86; N, 7.40. Found: C, 69.31; H, 3.91; N, 7.13.

Synthesis of mono-bromo porphyrin cage compound (8)

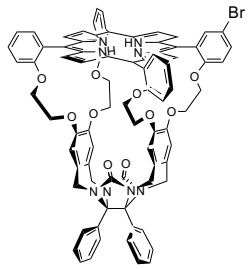

To compound **7** (549.09 mg, 0.41 mmol, 1 eq.), potassium carbonate (1.406 g, 10.19 mmol, 25 eq.), 5-(5-bromo-2-hydroxyphenyl)-10,15,20-tris(2-hydroxyphenyl)porphyrin (**6**, 306.97 mg, 0.41 mmol, 1 eq.), and acetonitrile (750 mL) were added. Argon was led through the reaction mixture for 30 min, and the solution was subsequently refluxed for 16 h. After cooling, the mixture was filtered over celite and the filtrate was evaporated to dryness. The crude product was purified by column chromatography (alumina brock III) using chloroform as the eluent. Precipitation from DCM/*n*-heptane followed by washing with *n*-pentane (4x) and drying *in vacuo* yielded the product (**8**, 92.6 mg, 0.07 mmol, 16%, racemate of two enantiomers) as a purple solid.
^{1}H-NMR ($CDCl_3$, 500 MHz): ∂ 8.80-8.74 (m, 4H, ß-pyrrole-*H*-**3,4,13,14**), 8.70-8.64 (m, 4H, ß-pyrrole-*H*-**8,9,18,19**), 8.21 (d, 1H, Ar*H*-**22**, *J* = 2.5 Hz), 8.10-8.03 (m, 3H, Ar*H*-**28,34,40**), 7.86 (dd, 1H, Ar*H*-**24**, *J* = 8.9, 2.5 Hz), 7.78-7.73 (m, 3H, Ar*H*-**30,36,42**), 7.41-7.36 (m, 3H, Ar*H*-**29,35,41**), 7.35-7.32 (m, 3H, Ar*H*-**31,37,43**), 7.21 (d, 1H, Ar*H*-**25**, *J* = 8.9 Hz), 6.98-6.91 (m, 6H, Ar*H*-**55,56**), 6.83-6.80 (m, 4H, Ar*H*-**54**), 6.19 (s, 3H, Ar*H*-**48(II, III, IV)**), 6.18 (s, 1H, Ar*H*-**48(I)**), 4.31-4.23 (m, 4H, CH_2-**45a**), 4.23 (d, 4H, CH_2-**50a**, *J* = 15.9 Hz), 4.10-4.00 (m, 4H, CH_2-**45b**), 3.74 (d, 4H, CH_2-**50b**, *J* = 15.6 Hz), 3.55-3.48 (m, 4H, CH_2-**46a**), 3.39-3.30 (m, 4H, CH_2-**46b**), -2.75 (s, 2H, N*H*); ^{13}C{^{1}H}-NMR ($CDCl_3$, 126 MHz): ∂ 158.72 (Ar*C*-**32,38,44**), 158.01 (Ar*C*-**26**), 156.99 (C=O-**51**), 146.58-146.49 (Ar*C*-**47**), 138.01 (Ar*C*-**22**), 135.77 (Ar*C*-**28,34,40**), 134.03 (Ar*C*-**21**), 133.64 (Ar*C*-**53**), 132.34 (Ar*C*-**24**), 131.80-131.76 (Ar*C*-**27,33,39**), 129.93-129.83 (Ar*C*-**49**), 129.64 (Ar*C*-**30,36,42**), 128.52-128.45 (Ar*C*-**55,56**), 128.11 (Ar*C*-**54**),

119.88-119.84 (Ar*C*-**29,35,41**), 115.59-115.39 (Ar*C*-**6,11,16**), 115.18 (Ar*C*-**48**), 113.51 (Ar*C*-**25**), 113.16 (Ar*C*-**1**), 112.33 (Ar*C*-**23**), 111.93-111.87 (Ar*C*-**31,37,43**), 84.77 (*C*-**52**), 67.43 (*C*H_2-**46**), 66.86 (*C*H_2-**45**), 44.41 (*C*H_2-**50**); UV-Vis ($CHCl_3$) *λ*/nm (log(*ε*/M^{-1} cm^{-1})) 421 (5.46), 516 (4.18); Accurate mass; m/z: 1423.39108 (M(^{79}Br)+H)$^+$, 1425.39106 (M(^{81}Br)+H)$^+$; calculated for $C_{84}H_{64}BrN_8O_{10}$ 1423.39288 (^{79}Br); 1425.39083 (^{81}Br).

Synthesis of zinc mono-bromo porphyrin cage compound (9)

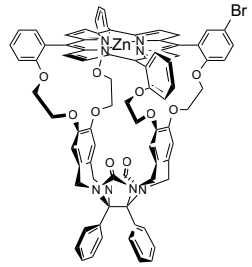

The mono-bromo porphyrin cage compound (**8**, 220 mg, 0.15 mmol, 1 eq.) was dissolved in chloroform (15 mL) and methanol (7.5 mL). Zinc(II) acetate dihydrate (119.60 mg, 0.54 mmol, 3.5 eq.) was added and the reaction mixture was stirred at r.t. for 1 h. After evaporating the mixture to dryness, the residue was purified by silicagel column chromatography using chloroform as the eluent. Precipitation from DCM/*n*-heptane followed by washing with *n*-pentane (4x) and drying *in vacuo* yielded the product (**9**, 229.4 mg, 0.15 mmol, 100%, racemate of two enantiomers) as a purple solid.
^{1}H-NMR ($CDCl_3$, 500 MHz): ∂ 8.94-8.87 (m, 4H, ß-pyrrole-*H*-**3,4,13,14**), 8.80-8.73 (m, 4H, ß-pyrrole-*H*-**8,9,18,19**), 8.23 (d, 1H, Ar*H*-**22**, *J* = 2.5 Hz), 8.12-8.03 (m, 3H, Ar*H*-**28,34,40**), 7.85 (dd, 1H, Ar*H*-**24**, *J* = 8.9, 2.6 Hz), 7.78-7.72 (m, 3H, Ar*H*-**30,36,42**), 7.40-7.35 (m, 3H, Ar*H*-**29,35,41**), 7.35-7.31 (m, 3H, Ar*H*-**31,37,43**), 7.21 (d, 1H, Ar*H*-**25**, *J* = 8.9 Hz), 6.99-6.90 (m, 6H, Ar*H*-**55,56**), 6.77-6.72 (m, 4H, Ar*H*-**54**), 6.11 (s, 3H, Ar*H*-**48(II, III, IV)**), 6.10 (s, 1H, Ar*H*-**48(I)**), 4.26-4.16 (m, 4H, CH_2-**45a**), 4.09 (d, 4H, CH_2-**50a**, *J* = 15.6 Hz), 4.06-3.94 (m, 4H, CH_2-**45b**), 3.66 (d, 4H, CH_2-**50b**, *J* = 15.8 Hz), 3.55-3.46 (m, 4H, CH_2-**46a**), 3.32-3.23 (m, 4H, CH_2-**46b**); ^{13}C{^{1}H}-NMR ($CDCl_3$, 126 MHz): ∂ 158.75 (Ar*C*-**32,38,44**), 158.04 (Ar*C*-**26**), 156.84 (C=O-**51**), 150.23-149.45 (Ar*C*-**2,5,7,10,12,15,17,20**), 146.51-146.42 (Ar*C*-**47**), 137.89 (Ar*C*-**22**), 135.56 (Ar*C*-**28,34,40**), 134.78 (Ar*C*-**21**), 133.58 (Ar*C*-**53**), 132.53 (Ar*C*-**27,33,39**), 132.10 (Ar*C*-**24**), 131.70-130.50 (Ar*C*-**3,4,8,9,13,14,18,19**), 129.89-129.79 (Ar*C*-**49**), 129.41 (Ar*C*-**30,36,42**), 128.54-128.46 (Ar*C*-**55,56**), 128.05 (Ar*C*-**54**), 119.85 (Ar*C*-**29,35,41**), 116.51-116.28 (Ar*C*-**6,11,16**), 115.19 (Ar*C*-**48**), 114.11 (Ar*C*-**1**), 113.68 (Ar*C*-**25**), 112.33 (Ar*C*-**23**), 112.11-112.04 (Ar*C*-**31,37,43**), 84.68 (*C*-**52**), 67.45 (*C*H_2-**46**), 66.94 (*C*H_2-**45**), 44.26 (*C*H_2-**50**); UV-Vis ($CHCl_3$) *λ*/nm (log(*ε*/M^{-1} cm^{-1})) 422 (5.64), 549 (4.29); MALDI-TOF; m/z: 1485.3 (M(^{79}Br)+H)$^+$, 1487.3 (M(^{81}Br)+H)$^+$; calculated for $C_{84}H_{62}BrN_8O_{10}Zn$ 1485.3 (^{79}Br); 1487.3 (^{81}Br).

Synthesis of potassium triisopropylsilylacetylene trifluoroborate (TIPSA BF_3K)

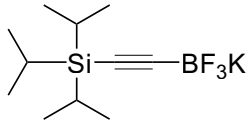

A solution of triisopropylsilylacetylene (2.0 mL, 8.9 mmol, 1 eq.) was dissolved in degassed THF (20 mL) and cooled to -78 °C. *n*-Butyl lithium (5.6 mL, 8.9 mmol, 1 eq.) was added dropwise and the reaction mixture was stirred for 1 hour. Trimethoxyborate (1.5 mL, 13 mmol, 1.5 eq.) was added dropwise, the mixture was stirred for 1 hour and then allowed to warm up to -20 °C over the course of 1 hour. Subsequently, a saturated solution of potassium bifluoride (4.30 g, 55.1 mmol, 6.2 eq.) in water was added under vigorous stirring. The mixture was stirred at -20 °C for 1 hour, after which it was allowed to warm to room temperature. The solvent was evaporated and the resulting white residue was dried under vacuum for 2 hours. The residue was washed with subsequently acetone and hot acetone and the filtrate was evaporated to yield a white solid, which was re-precipitated from hot acetone/petroleum ether (80-100). After cooling the suspension to -20°C, the precipitate was filtered off and the residue was washed with *n*-pentane. After drying in air and under vacuum, the product was obtained as a white, fluffy solid (1.0 g, 3.6 mmol, 40%).

^{1}H-NMR (Acetone-d_6, 400 MHz): δ 1.08-1.10 (m, 18H, CH(CH_3)$_2$), 0.93-1.03 (m, 3H, CH(CH$_3$)$_2$); ^{19}F-NMR (acetone-d_6, 380 MHz) δ 135.5 (1:1:1:1, *J* = 34 Hz); ^{29}Si-NMR (acetone-d_6, 80 MHz) δ (ppm) -5.63 (s); ^{11}B-NMR (acetone-d_6, 133 MHz,) δ -2.15 (q, *J* = 36 Hz).

Synthesis of the TIPS-protected acetylene functionalized porphyrin cage compound (10)

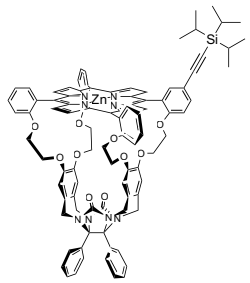

Zinc mono-bromo porphyrin cage compound (**9**, 288 mg, 0.19 mmol, 1 eq.), potassium triisopropylsilylacetylene trifluoroborate (111.7 mg, 0.39 mmol, 2 eq.), cesium carbonate (315.8 mg, 0.97 mmol, 5 eq.), and [1,1'-bis(diphenylphosphino) ferrocene]dichloropalladium(II) (39.8 mg, 0.05 mmol, 0.25 eq.) were dissolved in THF (42.75 mL) and water (2.25 mL) under an argon atmosphere. The reaction mixture was refluxed for 16 h. After cooling to r.t., the mixture was diluted with DCM and the solution was subsequently washed with water (4 x 50 mL). The organic layer was dried over $MgSO_4$, filtered, and evaporated to dryness. The crude product was purified by silicagel column chromatography using 1% MeOH in $CHCl_3$ as the eluent yielding the product (**10**, 285.4 mg, 0.18 mmol, 93%, racemate of two enantiomers) as a purple solid.

^{1}H-NMR ($CDCl_3$, 500 MHz): ∂ 8.93-8.85 (m, 4H, ß-pyrrole-H-**3,4,13,14**), 8.74-8.67 (m, 4H, ß-pyrrole-H-**8,9,18,19**), 8.19 (d, 1H, Ar*H*-**22**, *J* = 2.1 Hz), 8.01-7.96 (m, 2H, Ar*H*-**28,40**), 7.95-7.91 (m, 1H, Ar*H*-**34**), 7.87 (dd, 1H, Ar*H*-**24**, *J* = 8.5, 2.1 Hz), 7.74-7.68 (m, 3H, Ar*H*-**30,36,42**), 7.33-7.29 (m, 3H, Ar*H*-**31,37,43**), 7.29-7.24 (m, 3H,

Ar*H*-**29,35,41**), 7.22 (d, 1H, Ar*H*-**25**, *J* = 8.6 Hz), 6.97-6.91 (m, 6H, Ar*H*-**55,56**), 6.44 (bs, 4H, Ar*H*-**54**), 5.86-5.73 (m, 4H, Ar*H*-**48**), 4.17-4.07 (m, 4H, CH_2-**45a**), 3.95-3.84 (m, 4H, CH_2-**45b**), 3.55 (bs, 4H, CH_2-**50a**), 3.47-3.39 (m, 4H, CH_2-**46a**), 3.39-3.29 (m, 4H, CH_2-**50b**), 3.17-3.05 (m, 4H, CH_2-**46b**), 1.07 (bs, 21H, TIPS); ^{13}C{^{1}H}-NMR ($CDCl_3$, 126 MHz): ∂ 159.05 (Ar*C*-**26**), 158.84-158.81 (Ar*C*-**32,44**), 158.76 (Ar*C*-**38**), 156.40-156.37 (C=O-**51**), 150.10-149.60 (Ar*C*-**2,5,7,10,12,15,17,20**), 146.32-146.08 (Ar*C*-**47**), 138.60 (Ar*C*-**22**), 135.54 (Ar*C*-**28,40**), 135.39 (Ar*C*-**34**), 133.51 (Ar*C*-**24**), 133.23 (Ar*C*-**53**), 132.85 (Ar*C*-**21**), 132.79-132.75 (Ar*C*-**27,33,39**), 131.50-130.50 (Ar*C*-**3,4,8,9,13,14,18,19**), 129.37 (Ar*C*-**49**), 129.31-129.22 (Ar*C*-**30,36,42**), 128.51 (Ar*C*-**55,56**), 127.86 (Ar*C*-**54**), 119.94-119.82 (Ar*C*-**29,35,41**), 116.07 (Ar*C*-**11**), 115.91-115.88 (Ar*C*-**6,16**), 114.87 (Ar*C*-**23**), 114.78 (Ar*C*-**48**), 114.38 (Ar*C*-**1**), 112.39-112.27 (Ar*C*-**31,37,43**), 111.92 (Ar*C*-**25**), 107.10 (Ar*C*-**57**), 88.95 (Ar*C*-**58**), 84.37 (*C*-**52**), 67.37-67.19 (*C*H$_2$-**46**), 67.02-66.96 (*C*H$_2$-**45**), 43.76 (*C*H$_2$-**50**), 18.69 (TIPS-*C*), 11.33 (TIPS-*C*); MALDI-TOF; m/z: 1587.5 $(M+H)^+$, calculated for $C_{95}H_{83}N_8O_{10}SiZn$ 1587.5.

Synthesis of the acetylene functionalized porphyrin cage compound (11)

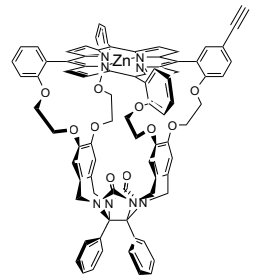

Argon was led through THF (75 mL) for 30 min and compound **10** (372 mg, 0.23 mmol, 1 eq.) and tetrabutylammonium fluoride trihydrate (739.5 mg, 2.34 mmol, 10 eq.) were added. The reaction mixture was stirred in the dark at r.t. for 4 h and was then evaporated to dryness. The residue was dissolved in DCM and this solution was washed with water (3 x 50 mL), dried over Na_2SO_4, filtered and evaporated to dryness. The crude product was purified by silicagel column chromatography using 0.5% MeOH in $CHCl_3$ as the eluent. Precipitation from DCM/*n*-heptane followed by washing with *n*-pentane (4x) and drying *in vacuo* yielded the product (**11**, 244 mg, 0.17 mmol, 73%, racemate of two enantiomers) as a purple solid.

^{1}H-NMR ($CDCl_3$, 500 MHz): ∂ 8.91-8.87 (m, 4H, ß-pyrrole-*H*-**3,4,13,14**), 8.77-8.71 (m, 4H, ß-pyrrole-*H*-**8,9,18,19**), 8.24 (d, 1H, Ar*H*-**22**, *J* = 2.2 Hz), 8.10-8.03 (m, 3H, Ar*H*-**28,34,40**), 7.89 (dd, 1H, Ar*H*-**24**, *J* = 8.6, 2.2 Hz), 7.77-7.72 (m, 3H, Ar*H*-**30,36,42**), 7.38-7.34 (m, 3H, Ar*H*-**29,35,41**), 7.34-7.32 (m, 3H, Ar*H*-**31,37,43**), 7.27 (d, 1H, Ar*H*-**25**, *J* = 8.7 Hz), 6.97-6.92 (m, 6H, Ar*H*-**55,56**), 6.74-6.68 (m, 4H, Ar*H*-**54**), 6.09-6.05 (m, 4H, Ar*H*-**48**), 4.28-4.15 (m, 4H, CH_2-**45a**), 4.07-3.96 (m, 8H, CH_2-**45b**, CH_2-**50a**), 3.63 (d, 4H, CH_2-**50b**, *J* = 16.0 Hz), 3.54-3.47 (m, 4H, CH_2-**46a**), 3.32-3.22 (m, 4H, CH_2-**46b**), 3.05 (s, 1H, alkyne*H*-**58**); ^{13}C{^{1}H}-NMR ($CDCl_3$, 126 MHz): ∂ 159.22 (Ar*C*-**26**), 158.80-158.74 (Ar*C*-**32,38,44**), 156.80 (C=O-**51**), 150.18-149.55 (Ar*C*-**2,5,7,10,12,15,17,20**), 146.49-146.35 (Ar*C*-**47**), 139.07 (Ar*C*-**22**), 135.58-135.59 (Ar*C*-**28,34,40**), 133.54 (Ar*C*-**24**), 133.50 (Ar*C*-**53**), 132.81 (Ar*C*-**21**), 132.67-132.59 (Ar*C*-**27,33,39**), 131.60-130.56 (Ar*C*-**3,4,8,9,13,14,18,19**), 129.83-129.67 (Ar*C*-**49**), 129.36

(Ar*C*-**30,36,42**), 128.53-128.47 (Ar*C*-**55,56**), 128.04 (Ar*C*-**54**), 119.85 (Ar*C*-**29,35,41**), 116.32-116.13 (Ar*C*-**6,11,16**), 115.16-114.97 (Ar*C*-**48**), 114.46 (Ar*C*-**1**), 113.37 (Ar*C*-**23**), 112.18-112.07 (Ar*C*-**31,37,43**), 111.70 (Ar*C*-**25**), 84.66 (*C*-**52**), 83.76 (alkyne*C*-**57**), 76.12 (alkyne*C*-**58**), 67.45-67.40 (CH_2-**46**), 66.95-66.93 (CH_2-**45**), 44.21 (CH_2-**50**); MALDI-TOF; m/z: 1431.3 $(M+H)^+$, calculated for $C_{86}H_{63}N_8O_{10}Zn$ 1431.4.

Synthesis of 1,3-Diazidopropane

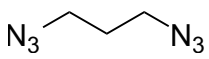

Sodium azide-1-^{15}N (490 mg, 7.43 mmol, 3 eq.) and 1,3-dibromopropane (0.25 mL, 2.48 mmol, 1 eq.) were dissolved in DMF (16 mL) and the reaction mixture was heated at 85°C for 20 h. After cooling to r.t., water (100 mL) was added to the mixture and the resulting solution was extracted with diethyl ether. Subsequently the organic layer was washed with water (5 x 100 mL) and brine (2 x 100 mL), dried over Na_2SO_4, filtrated, and evaporated to almost dryness to yield the product as a clear solution in diethyl ether (96%, based on ^{1}H NMR integrals).

^{1}H NMR ($CDCl_3$, 500 MHz): ∂ 3.42 (t, 4H, $N_3CH_2CH_2CH_2N_3$, *J* = 6.5 Hz), 1.87-1.80 (m, 2H, $N_3CH_2CH_2CH_2N_3$); ^{13}C NMR ($CDCl_3$, 126 MHz): ∂ 48.58 ($N_3CH_2CH_2CH_2N_3$), 28.47 ($N_3CH_2CH_2CH_2N_3$); ^{15}N NMR▪ ($CDCl_3$, 51 MHz): ∂ 247.78 (s, N**N*N*$CH_2CH_2CH_2$N**N*N*), 211.36 (s, *N**NN*$CH_2CH_2CH_2$N*N*N**), 69.69 (s, N*N*N**$CH_2CH_2CH_2$*N**NN*); ▪ 50% of the indicated N atoms are ^{15}N-labeled.

Synthesis of 1,5-Diazidopentane

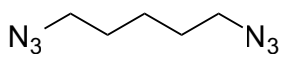

Sodium azide-1-^{15}N (486 mg, 7.37 mmol, 2.8 eq.) and 1,5-dibromopentane (0.35 mL, 2.57 mmol, 1 eq.) were dissolved in DMF (15 mL) and the reaction mixture was heated at 80°C for 16 h. After cooling to r.t., water (100 mL) was added to the mixture and the resulting solution was extracted with diethyl ether (2 x 150 mL). Subsequently the organic layer washed with brine (2 x 100 mL), dried over Na_2SO_4, filtrated and the evaporated to almost dryness to yield the product as a clear solution in diethyl ether (75%, based on ^{1}H NMR integrals).

^{1}H NMR ($CDCl_3$, 500 MHz): ∂ 3.29 (t, 4H, $N_3CH_2(CH_2)_3CH_2N_3$, *J* = 6.8 Hz), 1.60-1.52 (m, 4H, $N_3CH_2CH_2CH_2CH_2CH_2N_3$), 1.45-1.35 (m, 2H, $N_3(CH_2)_2CH_2(CH_2)_2N_3$); ^{15}N NMR▪ ($CDCl_3$, 51 MHz): ∂ 242.94 (s, N**N*N*$CH_2(CH_2)_3CH_2$N**N*N*), 205.87 (s, *N**N-N*$CH_2(CH_2)_5CH_2$N*N*N**), 66.78 (s, N*N*N**$CH_2(CH_2)_3CH_2$*N**NN*); ▪ 50% of the indicated N atoms are ^{15}N-labeled.

Synthesis of 1,11-Diazidoundecane

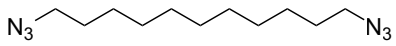

Sodium azide-1-^{15}N (500 mg, 7.58 mmol, 3 eq.) and 1,11-dibromoundecane (0.60 mL, 2.53 mmol, 1 eq.) were dissolved in DMF (15 mL). The reaction mixture was stirred at 80°C for 20 h. After cooling to r.t., water

(150 mL) was added to the mixture and the resulting solution was extracted with diethyl ether (2 x 100 mL). Subsequently, the organic layer was washed with water (10 x 200 mL) and brine (2 x 200 mL), dried over Na_2SO_4, filtered and evaporated to almost dryness to yield the product as a clear solution in diethyl ether (45 %, based on ^{1}H NMR integrals).

^{1}H-NMR ($CDCl_3$, 500 MHz): ∂ 3.26 (t, 4H, $N_3CH_2(CH_2)_9CH_2N_3$, *J* = 7 Hz), 1.62-1.56 (m, 4H, $N_3CH_2CH_2(CH_2)_7CH_2CH_2N_3$), 1.39-1.28 (m, 14H, $N_3(CH_2)_2(CH_2)_7(CH_2)_2N_3$); ^{13}C NMR ($CDCl_3$, 126 MHz): ∂ 51.49 ($N_3CH_2CH_2CH_2(CH_2)_5CH_2CH_2CH_2N_3$), 51.46 ($N_3CH_2CH_2CH_2(CH_2)_5CH_2CH_2CH_2N_3$), 29.44 ($N_3CH_2CH_2CH_2(CH_2)_5CH_2CH_2CH_2N_3$), 29.41 ($N_3CH_2CH_2CH_2(CH_2)_5CH_2CH_2CH_2N_3$), 29.14 ($N_3CH_2CH_2CH_2(CH_2)_5CH_2CH_2CH_2N_3$), 28.8 ($N_3CH_2CH_2CH_2(CH_2)_5CH_2CH_2CH_2N_3$), 26.7 ($N_3CH_2CH_2CH_2(CH_2)_5CH_2CH_2CH_2N_3$; ^{15}N NMR▪ ($CDCl_3$, 51 MHz): *δ* 248.5 (s, N**N*N*$CH_2(CH_2)_9CH_2$N**N*N*), 210.5 (s, *N**N-N*$CH_2(CH_2)_9CH_2$N*N*N**), 71.9 (s, N*N*N**$CH_2(CH_2)_9CH_2$*N**NN*); ▪ 50% of the indicated N atoms are ^{15}N-labeled.

Synthesis of Zn_2C_3DC

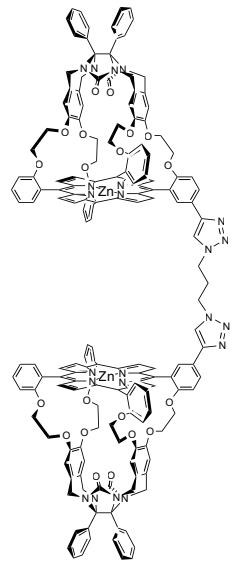

To a mixture of compound **11** (135.5 mg, 0.09 mmol, 2 eq.) and copper(I) iodide (9.36 mg, 0.05 mmol, 1 eq.) in freshly distilled THF (19 mL) and freshly distilled MeCN (19 mL), DIPEA (15.80 µL, 0.09 mmol, 2 eq.) was added. A solution of 1,3-diazidopropane-^{15}N enriched in THF (74.3 µL, 0.57 M, 0.04 mmol, 0.9 eq.) was added and the reaction mixture was stirred in the dark at r.t. for 9 days. On days 2 and 4 additional CuI (12.08 mg and 21.15 mg, resp.) and DIPEA (2 x 15.80 µl) were added. The mixture was diluted with DCM (50 mL) and washed with water (3 x 50 mL). The organic layer was evaporated and the crude product was purified by silicagel column chromatography starting using a gradient of 1-5% of MeOH in $CHCl_3$ as the eluent. Precipitation from DCM/*n*-heptane followed by washing with *n*-pentane (4x) and drying *in vacuo* yielded the product (**Zn_2C_3DC**, 44.8 mg, 0.02 mmol, 35%) as a purple solid.

^{1}H-NMR (DMSO-d_6 at 333.15 K, 500 MHz): ∂ 8.79 (dd, 2H, β-pyrrole-*H*, *J* = 4.6, 1.2 Hz), 8.75-8.70 (m, 6H, β-pyrrole-*H*), 8.58-8.49 (m, 8H, β-pyrrole-*H*) 8.50-8.47 (m, 2H, Triazole-*H*-**58**), 8.33 (t, 2H, Ar*H*-**22**, *J* = 2.4 Hz), 8.19 (dd, 1H, Ar*H*-**24***, *J* = 8.5, 2.3 Hz), 8.18 (dd, 1H, Ar*H*-**24***, *J* = 8.5, 2.3 Hz) 7.92-7.82 (m, 6H, Ar*H*-**28**, **34**, **40**), 7.79-7.66 (m, 6H, Ar*H*-**30**, **36**, **42**), 7.56-7.48 (m, 6H, Ar*H*-**31**, **37**, **43**), 7.46 (d, 1H, Ar*H*-**25***, *J* = 8.7 Hz), 7.39 (d, 1H, Ar*H*-**25***, *J* = 8.9 Hz), 7.37-7.19 (m, 6H, Ar*H*-**29**, **35**, **41**), 7.05-6.94 (m, 12H, Ar*H*-**55**, **56**), 6.84-6.78 (m, 6H, Ar*H*-**48(II,III,IV)**), 6.20 (s, 1H, Ar*H*-**48(I)***), 6.19 (s, 1H, Ar*H*-**48(I)***), 4.43 (t, 4H, CH_2-**62**, *J* = 6.8 Hz), 4.22-4.03 (m, 24H, CH_2-**45**, CH_2-**50a**), 3.65

(d, 8H, CH_2-**50b**, *J* = 15.7 Hz), 3.51-3.40 (m, 8H, CH_2-**46a**), 3.28-3.22 (m, 8H, CH_2-**46b**), 2.51-2.46 (m, 2H, CH_2-**63**); ^{13}C NMR† (DMSO-d_6 at 333.15 K, 126 MHz): ∂ 158.40 (Ar*C*-**32**, **38**, **44**), 156.00 (*C*=O-**51**), 155.86 (*C*=O-**51**), 149.37 (Ar*C*-**2**, **5**, **7**, **10**, **12**, **15**, **17**, **20**), 148.57 (Ar*C*-**2**, **5**, **7**, **10**, **12**, **15**, **17**, **20**), 146.07 (*C*-**57**), 145.69 (Ar*C*-**47**), 134.53 (Ar*C*-**28**, **34**, **40**), 133.06 (Ar*C*-**53**), 132.40 (Ar*C*-**27**, **33**, **39**), 131.70 (Ar*C*-**22**), 130.21 (Ar*C*-**3**, **4**, **8**, **9**, **13**, **14**, **18**, **19**), 129.89 (Ar*C*-**3**, **4**, **8**, **9**, **13**, **14**, **18**, **19**), 129.81 (Ar*C*-**49**), 128.83 (Ar*C*-**30**, **36**, **42**), 127.79 (Ar*C*-**55**, **56**), 127.40 (Ar*C*-**54**), 125.67 (Ar*C*-**24**), 120.44 (*C*H-**58**), 119.16 (Ar*C*-**29**, **35**, **41**), 114.79 (Ar*C*-**48(II,III,IV)**), 114.46 (Ar*C*-**48(I)**), 112.62 (Ar*C*-**25**), 112.60 (Ar*C*-**31**, **37**, **43**), 84.00 (*C*-**52**), 83.83 (*C*-**52**), 67.06 (*C*H_2-**46**), 66.66 (*C*H_2-**45**), 46.44 (*C*H_2-**62**), 43.18 (*C*H_2-**50**), 29.28 (*C*H_2-**63**); ^{15}N{^{1}H}-NMR▪ (DMSO-d_6 at 333.15 K, 51 MHz): ∂ 346.54 (Triazole-*N*-**61***), 346.47 (Triazole-*N*-**61***), 248.55 (Triazole-*N*-**59***), 248.50 (Triazole-*N*-**59***); Accurate MALDI-TOF; m/z: 2988.7613 $(M)^+$, calculated for $C_{175}H_{130}N_{20}{}^{15}N_2O_{20}{}^{64}Zn_2$ 2988.8355. *Peaks belonging to the two different diastereoisomers that could not be separated. † ^{13}C-NMR shifts obtained via HSQC and HMBC spectra as no ^{13}C{^{1}H}-NMR spectrum was recorded. ▪ 50% of the indicated N atoms are ^{15}N-labeled.

Synthesis of Zn_2C_5DC

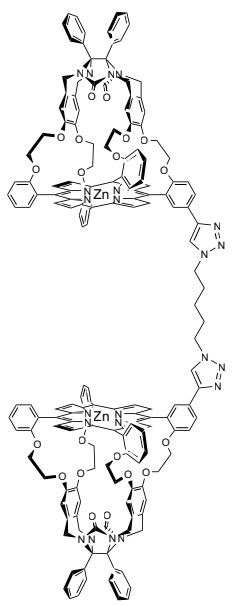

To a mixture of compound **11** (134.1 mg, 0.09 mmol, 2 eq.) and copper(I) iodide (10.2 mg, 0.05 mmol, 1 eq.) in freshly distilled THF (19 mL) and freshly distilled MeCN (19 mL), DIPEA (15.80 µL, 0.09 mmol, 2 eq.) was added. A solution of 1,5-diazidopentane-^{15}N enriched in THF (51.2 µL, 0.83 M, 0.04 mmol, 0.9 eq.) was added and the reaction mixture was stirred in the dark at r.t. for 7 days. On days 2 and 4 additional CuI (20.26 mg and 10.44 mg, resp.) and DIPEA (2 x 15.80 µL) were added. The mixture was concentrated *in vacuo* and the crude product was purified by silicagel column chromatography using a gradient of 0.7-5% MeOH in $CHCl_3$ as the eluent. Precipitation from DCM/*n*-heptane followed by washing with *n*-pentane (4x) and drying *in vacuo* yielded the product (**Zn_2C_5DC**, 39.7 mg, 0.01 mmol, 31%) as a purple solid.

^{1}H-NMR (DMSO-d_6 at 333.15 K, 500 MHz): ∂ 8.80 (dd, 2H, β-pyrrole-*H*, *J* = 4.7, 3.5 Hz), 8.76-8.72 (m, 6H, β-pyrrole-*H*), 8.59 (d, 2H, β-pyrrole-*H*, *J* = 4.6 Hz) 8.55-8.52 (m, 6H, β-pyrrole-*H*), 8.48-8.45 (m, 2H, Triazole-*H*-**58**), 8.34 (t, 2H, Ar*H*-**22**, *J* = 1.9 Hz), 8.20 (dd, 2H, Ar*H*-**24**, *J* = 8.6, 2.2 Hz), 7.91-7.86 (m, 6H, Ar*H*-**28**, **34**, **40**), 7.79-7.67 (m, 6H, Ar*H*-**30**, **36**, **42**), 7.54-7.46 (m, 6H, Ar*H*-**31**, **37**, **43**), 7.44 (dd, 2H, Ar*H*-**25***, *J* = 8.8, 5.9 Hz), 7.38-7.27 (m, 6H, Ar*H*-**29**, **35**, **41**), 7.04-6.95 (m, 12H, Ar*H*-**55**, **56**), 6.83-6.78 (m, 8H, Ar*H*-**54**), 6.27-6.23 (m, 6H, Ar*H*-

48(II,III,IV)), 6.18 (s, 1H, Ar*H*-**48(I)***), 6.16 (s, 1H, Ar*H*-**48(I)***), 4.41 (t, 4H, CH_2-**62**, *J* = 6.9 Hz), 4.20-4.00 (m, 24H, CH_2-**45**, CH_2-**50a**), 3.68-3.57 (m, 8H, CH_2-**50b**), 3.53-3.40 (m, 8H, CH_2-**46a**), 3.27-3.20 (m, 8H, CH_2-**46b**), 1.85 (p, 4H, CH_2-**63**, *J* = 7.3 Hz), 1.30-1.22 (m, 2H, CH_2-**64**); ^{13}C NMR† (DMSO-d_6 at 333.15 K, 126 MHz): ∂ 158.27 (Ar*C*-**32**, **38**, **44**), 157.92 (Ar*C*-**26**), 155.88 (*C*=O-**51**), 155.72 (*C*=O-**51**), 149.20 (Ar*C*-**2**, **5**, **7**, **10**, **12**, **15**, **17**, **20**), 148.47 (Ar*C*-**2**, **5**, **7**, **10**, **12**, **15**, **17**, **20**), 145.84 (*C*-**57**), 145.55 (Ar*C*-**47(II, III, IV)**), 145.42 (Ar*C*-**47(I)**), 134.60 (Ar*C*-**28**, **34**, **40**), 132.92 (Ar*C*-**53**), 132.42 (Ar*C*-**21**), 132.24 (Ar*C*-**27**, **33**, **39**), 131.75 (Ar*C*-**22**), 130.28 (Ar*C*-**3**, **4**, **8**, **9**, **13**, **14**, **18**, **19**), 129.91 (Ar*C*-**3**, **4**, **8**, **9**, **13**, **14**, **18**, **19**), 129.66 (Ar*C*-**49(II, III, IV)**), 129.51 (Ar*C*-**49(I)**), 128.89 (Ar*C*-**30**, **36**, **42**), 127.84 (Ar*C*-**55**, **56**), 127.41 (Ar*C*-**54**), 125.68 (Ar*C*-**24**), 122.16 (Ar*C*-**23**), 120.17 (*C*H-**58**), 119.21 (Ar*C*-**29**, **35**, **41**), 115.13 (Ar*C*-**6**, **11**, **16**), 114.82 (Ar*C*-**48(II,III,IV)**), 114.67 (Ar*C*-**1**), 114.47 (Ar*C*-**48(I)***), 114.36 (Ar*C*-**48(I)***), 112.67 (Ar*C*-**25**, **31**, **37**, **43**), 83.83 (*C*-**52**), 83.71 (*C*-**52**), 67.07 (*C*H_2-**46**), 66.69 (*C*H_2-**45**), 48.68 (*C*H_2-**62**), 43.19 (*C*H_2-**50**), 28.33 (*C*H_2-**64**), 28.27 (*C*H_2-**63**); ^{15}N{^{1}H}-NMR▪ (DMSO-d_6 at 333.15 K, 51 MHz): ∂ 345.64 (Triazole-*N*-**61***), 345.61 (Triazole-*N*-**61***), 250.67 (Triazole-*N*-**59***), 250.59 (Triazole-*N*-**59***); Accurate MALDI-TOF; m/z: 3016.8603 $(M)^+$, calculated for $C_{177}H_{134}N_{20}{}^{15}N_2O_{20}{}^{64}Zn_2$ 3016.8668. *Peaks belonging to the two different diastereoisomers that could not be separated. † ^{13}C-NMR shifts obtained via HSQC and HMBC spectra as no ^{13}C{^{1}H}-NMR spectrum was recorded. ▪ 50% of the indicated N atoms are ^{15}N-labeled.

Synthesis of $Zn_2C_{11}DC$

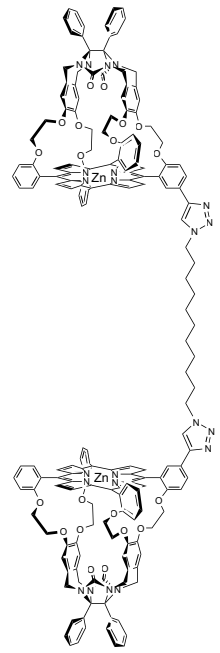

To a solution of compound **11** (134.8 mg, 0.09 mmol, 2 eq.) and copper(I) iodide (11.4 mg, 0.06 mmol, 1.5 eq.) in freshly distilled THF (19 mL) and freshly distilled MeCN (19 mL), DIPEA (15.80 µL, 0.09 mmol, 2 eq.) was added. A solution of 1,11-diazidoundecane-^{15}N enriched in THF (304 µL, 0.14 M, 0.04 mmol, 0.9 eq.) was added and the reaction mixture was stirred in the dark at r.t. for 6 days. On days 3 and 5 additional CuI (16.78 mg and 19.24 mg, resp.) and DIPEA (2x 15.80 µL) were added. The mixture was concentrated *in vacuo* and the crude products was purified by silicagel column chromatography using a gradient of 0.5%-5% MeOH in $CHCl_3$ as the eluent. Precipitation from DCM/*n*-heptane followed by washing with *n*-pentane (4x) and drying *in vacuo* yielded the product (**$Zn_2C_{11}DC$**, 81.9 mg, 0.03 mmol, 62%) as a purple solid.

^{1}H-NMR (DMSO-d_6 at 333.15 K, 500 MHz): ∂ 8.80 (dd, 2H, β-pyrrole-*H*, *J* = 4.6, 2.1 Hz), 8.76-8.70 (m, 6H, β-pyrrole-*H*), 8.59 (t, 2H, β-pyrrole-*H*, *J* = 4.2 Hz) 8.56-8.49 (m, 6H,

β-pyrrole-*H*), 8.47-8.44 (m, 2H, Triazole-*H*-**58**), 8.36-8.34 (m, 2H, Ar*H*-**22**), 8.23 (dt, 2H, Ar*H*-**24**, *J* = 8.7, 1.7 Hz), 7.92-7.88 (m, 6H, Ar*H*-**28**, **34**, **40**), 7.79-7.68 (m, 6H, Ar*H*-**30**, **36**, **42**), 7.56 (d, 2H, Ar*H*-**25**, *J* = 8.8 Hz), 7.54-7.41 (m, 6H, Ar*H*-**31**, **37**, **43**), 7.38-7.27 (m, 6H, Ar*H*-**29**, **35**, **41**), 7.04-6.95 (m, 12H, Ar*H*-**55**, **56**), 6.83-6.79 (m, 8H, Ar*H*-**54**), 6.26-6.20 (m, 8H, Ar*H*-**48**), 4.24 (t, 4H, CH_2-**62**, *J* = 6.9 Hz), 4.21-4.04 (m, 24H, CH_2-**45**, CH_2-**50a**), 3.69-3.59 (m, 8H, CH_2-**50b**), 3.53-3.38 (m, 8H, CH_2-**46a**), 3.29-3.18 (m, 8H, CH_2-**46b**), 1.79-1.71 (m, 4H, CH_2-**63**), 1.19-1.11 (m, 14H, CH_2-**64**, **65**, **66**, **67**); ^{13}C NMR† (DMSO-d_6 at 333.15 K, 126 MHz): ∂ 158.56 (Ar*C*-**32**, **38**, **44**), 158.23 (Ar*C*-**26**), 156.16 (*C*=O-**51**), 156.03 (*C*=O-**51**), 149.51 (Ar*C*-**2**, **5**, **7**, **10**, **12**, **15**, **17**, **20**), 148.75 (Ar*C*-**2**, **5**, **7**, **10**, **12**, **15**, **17**, **20**), 146.13 (*C*-**57**), 145.80 (Ar*C*-**47**), 134.57 (Ar*C*-**28**, **34**, **40**), 133.23 (Ar*C*-**53**), 132.81 (Ar*C*-**21**), 132.56 (Ar*C*-**27**, **33**, **39**), 131.70 (Ar*C*-**22**), 130.23 (Ar*C*-**3**, **4**, **8**, **9**, **13**, **14**, **18**, **19**), 129.93 (Ar*C*-**49**), 129.87 (Ar*C*-**3**, **4**, **8**, **9**, **13**, **14**, **18**, **19**), 128.84 (Ar*C*-**30**, **36**, **42**), 127.79 (Ar*C*-**55**, **56**), 127.34 (Ar*C*-**54**), 125.56 (ArC-**24**), 122.52 (Ar*C*-**23**), 120.10 (*C*H-**58**), 119.16 (Ar*C*-**29**, **35**, **41**), 115.52 (Ar*C*-**6**, **11**, **16**), 114.70 (Ar*C*-**48**), 112.66 (Ar*C*-**25**, **31**, **37**, **43**), 84.08 (*C*-**52**), 67.02 (*C*H_2-**46**), 66.61 (*C*H_2-**45**), 48.93 (*C*H_2-**62**), 43.20 (*C*H_2-**50**), 28.84 (*C*H_2-**63**), 28.08 (*C*H_2-**62**), 28.02 (*C*H_2-**64**), 27.67 (*C*H_2-**65**), 25.18 (*C*H_2-**66**, **67**); ^{15}N{^{1}H}-NMR▪ (DMSO-d_6 at 333.15 K, 51 MHz): ∂ 345.45 (Triazole-*N*-**61**), 251.16 (Triazole-*N*-**59**); Accurate MALDI-TOF; m/z: 3100.9959 $(M)^+$, calculated for $C_{183}H_{146}N_{20}{}^{15}N_2O_{20}{}^{64}Zn_2$ 3100.9607. *Peaks belonging to the two different diastereoisomers that could not be separated. † ^{13}C-NMR shifts obtained via HSQC and HMBC spectra as no ^{13}C{^{1}H}-NMR spectrum was recorded. ▪ 50% of the indicated N atoms are ^{15}N-labeled.

Synthesis of H_4C_3DC

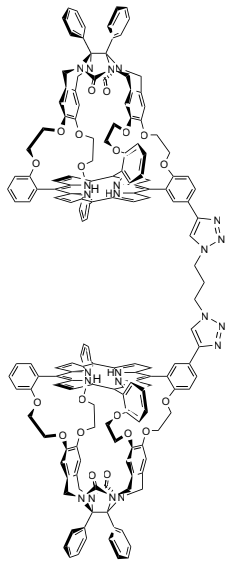

Zn_2C_3DC (65.93 mg, 22 µmol) was dissolved in $CHCl_3$ (100 mL) after which HCl (6M, 200 mL) was added and the reaction mixture was stirred at r.t. for 2 h. Subsequently, the organic layer was washed with sat. aq. $NaHCO_3$ (200 mL) and water (200 mL), dried over Na_2SO_4, filtrated, and evaporated to dryness. The crude product was purified by silicagel column chromatography using 1.5% MeOH in $CHCl_3$ as the eluent. Precipitation from DCM/*n*-heptane followed by washing with *n*-pentane (4x) and drying *in vacuo* yielded the product (**H_4C_3DC**, 43.16 mg, 15 µmol, 68%) as a purple solid.

^{1}H-NMR°,• ($CDCl_3$, 500 MHz): ∂ 8.80-8.76 (m, 4H, β-pyrrole-*H*), 8.76-8.70 (m, 4H, β-pyrrole-*H*), 8.69-8.65 (m, 4H, β-pyrrole-*H*), 8.65-8.59 (m, 4H, β-pyrrole-*H*), 8.40 (dd, 2H, Ar*H*-**22**, *J* = 4.3, 2.4 Hz), 8.28-8.21 (m, 2H, Ar*H*-**24**), 8.08-7.97 (m, 6H, Ar*H*-**28**, **34**, **40**), 7.79-7.75 (m, 2H, Triazole-*H*-**58**), 7.76-7.63 (m, 6H, ArH-**30**, **36**, **42**), 7.38-7.22

(m, 12H, Ar*H*-**29**, **31**, **35**, **37**, **41**, **43**), 7.26 (1H, Ar*H*-**25#**), 7.20 (1H, Ar*H*-**25◊**), 7.01-6.90 (m, 12H, Ar*H*-**55**, **56**), 6.85-6.77 (m, 8H, Ar*H*-**54**), 6.23-6.17 (m, 6H, Ar*H*-**48(II,III,IV)**), 6.16 (s, 1H, Ar*H*-**48(I)#**), 6.13 (s, 1H, Ar*H*-**48(I)◊**), 4.32 (t, 4H, CH_2-**62**, *J* = 6.1 Hz), 4.28-4.20 (m, 6H, CH_2-**45a(II, III, IV)**), 4.23 (d, 8H, CH_2-**50a**, *J* = 16.2 Hz), 4.20 (1H, CH_2-**45a(I)#**), 4.12 (1H, CH_2-**45a(I)◊**), 4.08-4.00 (m, 6H, CH_2-**45b(II, III, IV)**), 3.96 (1H, CH_2-**45b(I)#**), 3.88 (1H, CH_2-**45b(I)◊**), 3.80-3.67 (m, 8H, CH_2-**50b**, *J* = 15.4 Hz), 3.55-3.42 (m, 6H, CH_2-**46a(II, III, IV)**), 3.47 (1H, CH_2-**46a(I)#**), 3.39-3.28 (m, 6H, CH_2-**46b(II, III, IV)**), 3.37 (1H, CH_2-**46a(I)◊**), 3.33 (1H, CH_2-**46b(I)#**), 3.27 (1H, CH_2-**46b(I)◊**), 2.52-2.41 (m, 2H, CH_2-**63**), -2.74 (s, 2H, N*H*); ^{13}C NMR• ($CDCl_3$, 126 MHz): ∂ 158.86 (Ar*C*-**26**), 158.76 (Ar*C*-**32**, **38**, **44**), 157.07 (*C*=O-**51**), 147.84 (*C*-**57**), 146.62 (Ar*C*-**47**), 135.78 (Ar*C*-**28**, **34**, **40**), 133.21 (Ar*C*-**22**), 131.90 (Ar*C*-**27**, **33**, **39**), 132.20 (Ar*C*-**21**), 129.85 (Ar*C*-**49**), 129.63 (Ar*C*-**30**, **36**, **42**), 128.53 (Ar*C*-**55**, **56**), 128.20 (Ar*C*-**54**), 127.13 (Ar*C*-**24**), 122.10 (Ar*C*-**23**), 120.07 (*C*H-**58**), 119.83 (Ar*C*-**29**, **35**, **41**), 115.30 (Ar*C*-**6**, **11**, **16**) 115.27 (Ar*C*-**48(II,III,IV)**), 115.01 (Ar*C*-**48(I)**), 114.50 (Ar*C*-**1**), 112.20 (Ar*C*-**25**), 111.92 (Ar*C*-**31**, **37**, **43**), 84.78 (*C*-**52**), 67.44 (*C*H_2-**46(II, III, IV)**), 67.20 (*C*H_2-**46(I)#**), 67.13 (*C*H_2-**46(I)◊**), 66.90 (*C*H_2-**45(II, III, IV)**), 66.87 (*C*H_2-**45(I)#**), 66.78 (*C*H_2-**45(I)◊**), 46.65 (*C*H_2-**62**), 44.43 (*C*H_2-**50**), 30.54 (*C*H_2-**63**); ^{15}N{^{1}H}-NMR▪ ($CDCl_3$, 51 MHz): ∂ 346.54 (Triazole-*N*-**61***), 346.45 (Triazole-*N*-**61***), 244.89 (Triazole-*N*-**59***), 244.77 (Triazole-*N*-**59***); Accurate mass; m/z: 2867.01780 $(M+2H)^+$, calculated for $C_{175}H_{136}N_{20}{}^{15}N_2O_{20}$ 2867.02419. ° Multiplicity assigned as accurate as possible. • ^{1}H and ^{13}C-NMR shifts via COSY, ROESY, HSQC and HMBC spectra. ◊/#Peaks belonging to the two diastereoisomers. *Peaks belonging to the two different diastereoisomers that could not be separated. ▪ 50% of the indicated N atoms are ^{15}N-labeled.

Synthesis of H_4C_5DC

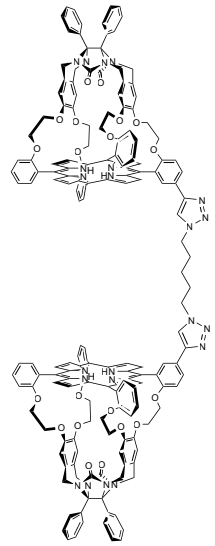

This compound was synthesized as described for **H_4C_3DC** using **Zn_2C_5DC** (45.53 mg, 15.1 µmol), $CHCl_3$ (75 mL) and HCl (6M, 200 mL) The product was obtained as a purple solid (**H_4C_5DC**, 35.66 mg, 12.3 µmol, 81%).

^{1}H-NMR°,• ($CDCl_3$, 500 MHz): ∂ 8.80-8.76 (m, 4H, β-pyrrole-*H*), 8.76-8.70 (m, 4H, β-pyrrole-*H*), 8.69-8.60 (m, 8H, β-pyrrole-*H*), 8.36 (t, 2H, Ar*H*-**22**, *J* = 2.0 Hz), 8.33-8.28 (m, 2H, Ar*H*-**24**), 8.06-7.98 (m, 6H, Ar*H*-**28**, **34**, **40**), 7.77-7.61 (m, 6H, Ar*H*-**30**, **36**, **42**), 7.65 (2H, Triazole-*H*-**58**), 7.37-7.23 (m, 12H, Ar*H*-**29**, **31**, **35**, **37**, **41**, **43**), 7.28 (1H, Ar*H*-**25#**), 7.25 (1H, Ar*H*-**25◊**), 6.98 -6.91 (m, 12H, Ar*H*-**55**, **56**), 6.84-6.78 (m, 8H, Ar*H*-**54**), 6.21-6.17 (m, 6H, Ar*H*-**48(II,III,IV)**), 6.16 (s, 1H, Ar*H*-**48(I)#**), 6.14 (s, 1H, Ar*H*-**48(I)◊**), 4.30 (t, 4H, CH_2-**62**, *J* = 6.9 Hz), 4.27-4.15 (m, 6H, CH_2-**45a(II, III, IV)**), 4.23 (d, 8H, CH_2-**50a**, *J* = 16.0 Hz), 4.20 (1H, CH_2-**45a(I)#**), 4.18 (1H, CH_2-**45a(I)◊**), 4.08-3.93

(m, 6H, CH_2-**45b(II, III, IV)**), 4.00 (1H, CH_2-**45b(I)#**), 3.95 (1H, CH_2-**45b(I)◊**), 3.74 (d, 8H, CH_2-**50b**, *J* = 15.7 Hz), 3.53-3.41 (m, 6H, CH_2-**46a(II, III, IV)**), 3.47 (1H, CH_2-**46a(I)#**), 3.37-3.27 (m, 6H, CH_2-**46b(II, III, IV)**), 3.44 (1H, CH_2-**46a(I)◊**), 3.32 (2H, CH_2-**46b(I)***), 1.94-1.87 (m, 4H, CH_2-**63**), 1.38-1.33 (m, 2H, CH_2-**64**), -2.74 (s, 2H, N*H*); ^{13}C NMR• ($CDCl_3$, 126 MHz): ∂ 158.75 (Ar*C*-**26**), 158.72 (Ar*C*-**32**, **38**, **44**), 156.90 (*C*=O-**51**), 147.70 (*C*-**57**), 146.61 (Ar*C*-**47**), 135.80 (Ar*C*-**28**, **34**, **40**), 133.31 (Ar*C*-**22**), 131.90 (Ar*C*-**27**, **33**, **39**), 131.33 (Ar*C*-**21**), 129.81 (Ar*C*-**49**), 129.51 (Ar*C*-**30**, **36**, **42**), 128.51 (Ar*C*-**55**, **56**), 128.12 (Ar*C*-**54**), 126.80 (Ar*C*-**24**), 122.30 (Ar*C*-**23**), 119.79 (Ar*C*-**29**, **35**, **41**), 119.14 (*C*H-**58**), 115.31 (Ar*C*-**48(II,III,IV)**), 115.30 (Ar*C*-**6**, **11**, **16**), 114.99 (Ar*C*-**48(I)**), 114.40 (Ar*C*-**1**), 112.04 (Ar*C*-**25**), 111.95 (Ar*C*-**31**, **37**, **43**), 84.77 (*C*-**52**), 67.45 (*C*H_2-**46(II, III, IV)**), 67.21 (*C*H_2-**46(I)***), 66.87 (*C*H_2-**45**), 49.90 (*C*H_2-**62**), 44.44 (*C*H_2-**50**), 29.62 (*C*H_2-**63**), 23.41(*C*H_2-**64**); ^{15}N{^{1}H}-NMR▪ ($CDCl_3$, 51 MHz): ∂ 344.54 (Triazole-*N*-**61***), 344.51 (Triazole-*N*-**61***), 247.74 (Traizole-*N*-**59***), 247.71 (Triazole-*N*-**59***); Accurate mass; m/z: 2895.04174 (M+2H)$^+$, calculated for $C_{177}H_{140}N_{20}{}^{15}N_2O_{20}$ 2895.05549. ○ Multiplicity assigned as accurate as possible. • ^{1}H and ^{13}C-NMR shifts via COSY, ROESY, HSQC and HMBC spectra. ◊/#Peaks belonging to the two diastereoisomers. *Peaks belonging to the two different diastereoisomers that could not be separated. ▪ 50% of the indicated N atoms are ^{15}N-labeled.

Synthesis of $H_4C_{11}DC$

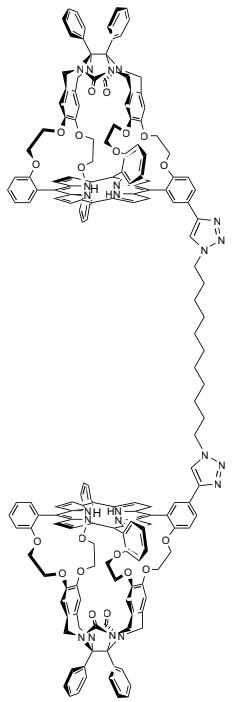

This compound was synthesized as described for **H_4C_3DC** using **$Zn_2C_{11}DC$** (39.03 mg, 12.6 µmol), $CHCl_3$ (50 mL) and HCl (6M, 200 mL). The product was obtained as a purple solid (**$H_4C_{11}DC$**, 34.59 mg, 11.6 µmol, 92%).

^{1}H-NMR○,• ($CDCl_3$, 500 MHz): ∂ 8.80-8.77 (m, 4H, β-pyrrole-*H*), 8.76-8.72 (m, 4H, β-pyrrole-*H*), 8.71-8.61 (m, 8H, β-pyrrole-*H*), 8.35-8.33 (m, 2H, Ar*H*-**22**), 8.33-8.31 (m, 2H, Ar*H*-**24**), 8.07-8.01 (m, 6H, Ar*H*-**28**, **34**, **40**), 7.75-7.66 (m, 6H, Ar*H*-**30**, **36**, **42**), 7.56-7.52 (m, 2H, Triazole-*H*-**58**), 7.38-7.273 (m, 12H, Ar*H*-**29**, **31**, **35**, **37**, **41**, **43**), 7.35 (2H, Ar*H*-**25**), 6.99 -6.91 (m, 12H, Ar*H*-**55**, **56**), 6.84-6.78 (m, 8H, Ar*H*-**54**), 6.21-6.15 (m, 8H, Ar*H*-**48**), 4.29 (2H, CH_2-**45a(I)**), 4.23 (6H, CH_2-**45a(II, III, IV)**), 4.23 (d, 8H, CH_2-**50a**, *J* = 15.6 Hz), 4.16 (t, 4H, CH_2-**62**, *J* = 7.2 Hz), 4.12-3.97 (m, 6H, CH_2-**45b(II, III, IV)**), 4.09 (2H, CH_2-**45b(I)**), 3.74 (d, 8H, CH_2-**50b**, *J* = 15.8 Hz), 3.57-3.44 (m, 6H, CH_2-**46a(II, III, IV)**), 3.55 (2H, CH_2-**46a(I)**), 3.39 (2H, CH_2-**46b(I)**), 3.36-3.28 (m, 6H, CH_2-**46b(II, III, IV)**), 1.73 (4H, CH_2-**63**), 1.19-1.08 (m, 14H, CH_2-**64**, **65**, **66**, **67**), -2.74 (s, 2H, N*H*); ^{13}C NMR• ($CDCl_3$, 126 MHz): ∂ 158.77 (Ar*C*-**32**, **38**, **44**), 158.72 (Ar*C*-**26**), 157.03 (*C*=O-**51**), 147.48

(*C*-**57**), 146.68 (Ar*C*-**47**), 135.88 (Ar*C*-**28**, **34**, **40**), 133.20 (Ar*C*-**22**), 131.99 (Ar*C*-**21**), 131.82 (Ar*C*-**27**, **33**, **39**), 129.82 (Ar*C*-**49**), 129.73 (Ar*C*-**30**, **36**, **42**), 128.66 (Ar*C*-**55**, **56**), 128.25 (Ar*C*-**54**), 127.20 (Ar*C*-**24**), 122.54 (Ar*C*-**23**), 119.96 (Ar*C*-**29**, **35**, **41**), 119.04 (*C*H-**58**), 115.47 (Ar*C*-**48(II,III,IV)**), 115.46 (Ar*C*-**48(I)**), 115.29 (Ar*C*-**6**, **11**, **16**) 114.54 (Ar*C*-**1**), 112.28 (Ar*C*-**25**), 112.15 (Ar*C*-**31**, **37**, **43**), 84.80 (*C*-**52**), 67.62 (*C*H_2-**46(II, III, IV)**), 67.37 (*C*H_2-**46(I)**), 67.20 (*C*H_2-**45(I)**), 67.04 (*C*H_2-**45(II, III, IV)**), 50.40 (*C*H_2-**62**), 44.42 (*C*H_2-**50**), 30.34 (*C*H_2-**63**), 26.60 (*C*H_2-**64**, **65**, **66**, **67**); ^{15}N{^{1}H}-NMR▪ ($CDCl_3$, 51 MHz): ∂ 343.55 (Triazole-*N*-**61**), 249.05 (Triazole-*N*-**59**); Accurate mass; m/z: 2979.14800 (M+2H)$^+$, calculated for $C_{183}H_{152}N_{20}{}^{15}N_2O_{20}$ 2979.14939. ○ Multiplicity assigned as accurate as possible. • ^{1}H and ^{13}C-NMR shifts via COSY, ROESY, HSQC and HMBC spectra. ▪ 50% of the indicated N atoms are ^{15}N-labeled.

2.5. References

(1) van Dongen, S. F. M.; Clerx, J.; Nørgaard, K.; Bloemberg, T. G.; Cornelissen, J. J. L. M.; Trakselis, M. A.; Nelson, S. W.; Benkovic, S. J.; Rowan, A. E.; Nolte, R. J. M. A Clamp-like Biohybrid Catalyst for DNA Oxidation. *Nat. Chem.* **2013**, *5* (11), 945–951.

(2) Johnson, A.; O'Donnell, M. Cellular DNA Replicases: Components and Dynamics at the Replication Fork. *Annu. Rev. Biochem.* **2005**, *74* (1), 283–315.

(3) Goldman, N.; Bertone, P.; Chen, S.; Dessimoz, C.; LeProust, E. M.; Sipos, B.; Birney, E. Towards Practical, High-Capacity, Low-Maintenance Information Storage in Synthesized DNA. *Nature* **2013**, *494* (7435), 77–80.

(4) Church, G. M.; Gao, Y.; Kosuri, S. Next-Generation Digital Information Storage in DNA. *Science* **2012**, *337* (6102), 1628.

(5) Zhirnov, V.; Zadegan, R. M.; Sandhu, G. S.; Church, G. M.; Hughes, W. L. Nucleic Acid Memory. *Nat. Mater.* **2016**, *15* (4), 366–370.

(6) Colquhoun, H.; Lutz, J.-F. Information-Containing Macromolecules. *Nat. Chem.* **2014**, *6* (6), 455–456.

(7) Lutz, J.-F. Coding Macromolecules: Inputting Information in Polymers Using Monomer-Based Alphabets. *Macromolecules* **2015**, *48* (14), 4759–4767.

(8) Mutlu, H.; Lutz, J.-F. Reading Polymers: Sequencing of Natural and Synthetic Macromolecules. *Angew. Chem. Int. Ed.* **2014**, *53* (48), 13010–13019.

(9) Lutz, J.-F. Writing on Polymer Chains. *Acc. Chem. Res.* **2013**, *46* (11), 2696–2705.

(10) Niu, J.; Hili, R.; Liu, D. R. Enzyme-Free Translation of DNA into Sequence-Defined Synthetic Polymers Structurally Unrelated to Nucleic Acids. *Nat. Chem.* **2013**, *5* (4), 282–292.

(11) Roy, R. K.; Meszynska, A.; Laure, C.; Charles, L.; Verchin, C.; Lutz, J.-F. Design and Synthesis of Digitally Encoded Polymers That Can Be Decoded and Erased. *Nat. Commun.* **2015**, *6*, 7237.

(12) Al Ouahabi, A.; Charles, L.; Lutz, J.-F. Synthesis of Non-Natural Sequence-Encoded Polymers Using Phosphoramidite Chemistry. *J. Am. Chem. Soc.* **2015**, *137* (16), 5629–5635.

(13) Pfeifer, S.; Zarafshani, Z.; Badi, N.; Lutz, J.-F. Liquid-Phase Synthesis of Block Copolymers Containing Sequence-Ordered Segments. *J. Am. Chem. Soc.* **2009**, *131* (26), 9195–9197.

(14) Trinh, T. T.; Oswald, L.; Chan-Seng, D.; Charles, L.; Lutz, J.-F. Preparation of Information-Containing Macromolecules by Ligation of Dyad-Encoded Oligomers. *Chem. – Eur. J.* **2015**, *21* (34), 11961–11965.

(15) Elemans, J. A. A. W.; Claase, M. B.; Aarts, P. P. M.; Rowan, A. E.; Schenning, A. P. H. J.; Nolte, R. J. M. Porphyrin Clips Derived from Diphenylglycoluril. Synthesis, Conformational Analysis, and Binding Properties. *J. Org. Chem.* **1999**, *64* (19), 7009–7016.

(16) Thordarson, P.; Bijsterveld, E. J. A.; Rowan, A. E.; Nolte, R. J. M. Epoxidation of Polybutadiene by a Topologically Linked Catalyst. *Nature* **2003**, *424* (6951), 915–918.

(17) Coumans, R. G. E.; Elemans, J. A. A. W.; Nolte, R. J. M.; Rowan, A. E. Processive Enzyme Mimic: Kinetics and Thermodynamics of the Threading and Sliding Process. *Proc. Natl. Acad. Sci. U. S. A.* **2006**, *103* (52), 19647–19651.

(18) Monnereau, C.; Ramos, P. H.; Deutman, A. B. C.; Elemans, J. A. A. W.; Nolte, R. J. M.; Rowan, A. E. Porphyrin Macrocyclic Catalysts for the Processive Oxidation of Polymer Substrates. *J. Am. Chem. Soc.* **2010**, *132* (5), 1529–1531.

(19) Deutman, A. B. C.; Cantekin, S.; Elemans, J. A. A. W.; Rowan, A. E.; Nolte, R. J. M. Designing Processive Catalytic Systems. Threading Polymers through a Flexible Macrocycle Ring. *J. Am. Chem. Soc.* **2014**, *136* (25), 9165–9172.

(20) Thordarson, P.; Bijsterveld, E. J. A.; Elemans, J. A. A. W.; Kasák, P.; Nolte, R. J. M.; Rowan, A. E. Highly Negative Homotropic Allosteric Binding of Viologens in a Double-Cavity Porphyrin. *J. Am. Chem. Soc.* **2003**, *125* (5), 1186–1187.

(21) Deutman, A. B. C.; Monnereau, C.; Moalin, M.; Coumans, R. G. E.; Veling, N.; Coenen, M.; Smits, J. M. M.; de Gelder, R.; Elemans, J. A. A. W.; Ercolani, G.; et al. Squaring Cooperative Binding Circles. *Proc. Natl. Acad. Sci. U. S. A.* **2009**, *106* (26), 10471–10476.

(22) Elemans, J. A. A. W.; Bijsterveld, E. J. A.; Rowan, A. E.; Nolte, R. J. M. Manganese Porphyrin Hosts as Epoxidation Catalysts – Activity and Stability Control by Axial Ligand Effects. *Eur. J. Org. Chem.* **2007**, *2007* (5), 751–757.

(23) van Hameren, R.; Schön, P.; van Buul, A. M.; Hoogboom, J.; Lazarenko, S. V.; Gerritsen, J. W.; Engelkamp, H.; Christianen, P. C. M.; Heus, H. A.; Maan, J. C.; et al. Macroscopic Hierarchical Surface Patterning of Porphyrin Trimers via Self-Assembly and Dewetting. *Science* **2006**, *314* (5804), 1433–1436.

(24) Koszarna, B.; Gryko, D. T. Efficient Synthesis of Meso-Substituted Corroles in a H2O–MeOH Mixture. *J. Org. Chem.* **2006**, *71* (10), 3707–3717.

(25) Chang, K.-H.; Huang, C.-C.; Liu, Y.-H.; Hu, Y.-H.; Chou, P.-T.; Lin, Y.-C. Synthesis of Photo-Luminescent Zn(II) Schiff Base Complexes and Its Derivative Containing Pd(II) Moiety. *Dalton Trans.* **2004**, *11*, 1731–1738.

(26) Fritz, J. S.; Schenk, G. H. Acid-Catalyzed Acetylation of Organic Hydroxyl Groups. *Anal. Chem.* **1959**, *31* (11), 1808–1812.

(27) Guillier, F.; Orain, D.; Bradley, M. Linkers and Cleavage Strategies in Solid-Phase Organic Synthesis and Combinatorial Chemistry. *Chem. Rev.* **2000**, *100* (6), 2091–2158.

(28) Reynhout, I. C.; Löwik, D. W. P. M.; van Hest, J. C. M.; Cornelissen, J. J. L. M.; Nolte, R. J. M. Solid Phase Synthesis of Biohybrid Block Copolymers. *Chem. Commun.* **2005**, No. 5, 602–604.

(29) Balaz, M.; Collins, H. A.; Dahlstedt, E.; Anderson, H. L. Synthesis of Hydrophilic Conjugated Porphyrin Dimers for One-Photon and Two-Photon Photodynamic Therapy at NIR Wavelengths. *Org. Biomol. Chem.* **2009**, *7* (5), 874–888.

(30) Littler, B. J.; Miller, M. A.; Hung, C.-H.; Wagner, R. W.; O'Shea, D. F.; Boyle, P. D.; Lindsey, J. S. Refined Synthesis of 5-Substituted Dipyrromethanes. *J. Org. Chem.* **1999**, *64* (4), 1391–1396.

(31) Plunkett, S.; Dahms, K.; Senge, M. O. Synthesis and Reactivity of Allenylporphyrins. *Eur. J. Org. Chem.* **2013**, (8), 1566–1579.

(32) Varamo, M.; Loock, B.; Maillard, P.; Grierson, D. S. Development of Strategies for the Regiocontrolled Synthesis of Meso-5,10,20-Triaryl-2,3-Chlorins. *Org. Lett.* **2007**, *9* (23), 4689–4692.

(33) Mathias O. Senge; Kalisch, W. W.; Bischoff, I. The Reaction of Porphyrins with Organolithium Reagents. *Chem. Eur. J.* **2000**, *6* (6), 2721–2738.

(34) Harder, S.; Boersma, J.; Brandsma, L.; van Mier, G. P. M.; Kanters, J. A. The Molecular Structure of 1-Lithio-2-Methoxybenzene in the Solid State and in Solution. *J. Organomet. Chem.* **1989**, *364* (1), 1–15.

(35) Senge, M. O.; Bischoff, I. Regioselective Synthesis of Conformationally Designed Porphyrins with Mixed Meso-Substituent Types and Distortion Modes. *Eur. J. Org. Chem.* **2001**, *(9)*, 1735–1751.

(36) Horn, S.; Senge, M. O. The Intermolecular Pauson–Khand Reaction of Meso-Substituted Porphyrins. *Eur. J. Org. Chem.* **2008,** (29), 4881–4890.

(37) Miyaura, N.; Suzuki, A. Palladium-Catalyzed Cross-Coupling Reactions of Organoboron Compounds. *Chem. Rev.* **1995**, *95* (7), 2457–2483.

(38) Singh, M. S.; Chowdhury, S.; Koley, S. Advances of Azide-Alkyne Cycloaddition-Click Chemistry over the Recent Decade. *Tetrahedron* **2016**, *72* (35), 5257–5283.

(39) Ladomenou, K.; Nikolaou, V.; Charalambidis, G.; Coutsolelos, A. G. "Click"-Reaction: An Alternative Tool for New Architectures of Porphyrin Based Derivatives. *Coord. Chem. Rev.* **2016**, *306*, 1–42.

(40) Liang, L.; Astruc, D. The copper(I)-Catalyzed Alkyne-Azide Cycloaddition (CuAAC) "click" Reaction and Its Applications. An Overview. *Coord. Chem. Rev.* **2011**, *255* (23), 2933–2945.

(41) Haldon, E.; Nicasio, M. C.; Perez, P. J. Copper-Catalysed Azide-Alkyne Cycloadditions (CuAAC): An Update. *Org. Biomol. Chem.* **2015**, *13* (37), 9528–9550.

(42) Thévenin, M.; Thoret, S.; Grellier, P.; Dubois, J. Synthesis of Polysubstituted Benzofuran Derivatives as Novel Inhibitors of Parasitic Growth. *Bioorg. Med. Chem.* **2013**, *21* (17), 4885–4892.

(43) Shultz, D. A.; Gwaltney, K. P.; Lee, H. A Modified Procedure for Sonogashira Couplings: Synthesis and Characterization of a Bisporphyrin, 1,1-Bis[zinc(II) 5'-Ethynyl-10',15',20'-Trimesitylporphyrinyl]methyl-enecyclohexane. *J. Org. Chem.* **1998**, *63* (12), 4034–4038.

(44) Cheng, J.; Sun, Y.; Wang, F.; Guo, M.; Xu, J.-H.; Pan, Y.; Zhang, Z. A Copper- and Amine-Free Sonogashira Reaction Employing Aminophosphines as Ligands. *J. Org. Chem.* **2004**, *69* (16), 5428–5432.

(45) Molander, G. A.; Katona, B. W.; Machrouhi, F. Development of the Suzuki–Miyaura Cross-Coupling Reaction: Use of Air-Stable Potassium Alkynyltrifluoroborates in Aryl Alkynylations. *J. Org. Chem.* **2002**, *67* (24), 8416–8423.

(46) Kocher, L.; Durot, S.; Heitz, V. Control of the Cavity Size of Flexible Covalent Cages by Silver Coordination to the Peripheral Binding Sites. *Chem. Commun.* **2015**, *51* (67), 13181–13184.

(47) Bhattacharya, S.; Biswas, J. Vesicle and Stable Monolayer Formation from Simple "Click" Chemistry Adducts in Water. *Langmuir* **2011**, *27* (5), 1581–1591.
(48) Ganapathi, E.; Madhu, S.; Ravikanth, M. Synthesis and Properties of Triazole Bridged BODIPY-Conjugates. *Tetrahedron* **2014**, *70* (3), 664–671.

2.6 Appendices

A1: Synthetic approaches employed to obtain various substituted porphyrins.

Table 1 Synthetic approaches employed to obtain various substituted porphyrins.

Entry	R^1	R^2	M	Method[a]	Adaptations	Comments
1	OCH_3	Br	2H	1a) Direct condensation of monopyrroles[23] 1b) Stepwise condensation via an a,c-bilane[24]	1a,b) 2-Methoxybenzaldehyde and 5-bromo-2-methoxybenzaldehyde were used as reagents	1a) No product was obtained due to poor separation caused by the presence of atropisomers 1b) No product was obtained due to the same reasons
2	OCH_3	Br	Zn	Zn insertion[15]	-	No product was obtained due to poor separation caused by the presence of atropisomers
3	OCH_3	$C{\equiv}CC(CH_3)_2OH$	2H	Sonogashira cross coupling[25]	-	No product was obtained due to poor separation of products
4	OH	Br	2H	Deprotection of OCH_3-groups[22]	-	No product was obtained due to poor separation of products
5	$OC(O)CH_3$	Br	2H	Acetylation[26]	-	No product was obtained due to poor separation caused by the presence of atropisomers
6	OCH_3	NO_2	2H	Direct condensation of monopyrroles[23]	2-Methoxybenzaldehyde and 5-nitro-2-methoxybenzaldehyde were used as reagents	Separation was obtained yielding a mixture of non-substituted and mono-substituted porphyrin. But during deprotection, β-pyrrolic protons were randomly substituted by bromine atoms from BBr_3

[a] Methods previously described for the preparation of analogous compounds.

A2: Synthetic approaches employed to obtain a mono-substituted porphyrin clip.

Table 2 Synthetic approaches employed to obtain a mono-substituted porphyrin clip.

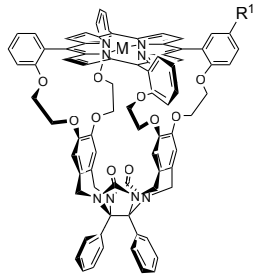

Entry	R^1	M	Method[a]	Adaptations	Comments
1	Br	2H	Substitution of the OTos groups of compound **7**[15] 1a) Stepwise substitution 1b) One pot substitution	-	1a,b) No product obtained due to poor separation of the obtained mixture
2	COOH	2H	Solid phase synthesis[27]	2-Chlorotrityl chloride resin with *p*-formyl-*o*-hydroxybenzoic acid as coupling group	No product was formed

[a] Methods previously described for the preparation of analogous compounds.

A3: Synthetic approaches employed to convert zinc mono-bromo porphyrin clip 9 into mono-acetylene porphyrin clip 11.

Table 3 Synthetic approaches employed to convert zinc mono-bromo porphyrin clip **9** into mono-acetylene porphyrin clip **11**.

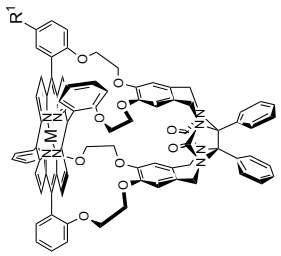

Entry	R^1	M	Method[a]	Adaptations	Comments
1	$C{\equiv}CSi(CH_3)_3$	Zn	Sonogashira cross coupling[42]	Toluene was used as the solvent and the reaction was carried out at 50 °C	No pure product could be obtained due to poor separation of the product and the starting compound **9**
2	$C{\equiv}CC(CH_3)_2OH$	Zn	Sonogashira cross coupling[43]	Toluene was used as the solvent and 2-methyl-3-butyn-2-ol as the acetylene functionality	Irreproducible yields and contamination of product with salts
3	C≡CH	Zn	Deprotection of the acetone protected acetylene of entry 2[44]	-	Irreproducible yields and no separation from salts
4	$[(CH_3)_2CH]_3SiC{\equiv}C$	Zn	Suzuki-Miyaura cross coupling[45]	TIPSA BF_3K was used as the acetylene functionality	Pure product could be isolated after column chromatography

[a] Methods previously described for the preparation of analogous compound.

3

Binding of DABCO to zinc double porphyrin cages

Part of this chapter will be published:

Synthesis of double porphyrin cage compounds and the formation of sandwich complexes with a ditopic ligand - *Manuscript in preparation*

K. Stout, T. Peters, M. F. J. Mabesoone, F. Visschers, E. M. Meijer, J. van den Berg, J-R. Klop, S. Cantekin, P. B. White, P. T. Tinnemans, J. A. A. W Elemans, A. E. Rowan and R. J. M Nolte

Abstract

The binding of 1,4-diazabicyclo[2.2.2]octane (DABCO) to zinc double porphyrin cages (**Zn_2C_xDC**) was investigated. The formation of 1:1 **Zn_2C_xDC**:DABCO sandwich-like complexes, in which one DABCO molecule is bound in between two zinc porphyrins, and 1:2 **Zn_2C_xDC**:DABCO open complexes, in which each zinc porphyrin is bound to a DABCO molecule, was demonstrated in chloroform and in a 1:1 (v/v) solvent mixture of chloroform and acetonitrile. **Zn_2C_3DC** formed the strongest 1:1 sandwich complex with DABCO in the solvent mixture of chloroform and acetonitrile, while the differences in binding strength of the complexes between DABCO and the other **Zn_2C_xDC** hosts were rather small. The association constants of the 1:2 open complexes were about 3 orders of magnitude smaller than those of the 1:1 sandwich complexes. In chloroform, up to the addition of 10 equivalents of DABCO, the experimental titration curves significantly deviated from the theoretical binding curves assuming a 1:2 binding model. To explain this deviation, two modified binding models, which assume the creation of additional binding sites for the ligand as a result of specific solvation effects in chloroform, were proposed. When dichloromethane was employed as the solvent, a solvolysis reaction with DABCO took place, interfering with the formation of well-defined 1:1 **Zn_2C_xDC**:DABCO sandwich complexes. With the help of variable temperature ^{1}H-NMR studies in a solvent mixture of $CDCl_3$ and acetonitrile-d_3 the formation of the various complexes between DABCO and the host was confirmed. The successful formation of the 1:1 **Zn_2C_xDC**:DABCO sandwich complexes in chloroform and in a solvent mixture of chloroform and acetonitrile provides an essential step towards the construction of double porphyrin cages, which will be used for binary data storage in synthetic polymers.

3.1. Introduction

Nowadays the development of new and efficient data storage systems is an emerging research field, given the expectation that the global digital archive will contain 3×10^{24} bits by 2040.[1] Hence, alternative methods to silicon memory chips are needed to facilitate the storage of big data. Recently, the storage of non-biological data on DNA was reported, creating new possibilities for alternative storage media. In this connection it is worthwhile to mention that synthetic polymers are more desirable than DNA as storage media, because they are more robust, easier to handle, and can make use of a binary code in computing compared to a quaternary code in the case of DNA.[2–6] With the objective to storage binary data on a synthetic polymer with the help of a catalytic machine that writes digital data in the form of epoxide functions, a series of double porphyrin cage compounds was designed, synthesized and characterized (Figure 1 and Chapter 2).[7]

It is expected that when one of the porphyrin cages contains a zinc ion, an instructing cavity can be created, capable of influencing the catalytic activity exhibited by the manganese ion in the other porphyrin cage via allosteric interactions transferred through the coordination of a ditopic axial ligand. The ditopic ligand selected for this purpose was 1,4-diazabicyclo[2.2.2]octane (DABCO), which is known to form strong coordination complexes with zinc porphyrins because of its relatively high basicity.[8] The binding of DABCO to zinc porphyrins and the typical changes in the UV-Vis and NMR spectra that are observed upon coordination of the ligand have been extensively reported.[8–18] DABCO can form sandwich-type structures by binding in between two porphyrins. The porphyrin ladders reported by Anderson *et al.* are amongst the best known examples of such complexes.[8,19] In an analogous way, DABCO is also expected to fit in between the two porphyrin planes of the different zinc double porphyrin cages (**Zn_2C_xDC**s). The binding of this axial ligand is considered to be essential for the transfer of information between the two metal centers in a zinc-manganese double porphyrin cage derivative. Binding of a guest such as dimethylviologen hexafluorophosphate (**Me_2V**) in the instructing zinc porphyrin cavity may change the catalytic activity of the manganese center in the writing cavity via allosteric interactions mediated by the ditopic ligand that links the two metal centers. In this chapter the binding of DABCO to the **Zn_2C_xDC** compounds was investigated with the help of UV-Vis and NMR spectroscopy in different solvents. The main objective was to investigate if there is an optimal length of the spacer linking the cavities of the **Zn_2C_xDC** compounds, which may lead to the strongest binding of DABCO in the sandwich-type complexes.

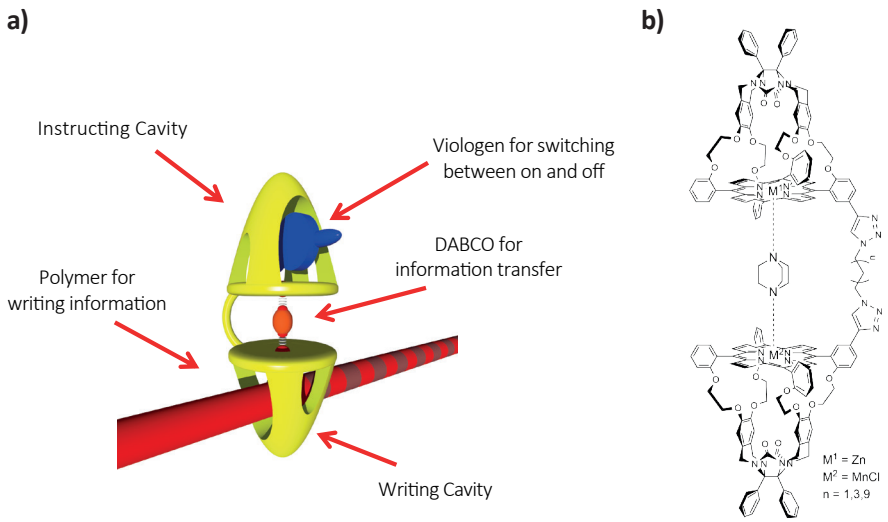

Figure 1 *a) Schematic representation of a double porphyrin cage (yellow) consisting of two receptor molecules capped with a porphyrin roof that are covalently linked. The instructing cavity contains a zinc center and the writing cavity a manganese center. The coordination of a ditopic ligand such as DABCO (orange) in between the two porphyrins might allow the transfer of information from the instructing cavity to the writing cavity, thus enabling the possibility of influencing the catalytic reaction. The binding of a viologen guest (blue) inside the instructing cavity may influence the coordination of DABCO to the manganese center, which can perform a catalytic reaction on, for example, a polymer substrate (red), via a series of allosteric interactions. b) Chemical structure of the zinc-manganese double porphyrin cages with alkyl spacer lengths of 3, 5, and 11 carbon atoms, binding DABCO as a ditopic axial ligand.*

3.2. Results and discussion

3.2.1 Introduction to the spectral studies on the binding of DABCO to zinc bis-porphyrin systems

The binding of DABCO to the double zinc porphyrin cages was investigated with the help of UV-Vis and NMR spectroscopy. Previously reported zinc bis-porphyrin systems (**Zn_2BisP**), including for example zinc porphyrin tweezers or porphyrin ladders, exhibited well-defined Soret bands in their UV-Vis spectra, which shifted upon the binding of a ditopic axial ligand like DABCO.[8–16] The Soret band of a zinc bis-porphyrin (Figure 2a) can typically be found around 420 nm, while in a 1:1 sandwich complex with DABCO (Figure 2b) the absorption displays a red shift to around 426 nm.[10–12] Upon the addition of more DABCO molecules to this complex, the Soret band shifts further to around 431 nm, indicative of the formation of a 1:2 **Zn_2BisP**:DABCO "open" complex (Figure 2c).[10,11] The binding between DABCO and **Zn_2BisP** compounds can also be investigated by NMR spectroscopy. The ^{1}H resonance

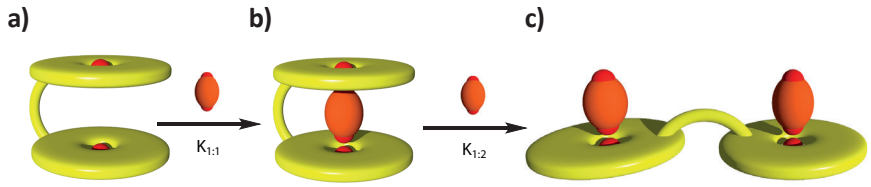

Figure 2 *Schematic representation of the binding of DABCO to a zinc bis-porphyrin complex (**Zn_2BisP** (a)), in which the first DABCO molecule (orange) is coordinated to the two zinc centers in the porphyrin planes forming a 1:1 **Zn_2BisP**:DABCO sandwich complex with a binding constant $K_{1:1}$ (b). Upon binding of an additional DABCO molecule, the 1:2 open **Zn_2BisP**:DABCO complex is formed, in which the zinc center in each porphyrin plane binds to a DABCO molecule, with an overall binding constant $K_{1:2}$ (c).*

of the 12 chemically equivalent methylene protons of DABCO in a 1:1 sandwich complex with a **Zn_2BisP** compound can be expected at around δ –4.5 ppm, because these protons experience the ring current of two porphyrin planes.[9–13,15,17,18] In a 1:2 **Zn_2BisP**:DABCO open complex, the methylene protons are no longer chemically equivalent: the 6 methylene protons close to the DABCO nitrogen atom bound to the zinc porphyrin resonate around δ –3 ppm, while the resonance of the other 6 methylene protons is expected around δ 0.8 ppm.[9,11,20,21]

3.2.2 Formation of the different DABCO complexes: UV-Vis titrations in dichloromethane

For the UV-Vis titrations, first dichloromethane (DCM) was selected as the solvent because it dissolves the **Zn_2C_xDC** compounds easily and can be used in future catalytic epoxidation studies that employ iodosylbenzene as the oxidant.[22–24] During the UV-Vis titrations, the absorbance and shifts in the UV-Vis spectra of a 1.5 μM **Zn_2C_xDC** solution in DCM, to which increasing amounts of ligand (DABCO) were added, were recorded. By adding a solution that contains both the host and the ligand, the concentration of host remains constant while the concentration of ligand increases. Because DABCO is a 'silent' ligand, which does not absorb in the UV-Vis region studied, all the changes in absorbance can be attributed to the formation of the different host-ligand complexes.[25]

A series of UV-Vis spectra, which were obtained by adding increasing amounts of DABCO to **Zn_2C_3DC** in DCM, is shown in Figure 3a. They show three Soret bands between 400 and 450 nm. The Soret band at 422 originates from the free **Zn_2C_3DC** host and is at a similar wavelength as that of Soret bands of related zinc bis-porphyrin systems.[10–12] The intensity of this Soret band lowered upon the addition of DABCO, and simultaneously a new Soret band at 426 nm started to emerge.[8,10–16] The presence of an isosbestic point and the observed red-shift are characteristic for the formation of a 1:1 **Zn_2C_3DC**:DABCO sandwich complex.[8,10–16] When increasing

aliquots of DABCO were added, the Soret band at 426 nm also decreased in intensity, while a new Soret band at 431 nm arose, accompanied by an isosbestic point at 428 nm. These spectral changes indicate the formation of a 1:2 **Zn_2C_3DC**:DABCO open complex.[8,10–16] The Q-bands of the porphyrins are located between 525 and 625 nm and showed a red-shift upon the formation of the 1:1 **Zn_2C_3DC**:DABCO sandwich complex and no further shifts upon the addition of more DABCO.[26,27] For the binding between DABCO and **Zn_2C_5DC** and **$Zn_2C_{11}DC$**, similar spectra and transitions were observed, indicating a similar complexation behavior as observed for **Zn_2C_3DC** (data shown in appendix A1).

By plotting the absorbance of all the Soret bands as function of the number of equivalents of DABCO added, titration curves can be extracted from the UV-Vis spectra, as shown in Figure 3a. Surprisingly, when a titration was performed with the same solution on two consecutive days, i.e. 2 and 22 h after its preparation, the

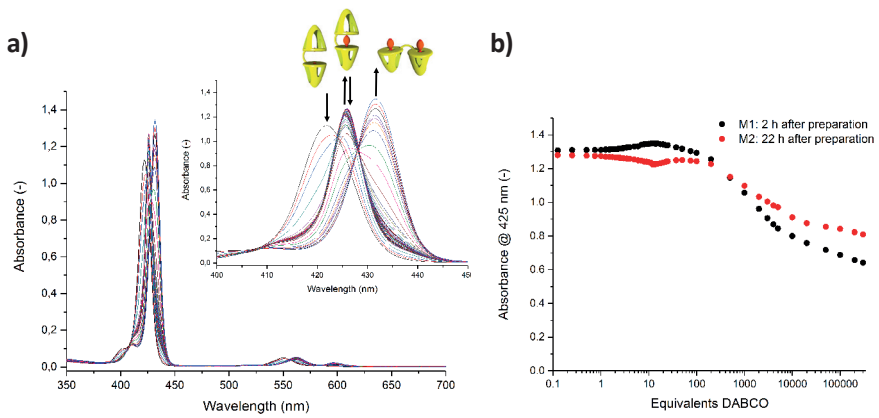

Figure 3 *a) UV-Vis spectra recorded during the titration of **Zn_2C_3DC** with increasing amounts of DABCO in DCM. The inset shows a zoom-in of the Soret band region and provides schematic representations of the various complexes that correspond to the observed Soret bands. b) Titration curves for the binding of DABCO to **Zn_2C_5DC** measured on two consecutive days, in which the number of equivalents of DABCO is plotted against the absorbance of the Soret band at 425 nm. The titration curves were measured using the same solutions 2 hours (M1, black) and 22 hours (M2, red), respectively, after their preparation. c) Reaction of DABCO with DCM, yielding a quaternary ammonium salt. d) Crystal structure of this compound. Cl, green; N, blue; C, black; covalent bond, grey.*

titration curves were not the same (Figure 3b). In subsequent studies it was discovered that DCM reacts with DABCO to give a quaternary ammonium salt (Figure 3c). The formation of this product by a solvolysis reaction under reflux conditions has been described in the literature.[28] However, also when a solution of DABCO in DCM was stirred overnight at room temperature a substantial amount of a white precipitate was formed. Mass spectrometry, NMR spectroscopy and a crystal structure determination (Figure 3d) confirmed that this precipitate was the quaternary ammonium salt. The occurrence of this reaction explained the poor reproducibility of the titrations, because the quaternary ammonium salt cannot bind anymore in a ditopic fashion, while in addition it might also interact via ion-dipole interactions with the ethylene oxide spacers of the **Zn_2C_xDC** hosts (Figure 4).

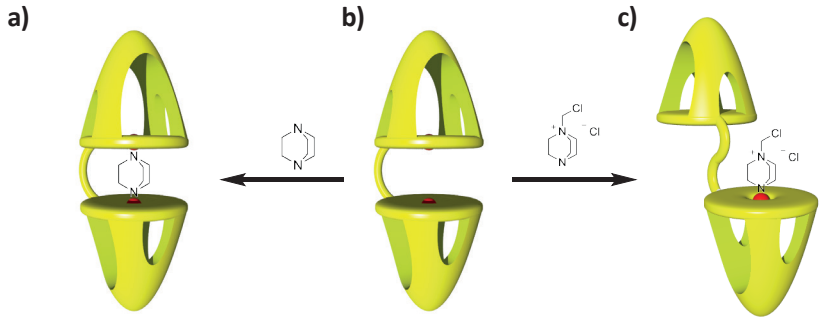

Figure 4 *(a) Schematic representation of the 1:1 **Zn_2C_xDC**:DABCO sandwich complex that is formed when DABCO is coordinated to both zinc porphyrins, (b) of uncomplexed **Zn_2C_xDC**, and (c) of a 1:1 complex between **Zn_2C_xDC** and 1-(chloromethyl)-1,4-diazabicyclo[2.2.2]octan-1-ium.*

The binding constants obtained from the titrations could in theory be corrected for the formation of the quaternary ammonium salt by taking into account the rate constant of the solvolysis reaction, which can be used to calculate the actual DABCO concentration at each addition step of the ligand. However, this correction cannot account for possible interactions of the formed quaternary ammonium salt with the **Zn_2C_xDC** hosts. To further investigate these interactions, ^{1}H-NMR studies were carried out with the reference compound **H_2SC** (Figure 5). Upon the addition of the salt to a solution of **H_2SC** in a solvent mixture of CD_2Cl_2/MeCN-d_3 (1:1, (v/v)) the resonances of the crown-ether protons between 3.1 and 4.2 ppm and those of the β-pyrrole protons at 8.81 ppm shifted downfield by 0.38 (on average) and 0.19 ppm, respectively. These shifts indicate that the salt has ion-dipole interactions with the crown ether linkers of **H_2SC**.[29] Besides the shifts of the crown-ether protons, the resonances of the NH-protons of the porphyrin are shifted upfield by 0.2 ppm, indicating that they experience additional shielding upon the addition of the salt. This

upfield shift is most likely caused by the binding of the CH_2Cl-portion of the salt in the cavity, while the positively charged nitrogen atom resides in between the crown-ether spacers. In addition, the resonances of the ammonium salt are broadened, which is probably caused by rapid exchange between a bound and unbound state. Due to this broadening, it could not be determined with the help of a ROESY-spectrum how the salt binds to **H_2SC**, because no ROE effects could be observed. It can be expected that the salt will have similar interactions with the cavities of all the zinc double porphyrin cages. In addition, it can in those cases still coordinate with its free amine to a zinc center (Figure 4). While 1:1 **Zn_2C_xDC**:DABCO sandwich complexes can still be formed, at increasing amounts of the salt, the competition of the latter for binding to the zinc centers will increase. The generation of such complexes will hamper the formation of the 1:1 **Zn_2C_xDC**:DABCO sandwich complex and facilitate the formation of an open-folded complex. Based on the above experiments and reasonings, it was concluded that DCM is not a suitable solvent for the determination of reliable binding constants for the binding of DABCO to **Zn_2C_xDC** compounds. The titration curves, therefore, were not further analyzed and no binding constants were calculated.

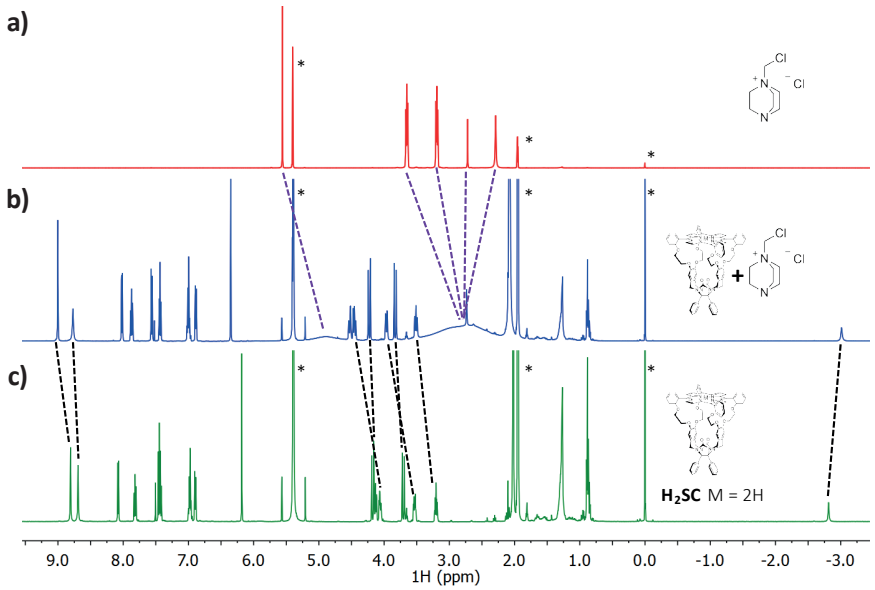

Figure 5 *^{1}H-NMR spectra of 1-(chloromethyl)-1,4-diazabicyclo[2.2.2]octan-1-ium (a, red), **H_2SC** with 10 equivalents of 1-(chloromethyl)-1,4-diazabicyclo[2.2.2]octan-1-ium (b, blue, 1 mM) and of **H_2SC** (c, green, 1 mM) in CD_2Cl_2/MeCN-d_3 (1:1, (v/v)). The shifts of the β-pyrrole, the crown ether, and the NH proton resonances of **H_2SC** are indicated by black dotted lines and the shifts of the proton resonances of the ammonium salt as purple dotted lines. Stars (*) indicate the resonances of CH_2Cl_2, MeCN, and tetramethylsilane.*

3.2.3 Formation of the different DABCO complexes: UV-Vis titrations in chloroform

Due to the problems encountered with DCM as the solvent, the binding between DABCO and the **Zn_2C_xDC** hosts was subsequently studied in chloroform. It turned out that refluxing solutions of DABCO in chloroform did not yield a quaternary ammonium salt or any other product, meaning that the ligand is inert to this solvent.

Depending on the concentration of DABCO, the UV-Vis spectra of the titration of **Zn_2C_3DC** with this ligand again revealed the occurrence of three different Soret bands (Figure 6a). The Soret band of the uncoordinated free host, **Zn_2C_3DC**, was located at 421.5 nm, which is a wavelength that was also found for related zinc bis-porphyrin systems.[8,10–16] Similar as was observed for the titration in DCM, this Soret band first decreased in intensity, accompanied by the emergence of a new Soret band at 426.5 nm and an isosbestic point, which is characteristic for the formation of a 1:1 sandwich complex.[8,10–16] Upon adding more DABCO, the band at 426.5 nm again decreased in intensity and a new band emerged at 432.5 nm, characteristic for the 1:2 **Zn_2C_3DC**:DABCO open complex.[8,10–16] The Q-bands were located between 525 and 625 nm and only the Q-band at 549 nm showed a

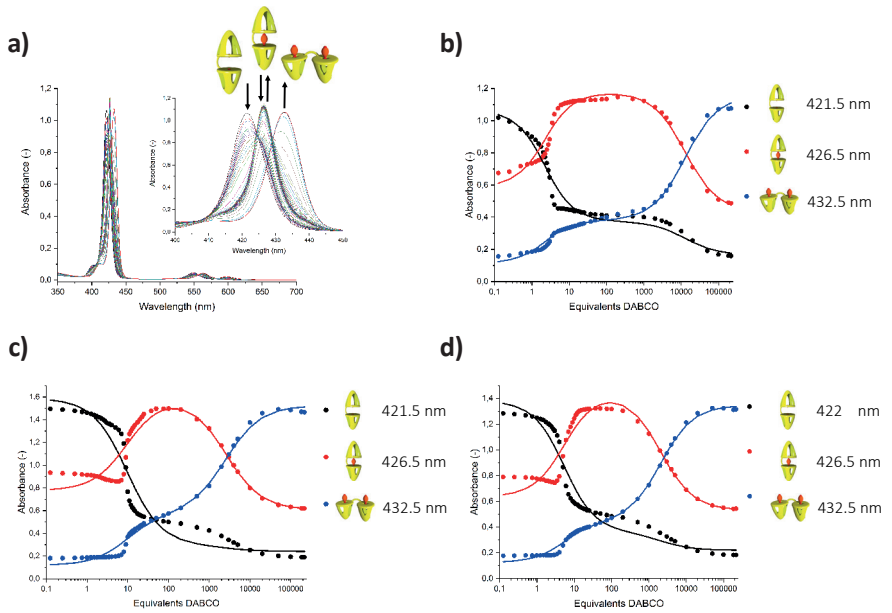

Figure 6 *a) UV-Vis spectra of the titration of **Zn_2C_3DC** with increasing amounts of DABCO in chloroform. The inset shows a zoom-in of the Soret band region. b, c, d) Titration curves (dotted traces) of **Zn_2C_3DC** (b), **Zn_2C_5DC** (c) and **Zn_2C_{11}DC** (d) in which the absorbance is plotted as a function of the number of equivalents of DABCO, with fits (solid lines) obtained from http://supramolecular.org/.*

red-shifted transition when going from the uncoordinated to coordinated zinc porphyrins.[26,27] The same UV-Vis transitions were observed when DABCO was added to a solution of **Zn_2C_5DC** or **Zn_2C_{11}DC** in chloroform, indicating similar binding behavior of the ligand as observed for **Zn_2C_3DC** (data shown in appendix A2). In chloroform, all the 1:1 **Zn_2C_xDC**:DABCO sandwich complexes appeared to be stable (i.e. no undesired side reactions between the ligand and the solvent occurred), which is an important condition for the possible use of a double porphyrin cage compound in future binary coded data storage systems.

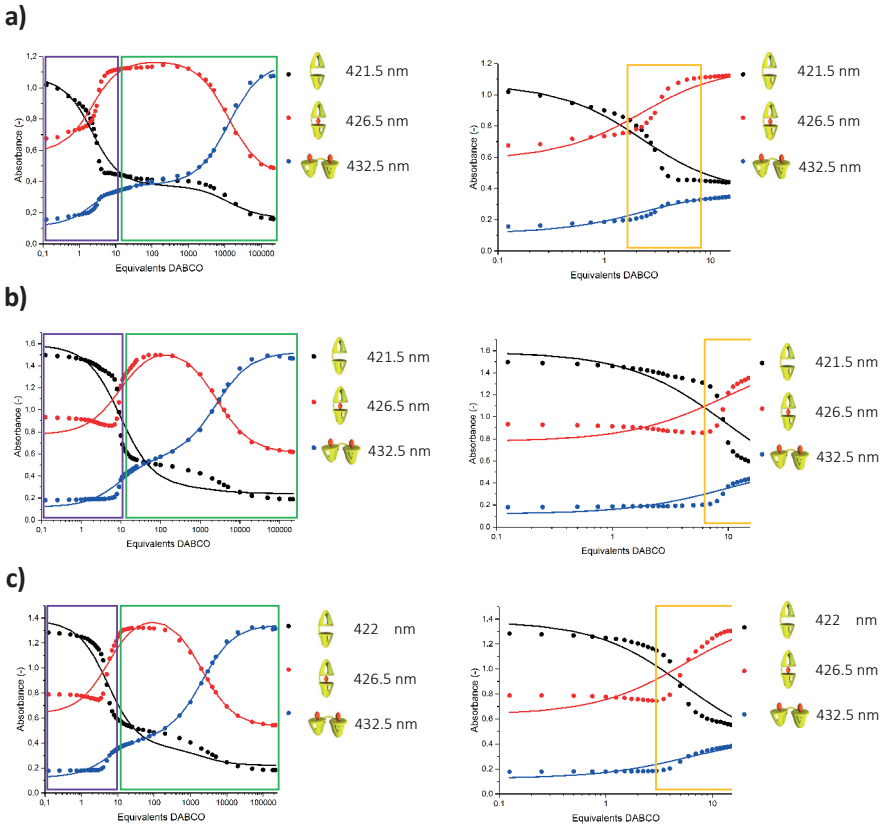

Figure 7 *Titration curves (left) and zoomed-in (0 to 15 equivalents of DABCO, right) titration curves of (a) **Zn_2C_3DC**, (b) **Zn_2C_5DC** and (c) **Zn_2C_{11}DC** in which the absorbance of the Soret band is plotted as a function of the number of equivalents of DABCO in chloroform. Fits (solid curves) were obtained using http://supramolecular.org/. For the first 10 equivalents of DABCO the titration curves are not adequately fitted by the predictions of the standard 1:2 binding model (purple boxes), while the second binding event in which the 1:2 **Zn_2C_xDC**:DABCO open complexes are formed is fitted better using the standard 1:2 binding model (green boxes). The yellow boxes highlight the start of or the complete transition from the uncomplexed **Zn_2C_xDC** compounds to the 1:1 **Zn_2C_xDC**:DABCO sandwich complexes.*

The titration curves that can be extracted from the UV-Vis spectra, such as depicted in Figure 6a, are shown in Figures 6b-d for the coordination of DABCO to **Zn_2C_3DC**, **Zn_2C_5DC** and **Zn_2C_{11}DC**, respectively. To derive the respective binding constants, the curves were fitted assuming a standard 1:2 binding model in which a single host can bind up to two ligands.[30] The resulting fitting curves are included in Figures 6b-d as solid lines.[25] The standard 1:2 binding model involves two binding constants: $K_{1:1}$ for the formation of the 1:1 **Zn_2C_xDC**:DABCO sandwich complex, and $K_{1:2}$ for the formation of the 1:2 **Zn_2C_xDC**:DABCO open complex.[25] The full derivation of the formulas employed in the standard 1:2 binding model can be found in the experimental section.

The obtained fits matched the experimentally obtained data relatively well for the second parts of the titration curves, reflecting the conversion of the 1:1 **Zn_2C_xDC**:DABCO sandwich complexes to the 1:2 **Zn_2C_xDC**:DABCO open complexes (Figure 7). However, the obtained fits deviated substantially from the experimentally obtained data at the transition of the uncomplexed **Zn_2C_xDC** compound to the 1:1 **Zn_2C_xDC**:DABCO sandwich complex. This deviation is most pronounced in the region from 0 to 10 equivalents of DABCO (right side of Figure 7, zooms of the titration curves). The Soret band at 421.5 nm of the uncomplexed **Zn_2C_3DC** compound showed a slight decay while the Soret band indicative for the formation of the 1:1 **Zn_2C_3DC**:DABCO sandwich complex did not yet significantly emerge. Upon the addition of more than 1.75 equivalents of DABCO, a sudden steep change in the absorbance of the Soret band is observed, indicating the start of the coordination of DABCO to the zinc centers. This steep transition indicates the formation of the 1:1 **Zn_2C_3DC**:DABCO sandwich complex and is completed after the addition of 8 equivalents of DABCO. Because there is a slight change in the absorbance of the Soret band of the uncomplexed **Zn_2C_3DC** from 0 to 1.75 equivalents of DABCO, but much less significantly in the Soret band of the 1:1 **Zn_2C_3DC**:DABCO sandwich complex, there appears to be a change in the environment of the zinc porphyrins, while at the same time the binding of DABCO to the zinc centers does not yet occur. Based on these observations, it is concluded that, in chloroform, the formation of the 1:1 **Zn_2C_3DC**:DABCO sandwich complex is initially hindered. **Zn_2C_5DC** and **Zn_2C_{11}DC** showed the same behavior, although the decay of the Soret band of the uncomplexed compounds was less pronounced than that observed for **Zn_2C_3DC**, while in contrast the steep rises of the Soret band belonging to the sandwich complexes were more pronounced. The transition from the uncomplexed compounds to the sandwich complex occurred from 6 to 37 and 3 to 25 equivalents of DABCO for **Zn_2C_5DC** and **Zn_2C_{11}DC**, respectively.

These unexpected results can have several causes, the first being that the zinc porphyrins of the **Zn_2C_xDC** compounds are blocked by another ligand that competes with the binding of DABCO. Since the solution of the free host only contains **Zn_2C_xDC**, chloroform, and traces of water, this blocking can either originate from the

coordination of one of the nitrogen atoms of the triazole group present in the linker or from the coordination of a chloroform or water molecule. Coordination of chloroform is unlikely since to the best of our knowledge no records of the coordination of this solvent to zinc porphyrins are known, and the wavelengths of the Soret bands of uncomplexed **Zn_2C_xDC** compound dissolved in chloroform and DCM are equal. It can be assumed, therefore, that DCM and chloroform solvate the zinc porphyrins in a similar way, which should not lead to different coordination behavior of DABCO, at least in principle. In DCM, however, no delay in the emergence of the Soret band belonging to the 1:1 **Zn_2C_xDC**:DABCO sandwich complex was observed, implying that in chloroform another interaction than that with the bulk solvent must play a role in the anomalous coordination behavior. Coordination of one of the nitrogen atoms of the triazole groups in the linker to the zinc center is possible, either in an intramolecular or in an intermolecular fashion (Chapter 2). However, zinc porphyrin systems containing triazole groups have been reported to display broad Soret bands at 420 nm and to contain a red-shifted shoulder at 430 nm or a complete split of this Soret band in chloroform.[31,32] The Soret band of the **Zn_2C_xDC** compounds is present at 421 nm and although it is broad, it shows no shoulder at 430 nm. Therefore, no coordination of the triazole nitrogen atoms to the zinc center occurs at our UV-Vis concentrations. At NMR concentrations (1 mM), the proton signals showed broadening when the **Zn_2C_xDC** compounds were measured in $CDCl_3$ and this effect may originate from intermolecular or intramolecular coordination of the triazole nitrogen atoms to the porphyrin zinc centers (Chapter 2, Figure 15). Due to the concentration difference between the NMR-studies (1 mM) and UV-Vis studies (1.5 µM), it can be concluded that the coordination observed in the ^{1}H-NMR spectra in $CDCl_3$ originates from intermolecular coordination of the triazole nitrogen atoms to the zinc center of another **Zn_2C_xDC** compound, since such a process will be concentration dependent.

Another cause, which cannot be neglected, because zinc centers in porphyrins have typically a 5-coordination, is that the zinc centers are coordinated to an axial ligand that is situated inside the receptor cavities. An obvious ligand that is known to coordinate to the zinc center at the inside of the cavity of **ZnSC** compounds is water.[23] Although great care was taken to expel all water from the system during the preparation of the solutions for the titrations and during the titrations, it is not unlikely that a water molecule is associated to the zinc porphyrins since these compounds always require an axial ligand. However, during the titration measurements in DCM, no deviating behavior was observed although water is expected to be present in a similar amount as in chloroform. A difference in the binding behavior can cause a difference in the binding constants of water to the zinc center. And therefore, **Zn_2C_xDC** compounds dissolved in DCM or chloroform may behave differently towards the binding of ligands. However, it is expected that if water is associated to the zinc centers in the **Zn_2C_xDC** compounds and DABCO binds

to the zinc center, a decrease in the Soret band of the unbound zinc centers and a simultaneous increase in the Soret band of the 1:1 **Zn_2C_xDC**:DABCO complex would be observed because the coordination sphere of the zinc centers is limited to 5 ligands. Since the decrease in the Soret band of the uncoordinated zinc centers is not accompanied by an immediate increase in the Soret band of the coordinated complex, it is possible that a water molecule is associated to the zinc center but it is questionable whether its binding is will cause the observed deviating behavior in the titration for the addition of the first 10 equivalents of DABCO to the **Zn_2C_xDC** compounds.

A final possibility is that DABCO first interacts with other binding sites at the **Zn_2C_xDC** compounds, before it binds to the zinc centers. These binding sites in chloroform may be located at the porphyrin planes, the bis-triazole linkers, or the diphenylglycoluril-based cavities of the **Zn_2C_xDC** compounds. The **Zn_2C_xDC** compounds can be divided into two parts, the diphenylglycoluril-based cage equipped with a porphyrin plane and the two porphyrin planes that are connected via a bistriazole linker. The latter part has a similar structure as other covalently linked zinc bis-porphyrin systems reported in the literature, such as porphyrin tweezers, although these systems lack triazole groups in their linkers.[8,10,14,15] Binding of DABCO to such systems in chloroform did not exhibit deviations in the titration curves as observed for our **Zn_2C_xDC** compounds.[8,10,14,15] Therefore, it is unlikely that the anomalies in the titration curves of the **Zn_2C_xDC** compounds with DABCO originate solely from the porphyrin planes. However, it is possible that the bistriazole linker and/or the solvent induce a specifically folded geometry in the **Zn_2C_xDC** compounds that may serve as a new binding site for DABCO (Figure 8a). Another possibility is that chloroform, with its slightly acidic proton, forms weak hydrogen bonds with for example the carbonyl groups and/or the ethylenedioxy groups of the cavity (Figure

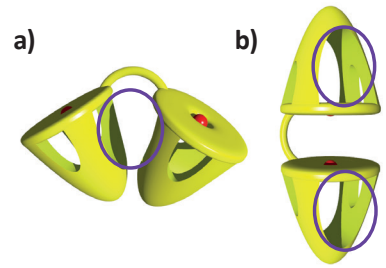

Figure 8 *Schematic representation of two possible orientations of* ***Zn_2C_xDC*** *dissolved in chloroform. (a) A possible binding cavity for DABCO is created in between the two cavities (purple ellipse). (b) Chloroform molecules might have interactions with the carbonyl groups and/or the ethylenedioxy groups in the cavity of* ***Zn_2C_xDC*** *(purple ellipse), generating additional binding sites.*

8b), thereby creating new binding sites or spaces for DABCO.[33,34] To exclude the binding of DABCO inside of the cavity of the **Zn_2C_xDC** compounds, DABCO was added in a >10 fold excess to the reference compound **H_2SC** in $CDCl_3$ at NMR concentration (1 mM). The NH protons in the porphyrin can yield additional information if DABCO binds inside of the cavity since they are expected to exhibit a change in chemical shift if the environment of the cavity changes. However when the ^{1}H-spectra of **H_2SC** with and without the presence of a >10 fold excess of DABCO were compared, no change in chemical shift was observed for the proton signals of the cavity neither for the NH protons. Therefore, binding of DABCO to the inside of the cavity of the **Zn_2C_xDC** compounds is not present and was discarded as a cause for the deviating binding behavior of DABCO.

3.2.3.1 DABCO binding to two zinc porphyrins that are connected with a bistriazole linker

In order to systematically identify possible binding locations for DABCO ligands other than the porphyrin zinc centers, a model compound for **Zn_2C_xDC** in which the diphenylglycoluril-based cavities are absent, was synthesized. It consists of two tri-tolylporphyrins that are linked via a bistriazole-undecyl spacer (**Zn_2C_{11}TTBP**, Figure 9a). It serves as a reference compound for **$Zn_2C_{11}DC$**, since for that compound the deviation between the first part of the titration curves and the fits assuming a 1:2 binding model was most pronounced (Figures 6d and 7c). When up to 10 equivalents of DABCO were added to a solution of **Zn_2C_{11}TTBP** in chloroform, the initial Soret band at 420.5 nm, decreased in intensity (Figure 9b).[8,10–16,19] This decrease was accompanied by a simultaneously increase of a new red-shifted Soret band at 424.5 nm, indicative of the formation of the 1:1 **Zn_2C_{11}TTBP**:DABCO sandwich complex.[8,10–16,19] The emergence of the new Soret band at 424.5 nm already occurred during the addition of the first equivalents of DABCO, which is in contrast to the behavior observed in case of the **Zn_2C_xDC** compounds. The titration curve shows that after the addition of 1.5 equivalents of DABCO no more increase in absorbance of the Soret band at 424.5 nm occurs (Figure 9c), indicating the full formation of the 1:1 **Zn_2C_{11}TTBP**:DABCO sandwich complex. Although the measured maximum absorbance is high (A_{max} = 2), which gives rise to some uncertainty about the measurement, the coordination behavior of DABCO to **Zn_2C_{11}TTBP** in chloroform does not show the anomalies observed for the coordination of DABCO to the **Zn_2C_xDC** compounds in chloroform. Therefore, it is concluded that these anomalies do not originate from a specific geometry imposed by the porphyrin planes and the bis-triazole linker.

3.2.3.2 Role of the diphenylglycoluril-based cavity

Subsequently, it was investigated whether the deviating titration characteristics of the **Zn_2C_xDC** compounds could be ascribed to their diphenylglycoluril-based cavities in combination with a porphyrin plane, which contain parts that may have non-

covalent interactions with DABCO or solvent molecules. First, the titration of the zinc tetrahydroxy porphyrin cage compound (**$Zn(OH)_4SC$**, Figure 10a) with DABCO in chloroform, which had been published previously by our group, was re-analyzed (Figure 10).[13] During the addition of the first half equivalent of DABCO, the absorbance of the Soret band of **$Zn(OH)_4SC$** hardly changes (Figure 10c, purple box up to 0.5 equivalents of DABCO). After this initial delay, a steep decrease in absorbance of the Soret band at 421 nm and a steep increase in the Soret band at 426 nm, which is indicative of the formation of the 2:1 **$Zn(OH)_4SC$**:DABCO sandwich complex, are observed. Further addition of DABCO, up to 5 equivalents, leads to the simultaneous increase of the Soret band at 426 nm and a Soret band at 428 nm. Both bands heavily overlapped. The emergence of the Soret band at 428 nm points to the formation of the 1:1 **$Zn(OH)_4SC$**:DABCO complex. The observed delay displays similarities to the delays in the titration curves of DABCO with the **Zn_2C_xDC** compounds, although it is significantly shorter in the case of **$Zn(OH)_4SC$**. **$Zn(OH)_4SC$** contains a diphenylglycolu-

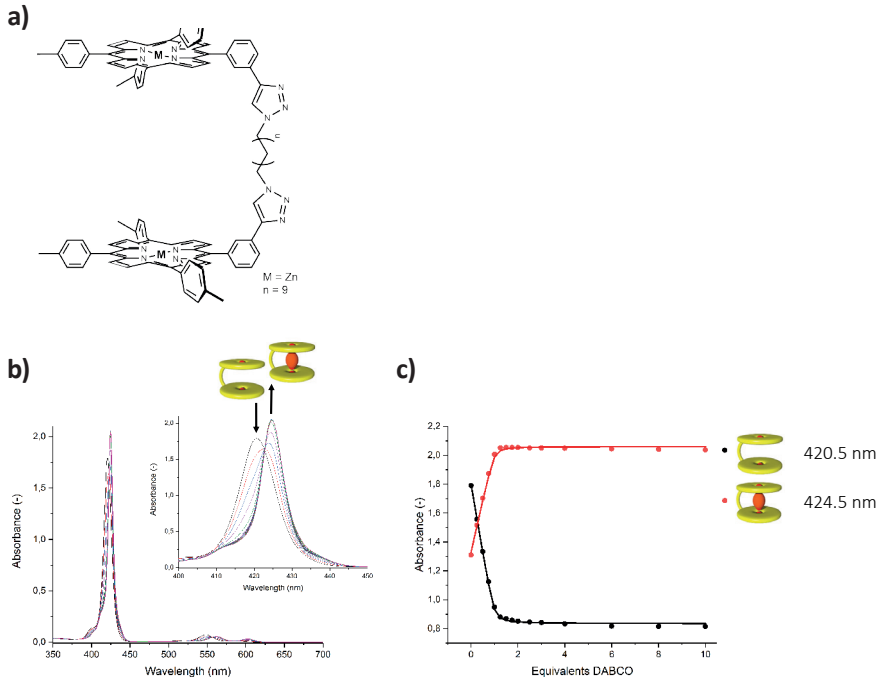

Figure 9 *a) Chemical structure of reference compound **Zn_2C_{11}TTBP**. b) Representative UV-Vis spectra of the titration of **Zn_2C_{11}TTBP** with DABCO in chloroform. The inset shows a zoom-in of the Soret band region. c) Titration curves of **Zn_2C_{11}TTBP** in which the absorbance is plotted as a function of the number of equivalents of DABCO added. The solid lines represent fits assuming a standard 1:1 binding model. For clarity reasons, the number of equivalents of DABCO is plotted on a linear scale.*

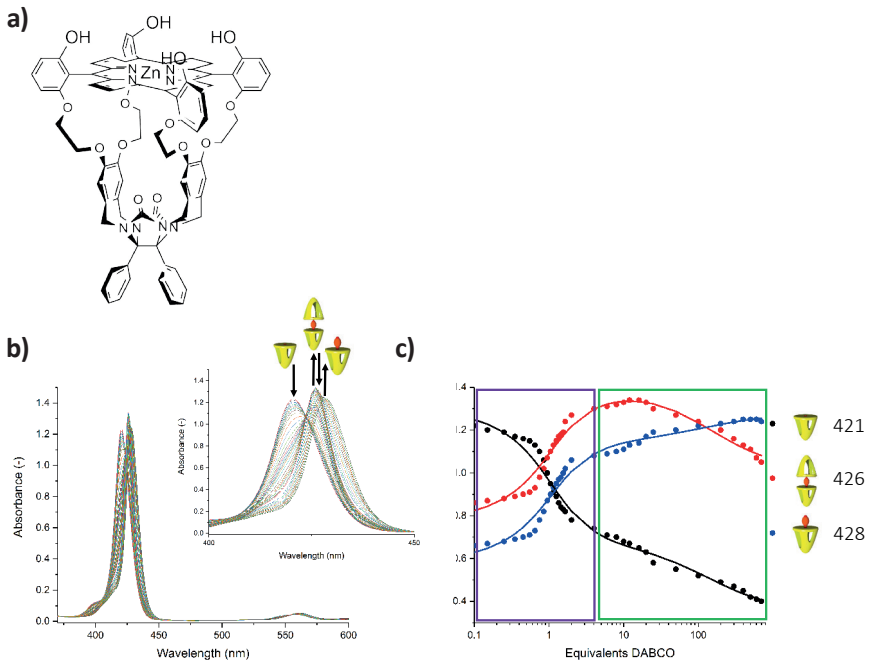

Figure 10 *a) Chemical structure of the reference tetrahydroxy porphyrin cage compound* ***Zn(OH)$_4$SC****. b) Representative UV-Vis spectra of the titration of* ***Zn(OH)$_4$SC*** *with DABCO in chloroform. The inset shows a zoom-in of the Soret band region. c) Titration curves of the Soret bands at 421 nm (black), 426 nm (red), and 428 nm (blue) with fits (solid lines) assuming a standard 1:2 binding model.*

ril-based cavity in combination with a porphyrin plane, but it does not contain a linker. Since it was concluded in the previous section that the anomaly in the titration curves does not originate from the combination of a porphyrin plane and a bistriazole linker, the titration of **Zn(OH)$_4$SC** with DABCO suggests that it originates from the diphenylglycoluril-based cavity in combination with the porphyrin plane. The fact that **Zn(OH)$_4$SC** contains one cavity and the **Zn$_2$C$_x$DC** compounds two may explain why the steep change in the Soret absorbance occurs at a lower number of added DABCO equivalents in the titration with **Zn(OH)$_4$SC**.

3.2.3.3 Concluding remarks on the observed deviating binding behavior

Assuming that the deviating binding behavior during the titration of DABCO with the **Zn$_2$C$_x$DC** compounds in chloroform can be ascribed to the presence of the cavities in combination with the porphyrins, it was hypothesized that it can originate from interactions between chloroform solvent molecules and the cavity parts of the **Zn$_2$C$_x$DC** compounds, or from specifically folded geometries adopted by the **Zn$_2$C$_x$DC**

compounds induced by chloroform solvation effects (Figure 8). This hypothesis was supported by the fact that in DCM the experimentally obtained titration curves adequately match the calculated fits for the formation of a 1:1 **Zn$_2$C$_x$DC**:DABCO sandwich complex (Figure 3). In contrast to DCM, chloroform can form weak hydrogen bonds with the ethyleneoxy spacers and/or the carbonyl groups of the cavities of the **Zn$_2$C$_x$DC** compounds (Figure 11), and this may lead to differences in solvation.

These hydrogen bonds could cause the association of chloroform molecules around the cavities and thereby create additional binding sites for DABCO other than the zinc centers in the porphyrins. The deviating titration curves were not observed in a solvent mixture of chloroform and MeCN (1:1, (v/v), see section 2.4), possibly because in that case MeCN molecules coordinate to the porphyrin zinc centers giving rise to a Soret band at 426 nm, while no Soret band of the uncomplexed zinc centers at 421 nm is observed. Hence, no transition between these two Soret bands takes place. Also, it is more likely that hydrogen bonds will be formed between chloroform and MeCN instead of between chloroform and the cavities of the **Zn$_2$C$_x$DC** compounds. To test if there are weak interactions between chloroform molecules and the **Zn$_2$C$_x$DC** compounds, we may adapt the binding model that is used to fit the

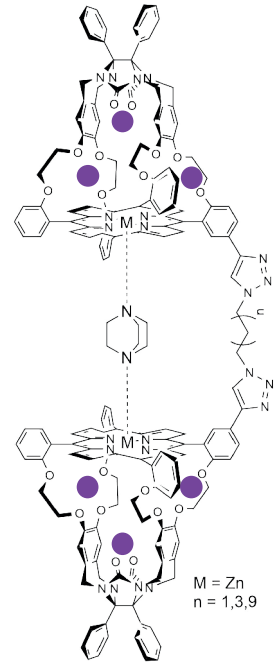

Figure 11 *Possible sites at the cavities of the* ***Zn$_2$C$_x$DC*** *compounds to which chloroform molecules (purple circles) can associate: the carbonyl groups (two binding sites per cavity) and/or at the ethyleneoxy spacers (eight binding sites per cavity).*

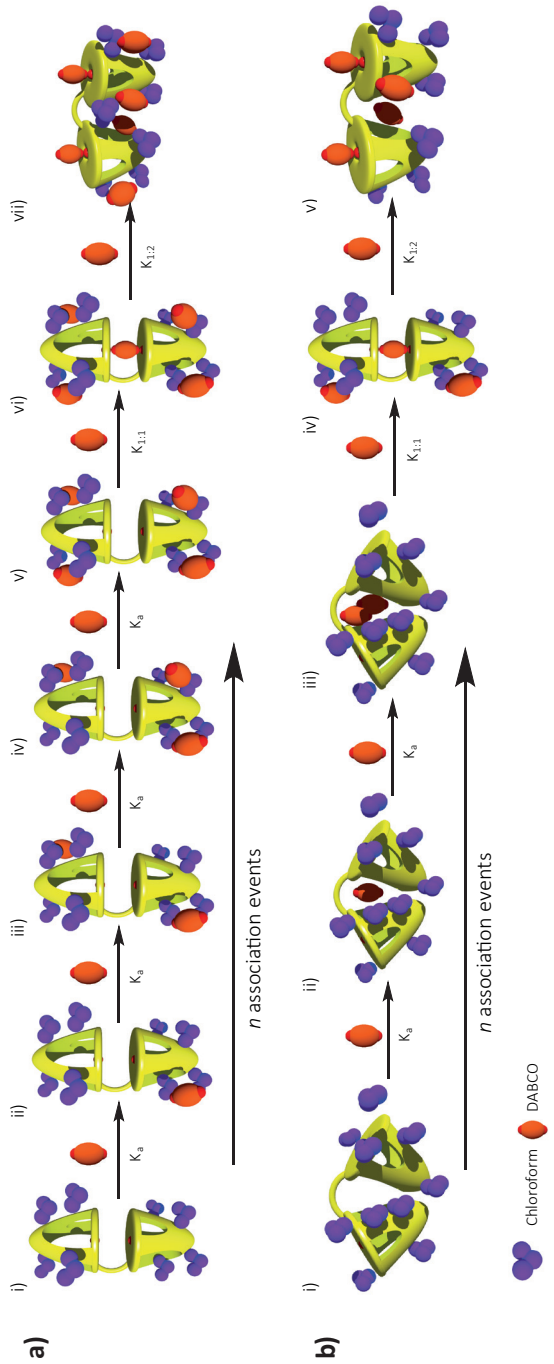

Figure 12 *Schematic representations of the possible adapted binding models, which describe the binding of DABCO molecules (orange) to a* ***Zn_2C_xDC*** *compound (yellow) dissolved in chloroform (purple). (a, i) Association of chloroform molecules in the first possible adapted binding model at the cavity parts of* ***Zn_2C_xDC****, creating hydrogen bonding "binding sites" for DABCO. (a, ii-v) DABCO molecules interact with these binding sites with binding constants K_a. (a, vi) Once all the possible hydrogen bonding binding sites are occupied, coordination of DABCO to the two zinc centers in the porphyrin planes to form a sandwich complex with binding constant $K_{1:1}$ can take place. (a, vi) Upon addition of more equivalents of DABCO, the 1:2 open* ***Zn_2C_xDC****:DABCO complex is eventually formed with a binding constant $K_{1:2}$. (b, i)* ***Zn_2C_xDC*** *is solvated by chloroform molecules creating hydrogen bonding "binding sites" for DABCO between the two cavities. (b, ii-iii) DABCO molecules interact with these binding sites with binding constants K_a. (b, iv) When all the binding sites are occupied by DABCO, a DABCO molecule can be bound to the two zinc centers in the porphyrin planes forming the 1:1* ***Zn_2C_xDC****:DABCO sandwich complex with a binding constant $K_{1:1}$. (b, v) When more equivalents of DABCO are added, the 1:2* ***Zn_2C_xDC****:DABCO open complex can be formed with a binding constant $K_{1:2}$. The exact locations and nature of the interactions of chloroform as well as DABCO with the* ***Zn_2C_xDC*** *compounds and with each other are not precisely known, and an equal distribution of the molecules at the cavities of* ***Zn_2C_xDC*** *is schematically (a) and randomly (b) depicted.*

titration curves. Assuming that specific solvation of the cavities of the **Zn_2C_xDC** compounds by chloroform molecules occurs, leading to additional weak binding sites for DABCO via hydrogen bonding interactions with the DABCO nitrogen atoms (Figure 12), the binding model should include the association of *n* DABCO molecules to these binding sites, each with an equilibrium constant K_a (Figure 12a, i-v). It should be noted that the binding process might be cooperative. After the occupation of these sites by ligand molecules, the zinc porphyrins subsequently can coordinate one additional DABCO molecule, forming the 1:1 **Zn_2C_xDC**:DABCO sandwich complex with a binding constant $K_{1:1}$ (Figure 12a, vi). Finally, another DABCO molecule can coordinate to the zinc porphyrins and form the 1:2 **Zn_2C_xDC**:DABCO open complex with a binding constant $K_{1:2}$ (Figure 12a, vii). This second binding event is assumed not to differ from $K_{1:2}$, i.e. the binding constant for the same event in the standard 1:2 binding model. In the case that the **Zn_2C_xDC** compounds assume a specifically folded geometry as a result of the solvation by chloroform molecules, also new binding sites for DABCO may be created, involving a possibly cooperative equilibrium constant K_a , which accounts for each individual association of *n* DABCO molecules (Figure 12b, i-iii), before the regular 1:1 **Zn_2C_xDC**:DABCO sandwich complex (Figure 12b, iv) and the 1:2 **Zn_2C_xDC**:DABCO open complex are formed (Figure 12b, v).

Unfortunately, however, based on the currently available experimental data, the precise geometry of the **Zn_2C_xDC** compounds in solution and the nature of the additional binding sites for DABCO are still unknown. Therefore, an accurate adapted binding model could not yet be constructed and used to fit the experimentally obtained titration curves.

3.2.4 Titrations in a solvent mixture of chloroform and acetonitrile (1:1, (v/v))

For the intended application of the double porphyrin cage as a component in a catalytic machine that can write information on a polymer chain (*vide infra*), the binding of a guest that can induce an allosteric interaction, i.e. a viologen-based molecule, in one of the cavities is required. However, such a guest is generally insoluble in chloroform. For this reason, acetonitrile (MeCN) was added as a co-solvent and it was investigated whether also in this solvent mixture stable 1:1 **Zn_2C_xDC**:DABCO sandwich complexes would be formed.

Figure 13a presents the UV-Vis spectra of the titration of **Zn_2C_3DC** with DABCO in the solvent mixture chloroform and MeCN (1:1, (v/v)). In the UV-Vis spectra, two Soret bands and the expected Q-bands are observed between 400 and 450 nm, and 525 and 652 nm, respectively. According to the literature available for similar zinc bisporphyrin systems and our previous UV-Vis experiments in the solvents DCM and chloroform, the Soret band of the free host, **Zn_2C_3DC**, is expected to be located around 420 nm.[10] However, this Soret band was not observed in any of the titrations of the **Zn_2C_xDC** compounds with DABCO in this solvent mixture. Its absence can be

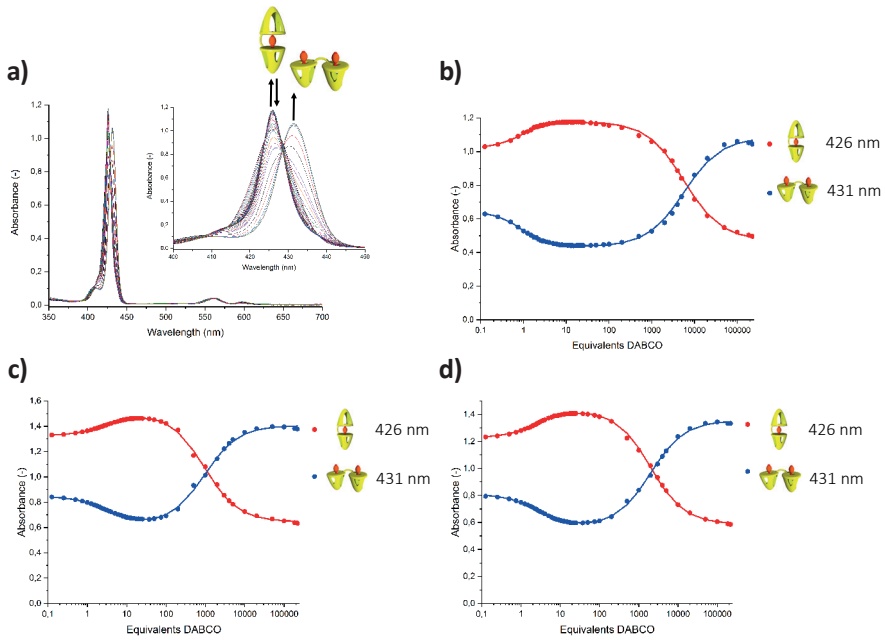

Figure 13 *a) UV-Vis spectra of the titration of* ***Zn_2C_3DC*** *with increasing amounts of DABCO in a solvent mixture of chloroform and MeCN (1:1, (v/v)). The inset shows a zoom-in of the Soret band region. b, c, d) Titration curves of* ***Zn_2C_3DC*** *(b),* ***Zn_2C_5DC*** *(c), and* ***$Zn_2C_{11}DC$*** *(d) in which the absorbance is plotted as a function of the number of added equivalents of DABCO. The dotted curves are the experimentally obtained data and the solid lines the fits calculated for the two Soret bands (see text).*

explained by the fact that a molecule of MeCN is coordinated to the zinc porphyrin, eliminating the presence of zinc centers that are not complexed to nitrogen-containing ligands and, hence, the occurrence of the Soret band corresponding to such species (data shown in appendix A4).[29]

The band at 426 nm, which thus most probably originates from the **Zn_2C_xDC**:MeCN complex, sharpens upon the addition of DABCO and increases in intensity (Figure 13a). These special spectral changes likely reflect the replacement of MeCN by DABCO. No shift in wavelength occurs since only two nitrogen-containing ligands are exchanged.[26,27] The sharpening of the Soret band indicates the formation of a more well-defined species, being the 1:1 **Zn_2C_3DC**:DABCO sandwich complex.[35] It is more defined and rigid because it has less rotational and translational freedom when the two porphyrins are pinched together compared to the situation when MeCN molecules are coordinated to the zinc porphyrins in an open complex. When more aliquots of DABCO are added, the emergence of a red shifted Soret band at 431 nm reflects the formation of a 1:2 **Zn_2C_xDC**:DABCO open complex.[8,10–16]

Table 1 Microscopic binding constants $K_{1:1}$ and $K_{1:2}$ obtained from the titrations of ***Zn_2C_3DC***, ***Zn_2C_5DC***, and ***$Zn_2C_{11}DC$*** with DABCO in the solvent mixture chloroform and MeCN (1:1, (v/v)). The K-values are given as their logarithmic values, with a reported error of 2 times the standard deviation over the measurement, which was performed fourfold. The number of equivalents of DABCO needed to obtain the maximum amount of 1:1 ***Zn_2C_xDC***:DABCO sandwich complex is also reported.

	Zn_2C_3DC	**Zn_2C_5DC**	**$Zn_2C_{11}DC$**[a]
Log($K_{1:1}$)	6.29 ± 0.06	5.37 ± 0.04	5.52 ± 0.04
Log($K_{1:2}$)	2.11 ± 0.09	2.87 ± 0.05	2.54 ± 0.03
Equivalents DABCO (1:1)	43	51	63

[a] Determined in threefold

The obtained titration curves were fitted to a standard 1:2 binding model (Figure 13b-d), and the corresponding binding constants can be found in Table 1.[25] The binding constants appear to be rather similar for the **Zn_2C_xDC** compounds with different spacer lengths. The binding constant of the 1:1 **Zn_2C_xDC**:DABCO sandwich complex ($K_{1:1}$) is the highest for **Zn_2C_3DC**. Binding constants for other, previously reported bis-porphyrin systems range from 4 to 8 for log($K_{1:1}$) and 2 to 3 for log($K_{1:2}$) in various solvents (DCM, chloroform, toluene) and are thus comparable with the binding constants obtained for our **Zn_2C_xDC** compounds. It should be noted, however, that in the case of our compounds competition for binding to the zinc centers occurs between DABCO and MeCN molecules in the used solvent mixture, probably leading to lower binding constants compared to systems in which MeCN is absent.[8,10,18,19,36–38] Previously, the coordination behavior of DABCO with **$Zn(OH)_4SC$** was studied in the same solvent mixture of chloroform and MeCN (1:1, (v/v), see above).[13] In that case, the 2:1 **$Zn(OH)_4SC$**:DABCO sandwich complex was formed with a very high binding constant of log($K_{1:1}$) = 10.9, which is the result of additional enhancing interactions between the two porphyrin cages via their hydroxyl groups. The **Zn_2C_xDC** compounds lack these hydroxyl groups but are covalently connected, placing the porphyrins in close proximity and making binding of a ditopic axial ligand more favorable. On the other hand, this connection between the porphyrins also causes conformational strains, which can lead to a less favorable coordination geometry. The combination of these factors may explain the lower binding constants which were observed for the first binding event in our **Zn_2C_xDC** compounds. Taking into account both $K_{1:1}$ and $K_{1:2}$, a total of 43 equivalents of DABCO need to be present to generate the maximum amount of sandwich complexes for **Zn_2C_3DC** (at the used concentration of host (1.5 µM) during the titration). When the spacer length of the **Zn_2C_xDC** hosts increases, the number of equivalents of DABCO that need to be present to form the maximum

amount of sandwich complex turned out to increase as well. Upon an increase in spacer length, more degrees of freedom are present in the host compounds, and this apparently influences both $K_{1:1}$ and $K_{1:2}$. When $K_{1:1}$ is relatively high and $K_{1:2}$ relatively low, a relatively small amount of DABCO is needed to form the maximum amount of the 1:1 sandwich complex. In order to form the 1:1 sandwich complex, the DABCO ligand has to coordinate simultaneously to both zinc porphyrins of the host, and therefore these moieties have to be in close proximity, which is less likely when the spacer is longer and has more degrees of freedom. As a result, the binding strength of the **Zn_2C_xDC**:DABCO complex will become weaker and more equivalents of the ligand are needed to obtain the maximum amount of sandwich complex.

3.2.5 Formation of the different DABCO complexes: NMR studies

In order to corroborate the formation of the respective complexes that were identified by the UV-Vis experiments, NMR studies were conducted for **Zn_2C_3DC** in the presence of various equivalents of DABCO and at various temperatures in a solvent mixture of $CDCl_3$ and MeCN-d_3 (1:1, (v/v)). Figure 14 shows the spectral changes in the ^{1}H-NMR spectra when up to 8 equivalents of DABCO were added to a 1 mM solution of **Zn_2C_3DC** at room temperature. In the presence of one equivalent of DABCO, the β-pyrrole signals, which originally resonated in the range from δ 8.87-8.54 ppm shifted upfield to δ 8.49-8.31 ppm, while a new very broad signal appeared at δ −4.46 ppm (Figure 14, blue box and arrow). The peak at δ −4.46 ppm is proposed to originate from the twelve chemically equivalent methylene protons of DABCO, which is bound in between two zinc porphyrin planes.[9–13,15,17,18] Due to fast exchange of the components in solution on the NMR timescale, the proton resonance of DABCO at δ −4.46 ppm was broad. In the presence of two or more equivalents of DABCO, uncomplexed DABCO (δ 2.59 ppm) was found to be present, as was confirmed by recording a reference spectrum in the same solvent mixture, which gave rise to a similar peak at δ 2.59 ppm (Figure 14, red arrow). However, the 1:2 **Zn_2C_3DC**:DABCO open complex, which is expected to generate a resonance at around δ −3 ppm for the six methylene protons of DABCO located in close proximity to the nitrogen atom coordinated to the zinc porphyrin, was not observed. This absence may be due to signal broadening as a result of rapid exchange between the bound and unbound state at 298 K.[9,10,20,21]

To lower the dynamics of the molecules in solution, which would help sharpen the resonances in the ^{1}H-NMR spectra, the solution of **Zn_2C_3DC** with one equivalent of DABCO was measured at different temperatures ranging from 238 K to 323 K (Figure 15). At high temperatures, the resonance of bound DABCO broadened and could not be observed in the spectrum. However, at temperatures lower than 278 K the broad resonance sharpened into a well-defined peak, which shifted to δ −4.6 ppm at 238 K, while the signals originating from **Zn_2C_3DC** gradually broadened.

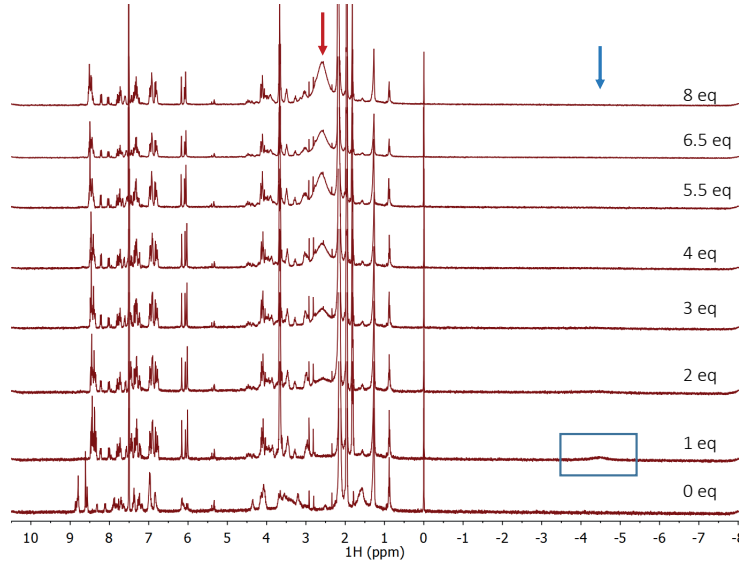

Figure 14 *^{1}H-NMR spectra of **Zn_2C_3DC** (1 mM) with an increasing number of equivalents of DABCO in a solvent mixture of $CDCl_3$ and MeCN-d_3 (1:1, (v/v)). The blue box and arrow point at the signal at −4.46 ppm that appears in the presence of one equivalent of DABCO. The red arrow points at the signal of uncomplexed DABCO at 2.59 ppm, which is observed in the presence of two or more equivalents of the ligand.*

To investigate the binding of DABCO into further detail, up to 4 equivalents of the ligand were added to **Zn_2C_3DC** and NMR spectra were recorded at 248 K (Figure 16). In the presence of 0.25 equivalents of DABCO, the signals of **Zn_2C_3DC** sharpened, indicating that a less dynamic species is present in solution. A gradual broadening of the resonance of DABCO at δ −4.58 ppm could be observed when the addition of this ligand was increased from 0.25 to one equivalent. Upon the addition of more equivalents, the peak of the ligand in the 1:2 **Zn_2C_3DC**:DABCO open complex started to arise at δ −2.92 ppm, while the resonance at δ −4.58 ppm decreased in intensity. Due to the gradual broadening of the DABCO resonances, no reliable baseline correction could be applied and, therefore, no ratio of the 1:1 and 1:2 complexes could be determined by integration of the signals. NMR studies on the formation of 1:1 sandwich complexes upon the addition of up to one equivalent of DABCO to other bis-porphyrin systems have been reported in the literature, and depending on the solvent and the temperature, these systems also displayed broad resonances for the DABCO protons in a sandwich-like complex.[9–11,21] When the amount of DABCO in those systems was increased, also resonances corresponding to the 1:2 complexes arose.[9–11,21] The signals of **Zn_2C_3DC** broadened and became less defined upon the addition of more equivalents of DABCO, which indicates an increase in the dynamics

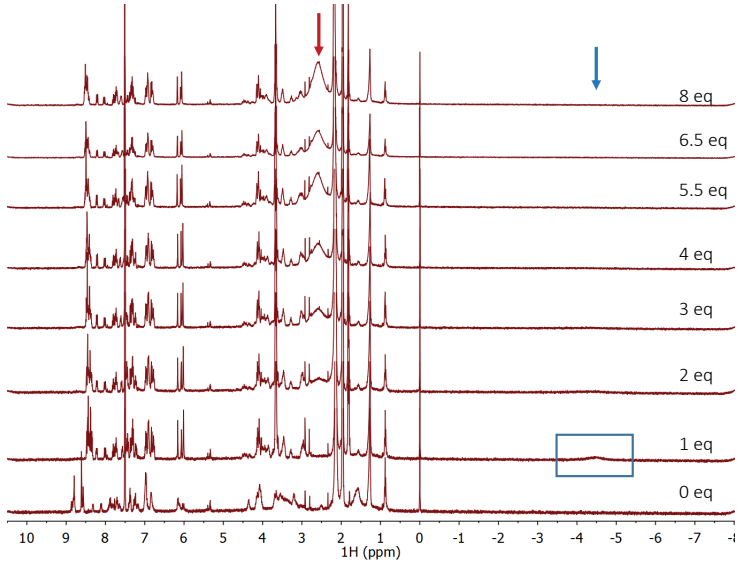

Figure 15 *Variable temperature ^{1}H-NMR spectra of **Zn_2C_3DC** (1 mM) with one equivalent of DABCO in a solvent mixture of $CDCl_3$ and MeCN-d_3 (1:1, (v/v)). The blue arrow points at the signal of DABCO bound in a sandwich-like geometry between the two zinc porphyrin planes.*

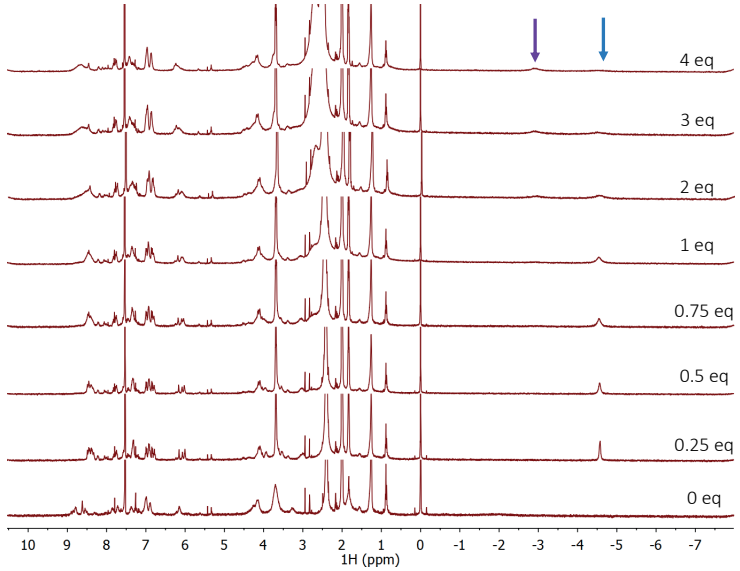

Figure 16 *^{1}H-NMR spectra of **Zn_2C_3DC** (1 mM) and various amounts of DABCO in a solvent mixture of $CDCl_3$ and MeCN-d_3 (1:1, (v/v)) at 248 K. The blue arrow points at the signal of DABCO bound in a sandwich-like geometry between the two zinc porphyrin planes, and the purple arrow at the signal of DABCO bound to a zinc porphyrin in a mono-dentate geometry.*

of the host. In the presence of 4 equivalents of DABCO, the signals of DABCO ligands that are bound both in monotopic and ditopic geometries were present as broad resonances (Figure 16, blue and purple arrows).

All formed complexes were more clearly observed by NMR spectroscopy at temperatures lower than 288 K, but it can be expected that these complexes also exist at room temperature when the same concentrations and ratios of **Zn_2C_3DC** and DABCO are present, albeit involved in higher exchange rate processes and in a distribution according to the binding constants operating at room temperature.

3.3. Conclusion

The coordination of DABCO to covalently linked zinc double porphyrin cages (**Zn_2C_xDC**) was investigated by UV-Vis and NMR titrations. When the titrations were carried out in dichloromethane (DCM), a solvolysis reaction between the solvent and DABCO took place, leading to the formation of 1-(chloromethyl)-1,4-diazabicyclo [2.2.2]octan-1-ium. This compound competes with DABCO for binding to the host molecules and as a result irreproducible titration curves were obtained. For this reason, DCM was discarded as a suitable solvent. Chloroform did not react with DABCO and in this solvent the 1:1 **Zn_2C_xDC**:DABCO sandwich complexes remained stable. However, up to the addition of 10 equivalents of the ligand the obtained binding curves deviated from the theoretically calculated curves corresponding to standard 1:2 binding models. Systematic variations in the structure of the bis-porphyrin hosts suggested that this deviation originates from the presence of the diphenylglycoluril-based cavity in combination with the porphyrins. The deviating results might be the result of the fact that the **Zn_2C_xDC** compounds adopt a specific geometry in solution, or might be caused by the association of chloroform molecules to the host molecules. These two possible effects could lead to the creation of additional binding spaces for DABCO. Unfortunately, with the currently available experimental data, no binding model that is in line with these phenomena could be constructed. To circumvent the problems with DCM and chloroform as solvents the formation of the sandwich complexes was also studied in a mixture of chloroform and MeCN (1:1, (v/v)). UV-Vis studies indicated that MeCN already from the beginning coordinates to the zinc porphyrins and is replaced by DABCO when this ligand is added, to form stable 1:1 **Zn_2C_xDC**:DABCO sandwich complexes. Upon the addition of more equivalents of DABCO, the open 1:2 **Zn_2C_xDC**:DABCO complexes were formed. The titrations revealed that **Zn_2C_3DC** formed the strongest 1:1 sandwich complex with DABCO, although the differences in binding strength of DABCO to the other **Zn_2C_xDC** hosts were rather small. The 1:2 open complexes had an association constant of about 3 orders of magnitude lower than those of the respective 1:1 complexes. The formation of the 1:1 and 1:2 complexes of **Zn_2C_3DC** and DABCO were

corroborated by variable temperature ^{1}H-NMR titrations in a solvent mixture of $CDCl_3$ and MeCN-d_3 (1:1, (v/v)). It was concluded that the formation of the 1:1 **Zn_2C_xDC**:DABCO sandwich complexes in chloroform and in a solvent mixture of chloroform and acetonitrile (1:1, (v/v)) was successful, providing an essential step forward to the use of these double porphyrin cages as components in catalytic systems that can write information on single polymer chains.

3.4. Experimental

All chemicals were commercially obtained and used without further purification unless stated otherwise. DCM was distilled under nitrogen from calcium hydride and MeCN was distilled under argon from calcium chloride. Chloroform (anhydrous, contains amylenes as stabilizers, ≥99%) was filtered over potassium carbonate under argon before use. DABCO was sublimated at 60-70 ^{0}C under vacuum prior to use.

^{1}H and ^{13}C-NMR spectra were recorded on Bruker Avance III 400 or 500 MHz spectrometers at 25˚C unless stated otherwise. Chemical shifts are reported in parts per million (ppm) relative to tetramethylsilane (TMS) as the internal reference. NMR data are presented as follows: chemical shift (ð) in ppm, multiplicity (s = singlet, bs = broad singlet, d = doublet, t = triplet, q=quartet, td = triplet of doublets, m = multiplet and/or multiple resonances), integration, assignment and coupling constant (J) in Hertz (Hz). All NMR signals were assigned on the basis of ^{1}H, ^{13}C-NMR, COSY, ROESY, HSQC and HMBC experiments. The numbering of the proton, carbon and nitrogen atoms used in the assignments is depicted in Figure 17. Phase and baseline corrections were applied to all ^{1}H-NMR and ^{13}C spectra. LCQ mass spectra were recorded in methanol on a Thermo Finnigan LCQ Advantage Max mass spectrometer. X-ray reflections were measured on a Bruker D8 Quest diffractometer with sealed tube and Triumph monochromator (λ = 0.71073Å). The software package used for the

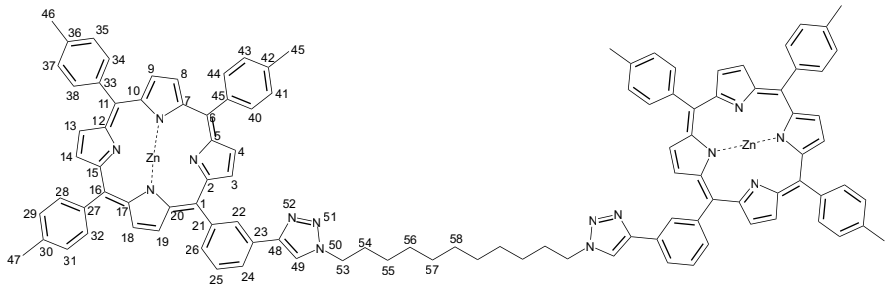

Figure 17 *Carbon, proton and nitrogen numbering of* ***Zn_2C_{11}TTBP*** *used for all NMR analyses. The same numbers are employed for the unnumbered (right) part of the molecule.*

intensity integration was Saint. Absorption correction was performed with SADABS. The X-ray structure was solved with direct methods using SHELXT. Least-squares refinement was performed with SHELXL-2014 against of all reflections. Non-hydrogen atoms were refined freely with anisotropic displacement parameters. Hydrogen atoms were calculated at positions or located in difference Fourier maps. All calculated hydrogen atoms were refined with a riding model. UV-Vis spectra were recorded using the software UV Probe on a Shimadzu UV 1800 spectrometer in a quartz cuvette with 1 cm path length and 3.8 mL total volume. The spectrum of the solvent was used as the baseline for the spectra.

3.4.1 Titration methods

UV-Vis titrations

All titrations were carried out in two-, tree- or fourfold. The 1:1 solvent mixtures were prepared by weighing the desired amounts of the two solvents in a closed Erlenmeyer flask. After thorough mixing of the solvents, the density of the solvent mixture was determined from the weight increase of a 50 mL volumetric flask.

A host stock solution was prepared by quantitatively weighing an amount of the host of between 1 and 2 mg, which was subsequently dissolved in 10 mL solvent or solvent mixture (HostStock). The HostStock was diluted to 1.5 µM (10 mL). All ligand solutions (10 mL) contained 1.5 µM host from diluting HostStock and 5.00^{-5} M (L1), 0.0001 M (L2), 0.0005 M (L3), 0.001 M (L4), 0.1 M (L5) and 1 M (L6) DABCO solution. Solution L6 was prepared by directly weighing the required amount of DABCO in 10 mL of solvent. Solution L5 was prepared from a 0.5 M DABCO stock solution. Solutions L4 and L3 were prepared by diluting solution L5. Solutions L2 and L1 were prepared by diluting solution L3. The volumes of solvents or solvent mixtures required for the host and host-ligand solutions were weighed on an analytical balance and the addition of the ligand solutions to the host solution was carried out with Gilson pipets (up to a volume of 1000 µL).

A UV-Vis spectrum was recorded after every addition of DABCO. The amounts of DABCO ligand solutions titrated to the host are given in Table 2.

Table 2 Table of titrated amounts of DABCO to a solution of **Zn_2C_xDC** (1.5 µM)

[DABCO] (M)	Equivalents	Volume to add (µL)	Total volume (µL)
5.00^{-05}	0	0.00	1500
	0.125	5.65	1505.65
	0.25	5.69	1511.34
0.0001	0.5	5.71	1517.05
	0.75	5.75	1522.80
	1	5.80	1528.60
	1.25	5.84	1534.44
	1.5	5.89	1540.32
	1.75	5.93	1546.26
	2	5.98	1552.23
	2.25	6.02	1558.26
	2.5	6.07	1564.33
	2.75	6.12	1570.45
	3	6.17	1576.62
	3.5	12.48	1589.09
	4	12.68	1601.77
0.0005	5	4.88	1606.65
	6	4.91	1611.56
	7	4.94	1616.50
	8	4.97	1621.47
	9	5.00	1626.47
	10	5.03	1631.50
	11	5.06	1636.56
	12	5.09	1641.65
	13	5.12	1646.78
	14	5.16	1651.93
	15	5.19	1657.12
0.001	17.5	6.38	1663.50
	20	6.43	1669.94
	22.5	6.48	1676.42
	25	6.53	1682.95
	37.5	33.40	1716.35
	50	34.80	1751.15
	75	74.00	1825.15
	100	80.50	1905.65
	200	409.00	2314.65
0.1	500	10.49	2325.14
	1000	17.70	2342.84

Table 2 Continued

[DABCO] (M)	Equivalents	Volume to add (µL)	Total volume (µL)
	2000	36.20	2379.04
	3000	37.40	2416.44
	4000	38.60	2455.04
	5000	39.80	2494.84
1	10000	19.00	2513.84
	20000	38.90	2552.74
	50000	124.20	2676.94
	100000	236.20	2913.14
	185000	514.00	3427.14
	218000	250.00	3677.14

The change in absorbance intensity of the Soret band was plotted against the number of equivalents of DABCO added, which gave titration curves that were fitted with the program Bindfit at http://supramolecular.org/ using a standard 1:2 binding model. This model involves two binding constants: $K_{1:1}$ for the formation of the 1:1 **Zn_2C_xDC**:DABCO sandwich complex and $K_{1:2}$ for the formation of the 1:2 **Zn_2C_xDC**:DABCO open complex. $K_{1:1}$ and $K_{1:2}$ are defined by equations (1) and (2), in which [H] is the concentration of free host, and [HL] and [HL_2] are the concentrations of host-ligand and host-ligand$_2$ complex, respectively.

$$K_{1:1} = \frac{[HL]}{[H]\,[L]} \tag{1}$$

$$K_{1:2} = \frac{[HL_2]}{[HL]\,[L]} \tag{2}$$

Equations (1) and (2) can be expressed in terms of absorption of the different Soret bands present in the sample and this yields the binding isotherm to which the titration curves can be fitted as equation (3), in which ΔA is the difference between the total absorption (A) and the initial absorption (A_0), $[H]_0$ is the total concentration of host, and $\Delta\varepsilon_{HL}$ and $\Delta\varepsilon_{HL_2}$ are the molar absorption coefficients in M^{-1}, which are defined from the molar absorption coefficients (ε) of the four individual species that are present during the titration (equations (4) and (5)).

$$\Delta A = A - A_0\,\frac{\Delta\varepsilon_{HL}\,(K_{11}[H]_0[L]) + \Delta\varepsilon_{HL_2}\,(K_{11}K_{12}[H]_0[L]^2)}{K_{11}K_{12}[L]^2 + K_{11}[L] + 1} \tag{3}$$

$$\Delta\varepsilon_{HL} = \varepsilon_{HL} - \varepsilon_H - \varepsilon_L \quad (4)$$

$$\Delta\varepsilon_{HL_2} = \varepsilon_{HL_2} - \varepsilon_H - \varepsilon_L \quad (5)$$

For each of the Soret bands equation (3) is calculated, thereby iteratively varying both binding constants simultaneously to yield the smallest error between the fit and the experimentally acquired data per wavelength. Each fitted wavelength has its own set of molar absorption coefficients as these are iteratively varied during the fitting procedure.

^{1}H-NMR titrations

The 1:1 solvent mixture used for the NMR experiments was prepared by the addition of equal volumes of $CDCl_3$ and MeCN-d_3 with Gilson pipets (up to a volume of 1000 µL) in a test tube. After thorough mixing of the solvents, the desired volume was added to the weighed host (1 – 2 mg) to obtain a host solution with a concentration of about 1 mM. Small amounts of ligand solution (up to 134 µL) were added with a Gilson pipet to the host solution until up to 8 equivalents of ligand were present. After each addition of ligand, a ^{1}H-NMR spectrum was recorded after an equilibration time of 5 minutes at the desired temperature.

3.4.2 Synthesis

1-(Chloromethyl)-1,4-diazabicyclo[2.2.2]octan-1-ium[28]

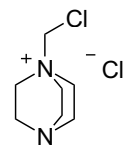

Freshly sublimated DABCO (3.0 g, 26.8 mmol) was dissolved in freshly distilled DCM (30 mL) under inert atmosphere. The solution was refluxed for 4 hours, after which it was allowed to cool to room temperature. The formed white precipitate was isolated by filtration under an inert atmosphere, subsequently washed with distilled DCM (5x10 mL), and dried under vacuum overnight. The product was obtained as a white powder (4.22 g, 80%).

^{1}H-NMR (acetonitrile-d_3, 500 MHz): ð 5.36 (s, 2H, CH_2), 3.53 (t, 6H, $N^+CH_2CH_2N$, J = 7.2 Hz), 3.18 (t, 6H, $N^+CH_2CH_2N$, J=7.2 Hz); LCQ (ESI); m/z 161.6 $(M(^{35}Cl))^+$, 163.1 $(M(^{37}Cl))^+$; calculated for $C_7H_{14}ClN_2$ 161.1 (^{35}Cl); 163.1 (^{37}Cl);

Synthesis of tri-tolyl-mono-{5-bromo-phenyl}-zinc-porphyrin

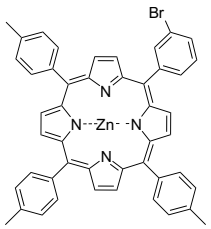

4-Methylbenzaldehyde (7.21 g, 60 mmol, 3 eq.) and 3-bromo-benzaldehyde (3.70 g, 20 mmol, 1 eq.) were dissolved in propionic acid (500 mL). The solution was heated to 90 ^{0}C and pyrrole (5.55 mL, 80 mmol, 4 eq.) was added dropwise. The reaction mixture was refluxed for 4 h, cooled to r.t. and the solvent was evaporated. The residue was purified by silicagel column chromatography using *n*-heptane/chloroform (50/50,

Table 3 Crystal data and data collection parameters for 1-(chloromethyl)-1,4-diazabicyclo[2.2.2]octan-1-ium

CCDC Number	1579101
Formula	$C_7H_{14}ClN_2Cl$
Formula Weight	197.10
Crystal System	orthorhombic
Space Group	Cmc21 (No 36)
a (Å)	6.6480(5)
b (Å)	12.0063(9)
c (Å)	11.5307(9)
V (Å ^{3})	920.36(12)
Z	4
D_{calc} (g/cm^3)	1.423
Mu_{MoKa} (mm^{-1})	0.645
$F_{(000)}$	416
Crystal Size (mm)	0.3x0.41x0.66
Temperature (K)	150
Radiation (Å)	MoKα 0.71073
$Θ_{min}$ (^{0})	3.4
$Θ_{max}$ (^{0})	36.3
Dataset	-11:11;-20:19;-19:19
Tot., Uniq. Data, R (int)	26377, 2381, 0.019
Observed Data (I > 2.0 σ (I))	2369
N_{ref}	2381
N_{par}	61
R	0.0246
wR^2	0.0651
S	1.07
Max and Av Shift/Error	0.00; 0.00
Flack x	-0.005(9)
Min and Max Resd. Dens (e/ Å ^{3})	-0.44; 0.27

(v/v)) as the eluent. The combined product fractions were evaporated to dryness and zinc(II) acetate dihydrate (0.925 g, 4.21 mmol, 0.21 eq.), methanol (50 mL) and chloroform (125 mL) were added. The resulting reaction mixture was refluxed for 2 h, cooled to r.t. and the solvent was evaporated. The crude product was purified by silicagel column chromatography using *n*-heptane/chloroform (40/60, (v/v)) as the eluent. Precipitation from DCM/*n*-heptane and drying *in vacuo* yielded the product (tri-tolyl-mono-{5-bromo-phenyl}-zinc-porphyrin, 1.03 g, 6.5%) as a purple solid.

^{1}H NMR (500 MHz, $CDCl_3$): δ 8.99 (d, 2H, ß-pyrrole-*H*-**4,18**, J = 4.7 Hz), 8.97 (s, 4H, ß-pyrrole-*H*-**8,9,13,14**), 8.91 (d, 2H, ß-pyrrole-*H*-**3,19**, J = 4.6 Hz), 8.39 (s, 1H, Ar*H*-**22**), 8.16 (d, *J* = 7.5, 1H, Ar*H*-**26**), 8.10 (d, *J* = 6.6 Hz, 6H, Ar*H*-**28,32,34,38,40,44**), 7.92 (d, *J* = 8.1 Hz, 1H, Ar*H*-**24**), 7.62 (t, *J* = 7.8 Hz, 1H, Ar*H*-**25**), 7.56 (d, *J* = 6.8 Hz, 6H, Ar*H*-**29,31,35,37,41,43**), 2.72 (s, 9H, CH_3-**45,46,47**); ^{13}C-NMR ($CDCl_3$, 126 MHz): δ 150.75-149.89 (Ar*C*-**12,15,20,17**) 145.17 (Ar*C*-**21**), 139.91 (Ar*C*-**27,33,39**), 137.31 (Ar*C*-**30,36,42**), 137.24 (Ar*C*-**22**), 134.50 (Ar*C*-**28,32,34,38,40,44**), 133.10 (Ar*C*-**26**), 132.45-132.17 (Ar*C*-**13,14,18**), 131.56 (Ar*C*-**19**), 130.79 (Ar*C*-**24**), 128.10 (Ar*C*-**25**), 127.46 (Ar*C*-**29,31,35,37,41,43**), 121.75-121.54 (Ar*C*-**6,11,16**), 121.11 (Ar*C*-**23**), 118.89 (Ar*C*-**1**), 21.69 (C**45,46,47**).

Synthesis of tri-tolyl-mono-{5-triisopropylsilylacetylene-phenyl}-zinc-porphyrin

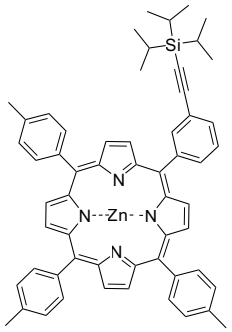

Tri-tolyl-mono-{5-bromo-phenyl}-zinc-porphyrin (213 mg, 267 µmol, 1 eq.), potassium triisopropylsilylacetylene trifluoroborate (152 mg, 528 µmol, 2 eq.), [1,1' bis(diphenylphosphino)ferrocene]dichloropalladium(II) complex with DCM (179 mg, 218 mmol, 0.9 eq.), and Cs_2CO_3 (414 mg, 1.27 mmol, 4.75 eq.) were dissolved in a mixture of THF and water (30 mL, 20:1, (v/v)). The reaction mixture was refluxed for 21 hours in the dark, and subsequently cooled to r.t. DCM was added, the organic layer was washed with water (3 x 15 mL), dried over $MgSO_4$, filtered, and evaporated to dryness. The crude product was purified by silicagel column chromatography using *n*-heptane/DCM (40/60, (v/v)) going to DCM as the eluent. All product-containing fractions were collected and the solvent was evaporated to yield a mixture of the product (major) and tri-tolyl-mono-phenyl-zinc-porphyrin (minor) as a purple solid.
^{1}H-NMR (500 MHz, $CDCl_3$): δ 8.89-8.81 (m, 8H, ß-pyrrole-*H*), 8.42 (t, 1H, Ar*H*, J= 2.4 Hz), 8.23 (dt, 1H, Ar*H*, J = 7.5 Hz, J = 1.5 Hz), 8.19-8.12 (m, 6H, Ar*H*), 7.96 (dt, 1H, Ar*H*, J= 8.0 Hz, J=1.5 Hz), 7.73 (t, 1H, Ar*H*, J=8.2 Hz), 7.58 (d, 6H, Ar*H*, J =7.5 Hz), 2.75 (s, 9H, tolyl-CH_3), 1.31 (br s, 3H, Si-C*H*-$(CH_3)_2$), 1.19 (s, 18H, Si-CH_2-$(CH_3)_2$)

Synthesis of tri-tolyl-mono-{5-acetylene-phenyl}-zinc-porphyrin

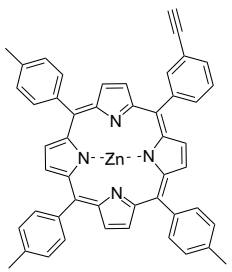

Tri-tolyl-mono-{5-triisopropylsiliylacetylene-phenyl}-zinc-porphyrin (176 mg, 195 µmol, 1 eq.) and tetrabutylammonium fluoride trihydrate (763 mg, 2.42 mmol, 10 eq.) were dissolved in THF (40 mL). The reaction mixture was stirred in the dark at r.t. for 4 h and was then evaporated to dryness. The residue was dissolved in DCM and this solution was washed with water (3 x 30 mL), dried over Na_2SO_4, filtered, and evaporated to dryness. The crude product was purified by silicagel column chromatography using *n*-heptane/DCM

(50/50, (v/v)) as the eluent. Precipitation from DCM/*n*-heptane and drying *in vacuo* yielded the product (tri-tolyl-mono-{m-acetylene-phenyl}-zinc-porphyrin, 31% with respect to tri-tolyl-mono-{5-bromo-phenyl}-zinc-porphyrin, 61.6 mg) as a purple solid.
^{1}H-NMR ($CDCl_3$, 500 MHz): δ (ppm) 8.98 (d, 2H, ß-pyrrole-*H*-**3,19**, J = 4.6 Hz), 8.97 (s, 4H, ß-pyrrole-*H*-**8,9,13,14**), 8.89 (d, 2H, ß-pyrrole-*H*-**4,18**, J = 4.6 Hz), 8.36 (t, 1H, Ar*H*-**22**, J = 1.5 Hz), 8.20 (dt, 1H, Ar*H*-**26**, J = 7.6 Hz, J = 1.5 Hz), 8.10-8.08 (m, 6H, Ar*H*-**28,32,34,38,40,44**), 7.90 (dt, 1H, Ar*H*-**24**, *J*=7.8 Hz, J = 1.4 Hz), 7.71-7.68 (m, 1H, Ar*H*-**25**), 7.55-7.53 (m, 6H, Ar*H*-**29,31,35,37,41,43**), 3.13 (s, 1H, alkyne*H*-**49**), 2.70 (s, 9H, CH_3-**45,46,47**); ^{13}C-NMR ($CDCl_3$, 126 MHz): δ 150.5 (Ar*C*-**5,17**), 150.4 (Ar*C*-**7,10,12,15**), 149.9 (Ar*C*-**2,20**), 143.2 (Ar*C*-**21**), 139.8 (Ar*C*-**27,33,39**), 137.6 (Ar*C*-**22**), 137.1 (Ar*C*-**30,36,42**), 134.7 (Ar*C*-**26**), 134.4 (Ar*C*-**28,32,34,38,40,44**), 132.3 (Ar*C*-**4,18**), 132.0 (Ar*C*-**8,9,13,14**), 131.6 (Ar*C*-**3,19**), 131.0 (Ar*C*-**24**), 127.3 (Ar*C*-**29,31,35,37,41,43**), 126.6 (Ar*C*-**25**), 121.3 (Ar*C*-**6,11,16**), 120.5 (Ar*C*-**23**), 119.0 (Ar*C*-**1**), 84 (alkyne*C*-**48**), 77 (alkyne*C*-**49**), 21.6 (C**45,46,47**); MALDI-TOF: m/z: 742.1 $(M+H)^+$; calculated for $[C_{49}H_{35}N_4Zn]^+$ 742.2.

Synthesis of Zn_2C_{11}TTBP

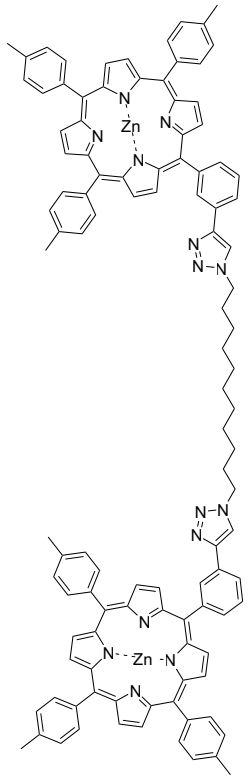

To a mixture of tri-tolyl-mono-{5-acetylene-phenyl}-zinc-porphyrin (90 mg, 121 µmol, 2 eq.) and copper(I) iodide (31 mg, 162 µmol, 1.3 eq.) in freshly distilled THF (25 mL) and freshly distilled MeCN (25 mL), DIPEA ((25 µl, 137 µmol, 2.2 eq.) was added. 1,11-Diazoundecane-^{15}N enriched (54.43 µmol, 0.9 eq., solution in diethyl ether) was added and the reaction mixture was stirred in the dark at r.t. for 7 days. The mixture was subsequently washed with water (3 x 50 mL). The organic layer was dried over Na_2SO_4, filtered and evaporated to dryness. The crude product was purified by silicagel column chromatography using *n*-heptane/ethyl acetate (34/66, (v/v)) as the eluent. Precipitation from DCM/*n*-heptane followed by washing with *n*-pentane (3 x) and drying *in vacuo* yielded the product (**Zn_2C_{11}TTBP**, 65 mg, 38.1 µmol, 63%) as a purple solid.
^{1}H-NMR ($CDCl_3$, 500 MHz): δ 8.95-8.91 (m, 16H, ß-pyrrole-*H*-**3,4,9,8,13,14,18,19**), 8.49 (t, 2H, Ar*H*-**22**, *J*=1.6 Hz), 8.18 (dt, 2H, Ar*H*-**24**, *J*=7.8 Hz, *J*=1.4 Hz), 8.14 (dt, 2H, Ar*H*-**26**, *J*=7.5 Hz, *J*=1.3 Hz), 8.10-8.06 (m, 12H, Ar*H*-**28,32,34,38,40,44**), 7.73 (t, 2H, Ar*H*-**25**, *J*=7.7 Hz), 7.67-7.66 (br s, 2H, Ar*H*-**49**), 7.55-7.46 (m, 12H, Ar*H*-**29,31,35,37,41,43**), 4.13 (t, 4H, CH_2-**53**, *J*=7.0 Hz), 2.69 (s,

6H, CH_3-**46**), 2.66 (s, 12H, CH_3-**45,47**), 1.75-1.71 (m, 4H, CH_2-**54**), 1.19-1.13 (m, 14H, CH_2-**55,56,57,58**); ^{13}C-NMR ($CDCl_3$, 126 MHz): δ (ppm) 150.40-150.01 (Ar*C*-**2,5,7,10,12,15,17,20**), 147.6 (Ar*C*-**48**), 143.43 (Ar*C*-**23**), 139.90 (Ar*C*-**33**), 139.86 (Ar*C*-**27,39**), 137.06 (Ar*C*-**30,36,42**), 134.04 (Ar*C*-**26**), 134.38-134.33 (Ar*C*-**28,32,34,38,40,44**), 132.08-131.72 (Ar*C*-**3,4,8,9,13,14,18,19**), 131.56 (Ar*C*-**22**), 128.9 (Ar*C*-**21**), 127.08 (Ar*C*-**25**), 127.28&127.25 (Ar*C*-**29,31,35,37,41,43**), 124.69 (Ar*C*-**24**), 121.32-121.20 (Ar*C*-**6,11,16,**) 120.21 (Ar*C*-**1**), 119.7 (Ar*C*-**49**), 50.2 (Ar*C*-**53**), 30.07 (Ar*C*-**54**), 26.19 (Ar*C*-**55,56,57,58**), 21.52 (C**46**), 21.50 (C**45,47**); ^{15}N-NMR▪ ($CDCl_3$, 51 MHz): δ 345.00 (Triazole-N-**52**), 249.15 (Triazole-N-**50**); ▪ 50% of the indicated N atoms are ^{15}N-labeled.

3.5. References

(1) Zhirnov, V.; Zadegan, R. M.; Sandhu, G. S.; Church, G. M.; Hughes, W. L. Nucleic Acid Memory. *Nat. Mater.* **2016**, *15* (4), 366–370.

(2) Goldman, N.; Bertone, P.; Chen, S.; Dessimoz, C.; LeProust, E. M.; Sipos, B.; Birney, E. Towards Practical, High-Capacity, Low-Maintenance Information Storage in Synthesized DNA. *Nature* **2013**, *494* (7435), 77–80.

(3) Church, G. M.; Gao, Y.; Kosuri, S. Next-Generation Digital Information Storage in DNA. *Science* **2012**, *337* (6102), 1628.

(4) Colquhoun, H.; Lutz, J.-F. Information-Containing Macromolecules. *Nat. Chem.* **2014**, *6* (6), 455–456.

(5) Lutz, J.-F. Coding Macromolecules: Inputting Information in Polymers Using Monomer-Based Alphabets. *Macromolecules* **2015**, *48* (14), 4759–4767.

(6) Mutlu, H.; Lutz, J.-F. Reading Polymers: Sequencing of Natural and Synthetic Macromolecules. *Angew. Chem. Int. Ed.* **2014**, *53* (48), 13010–13019.

(7) Stout, K. *Towards Double Cavity-Containing Porphyrin Clips for the Transfer of Information Chapter 2.*

(8) Taylor, P. N.; Anderson, H. L. Cooperative Self-Assembly of Double-Strand Conjugated Porphyrin Ladders. *J. Am. Chem. Soc.* **1999**, *121* (49), 11538–11545.

(9) Murphy, R. B.; Pham, D.-T.; Lincoln, S. F.; Johnston, M. R. Molecular Tweezers with Freely Rotating Linker and Porphyrin Moieties. *Eur. J. Org. Chem.* **2013**, *15*, 2985–2993.

(10) Ballester, P.; Costa, A.; Castilla, A. M.; Deyà, P. M.; Frontera, A.; Gomila, R. M.; Hunter, C. A. DABCO-Directed Self-Assembly of Bisporphyrins (DABCO=1,4-Diazabicyclo[2.2.2]octane). *Chem. – Eur. J.* **2005**, *11* (7), 2196–2206.

(11) Baldini, L.; Ballester, P.; Casnati, A.; Gomila, R. M.; Hunter, C. A.; Sansone, F.; Ungaro, R. Molecular Acrobatics: Self-Assembly of Calixarene-Porphyrin Cages. *J. Am. Chem. Soc.* **2003**, *125* (46), 14181–14189.

(12) Mak, C. C.; Bampos, N.; Sanders, J. K. M. Metalloporphyrin Dendrimers with Folding Arms. *Angew. Chem. Int. Ed.* **1998**, *37*, 3020–3023.

(13) Cantekin, S.; Markvoort, A. J.; Elemans, J. A. A. W.; Rowan, A. E.; Nolte, R. J. M. Allosterically Controlled Threading of Polymers through Macrocyclic Dimers. *J. Am. Chem. Soc.* **2015**, *137* (11), 3915–3923.

(14) Ballester, P.; Oliva, A. I.; Costa, A.; Deyà, P. M.; Frontera, A.; Gomila, R. M.; Hunter, C. A. DABCO-Induced Self-Assembly of a Trisporphyrin Double-Decker Cage: Thermodynamic Characterization and Guest Recognition. *J. Am. Chem. Soc.* **2006**, *128* (16), 5560–5569.

(15) Kim, D.; Lee, S.; Gao, G.; Seok Kang, H.; Ko, J. A Molecular-Clip-Based Approach to Cofacial Zinc–porphyrin Complexes. *J. Organomet. Chem.* **2010**, *695* (1), 111–119.

(16) Hunter, C. A.; Tregonning, R. Modular Assembly of Porphyrin Sandwiches as Potential Hosts. *Tetrahedron* **2002**, *58* (4), 691–697.

(17) Mikhailitsyna, E. A.; Tyurin, V. S.; Beletskaya, I. P. Synthesis of Supramolecular Complexes Based on Tetracrown–substituted Zinc Porphyrinates. *Prot. Met. Phys. Chem. Surf.* **2010**, *46* (6), 655–661.

(18) Mondal, P.; Rath, S. P. Cyclic Zinc(II) Bisporphyrin-Based Molecular Switches: Supramolecular Control of Complexation-Mediated Conformational Switching and Photoinduced Electron Transfer. *Chem. – Eur. J.* **2016**, *22* (16), 5607–5619.

(19) Anderson, H. L. Conjugated Porphyrin Ladders. *Inorg. Chem.* **1994**, *33* (5), 972–981.

(20) Hidalgo Ramos, P.; Saisaha, P.; Elemans, J. A. A. W.; Rowan, A. E.; Nolte, R. J. M. Conformational Analysis and Binding Properties of a Cavity Containing Porphyrin Catalyst Provided with Urea Functions. *Eur. J. Org. Chem.* **2016**, *26*, 4487–4495.

(21) Wang, H.-W.; Chen, C.-H.; Lim, T.-S.; Huang, S.-L.; Luh, T.-Y. Supramolecular Porphyrin–DABCO Array in Single- and Double-Stranded Polynorbornenes. *Chem. – Asian J.* **2011**, *6* (2), 524–533.

(22) Elemans, J. A. A. W.; Bijsterveld, E. J. A.; Rowan, A. E.; Nolte, R. J. M. Manganese Porphyrin Hosts as Epoxidation Catalysts – Activity and Stability Control by Axial Ligand Effects. *Eur. J. Org. Chem.* **2007**, *5*, 751–757.

(23) Thordarson, P.; Coumans, R. G. E.; Elemans, J. A. A. W.; Thomassen, P. J.; Visser, J.; Rowan, A. E.; Nolte, R. J. M. Allosterically Driven Multicomponent Assembly. *Angew. Chem. Int. Ed.* **2004**, *43* (36), 4755–4759.

(24) Elemans, J. A. A. W.; Bijsterveld, E. J. A.; Rowan, A. E.; Nolte, R. J. M. A Host–guest Epoxidation Catalyst with Enhanced Activity and Stability. *Chem. Commun.* **2000**, *24*, 2443–2444.
(25) Thordarson, P. Determining Association Constants from Titration Experiments in Supramolecular Chemistry. *Chem. Soc. Rev.* **2011**, *40* (3), 1305–1323.
(26) Nappa, M.; Valentine, J. S. The Influence of Axial Ligands on Metalloporphyrin Visible Absorption Spectra. Complexes of Tetraphenylporphinatozinc. *J. Am. Chem. Soc.* **1978**, *100* (16), 5075–5080.
(27) Denden, Z.; Ezzayani, K.; Saint-Aman, E.; Loiseau, F.; Najmudin, S.; Bonifácio, C.; Daran, J.-C.; Nasri, H. Insights on the UV/Vis, Fluorescence, and Cyclic Voltammetry Properties and the Molecular Structures of ZnII Tetraphenylporphyrin Complexes with Pseudohalide Axial Azido, Cyanato-N, Thiocyanato-N, and Cyanido Ligands. *Eur. J. Inorg. Chem.* **2015**, *15*, 2596–2610.
(28) Banks, R. E.; Besheesh, M. K.; Mohialdin-Khaffaf, S. N.; Sharif, I. N-Halogeno Compounds Part 17. Precursors of NF-TEDA Reagents: Quaternary Salts of 1,4-Diazabicyclooctane Containing Fluoro-Anions, and Their Lewis Acid-Lewis Base Adducts with Boron Trifluoride, Phosphorus Pentafluoride and Sulphur Trioxide. *J. Fluor. Chem.* **1996**, *78* (1), 43–50.
(29) Elemans, J. A. A. W.; Claase, M. B.; Aarts, P. P. M.; Rowan, A. E.; Schenning, A. P. H. J.; Nolte, R. J. M. Porphyrin Clips Derived from Diphenylglycoluril. Synthesis, Conformational Analysis, and Binding Properties. *J. Org. Chem.* **1999**, *64* (19), 7009–7016.
(30) The Fit of the Standard 1:2 Binding Model Was Obtained from Http://supramolecular.org.
(31) Roberts Derrick A.; Schmidt Timothy W.; Crossley Maxwell J.; Perrier Sébastien. Tunable Self-Assembly of Triazole-Linked Porphyrin–Polymer Conjugates. *Chem. – Eur. J.* **2013**, *19* (38), 12759–12770.
(32) Maeda, C.; Yamaguchi, S.; Ikeda, C.; Shinokubo, H.; Osuka, A. Dimeric Assemblies from 1,2,3-Triazole-Appended Zn(II) Porphyrins with Control of NH-Tautomerism in 1,2,3-Triazole. *Org. Lett.* **2008**, *10* (4), 549–552.
(33) Goutev, N.; Matsuura, H. Hydrogen Bonding in Chloroform Solutions of Ethylenedioxy Ethers. Spectroscopic Evidence of Bifurcated Hydrogen Bonds. *J. Phys. Chem. A* **2001**, *105* (19), 4741–4748.
(34) Kwak, K.; Rosenfeld, D. E.; Chung, J. K.; Fayer, M. D. Solute–Solvent Complex Switching Dynamics of Chloroform between Acetone and Dimethylsulfoxide–Two-Dimensional IR Chemical Exchange Spectroscopy. *J. Phys. Chem. B* **2008**, *112* (44), 13906–13915.
(35) Hunter, C. A.; Sanders, J. K. M.; Stone, A. J. Exciton Coupling in Porphyrin Dimers. *Chem. Phys.* **1989**, *133* (3), 395–404.
(36) Merkaš, S.; Bouatra, S.; Rein, R.; Piantanida, I.; Zinic, M.; Solladié, N. Efficiency of Dinucleosides as the Backbone to Pre-Organize Multi-Porphyrins and Enhance Their Stability as Sandwich Type Complexes with DABCO. *Molecules* **2017**, *22* (7).
(37) Hunter, C. A.; Meah, M. N.; Sanders, J. K. M. Dabco-Metalloporphyrin Binding: Ternary Complexes, Host-Guest Chemistry and the Measurement of .pi.-.pi. Interactions. *J. Am. Chem. Soc.* **1990**, *112* (15), 5773–5780.
(38) Dudič, M.; Lhoták, P.; Petříčková, H.; Stibor, I.; Lang, K.; Sýkora, J. Calixarene-Based Metalloporphyrins: Molecular Tweezers for Complexation of DABCO. *Tetrahedron* **2003**, *59* (14), 2409–2415.
(39) Lindsey, J. S.; Schreiman, I. C.; Hsu, H. C.; Kearney, P. C.; Marguerettaz, A. M. Rothemund and Adler-Longo Reactions Revisited: Synthesis of Tetraphenylporphyrins under Equilibrium Conditions. *J. Org. Chem.* **1987**, *52* (5), 827–836.
(40) Molander, G. A.; Katona, B. W.; Machrouhi, F. Development of the Suzuki–Miyaura Cross-Coupling Reaction: Use of Air-Stable Potassium Alkynyltrifluoroborates in Aryl Alkynylations. *J. Org. Chem.* **2002**, *67* (24), 8416–8423.
(41) Kocher, L.; Durot, S.; Heitz, V. Control of the Cavity Size of Flexible Covalent Cages by Silver Coordination to the Peripheral Binding Sites. *Chem Commun* **2015**, *51* (67), 13181–13184.
(42) Ganapathi, E.; Madhu, S.; Ravikanth, M. Synthesis and Properties of Triazole Bridged BODIPY-Conjugates. *Tetrahedron* **2014**, *70* (3), 664–671.

3.6. Appendixes

A1: UV-Vis titrations of Zn_2C_5DC and $Zn_2C_{11}DC$ with DABCO in DCM

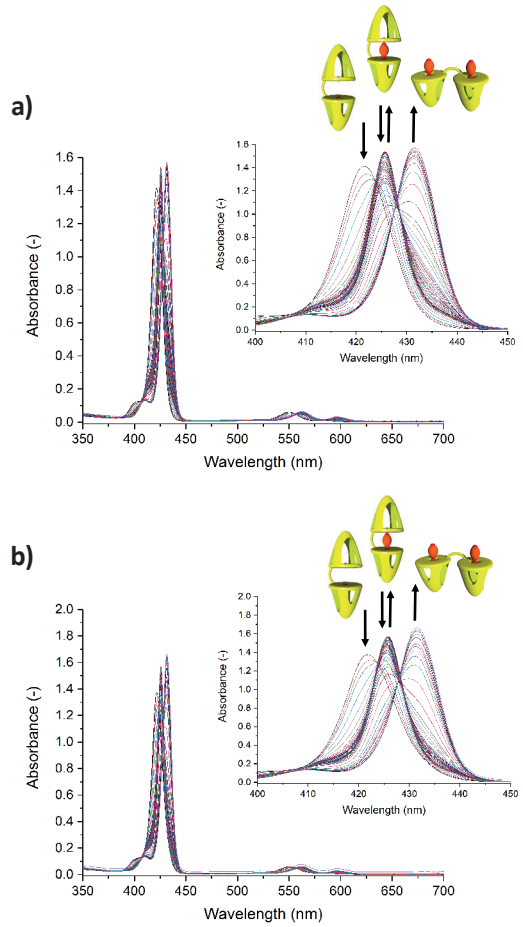

Figure 18 *Representative UV-Vis spectra of titrations of* ***Zn_2C_5DC*** *(a) and* ***$Zn_2C_{11}DC$*** *(b) with DABCO measured in DCM. The insets show zoom-ins of the Soret band regions between 400 – 450 nm.*

A2: UV-Vis titrations of Zn_2C_5DC and $Zn_2C_{11}DC$ with DABCO in chloroform

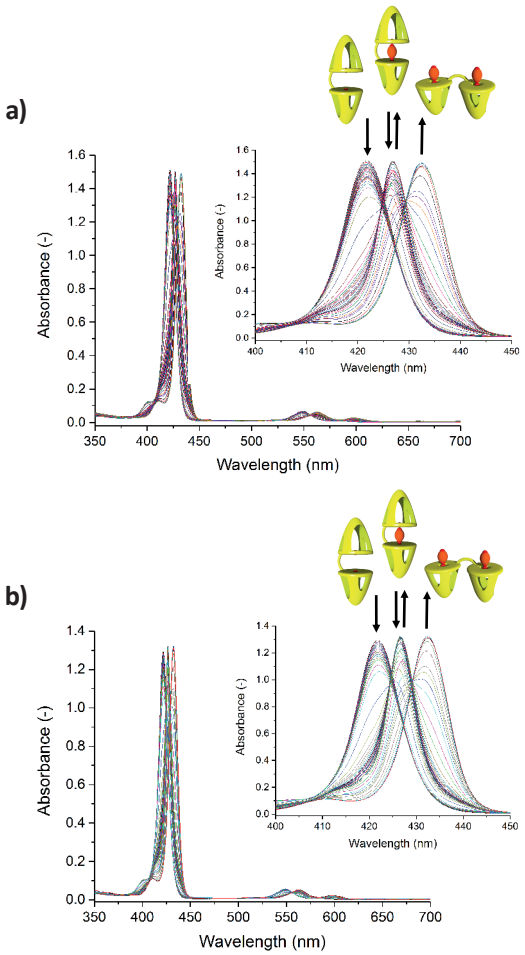

Figure 19 *Representative UV-Vis spectra of titrations of* ***Zn_2C_5DC*** *(a) and* ***$Zn_2C_{11}DC$*** *(b) with DABCO measured in chloroform. The insets show zoom-ins of the Soret band regions between 400 – 450 nm.*

A3: UV-Vis titrations of Zn_2C_5DC and $Zn_2C_{11}DC$ with DABCO in a solvent mixture of chloroform and MeCN (1:1, (v/v))

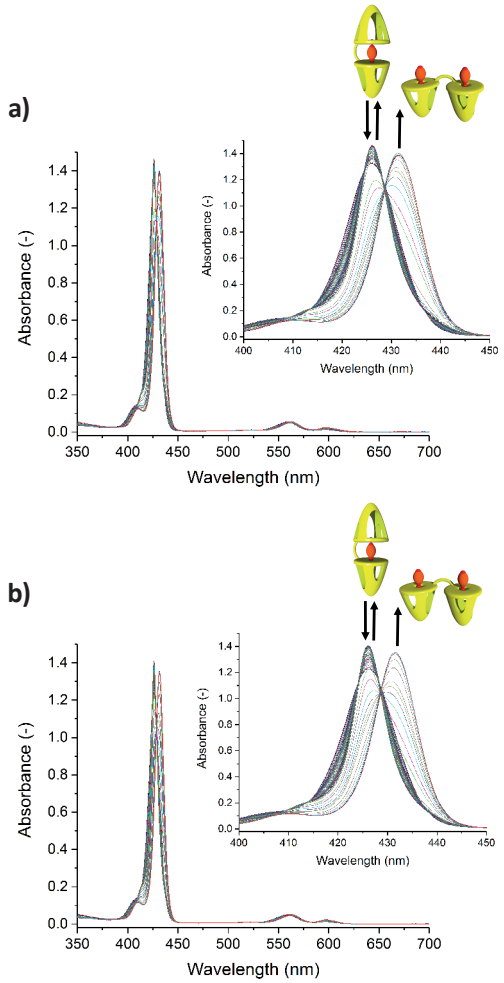

Figure 20 *Representative UV-Vis spectra of the titrations of* ***Zn_2C_5DC*** *(a) and* ***$Zn_2C_{11}DC$*** *(b) with DABCO measured in a solvent mixture of chloroform and MeCN (1:1, (v/v)). The insets show zoom-ins of the Soret band regions between 400 – 450 nm.*

A4: UV-Vis spectra of Zn_2C_5DC and $Zn_2C_{11}DC$ in chloroform and a solvent mixture of chloroform and MeCN (1:1, (v/v))

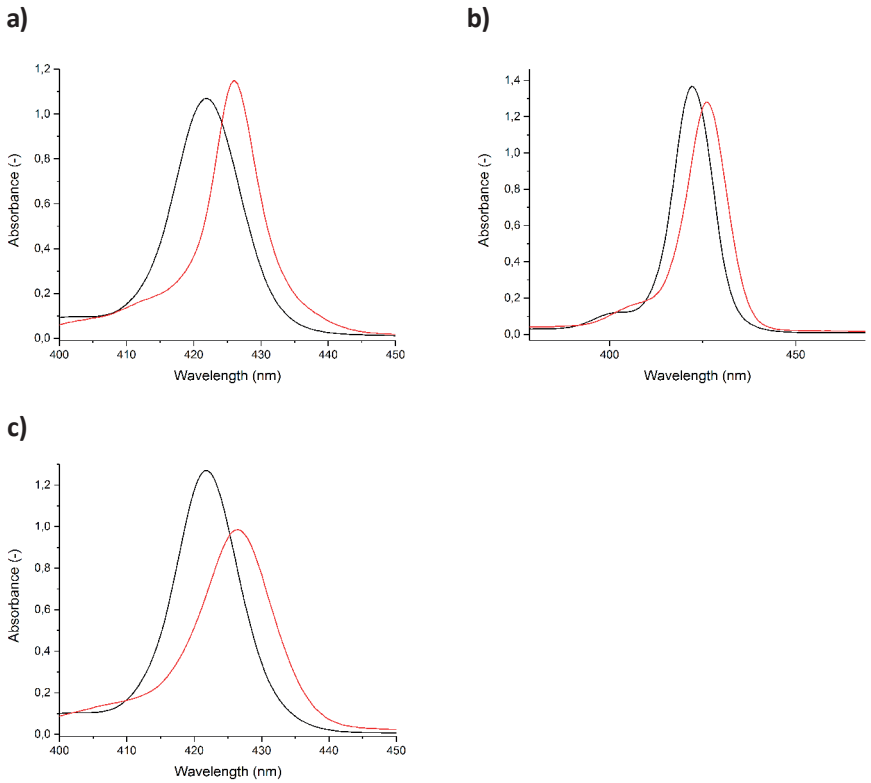

Figure 21 *Representative UV-Vis spectra of* ***Zn_2C_3DC*** *(a),* ***Zn_2C_5DC*** *(b), and* ***$Zn_2C_{11}DC$*** *(c) measured in chloroform (black), and of* ***Zn_2C_3DC*** *measured in a solvent mixture of chloroform and MeCN (1:1, (v/v), red)*

4

Binding of viologen guests in zinc double porphyrin cage compounds

This chapter will be published:

Allosteric binding of viologen guests in double zinc porphyrin cage complexes
- Manuscript in preparation

K. Stout, M. F. J. Mabesoone, J-R. Klop, P. B. White, J. A. A. W Elemans,
A. E. Rowan and R. J. M Nolte

Abstract

As a third step in the development of an enzyme mimic, capable of writing a binary code onto a synthetic polymer chain, the binding of dimethylviologen dihexafluorophosphate (**Me_2V**) guests in the cavities of complexes of covalently linked zinc double porphyrin cages, sandwiched via the ditopic axial ligand 1,4-diazabicyclo[2.2.2] octane (DABCO), **Zn_2C_xDC**:DABCO, was investigated. Already one equivalent of **Me_2V** guest was found to be capable of quenching more than 90% of the porphyrin fluorescence, which was explained by the fact that both porphyrins of the sandwich complex are within quenching distance when a **Me_2V** guest is bound in one of its two cavities. Upon hosting **Me_2V** guests in the sandwich complexes, the DABCO ligand remains bound between the two porphyrins. Binding of **Me_2V** in one cavity was shown to affect the coordination geometry of DABCO to the zinc porphyrins. The binding constants between **Me_2V** and the 1:1 **Zn_2C_xDC**:DABCO sandwich complexes were found to be independent of the spacer length between the two cage molecules. The binding constants between **Me_2V** and the **Zn_2C_xDC** compounds were found to be lower than those between **Me_2V** and the 1:1 **Zn_2C_xDC**:DABCO sandwich complexes. All complexes showed a highly negative cooperativity effect for the binding of **Me_2V** and therefore information transfer is present. For the 1:1 **Zn_2C_xDC**:DABCO sandwich complexes, this negative cooperativity probably influences the binding of DABCO to the zinc porphyrins. Variable temperature ^{1}H NMR studies confirmed that upon the addition of **Me_2V** DABCO remains bound in between the porphyrins of the 1:1 **Zn_2C_3DC**:DABCO sandwich complex. The binding of two equivalents of **Me_2V** to this sandwich complex gave rise to multiple proton resonances, which originate from the binding of the **Me_2V** guests to the different diastereoisomeric forms of the cage compound in solution.

4.1 Introduction

Nowadays data storage is an emerging research topic given the fact that it is expected that the global digital archive will contain 3×10^{24} bits by 2040, which cannot be sustained by the use of silicon memory chips.[1] Therefore, alternative methods are needed to facilitate the storage of big data. Data can be stored on biological polymers such as DNA or on synthetic polymers. The advantage of the latter is that synthetic polymers are easier to handle and can make use of the binary code, already commonly used in computing.[2–6] To enable the storage of data on a synthetic polymer, we designed, synthesized and characterized a double porphyrin cage compound, which is intrinsically capable of writing binary data on a polymer chain (Figure 1a).[7] This double porphyrin compound consists of two cage molecules, each equipped with a porphyrin 'roof', which are covalently linked together via a ditriazole spacer of different lengths, i.e. 3, 5, or 11 carbon atoms (Figure 1b).

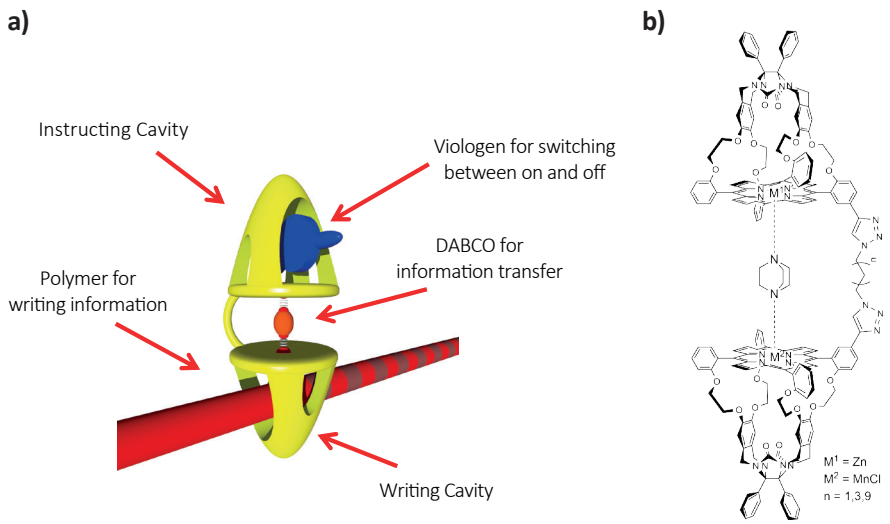

Figure 1 *a) Schematic representation of a double porphyrin cage (yellow) consisting of two receptor molecules capped with a porphyrin roof, which are covalently linked. The instructing cavity contains a zinc center and the writing cavity a manganese center. The coordination of a ditopic ligand such as DABCO (orange) in between the two porphyrins might allow the transfer of information from the instructing cavity to the writing cavity, thus enabling the possibility of influencing the catalytic reaction that is used to write the (chemical) information. The binding of a viologen guest (blue) inside the instructing cavity may influence the coordination of DABCO to the manganese center, which can perform a catalytic reaction on, for example, a polymer substrate (red), via a series of allosteric interactions. b) Chemical structure of the zinc-manganese double porphyrin cages with alkyl spacer lengths of 3, 5, and 11 carbon atoms, binding DABCO as a ditopic axial ligand.*

It is expected that when one of the porphyrin cages contains a zinc atom, an instructing cavity can be created, i.e. a cavity that can influence the catalytic activity exhibited by the manganese center in the other porphyrin cage via allosteric interactions transferred through a ditopic axial ligand such as 1,4-diazabicyclo[2.2.2]octane (DABCO). In the previous chapter of this thesis, it was shown that the binding of DABCO to zinc double porphyrin cages (**Zn_2C_xDC**s) results in stable 1:1 **Zn_2C_xDC**:DABCO sandwich complexes in chloroform or a solvent mixture of chloroform and acetonitrile (MeCN), 1:1, (v/v)).[8] The binding of this axial ligand to both porphyrin centers of the double cage could in theory facilitate the writing of information on a polymer chain by the writing cavity, because its coordination strength to both metal centers is expected to change upon the binding of a guest such as dimethylviologen hexafluorophosphate (**Me_2V**) in the instructing cavity.

The binding between **Me_2V** and single porphyrin clips (**SC**, Figure 2a) has been previously studied with the help of UV-Vis, fluorescence, and NMR spectroscopy.[9–19] Binding between **Me_2V** and **H_2SC** in a mixture of chloroform and acetonitrile (1:1, v/v) results in a small redshift of circa 2 nm of the Soret band in the UV-Vis spectrum.[14] In addition, the binding of **Me_2V** in cavity molecules that resemble, at least to some extent, the cavity of **SC** generates an additional charge-transfer absorption band around 425 nm.[20,21] If such a charge-transfer complex is also formed between **SC** and **Me_2V**, it will probably absorb in the same region as the Soret band. The superposition of these bands and the only small shift of the Soret band may result in unreliable results when host-guest binding constants are derived from spectral changes in UV-Vis. The binding between **Me_2V** and **SC** compounds can, however, also be studied with the help of fluorescence spectroscopy, because the fluorescence emission of the porphyrin of **H_2SC** and **ZnSC** is quenched when **Me_2V** is bound in the cavity.[10,14,16–19] The binding constants of the complexes between **Me_2V** and **H_2SC** or

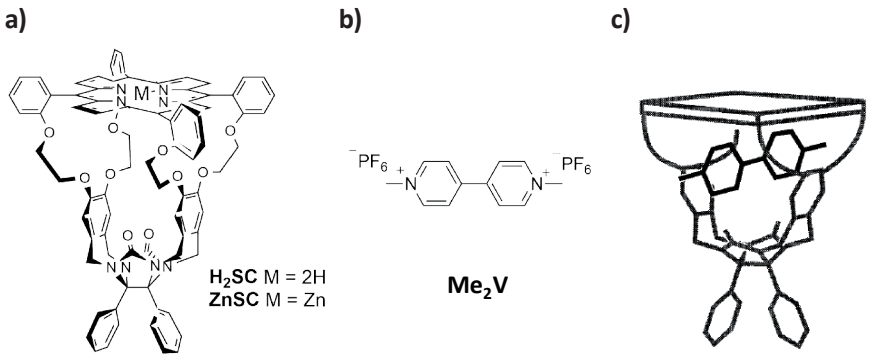

Figure 2 *a) Chemical structure of the single porphyrin cage compound (**SC**). b) Chemical structure of dimethylviologen hexafluorophosphate (**Me_2V**). c) Schematic representation of the complex between **SC** and **Me_2V**.[11]*

ZnSC are K_a >10^5 M^{-1}, indicating that at micromolar concentrations already at a low number of added equivalents of **Me_2V** nearly full saturation of the host-guest binding equilibria can be reached.[9–11,13–15,18,19,22] The binding between **Me_2V** and **H_2SC** has also been studied with the help of NMR spectroscopy, revealing that the proton resonances of the guest all broaden and shift upfield by -4.24, -2.66, and -1.05 ppm for the bipy-2,6, bipy-3,5, and the CH_3 protons of **Me_2V**, respectively.[9,14,15,23] Upon binding of **Me_2V** in the cavity of **H_2SC** its bipyridinium rings are located parallel to the aromatic sidewalls of the cage and nearly perpendicular to the porphyrin plane (Figure 2c), which causes considerable upfield shifts of the proton signals of the oxyethylene groups and a small upfield shift of the pyrrole NH resonances.[14]

Complexation of **Me_2V** in the cavity of **ZnSC** resulted in a stronger binding of an axial nitrogen-containing ligand, such as *t*-butylpyridine, to the outside of the porphyrin cage compound.[9] This positive heterotopic allosteric effect causes an increase in the abundance of zinc porphyrin molecules with a bound axial ligand, i.e. from 17 to >98% at a concentration of 1 µM of **ZnSC**.[9] This increase in binding constant was ascribed to a conformational change resulting from a squeezing of the cavity as a result of the clamping of **Me_2V** between the side walls of the **ZnSC**.[11] In addition, it is believed that upon the binding of **Me_2V** a solvent molecule (water or acetonitrile) that binds rather strongly to the zinc center at the inside of the cavity of **ZnSC** is expelled to the outside, where its binds weaker due to the lack of stabilizing cavity effects and thus is easier replaced by *t*-butylpyridine. As a result of these effects, binding of the **Me_2V** guest causes a positive allosteric effect towards the coordination of *t*-butyl pyridine which binds 250 times stronger than in the absence of **Me_2V**. Likewise, in a solution of the ditopic ligand DABCO (0.5 mM) and **ZnSC** (1 mM), 22% of **ZnSC** was in complex with DABCO in a sandwich-like species of type **ZnSC**:DABCO:**ZnSC**. When one equivalent of **Me_2V** was added to this solution, 57% of **ZnSC** was bound in one of the possible sandwich complexes (**ZnSC**:DABCO:**ZnSC**, **Me_2V**:**ZnSC**:DABCO:**ZnSC**, or **Me_2V**:**ZnSC**:DABCO:**ZnSC**:**Me_2V**, (for structures see Figure 3), hence the formation of assemblies of **ZnSC** around the DABCO ligand was promoted .[9] This allosteric magnification effect was also evident from NMR spectra, in which the porphyrin resonances of **ZnSC** bound and unbound to DABCO were in fast exchange in the absence of **Me_2V** and in slow exchange in the presence of this guest. This change in exchange dynamics allowed the determination of the ratio between the different complexes (**Me_2V**:**ZnSC**:DABCO:**ZnSC** and **Me_2V**:**ZnSC**:DABCO:**ZnSC**:**Me_2V**). In order to drive the equilibrium of this assembly even further towards the **Me_2V**:**ZnSC**:DABCO:**ZnSC**:**Me_2V** complex, the porphyrin *meso*-phenyl groups were equipped with four hydroxy functions at the outside of the cage molecule. The additional hydrogen bonds that are formed between the hydroxy functions during the dimerization of the cages pushed the equilibrium towards the pentameric complex with two viologen guests and one DABCO ligand, which now was present in an abundance of 98%.[9] The aim of the study described in this chapter

is to investigate the binding affinities between **Me_2V** and 1:1 **Zn_2C_xDC**:DABCO sandwich complexes with the help of UV-Vis, fluorescence, and NMR spectroscopy.

4.2. Results and discussion

4.2.1 Binding between Me_2V and 1:1 Zn_2C_xDC:DABCO sandwich complexes: fluorescence & UV-Vis studies

Me_2V is not soluble in chloroform but can be dissolved in acetonitrile (MeCN), hence, binding experiments with this guest were carried out in a 1:1 (v/v) solvent mixture of chloroform and MeCN. Since, as was outlined above, the binding of **Me_2V** in porphyrin cages is accompanied by only a small shift of the Soret band in combination with the emergence of a charge transfer absorption band, studying the complexation of this guest in the double porphyrin cage compounds with the help of UV-Vis spectroscopy may result in unreliable binding constants.[14,20,21] In addition, the presence of MeCN may hamper the use of UV-Vis spectroscopy because it can coordinate to the zinc centers in the porphyrin (see Chapter 3). It has been shown previously that **Me_2V** quenches the fluorescence emission of the porphyrin when it binds in a single porphyrin cage molecule.[10,14,16–19] This phenomenon made us decide to employ fluorescence spectroscopy as the technique to study the binding between **Me_2V** and the 1:1 **Zn_2C_xDC**:DABCO sandwich complexes.

To determine how **Me_2V** binds to the 1:1 **Zn_2C_xDC**:DABCO sandwich complexes, increasing amounts of the guest (up to 50 equivalents) were added to a solution containing these sandwich complexes. It was of special interest to investigate the binding of one and two equivalents of viologen guest, because such complexes are crucial in the development of the double cage compounds for the storage of binary

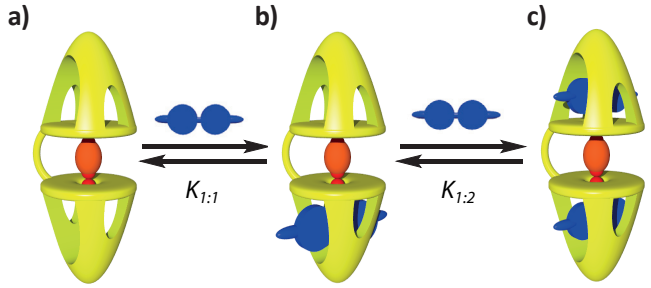

Figure 3 *Schematic representation of the binding between **Me_2V** (blue) and the 1:1 sandwich **Zn_2C_xDC**:DABCO complex (a) where the first **Me_2V** molecule is bound in one of the cavities forming a 1:1:1 **Zn_2C_xDC**:DABCO:**Me_2V** complex with a binding constant $K_{1:1}$ (b). Upon binding of an additional **Me_2V** molecule, the 1:1:2 **Zn_2C_xDC**:DABCO:**Me_2V** complex (c) is formed with a binding constant $K_{1:2}$.*

data in polymers. Since **Me_2V** is known to bind strongly in the cavity of porphyrin cages, it was hypothesized that the binding of one equivalent of this guest to the 1:1 **Zn_2C_xDC**:DABCO sandwich complex (Figure 3a), would cause the quenching of at most 50% of the fluorescence emission.[9–11] This 50% quenching originates from an presumed statistical distribution of the guest over the possible complexes, i.e. a 1:1:0, a 1:1:1, and a 1:1:2 **Zn_2C_xDC**:DABCO:**Me_2V** complex (Figure 3). The latter two complexes are assumed to cause 50% and 100% fluorescence quenching, respectively, while the first is not expected to exhibit any quenching. It is speculated that in the presence of two equivalents of **Me_2V**, full fluorescence quenching occurs because both cavities are supposed to be occupied (Figure 3c).

During the titrations, fluorescence spectra of solutions of 1.5 µM 1:1 **Zn_2C_xDC**:DABCO sandwich complex (prepared by taking into account the amount of DABCO required to ensure a maximum abundance of this complex based on the binding constants reported in Chapter 3) in a solvent mixture of chloroform and MeCN (1:1,

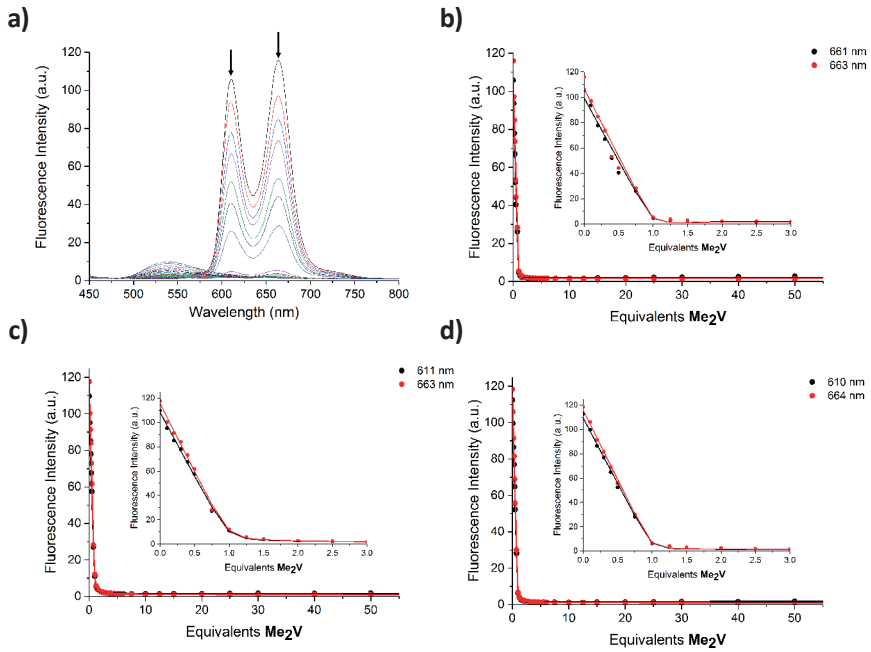

Figure 4 *a) Fluorescence spectra recorded during the titration of the 1:1 **Zn_2C_3DC**:DABCO sandwich complex with **Me_2V**, measured in a solvent mixture of chloroform and MeCN (1:1, (v/v)). b, c, d) Titration curves for (b) the 1:1 **Zn_2C_3DC**:DABCO, (c) **Zn_2C_5DC**:DABCO, and (d) **$Zn_2C_{11}DC$**:DABCO sandwich complexes, in which the fluorescence intensity is plotted as a function of the number of added equivalents of **Me_2V**. The insets show a zoom-in of the region of up to 3 added equivalents of **Me_2V**. Fits through the data points were obtained from http://supramolecular.org, assuming 1:2 host-guest stoichiometry.*

(v/v)), to which increasing amounts of guest (**Me_2V**) were added, were recorded. By adding a solution that contains both the sandwich complex and the guest, the concentration of the former remains constant during the titration. Because **Me_2V** is a 'silent' guest that does not absorb at the excitation wavelength, all changes in fluorescence emission can be attributed to the formation of the different host-guest complexes.[24]

The fluorescence titration spectra for the binding of **Me_2V** to the 1:1 **Zn_2C_3DC**:DABCO sandwich complex, and the titration curves for the binding of **Me_2V** to all 1:1 **Zn_2C_xDC**:DABCO sandwich complexes are presented in Figure 4. The fluorescence spectrum of the 1:1 **Zn_2C_3DC**:DABCO sandwich complex shows two bands at 611 and 663 nm, which rapidly decrease in intensity upon the addition of **Me_2V**, because of quenching as a result of binding of the guest (Figure 4a). For the binding of **Me_2V** to the other two sandwich complexes, similar fluorescence behavior was observed (data shown in appendix A1).

Surprisingly, after the addition of one equivalent of **Me_2V**, 94.8±0.98% of the fluorescence of the **Zn_2C_3DC**:DABCO complex, 90.8±0.66% of the **Zn_2C_5DC**:DABCO complex, and 92.3±4.92% of the **$Zn_2C_{11}DC$**:DABCO complex was quenched (Figure 4). It is remarkable that only one available **Me_2V** guest per 1:1 **Zn_2C_xDC**:DABCO sandwich complex is capable of almost fully quenching the fluorescence emission of both porphyrins within the complex. For comparison we also added **Me_2V** to the 1:1 **ZnSC**:DABCO reference complex under the same conditions and in the same solvent mixture (ensuring a maximum abundance of 1:1 **ZnSC**:DABCO complex) (Figure 5a). In this case, in the presence of 0.5 equivalents of the guest half of the porphyrin fluorescence was quenched and 1.5 equivalents of guest were needed to reach full quenching (Figure 5b), which is the expected quenching behavior.

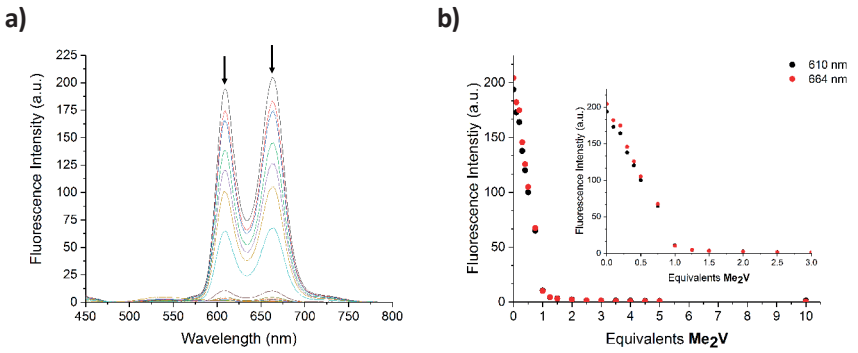

Figure 5 *a) Fluorescence spectra recorded during the titration of the 1:1* ***ZnSC****:DABCO complex with* ***Me_2V*** *in a solvent mixture of chloroform and MeCN (1:1, (v/v)). b) Corresponding titration curve in which the fluorescence intensity is plotted versus the number of added equivalents of* ***Me_2V****. The inset shows a zoom-in of the region of 0 to 3 added equivalents of* ***Me_2V****.*

It is not immediately clear how this unexpected quenching result should be explained. It might be that when one **Me_2V** guest is bound to the 1:1 **Zn_2C_xDC**:DABCO sandwich complex, the emission of both porphyrins is quenched simultaneously. This is possible, for instance, if the sandwich complex folds open so that **Me_2V** sits in between the two cages. In that case the DABCO ligand binds in a mono-dentate fashion to the porphyrin at the outside of the cage compound. However, in none of the UV-Vis spectra of the 1:1 **Zn_2C_xDC**:DABCO sandwich complexes a red shift of the Soret band was observed upon the addition of an increasing number of equivalents of **Me_2V** (Figure 6), which thus excludes the formation of complexes with mono-dentate-coordinated DABCO ligands. Hence, it can be concluded that the sandwich complexes remain intact during the addition of **Me_2V** (Figure 3).

The most likely explanation for the nearly full quenching of the porphyrin fluorescence, therefore, is that when the **Me_2V** guest is bound in one of the cavities of the sandwich complex, it is positioned close enough and in a proper orientation to quench the fluorescence of the second porphyrin as well. Fluorescence quenching by electron transfer is distance dependent, and systems have been reported in the

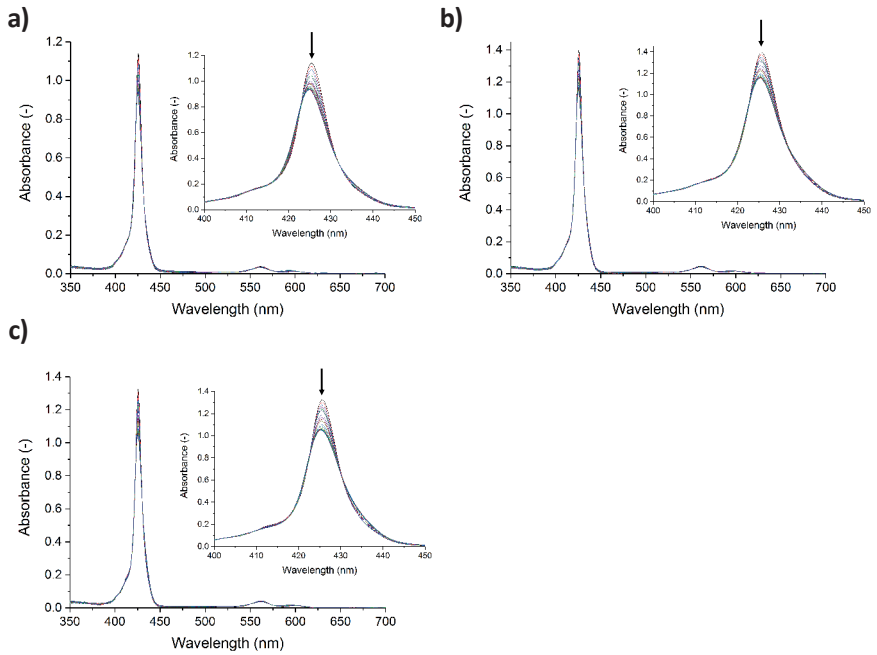

Figure 6 *UV-Vis spectra of (a) the titration of the 1:1* ***Zn_2C_3DC****:DABCO, (b) 1:1* ***Zn_2C_5DC****:DABCO, and (c) 1:1* ***$Zn_2C_{11}DC$****:DABCO sandwich complexes with* ***Me_2V*** *(up to 55 equivalents) in a solvent mixture of chloroform and MeCN (1:1, (v/v)). The insets show a zoom of the Soret band region of 400-450 nm.*

literature in which distances as far as 11 to 14.8 Å between a porphyrin and a **Me_2V** molecule still lead to quenching of the fluorescence, although the precise distance dependency of the efficiency of this quenching was not quantified.[25,26] The distance between the center of the **Me_2V** guest and the porphyrin plane in the **H_2SC** porphyrin cage compound is, based on molecular modeling, approximately 5 Angstrom (Å). The distance between the two porphyrins in the 1:1 **Zn_2C_xDC**:DABCO sandwich complexes is circa 7 Å (7.155 (**Zn_2C_3DC**), 6.653 (**Zn_2C_5DC**) and 7.152 Å (**$Zn_2C_{11}DC$**) for the 1:1 **Zn_2C_xDC**:DABCO sandwich complexes, based on Spartan modeling).[27] Together this provides a distance of about 12 Å between the **Me_2V** guest and the second porphyrin in the sandwich complexes, indicating that both porphyrin molecules are probably within the quenching distance of a bound **Me_2V**.[11,25,26]

Although it was not clear yet why the porphyrin fluorescence quenching by **Me_2V** was so efficient and how this result should be interpreted, we decided to calculate the binding constants for the complexation of this guest to the 1:1 **Zn_2C_xDC**:DABCO sandwich complexes. To this end the binding model shown in Figure 3 was adopted and the experimentally obtained data points from the fluorescence titration curves (Figure 4) were fitted to standard 1:1 and 1:2 host-guest binding models. Despite the fact that over 90% of the fluorescence quenching was caused by the binding of the first **Me_2V** guest, also the binding constant for the binding of the second **Me_2V** could be estimated. The results are reported in Table 1 and reveal that the $K_{1:1}$ and the $K_{1:2}$ values for the binding of **Me_2V** guests to the different sandwich complexes are very high, particularly those for the 1:1 **Zn_2C_3DC**:DABCO complex.

Table 1 Binding constants $K_{1:1}$ and $K_{1:2}$ for the binding between **Me_2V** and 1:1 **Zn_2C_xDC**:DABCO sandwich complexes in the solvent mixture of chloroform and MeCN (1:1, (v/v)), obtained with the help of fluorescence titrations. K-values are given as their logarithmic values, with an error of two times the standard deviation over a threefold measurement. The number of equivalents of **Me_2V** needed to obtain the maximum amount of 1:1:1 **Zn_2C_xDC**:DABCO:**Me_2V** sandwich complex and the percentage (%) of quenching when one equivalent (eq) of **Me_2V** is present are shown, with a reported error of two times the standard deviation over the threefold measurement. The cooperativity factor (α) is also reported.

	Zn_2C_3DC:DABCO	**Zn_2C_5DC:DABCO**	**$Zn_2C_{11}DC$:DABCO[a]**
Log($K_{1:1}$)	15.85±4.08	8.87±1.42	8.29±0.26
Log($K_{1:2}$)	13.07±3.97	6.20±1.24	4.79±0.98
Equivalents Me_2V (1:1:1)	1.0±0.00	1.0±0.06	1.2±0.16
% Quenching at 1 eq Me_2V	94.8±0.98	90.8±0.66	92.3±4.92
Cooperativity factor (α)	0.00666	0.00851	0.00126

[a] Measured in twofold.

The cooperativity factor (α) is defined by equation 1 and if α < 1, the system displays negative cooperativity, which means that the second binding event is less favorable than the first.[24] If α > 1, positive cooperativity takes place and therefore the second binding event is more favorable than the first.

$$\alpha = \frac{4K_{1:2}}{K_{1:1}} \qquad (1)$$

Table 1 shows that all the 1:1 **Zn_2C_xDC**:DABCO sandwich complexes display highly negative cooperativities for the binding of **Me_2V**. How can this negative cooperativity be explained? The initial binding of the **Me_2V** guest in the first cage of the sandwich complex may result in a stronger binding of the first nitrogen atom of the DABCO ligand to the zinc porphyrin of this cage, similar to the reported enhanced binding of a pyridine ligand to the outside of a **ZnSC** cage compound when a **Me_2V** is bound inside.[9] This enhanced binding may weaken the coordination strength of the second nitrogen atom of DABCO to the zinc porphyrin of the empty cage in the sandwich complex. When subsequently, the second **Me_2V** guest binds in this empty cage, the complexation apparently is still strong (Table 1), but may experience, via the DABCO ligand, a negative cooperative effect induced by the binding of the first **Me_2V**. Geometry changes in the double cage complex after the complexation of the first **Me_2V** guest molecule may be responsible for this weakened binding of the second **Me_2V** guest, resulting in the negative cooperativity. A further analysis and discussion of the fluorescence titration data is presented in appendix A2 of this chapter.

4.2.2 Binding between Me_2V and the 1:1 Zn_2C_xDC:DABCO sandwich complexes: NMR studies

In order to validate the fluorescence binding experiments, it was decided to follow the complexation of **Me_2V** to one of the sandwich complexes with the help of ^{1}H-NMR. To this end the NMR spectra of the 1:1 **Zn_2C_3DC**:DABCO sandwich complex (1 mM) dissolved in a solvent mixture of $CDCl_3$/MeCN-d_3 (1:1, (v/v)) were recorded in the presence and absence of one and two equivalents of **Me_2V** (Figure 7). All samples were extensively analyzed using several NMR techniques in order to achieve a complete assignment of the proton signals in the complexes. The resonance of the twelve chemically equivalent protons of DABCO in the sandwich complex in the absence of **Me_2V** is located at -4.46 ppm. This signal considerably sharpened upon the addition of **Me_2V**, which indicates slower dynamics of the ligand bound between the two zinc porphyrins.[28–35] It is expected that the binding of **Me_2V** in one or both cavities of **Zn_2C_3DC** will influence the binding strength of the DABCO ligand in the sandwich complex (see section 4.2.1).[9] One of the DABCO CH_2 resonances of the 1:2 **Zn_2C_3DC**:DABCO open complex, which is expected to be located at circa –3 ppm, was only marginally visible in the spectrum in which two equivalents of **Me_2V** are present, indicating that the 1:1 **Zn_2C_3DC**:DABCO sandwich complex remains folded when it

binds **Me_2V** guests (Figure 7, the box labeled M&SW).[8,12,28,30,36] In the presence of one equivalent of **Me_2V**, many of the proton signals of **Zn_2C_3DC** and the guest are broad. Line broadening in NMR spectra is dependent on the rate of exchange at a certain temperature and on the frequency differences between signals of the host-guest complex and its free components. The broadening of the proton resonances indicates that the exchange between the host and guest is fast on the NMR time scale. Half of the β-pyrrole signals (Figure 7, black box) and the signals belonging to ArH-**1** and ArH-**4** of **Me_2V** (see Figure 7, purple box, and Figure 8 for proton numbering) have almost completely merged with the baseline. The more broadened β-pyrrole signals, which experience a larger downfield complexation-induced shift than the other half, likely belong to the β-pyrrole protons above the receptor cavity portal, close to the bound **Me_2V** guest (Figure 9). When a second equivalent of **Me_2V** is added, all signals of **Zn_2C_3DC**, DABCO, and **Me_2V** sharpen up, suggesting the formation of a well-defined complex with limited or no exchange of the components at the NMR timescale.

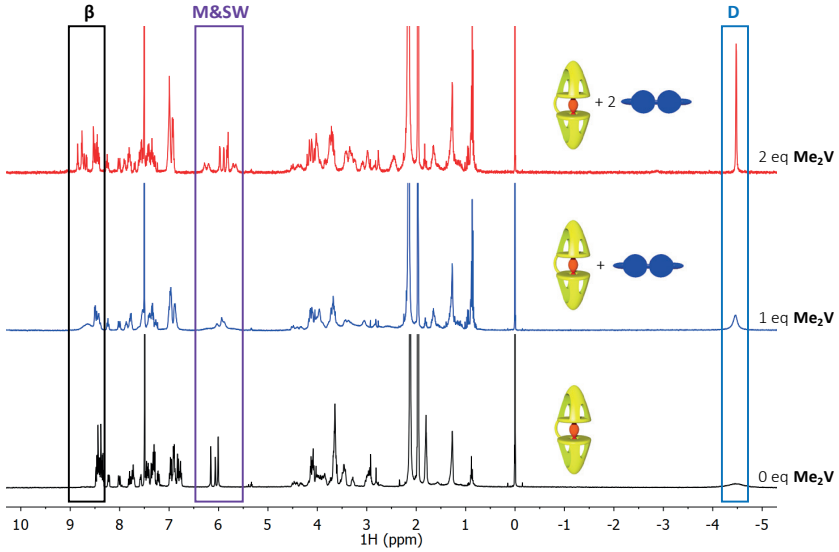

Figure 7 *^{1}H-NMR spectra of (bottom) the 1:1 **Zn_2C_3DC**:DABCO sandwich complex (1 mM), (middle) the complex in the presence of one and (top) two equivalent of **Me_2V** in a solvent mixture of $CDCl_3$ and MeCN-d_3 (1:1, (v/v)) at 298 K. The proton resonances of the DABCO ligand (blue box labeled D) in the sandwich complex are located at −4.49 ppm and sharpen upon the addition of **Me_2V**. The proton resonances of the β-pyrroles (black box labeled β), the **Me_2V** (ArH-**1** and ArH-**4**), and the side wall protons (purple box labeled M&SW) shift and broaden upon the addition of one equiv. of **Me_2V**.*

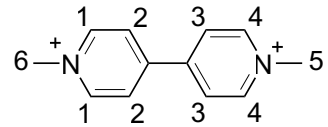

Figure 8 *Chemical structure and proton numbering of methyl viologen.*

In Chapter 3 it was shown that at higher temperatures the proton signals of **Zn_2C_3DC** in the NMR spectra sharpen up. To investigate if also the exchange dynamics of the host-guest complexes would change at higher temperatures, NMR spectra of the solutions of the 1:1 **Zn_2C_3DC**:DABCO sandwich complex in the presence of one or two

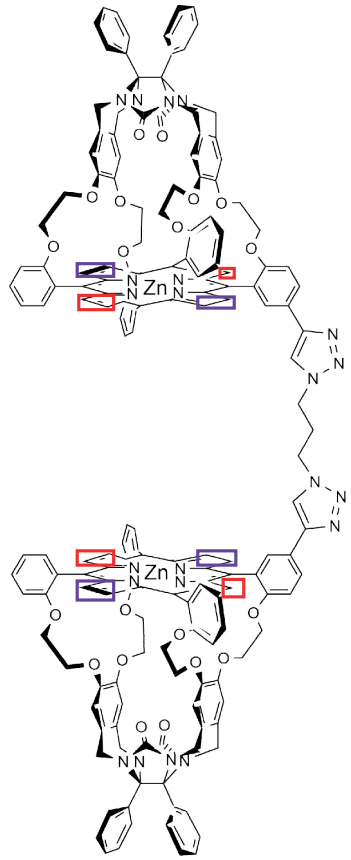

Figure 9 *Chemical structure of **Zn_2C_3DC**. The β-pyrrole protons are indicated by the purple and red boxes. The latter ones are located above the cavity side-walls.*

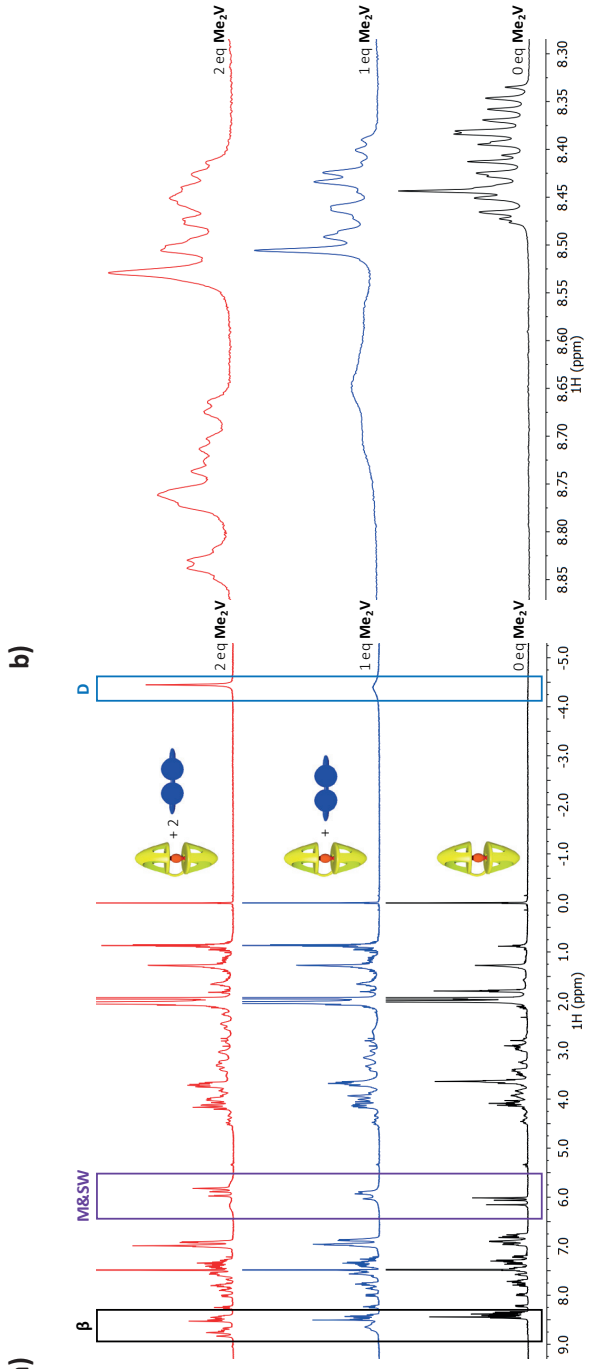

Figure 10 *a) ^{1}H-NMR spectra of (bottom) the 1:1 **Zn_2C_3DC**:DABCO sandwich complex (1 mM), (middle) the complex in the presence of one and (top) two equivalents of **Me_2V** in a solvent mixture of $CDCl_3$ and MeCN-d_3 (1:1, (v/v)) at 323 K. The resonances of the β-pyrrole protons are indicated by the black box (and β), those of the **Me_2V** (ArH-**1** and ArH-**4**) and the side wall protons by the purple box (and M&SW) and those of DABCO by the blue box (and D). b) Zoom-in of the β-pyrrole region.*

equivalents of **Me_2V** were recorded at 323 K (Figure 10). In the presence of one equivalent of **Me_2V**, half of the signals of the β-pyrrole protons and the side walls, as well as the **Me_2V** (ArH-**1** and ArH-**4**) resonances (6.20-5.75 ppm) were still broad. When two equivalents of **Me_2V** were present these resonances became sharp again. It can thus be concluded that elevation of the temperature has hardly an effect on the dynamics of the various complexes. The complexation induced shift values of both the broad and the sharp set of β-pyrrole resonances in the presence of one equivalent of **Me_2V** are located approximately halfway between these signals in the free sandwich complex and those in the sandwich complex in the presence of two equivalents of the guest (Figure 10b). This gradual shifting of the resonances in the presence of one equivalent of guest is more clearly visible at high temperatures and indicates that an ensemble of all possible host-guest complexes (1:1:0, 1:1:1, and 1:1:2 **Zn_2C_3DC**:DABCO:**Me_2V**) is present in solution. Their abundance ratio could not be precisely determined due to the overlap of the signals. Other signals in the NMR spectra, such as those of the side wall and the **Me_2V** protons, show this broadness and gradual shifting as well, albeit not so clearly.

Since in the presence of one equivalent of **Me_2V** no proton resonances of this guest were observed between 7 and 5 ppm at 323K, which is most likely due to fast exchange of the guest between the different complexes in solution, it was decided to do experiments at a lower temperature (238 K, Figure 11) as well. This temperature drop will slow down the dynamics of the molecules in solution and as a result sharpen the broad resonances in the ^{1}H-NMR spectra. Figure 11b shows that the resonance of the protons of the DABCO ligand bound between the two porphyrins changes from a single broad singlet in the free sandwich complex into two much sharper singlets in the presence of two equivalents of **Me_2V**. This splitting into two singlets of equal size indicates that DABCO binds to the zinc porphyrins in two somewhat different geometries, which is proposed to be the result of coordination of this ligand in two possible diastereoisomeric sandwich-like complexes (see Chapter 2 and below).[7] These well-defined 1:1:2 **Zn_2C_3DC**:DABCO:**Me_2V** complexes show sharp signals for all the components involved. When one equivalent of **Me_2V** was added, a similar split signal characteristic for the 1:1:2 **Zn_2C_3DC**:DABCO:**Me_2V** complex was observed. On either side of this split signal two very broad shoulders are present (Figure 11b). The slight 0.1 ppm difference in chemical shift between the DABCO resonances of the free sandwich complex and the resonance (broad shoulder at higher field) of the complex when one equivalent of **Me_2V** is present, may be attributed to a slight variation in the used solvent mixtures, as such a small shift is also observed for the chloroform resonance around 7.54 ppm. The splitting of the DABCO signal into a series of broad overlapping peaks may have two explanations. It might be that the observed signals originate solely from the 1:1:1 **Zn_2C_3DC**:DABCO:**Me_2V** complex or are a combination of the signals of the free sandwich complex and the sandwich complexes with one and two bound **Me_2V** guests. When only one

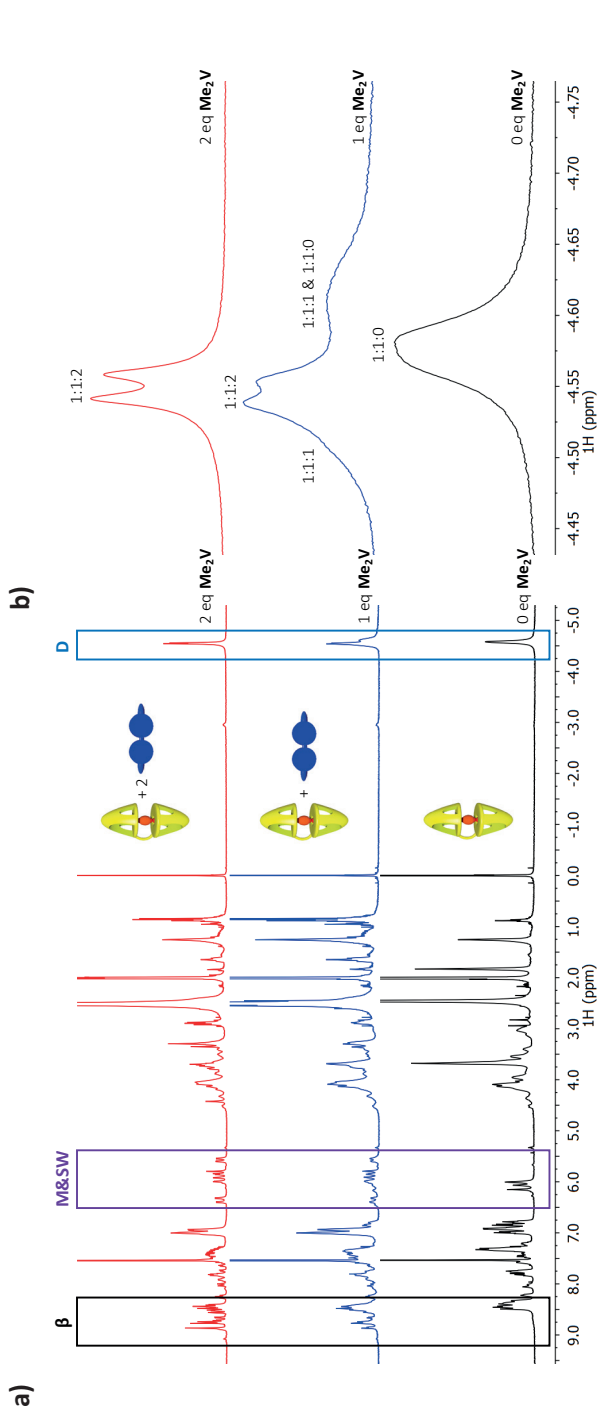

Figure 11 *a) ^{1}H-NMR spectra of (bottom) the 1:1 **Zn_2C_3DC**:DABCO sandwich complex (1 mM), (middle) the 1:1 **Zn_2C_3DC**:DABCO sandwich complex in the presence of one and (top) of two equivalents of **Me_2V**, in a solvent mixture of $CDCl_3$ and MeCN-d_3 (1:1, (v/v)) at 238 K. The resonances of the β-pyrrole protons are indicated by the black box (and β), those of the **Me_2V** (ArH-**1** and ArH-**4**) and the side wall protons by the purple box (and M&SW), and those of DABCO by the blue box (and D). b) Zoom-in of the DABCO region with the tentative assignments of the broad signals to the three sandwich complexes (1:1:0, 1:1:1, and 1:1:2) that are possibly present in solution.*

viologen guest is bound in a sandwich complex, it is expected that the coordinated DABCO ligand gives two signals, because half of the DABCO protons is adjacent to a cavity that is occupied by **Me_2V**, while the other half of the protons is adjacent to an empty cavity. Since at least three and probably more signals are observed for the DABCO protons, the exclusive presence of only one single 1:1:1 **Zn_2C_3DC**:DABCO:**Me_2V** complex is unlikely. Hence a dynamic equilibrium involving the above-mentioned three species as shown in Figure 3 (vide infra) is probably operative in solution. Figure 12 shows that the DABCO resonances of the sandwich complex with one guest present resemble the broad singlet of the free sandwich complex as well as the two singlets of the sandwich complex with two guests bound. Also, the **Me_2V** resonances in the host-guest mixture with one equivalent of **Me_2V** present resemble the signals of the free sandwich complex as well as those of the 1:1:2 **Zn_2C_3DC**:DABCO:**Me_2V** complex. If the 1:1:1 **Zn_2C_3DC**:DABCO:**Me_2V** complex is present in solution and in dynamic equilibrium with the other species, which is a realistic scenario, its proton resonances are likely to be broad and not clearly visible because they will overlap with the resonances of the other sandwich complexes, making their identification impossible.

In order to lower the dynamics in solution even further, in a subsequent series of NMR experiments the 1:1:2 **Zn_2C_3DC**:DABCO:**Me_2V** complex in the solvent mixture $CDCl_3$ and MeCN-d_3 (1:1, (v/v)) was studied at 223 K (Figure 12). As mentioned above, the presence of two singlets for the DABCO molecule, i.e. at -4.54 and -4.56 ppm, indicates that each diastereoisomeric complex creates its own set of resonances. Previously, it was reported that the aromatic protons ArH-**1** and ArH-**4** of **Me_2V** (Figure 8) appear as two doublet resonances in the region 5-7 ppm, when this guest is bound between the sidewalls of the single porphyrin cage **SC**.[11] The resonances of the same ArH-**1** and ArH-**4** protons in the spectrum of the complex 1:1:2 **Zn_2C_3DC**:DABCO:**Me_2V** complex appeared to consist of two sets of two doublets (Figure 12b), which at first sight did not correspond with the pattern visible in the 1:1 complex of **Me_2V** with **SC**.[11] At the lower temperature of 223 K, the J-coupling observed in the doublets at 238 K was barely visible. This phenomenon is ascribed to a lowering of the T_2 relaxation time and therefore these doublets appear as apparent singlets (Figure 12).

The differences in frequency between the doublets in these two sets of two doublets are 20 and 28 Hz, respectively, which are too large values for a typical 3-bond J-coupling. It was concluded, therefore, that these signals in fact must represent four separate doublets, which are proposed to originate from the different binding geometries of the **Me_2V** guests in the two diastereoisomeric forms (*RR*/*SS* and *RS*/*SR*) of the sandwich complexes and from the asymmetry present in the cavities of the **Zn_2C_xDC** compounds induced by the locations at which the linkers are attached (Figure 13). When the binding geometry of **Me_2V** in the *RR*/*SS* diastereoisomer is different from that in the *RS*/*SR* diastereoisomer, this will result in double sets of **Me_2V** resonances.

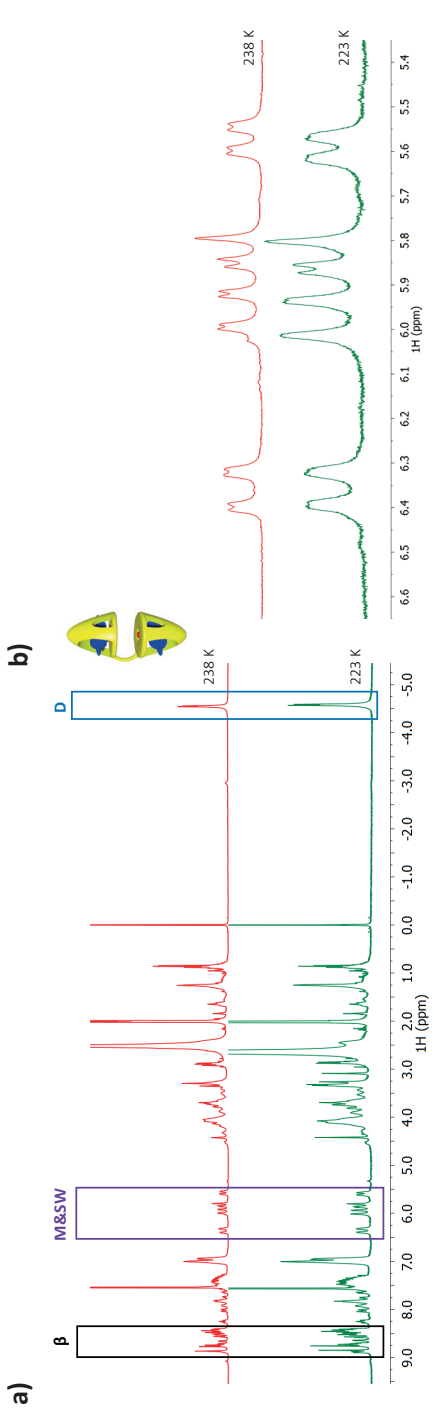

Figure 12 *a) ^{1}H-NMR spectra of the 1:1 **Zn_2C_3DC**:DABCO sandwich complex (1 mM) in the presence of two equivalents of **Me_2V**, in a solvent mixture of $CDCl_3$ and MeCN-d_3 (1:1, (v/v)) at 238 K (top) and 223 K (bottom). The resonances of the β-pyrrole protons are indicated by the black box (and β), those of the **Me_2V** (ArH-**1** and ArH-**4**) and the side wall protons by the purple box (and M&SW), and those of DABCO by the blue box (and D). b) Zoom-in of the **Me_2V** region (purple box).*

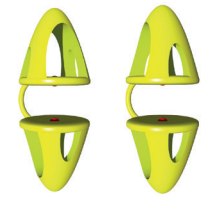

Figure 13 *Schematic representation of the two different diastereoisomeric forms of sets the **Zn_2C_xDC** compounds.*

For clarity, these double sets of **Me_2V** resonances will be labelled **a** and **b**. However, it is not known to which guest bound in which diastereoisomer the **Me_2V** protons belong. First, the proton resonances of the **Me_2V** guest in diastereoisomer **a** will be assigned, starting with the proton signal at 6.39 ppm originating from ArH-**1**. The COSY spectrum of the 1:1:2 **Zn_2C_3DC**:DABCO:**Me_2V** complex showed that this signal at 6.39 ppm (ArH-**1a**, Figure 14) couples with that of ArH-**2a** at 3.82 ppm. Via a ROE contact between the *meta* **Me_2V** protons in the 2D ROESY spectrum, ArH-**3a** could be assigned (3.34 ppm). ArH-**3a** subsequently couples with ArH-**4a** (5.56 ppm), which in turn has a ROE contact with the methyl protons H-**5a** (2.86 ppm). The other methyl-group (H-**6a**) could be located at 3.33 ppm via a ROE contact with ArH-**1a**. Next to the apparent singlet of ArH-**1a** (at 6.39 ppm), another apparent singlet is present at 6.32 ppm which originates from proton ArH-**1b** of the **Me_2V** guest that is bound in the other diastereoisomer. It has a cross peak in the COSY spectrum with ArH-**2b** at 3.75 ppm (Figure 14). With the help of the COSY and 2D ROESY spectra, the signals of the other protons of the guest could be assigned: 3.36, 5.62, 2.88 and 3.26 ppm for ArH-**3b**, ArH-**4b**, H-**5b**, and H-**6b**, respectively. A possible explanation for the unexpectedly large number of resonances could be that each proton of **Me_2V** is chemically unique as a result of restricted mobility of the guest inside the cavity due to hindered rotation of the aromatic rings around the bipyridyl-axis. However, in that case only two methyl resonances would be expected, instead of the four observed in the NMR spectra. Therefore, the sets of resonances must be attributed to the two different diastereoisomeric host-guest complexes. Based on this observation it is safe to assume that also the two singlets observed for the DABCO ligand bound between the zinc porphyrins originate from coordination to different diastereoisomers.

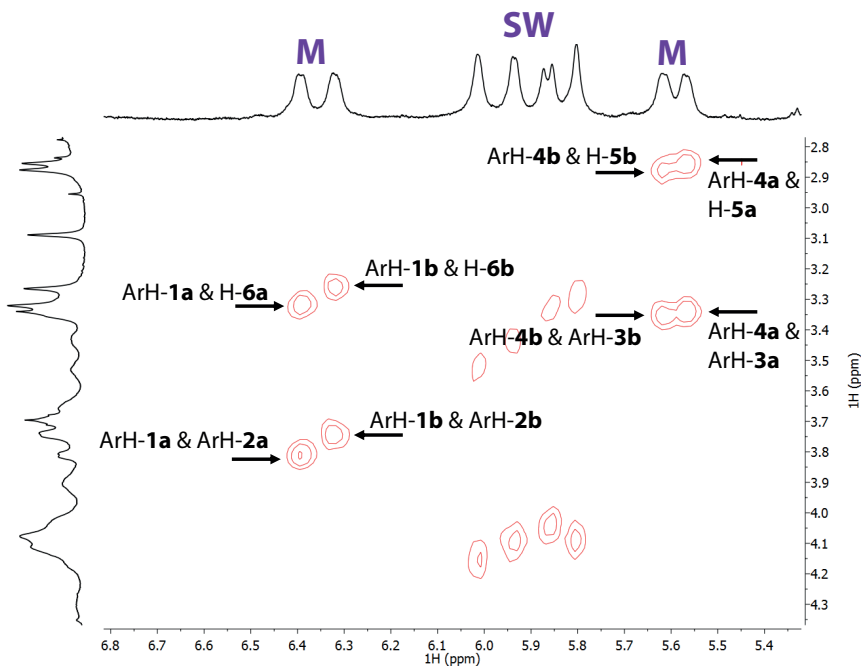

Figure 14 *Part of the 2D ROESY-spectrum of the 1:1:2* ***Zn_2C_3DC:DABCO:Me_2V*** *complex in a solvent mixture of $CDCl_3$ and MeCN-d_3 (1:1, (v/v)) at 223 K, showing the region of 6.8 to 5.3 ppm where the cross-coupling peaks of ArH-**1a** (6.39 ppm) & H-**6a** (3.33 ppm), ArH-**1a** (6.39 ppm) & ArH-**2a** (3.82 ppm), ArH-**1b** (6.32 ppm) & H-**6b** (3.26 ppm), ArH-**1b** (6.32 ppm) & ArH-**2b** (3.75 ppm), ArH-**4b** (5.62 ppm) & H-**5b** (2.88 ppm), ArH-**4b** (5.62 ppm) & ArH-**3b** (3.36 ppm), ArH-**4a** (5.56 ppm) & H-**5a** (2.86 ppm) and ArH-**4a** (5.56 ppm) & ArH-**3a** (3.34 ppm) are located. The **Me_2V** (ArH-**1** and ArH-**4**) and side wall proton resonances are indicated by M and SW, respectively.*

4.3. Conclusion

The binding of **Me_2V** in the cavities of 1:1 **Zn_2C_xDC**:DABCO sandwich complexes was investigated by fluorescence and NMR titrations. For all sandwich complexes, the addition of one equivalent of **Me_2V** caused the quenching of over 90% of the porphyrin fluorescence, which is remarkable. Both porphyrins in the sandwich complexes are probably within the quenching distance of a **Me_2V** guest when the latter is bound in one of the two cavities, and the **Me_2V** guest can therefore quench the fluorescence of both porphyrins simultaneously. It is likely that upon the addition of **Me_2V** the DABCO ligand in the sandwich complexes remains bound between the two porphyrins.

Analysis of the binding constants between **Me_2V** and the 1:1 **Zn_2C_xDC**:DABCO sandwich complexes indicated that the binding of the two **Me_2V** guests takes place in a negative cooperative fashion.

The formation of 1:1:2 complexes between **Zn_2C_xDC**, DABCO and **Me_2V** was corroborated by ^{1}H NMR titration experiments on the **Zn_2C_3DC** compound at varying temperatures. The NMR data confirmed that DABCO remains bound in between the porphyrins and hence that the sandwich complexes stay intact. When one equivalent of **Me_2V** was present at NMR concentrations (1 mM **Zn_2C_3DC**), exchange occurred between the 1:1:2 **Zn_2C_3DC**:DABCO:**Me_2V** and the 1:1 **Zn_2C_3DC**:DABCO sandwich complexes, a process that probably goes via the 1:1:1 **Zn_2C_3DC**:DABCO:**Me_2V** complex as an intermediate species. The binding of two equivalents of **Me_2V** to the sandwich complex gave rise to multiple proton resonances, which originate from the binding of the **Me_2V** guest in two different diastereoisomeric forms of the sandwich complexes.

Overall, the results of our studies on the complexation of **Me_2V** guests to the 1:1 **Zn_2C_xDC**:DABCO sandwich complexes with the help of fluorescence and NMR spectroscopy reveal that the binding of the DABCO ligand in between the porphyrin planes facilitates the transfer of information, i.e. in the form of a negative cooperative effect between the binding of the two **Me_2V** guests. This is an important prerequisite for the future development of a (double cage) catalytic device for the encoding of information into polymers.

4.4. Experimental

All chemicals were commercially obtained and used without further purification unless stated otherwise. MeCN was distilled under argon from calcium chloride. Chloroform (anhydrous, contains amylenes as stabilizers, ≥99%) was filtered over potassium carbonate under argon before use. DABCO was sublimated at 60-70 ^{0}C under vacuum prior to use. **Me_2V** was synthesized according to a literature reference.[11]

^{1}H and ^{13}C-NMR spectra were recorded on a Bruker Avance III 400 MHz spectrometer at 25˚C unless stated otherwise. Chemical shifts are reported in parts per million (ppm) relative to tetramethylsilane (TMS) as the internal reference. NMR data are presented as follows: Chemical shift (ð) in ppm and coupling constant (J) in Hertz (Hz). All NMR signals were assigned on the basis of ^{1}H, ^{13}C-NMR, COSY, ROESY, HSQC and HMBC experiments. Phase and baseline correction were applied to all ^{1}H-NMR and ^{13}C spectra. UV-Vis spectra were recorded with the program UV Probe on a Shimadzu UV 1800 spectrometer in a quartz cuvette with 1 cm path length and 3.8 mL total volume. The solvent was used as the baseline for the spectra. Fluorescence spectra were recorded with the program Labsolutions RF on a Shimadzu RF-5301PC Spectrofluorophotometer in a fluorescence cuvette with 1 cm path length

and 3.5 mL total volume. The solution was excited at the maximum wavelength determined by UV-Vis.

4.4.1 Titration methods

UV-Vis and fluorescence titrations

All titrations were carried out in threefold. The 1:1 solvent mixtures were prepared by weighing the desired amounts of both solvents into a closed Erlenmeyer flask. After thorough mixing, the density of the solvent mixture was determined from the weight increase of a 50 mL volumetric flask.

A host stock solution was prepared by quantitatively weighing an amount of the host (between 1 and 2 mg), which was dissolved in 10 mL solvent or solvent mixture (HostStock). The HostStock was diluted to 1.5 µM (10 mL) and if needed the appropriate amount of a DABCO stock solution (100 µL, 6.45 x10^{-3} M (**Zn_2C_3DC**), 7.65 x10^{-3} M (**Zn_2C_5DC**). 9.45 x10^{-3} M (**Zn_2C_{11}DC**)) was added thereby ensuring that the maximum amount of 1:1 **Zn_2C_xDC**:DABCO complex was present in solution. All ligand solutions (10 mL) contained 1.5 µM host from the diluted HostStock solution (if applicable with DABCO) and 4.00 x10^{-5} M (L1), 0. 4.00 x10^{-4} M (L2), 8.00x10^{-4} M (L3) of **Me_2V**. Solutions L1, L2 and L3 were prepared by diluting a 0.002 M **Me_2V** stock solution. The volumes of solvents or solvent mixtures required for the host and host-guest solutions were weighed on an analytical balance and the addition of the guest solutions to the host solution was carried out with Gilson pipets (up to a volume of 1000 µL).

A UV-Vis and fluorescence spectrum was recorded after every addition of **Me_2V**. The amounts of **Me_2V** ligand solutions titrated to the host are given in Table 2.

The change in the fluorescence emission was plotted against the number of added equivalents of **Me_2V**, which gave titration curves that were fitted with the program Bindfit at http://supramolecular.org/ which makes use of equation (2). In equation (2) ΔA is the difference between the total fluorescence intensity (A) and the initial fluorescence intensity (A_0), the $[H]_0$ is the total concentration of host, and $\Delta\varepsilon_{HL}$ and $\Delta\varepsilon_{HL_2}$ are the molar fluorescence coefficients in M^{-1}, which are determined from the molar fluorescence coefficients (ε) of the four individual species that are present during the titration, which in turn are defined by equations (3) and (4).

$$\Delta A = A - A_0 \frac{\Delta\varepsilon_{HL}\,(K_{11}[H]_0[L]) + \Delta\varepsilon_{HL_2}\,(K_{11}K_{12}[H]_0[L]^2)}{K_{11}K_{12}[L]^2 + K_{11}[L] + 1} \quad (2)$$

$$\Delta\varepsilon_{HL} = \varepsilon_{HL} - \varepsilon_H - \varepsilon_L \quad (3)$$

$$\Delta\varepsilon_{HL_2} = \varepsilon_{HL_2} - \varepsilon_H - \varepsilon_L \quad (4)$$

Table 2 Table of titrated amounts of **Me_2V** to a solution of 1:1 **Zn_2C_xDC**:DABCO sandwich complex (1.5 µM)

[Me_2V] (M)	Equivalents	Volume to add (µL)	Total volume (µL)
4.00x10^{-5}	0	0	2500
	0.1	9.41	2509.41
	0.2	9.48	2518.89
	0.3	9.55	2528.44
	0.4	9.63	2538.07
	0.5	9.70	2547.77
	0.75	24.58	2572.35
	1	25.1	2597.45
	1.25	25.6	2623.05
	1.5	26.0	2649.05
4.00x10^{-4}	2	5.00	2654.05
	2.5	5.02	2659.07
	3	5.04	2664.11
	3.5	5.06	2669.17
	4	5.08	2674.25
	4.5	5.10	2679.35
	5	5.12	2684.47
	5.5	5.14	2689.61
	6	5.16	2694.77
	7.5	15.60	2710.37
	10	26.4	2736.77
	12.5	26.9	2763.67
	15	27.5	2791.17
	20	56.6	2847.77
8.00x10^{-4}	25	28.0	2875.77
	30	28.6	2904.37
	40	58.9	2963.27
	50	61.3	3024.57
	60	63.9	3088.47

During the simultaneous iterative varying of the two binding constants to yield the smallest error between the fit and the experimentally acquired data, equation (2) was calculated per wavelength, while each wavelength has a specific set of molar fluorescence coefficients as these are wavelength-dependent.

^{1}H NMR titrations

The 1:1 solvent mixture for the ^{1}H NMR titrations was prepared by adding equal volumes of $CDCl_3$ and MeCN-d_3 with Gilson pipets (up to a volume of 1000 µL) to a test tube. After thorough mixing of the solvents, the desired volume was added to the weighed host (1 – 2 mg) to obtain a host solution with a concentration of circa 1 mM. One equivalent of DABCO was weighed and added to the host solution. Small amounts of guest (**Me_2V**) solution (up to 134 µL) were added to the host solution with a Gilson pipet until up to 2 equivalents of guest were present. After each addition of guest, a ^{1}H NMR spectrum was recorded at the desired temperature.

4.4.2 Spartan modeling

Modeling of the distance between the two zinc centers in the porphyrin planes was carried out with the Spartan14 program by applying first an MMFF geometry optimization followed by PM6 geometry optimization for **Zn_2C_3TTBP**, **Zn_2C_5TTBP**, and **Zn_2C_{11}TTBP** (see also Chapter 3). These compounds were used as reference compounds for **Zn_2C_3DC**, **Zn_2C_5DC**, and **Zn_2C_{11}DC**, respectively. These structures were chosen because the elimination of the cavity reduces the computational load and is not expected to influence the distance between the porphyrin planes.

4.5. References

(1) Zhirnov, V.; Zadegan, R. M.; Sandhu, G. S.; Church, G. M.; Hughes, W. L. Nucleic Acid Memory. *Nat. Mater.* **2016**, *15* (4), 366–370.

(2) Goldman, N.; Bertone, P.; Chen, S.; Dessimoz, C.; LeProust, E. M.; Sipos, B.; Birney, E. Towards Practical, High-Capacity, Low-Maintenance Information Storage in Synthesized DNA. *Nature* **2013**, *494* (7435), 77–80.

(3) Church, G. M.; Gao, Y.; Kosuri, S. Next-Generation Digital Information Storage in DNA. *Science* **2012**, *337* (6102), 1628.

(4) Colquhoun, H.; Lutz, J.-F. Information-Containing Macromolecules. *Nat. Chem.* **2014**, *6* (6), 455–456.

(5) Lutz, J.-F. Coding Macromolecules: Inputting Information in Polymers Using Monomer-Based Alphabets. *Macromolecules* **2015**, *48* (14), 4759–4767.

(6) Mutlu, H.; Lutz, J.-F. Reading Polymers: Sequencing of Natural and Synthetic Macromolecules. *Angew. Chem. Int. Ed.* **2014**, *53* (48), 13010–13019.

(7) *See Chapter 2 of This Thesis*.

(8) *See Chapter 3 of This Thesis*.

(9) Thordarson, P.; Coumans, R. G. E.; Elemans, J. A. A. W.; Thomassen, P. J.; Visser, J.; Rowan, A. E.; Nolte, R. J. M. Allosterically Driven Multicomponent Assembly. *Angew. Chem. Int. Ed.* **2004**, *43* (36), 4755–4759.

(10) Deutman, A. B. C.; Monnereau, C.; Moalin, M.; Coumans, R. G. E.; Veling, N.; Coenen, M.; Smits, J. M. M.; de Gelder, R.; Elemans, J. A. A. W.; Ercolani, G.; et al. Squaring Cooperative Binding Circles. *Proc. Natl. Acad. Sci. U. S. A.* **2009**, *106* (26), 10471–10476.

(11) Elemans, J. A. A. W.; Claase, M. B.; Aarts, P. P. M.; Rowan, A. E.; Schenning, A. P. H. J.; Nolte, R. J. M. Porphyrin Clips Derived from Diphenylglycoluril. Synthesis, Conformational Analysis, and Binding Properties. *J. Org. Chem.* **1999**, *64* (19), 7009–7016.

(12) Hidalgo Ramos, P.; Saisaha, P.; Elemans, J. A. A. W.; Rowan, A. E.; Nolte, R. J. M. Conformational Analysis and Binding Properties of a Cavity Containing Porphyrin Catalyst Provided with Urea Functions. *Eur. J. Org. Chem.* **2016**, *26*, 4487–4495.

(13) Deutman, A. B. C.; Smits, J. M. M.; de Gelder, R.; Elemans, J. A. A. W.; Nolte, R. J. M.; Rowan, A. E. Strong Induced-Fit Binding of Viologen and Pyridine Derivatives in Adjustable Porphyrin Cavities. *Chem. – Eur. J.* **2014**, *20* (36), 11574–11583.

(14) Rowan, A. E.; Aarts, P. P. M.; Koutstaal, K. W. M. Novel Porphyrin–viologen Rotaxanes. *Chem. Commun.* **1998**, *5*, 611–612.

(15) Coumans, R. G. E.; Elemans, J. A. A. W.; Thordarson, P.; Nolte, R. J. M.; Rowan, A. E. Synthesis of Porphyrin-Containing [3]Rotaxanes by Olefin Metathesis. *Angew. Chem. Int. Ed.* **2003**, *42* (6), 650–654.

(16) Coumans, R. G. E.; Elemans, J. A. A. W.; Nolte, R. J. M.; Rowan, A. E. Processive Enzyme Mimic: Kinetics and Thermodynamics of the Threading and Sliding Process. *Proc. Natl. Acad. Sci. U. S. A.* **2006**, *103* (52), 19647–19651.

(17) Deutman, A. B. C.; Cantekin, S.; Elemans, J. A. A. W.; Rowan, A. E.; Nolte, R. J. M. Designing Processive Catalytic Systems. Threading Polymers through a Flexible Macrocycle Ring. *J. Am. Chem. Soc.* **2014**, *136* (25), 9165–9172.

(18) Deutman, A. B. C.; Varghese, S.; Moalin, M.; Elemans, J. A. A. W.; Rowan, A. E.; Nolte, R. J. M. Slippage of a Porphyrin Macrocycle over Threads of Varying Bulkiness: Implications for the Mechanism of Threading Polymers through a Macrocyclic Ring. *Chem. – Eur. J.* **2015**, *21* (1), 360–370.

(19) Hidalgo Ramos, P.; Coumans, R. G. E.; Deutman, A. B. C.; Smits, J. M. M.; de Gelder, R.; Elemans, J. A. A. W.; Nolte, R. J. M.; Rowan, A. E. Processive Rotaxane Systems. Studies on the Mechanism and Control of the Threading Process. *J. Am. Chem. Soc.* **2007**, *129* (17), 5699–5702.

(20) Schenning, A. P. H. J.; de Bruin, B.; Rowan, A. E.; Kooijman, H.; Spek, A. L.; Nolte, R. J. M. Strong Binding of Paraquat and Polymeric Paraquat Derivatives by Basket-Shaped Hosts. *Angew. Chem. Int. Ed. Engl.* **1995**, *34* (19), 2132–2134.

(21) Allwood, B. L.; Spencer, N.; Shahriari-Zavareh, H.; Stoddart, J. F.; Williams, D. J. Complexation of Paraquat by a Bisparaphenylene-34-Crown-10 Derivative. *J. Chem. Soc. Chem. Commun.* **1987**, No. 14, 1064–1066.

(22) Thordarson, P.; Bijsterveld, E. J. A.; Rowan, A. E.; Nolte, R. J. M. Epoxidation of Polybutadiene by a Topologically Linked Catalyst. *Nature* **2003**, *424* (6951), 915–918.
(23) Elemans, J. A. A. W. *Nanosized Architectures from Glycoluril Building Blocks. PhD Thesis*; 2001.
(24) Thordarson, P. Determining Association Constants from Titration Experiments in Supramolecular Chemistry. *Chem. Soc. Rev.* **2011**, *40* (3), 1305–1323.
(25) Harriman, A. The Effect of Separation Distance on the Fluorescence Quenching for Zinc Porphyrin/viologen Systems. *Inorganica Chim. Acta* **1984**, *88* (2), 213–216.
(26) Jolliffe, K. A.; Bell, T. D. M.; Ghiggino, K. P.; Langford, S. J.; Paddon-Row, M. N. Efficient Photoinduced Electron Transfer in a Rigid U-Shaped Tetrad Bearing Terminal Porphyrin and Viologen Units. *Angew. Chem. Int. Ed.* **1998**, *37* (7), 915–919.
(27) Modeling of the distance between the two zinc centers in the porphyrin planes was carried out for **Zn_2C_3TTBP**, **Zn_2C_5TTBP** and **Zn_2C11TTBP** (see Chapter 3) as reference compounds for **Zn_2C3DC**, **Zn_2C5DC** and **Zn_2C_{11}DC**, respectively. These structures were chosen as reference compounds because the elimination of the cavity reduces the computational load and is not expected to influence the distance between the porphyrin planes.
(28) Murphy, R. B.; Pham, D.-T.; Lincoln, S. F.; Johnston, M. R. Molecular Tweezers with Freely Rotating Linker and Porphyrin Moieties. *Eur. J. Org. Chem.* **2013**, *15*, 2985–2993.
(29) Ballester, P.; Costa, A.; Castilla, A. M.; Deyà, P. M.; Frontera, A.; Gomila, R. M.; Hunter, C. A. DABCO-Directed Self-Assembly of Bisporphyrins (DABCO=1,4-Diazabicyclo[2.2.2]octane). *Chem. – Eur. J.* **2005**, *11* (7), 2196–2206.
(30) Baldini, L.; Ballester, P.; Casnati, A.; Gomila, R. M.; Hunter, C. A.; Sansone, F.; Ungaro, R. Molecular Acrobatics: Self-Assembly of Calixarene-Porphyrin Cages. *J. Am. Chem. Soc.* **2003**, *125* (46), 14181–14189.
(31) Mak, C. C.; Bampos, N.; Sanders, J. K. M. Metalloporphyrin Dendrimers with Folding Arms. *Angew. Chem. Int. Ed.* **1998**, *37*, 3020–3023.
(32) Cantekin, S.; Markvoort, A. J.; Elemans, J. A. A. W.; Rowan, A. E.; Nolte, R. J. M. Allosterically Controlled Threading of Polymers through Macrocyclic Dimers. *J. Am. Chem. Soc.* **2015**, *137* (11), 3915–3923.
(33) Kim, D.; Lee, S.; Gao, G.; Seok Kang, H.; Ko, J. A Molecular-Clip-Based Approach to Cofacial Zinc–porphyrin Complexes. *J. Organomet. Chem.* **2010**, *695* (1), 111–119.
(34) Mikhailitsyna, E. A.; Tyurin, V. S.; Beletskaya, I. P. Synthesis of Supramolecular Complexes Based on Tetracrown–substituted Zinc Porphyrinates. *Prot. Met. Phys. Chem. Surf.* **2010**, *46* (6), 655–661.
(35) Mondal, P.; Rath, S. P. Cyclic Zinc(II) Bisporphyrin-Based Molecular Switches: Supramolecular Control of Complexation-Mediated Conformational Switching and Photoinduced Electron Transfer. *Chem. – Eur. J.* **2016**, *22* (16), 5607–5619.
(36) Wang, H.-W.; Chen, C.-H.; Lim, T.-S.; Huang, S.-L.; Luh, T.-Y. Supramolecular Porphyrin–DABCO Array in Single- and Double-Stranded Polynorbornenes. *Chem. – Asian J.* **2011**, *6* (2), 524–533.

4.6. Appendices

A1: Fluorescence titration spectra of the 1:1 Zn_2C_5DC:DABCO and 1:1 Zn_2C_{11}DC:DABCO sandwich complexes with Me_2V in a solvent mixture of chloroform and MeCN (1:1, (v/v))

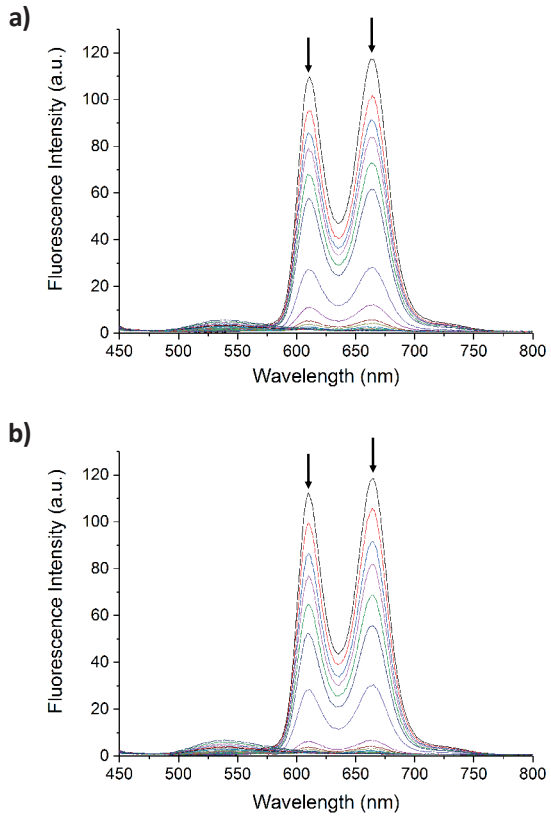

Figure 15 *Representative fluorescence spectra of titrations of (a) 1:1* ***Zn_2C_5DC****:DABCO and (b) 1:1* ***Zn_2C_{11}DC****:DABCO sandwich complex with* ***Me_2V*** *in a solvent mixture of chloroform and MeCN (1:1, (v/v)).*

A2: Further analysis and discussion of the fluorescence titration data

The binding constants of **Me_2V** with the 1:1 **Zn_2C_3DC**:DABCO sandwich complex as reported in Table 1 of the main text (page 148) are unexpectedly high for both the first and second binding event of the guest (log ($K_{1:1}$) and log ($K_{1:2}$) are ~16 and ~13, respectively). Complete formation of the 1:1:1 as well as the 1:1:2 **Zn_2C_3DC**:DABCO:**Me_2V** complexes occurs already at a low number of added equivalents of **Me_2V**.

It should be noted, however, that the error in the measurements (2σ) is high (2σ≈4), which indicates that the *K*-values extracted from the titration curves are very sensitive to small variations in the data points. However, the measurement of the 1:1 **Zn_2C_3DC**:DABCO sandwich complex with **Me_2V** was performed in triplicate and the results are consistent over all three measurements, not showing any outliers. How can these high binding constants be explained? As was mentioned in Chapter 3, molecular modeling studies using the Spartan software revealed that the distance between the two porphyrin planes in **Zn_2C_3TTBP** (model compound for **Zn_2C_3DC,** see Chapter 3, Figure 9) is 7.155 Å, a value that is higher than the distance between the porphyrin planes in **Zn_2C_5TTBP** and **$Zn_2C_{11}TTBP$**, which are model compounds for the other porphyrin cage compounds. The fact that the smallest spacer length leads to the largest distance between the porphyrins and assuming that this also holds for the related porphyrin cage complexes, indicates that there might be strain in the bonds of the spacer in the 1:1 **Zn_2C_3DC**:DABCO sandwich complex. It might be that due to the high binding constant of DABCO to the **Zn_2C_3DC** for this compound the zinc atoms are pulled out of the porphyrin planes the furthest. This may lead to a relatively large modification of the shape of the cage, to the extent that the interactions of its walls with **Me_2V** become stronger compared to the other **Zn_2C_xDC** compounds, eventually resulting in unexpectedly high binding constants for $K_{1:1}$ and $K_{1:2}$. It might also be that instead of a 1:1 **Zn_2C_3DC**:DABCO sandwich complex, a 2:2 **Zn_2C_3DC**:DABCO complex is formed in which two zinc centers of different **Zn_2C_3DC** compounds are bound to the same DABCO ligand, giving a ladder-like complex, which can still bind **Me_2V** guests in the cavities. However, it is less likely that such a complex of eight components is generated at the low concentrations used in the fluorescence studies (1.5 μM).

The binding constants for the first binding event of **Me_2V** with the 1:1 **Zn_2C_5DC**:DABCO and the 1:1 **$Zn_2C_{11}DC$**:DABCO sandwich complexes are both in the same order of magnitude, but more than seven orders of magnitude lower than the value obtained for the 1:1 **Zn_2C_3DC**:DABCO sandwich complex (Table 1, page 148). Nearly all binding constants found for the binding of **Me_2V** with the 1:1 **Zn_2C_xDC**:DABCO sandwich complexes are significantly larger than those previously obtained for the **Zn_2C_xDC** compounds (Table A1). This increase is proposed to be caused by an allosteric effect as a result of the coordination of DABCO. Similar allosteric effects have been observed before in other zinc porphyrin cage compounds.[9] This allosteric magnification effect also facilitates the quick and full occupation of the cavities of the zinc porphyrin cages by **Me_2V** already at low amounts of added guest, much lower than in the case of the porphyrin cages without DABCO present. The only case where no enhancement of binding was observed, albeit within the experimental error, was for the binding of the second **Me_2V** guest in **$Zn_2C_{11}DC$** (compare the log $K_{1:2}$ values for this compound in Tables 1 and A1). It might be that the second **Me_2V** guest binds in a similar fashion to **$Zn_2C_{11}DC$** and to the **$Zn_2C_{11}DC$**: DABCO sandwich complex, but

Table A1 Binding constants $K_{1:1}$ and $K_{1:2}$ for the binding between **Me_2V** and **Zn_2C_3DC**, **Zn_2C_5DC**, and **$Zn_2C_{11}DC$** in the solvent mixture chloroform and MeCN (1:1, (v/v)). K-values are given as their logarithmic values, with an error of two times the standard deviation over the threefold measurement. The number of equivalents of **Me_2V** needed to obtain the maximum amount of 1:1 **Zn_2C_xDC:Me_2V** sandwich complex is also shown, with a reported error of two times the standard deviation over the threefold measurement. The cooperativity factor (α) is also reported.

	Zn_2C_3DC	**Zn_2C_5DC**	**$Zn_2C_{11}DC$[a]**
Log($K_{1:1}$)	7.32±0.16	6.64±0.09	7.22±0.07
Log($K_{1:2}$)	4.70±0.05	4.13±0.22	5.29±0.04
Equivalents Me_2V (1:1)	1.7±0.47	3.8±1.25	1.4±0.25
Cooperativity factor (α)	0.00957	0.01271	0.04702

[a] measured in twofold

that this binding mode does not result in any structural changes because the spacer length is long enough to accommodate the second guest without any difficulties.

Tables 1 and A1 reveal that both the 1:1 **Zn_2C_xDC**:DABCO sandwich complexes and the **Zn_2C_xDC** compounds display highly negative cooperativity factors for the binding of **Me_2V** in all cases. These cooperativity factors are smaller for the former sandwich complexes than for the latter compounds by factors of 1.44, 1.49, and 373, respectively. As was explained in the main text this may be the result of geometry changes that occur after the binding of the first **Me_2V** guest, leading to a weakening of the binding of the second **Me_2V** guest. An alternative or additional explanation for the observed negative cooperativity is that the binding of two positively charged **Me_2V** guests in relative close proximity leads to electrostatic repulsion. The cooperativity factor is the lowest for the 1:1 **$Zn_2C_{11}DC$**:DABCO sandwich complex, indicating that binding of a second **Me_2V** guest in its second cavity is the least favorable compared to the other sandwich complexes. This might be the result of the longer spacer length, which requires that more degrees of freedom are lost upon the binding of the second **Me_2V** guest (entropy effect).

The negative cooperativity observed in the **Zn_2C_xDC** compounds might have a different cause, because there is no axial ligand present to bring the two cages together in a sandwich-like conformation. It might be that the first **Me_2V** guest binds in between the two cavities, having interactions with both of them simultaneously. If subsequently a second **Me_2V** guest is added, the first bound **Me_2V** guest has to relocate and move completely to one of the two cavities, while losing its interactions with the other cavity. The energy penalty associated with this relocation will result in an overall weaker binding of the second **Me_2V** guest, and hence in a negative

cooperativity. An additional contribution to the negative cooperativity may be the electrostatic repulsion between the two positively charged **Me_2V** guests bound in the two cavities, as mentioned before. This repulsion will be the lowest for **$Zn_2C_{11}DC$** compound, because its long spacer length enables a maximum distance between the two cavities. As a result, the binding cooperativity will be higher for this double cage compound. The lowest cooperativity is observed for **Zn_2C_3DC**, which is in line with the short distance between the two cavities as imposed by the short spacer. As a result, the electrostatic repulsion between the charged guests will be maximal, resulting in the observed low value.

5

Threading of polymer chains through double zinc porphyrin cages

This chapter will be published:

Threading of polymer chains through zinc double porphyrin cage compounds
- Manuscript in preparation

K. Stout, T. Peters, P. B. White, J. A. A. W Elemans, A. E. Rowan and R. J. M Nolte

Abstract

As a fourth step in the development of an enzyme mimic capable of writing a binary code onto a synthetic polymer, the threading of polytetrahydrofuran chains (polyTHF), equipped with a viologen (**V**) thermodynamic trap, through the cavities of porphyrin sandwich complexes is investigated. These complexes consist of covalently linked double zinc porphyrin cages, ligated by the ditopic axial ligand 1,4-diazabicyclo[2.2.2]octane (DABCO) to form 1:1 **Zn_2C_xDC**:DABCO (x = 3, 5, 11) sandwich structures. All three 1:1 **Zn_2C_xDC**:DABCO sandwich complexes can traverse polymer chains with lengths up to 69 nm. Fluorescence quenching experiments showed that 1:1:1 and 1:1:2 **Zn_2C_xDC**:DABCO:polymer architectures were formed and that the **V**-moiety of the polymer chain binds in a similar fashion as **Me_2V** to the 1:1 **Zn_2C_xDC**:DABCO sandwich complexes. MALDI-TOF spectrometry confirmed the formation of the 1:1:1 **Zn_2C_xDC**:DABCO:polymer complexes, but 1:1:2 **Zn_2C_xDC**:DABCO:polymer were not detected. It was demonstrated that an increase in polymer length decreases the threading-on rate, and that this rate and its related free energy of activation did not depend on the spacer length between the two cages in the sandwich complexes. The 1:1 **$Zn_2C_{11}DC$**:DABCO sandwich complex had a consistently lower energy penalty for the threading of the polymer chains than the other sandwich complexes, which was attributed to larger degrees of conformational freedom present in the former complex originating from the longer spacer length.

5.1. Introduction

Given the fact that is expected that the global digital archive cannot be sustained by the use of silicon memory chips by 2040, data storage is an emerging field of research.[1] As a result of this, new methods for data storage have to be developed and one possible approach is to use biological and synthetic polymers for this purpose (see Chapter 1). The storage of data in synthetic polymers is favored over the storage in biological polymers because the former macromolecules are easier to handle than the latter ones and can more favorably make use of a binary code, which is commonly used in computing.[2–6] To enable the storage of data in a synthetic polymer, we designed, synthesized, and characterized a double porphyrin cage compound, which is capable of writing binary codes onto a polymer chain, at least in principle (Figure 1a).[7] This double porphyrin cage compound consists of two cavities, which are both equipped with a porphyrin 'roof' and are covalently linked via bis-triazole-containing spacers of different lengths, i.e. 3, 5, or 11 carbon atoms (Figure 1b).

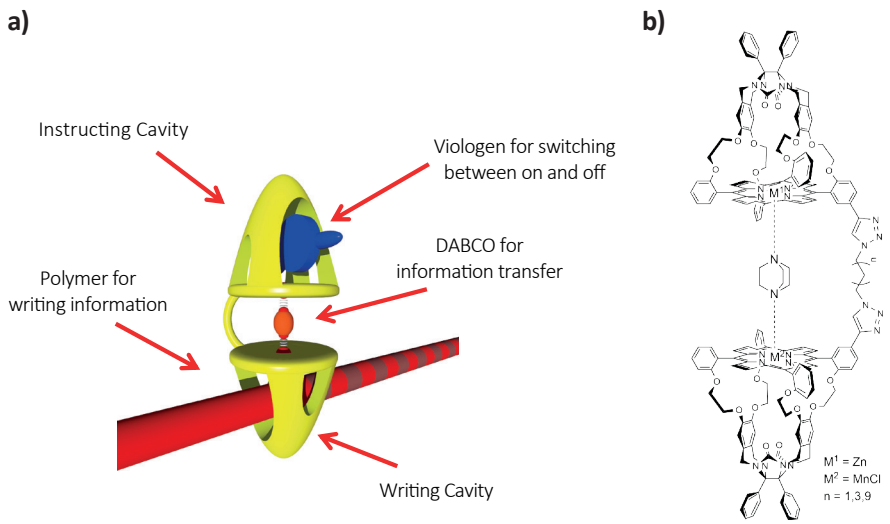

Figure 1 *a) Schematic representation of a double porphyrin cage compound consisting of two molecular cages capped with a porphyrin roof that are covalently connected (yellow). The instructing cavity contains a zinc center and the writing cavity a manganese ion. The binding of a ditopic ligand such as DABCO (orange) in between the two porphyrins might allow the transfer of information from the instructing cavity to the writing cavity. The binding of a viologen guest (blue) inside the instructing cavity may influence the binding of DABCO to the manganese center, which can perform a catalytic reaction on for example a polymer substrate (red), via a series of allosteric interactions. b) Chemical structure of the zinc-manganese double porphyrin cage compound with spacer lengths of 3, 5, and 11 carbon atoms, binding DABCO as ditopic axial ligand.*

It is expected that when one of the porphyrin cages contains a zinc ion, an instructing cavity is created that can influence the catalytic activity exhibited by the manganese center in the other porphyrin cage via allosteric interactions transferred through a ditopic axial ligand such as 1,4-diazabicyclo[2.2.2]octane (DABCO). It was shown in Chapter 3 that the binding of DABCO to double zinc porphyrin cage compounds (**Zn_2C_xDC**s) in chloroform or a solvent mixture of chloroform and acetonitrile (MeCN, 1:1, (v/v)) results in stable 1:1 **Zn_2C_xDC**:DABCO sandwich complexes. As mentioned above, the binding of this axial ligand to both porphyrins of the double cage compound could in theory facilitate information transfer, i.e. from the instructing cavity to the cavity that writes information onto a polymer chain, because its binding to both metal centers is expected to change upon the complexation of a guest such as *N,N*'-dimethylviologen dihexafluorophosphate (**Me_2V**) in the instructing cavity.

In connection with what is mentioned above, the aim of the present study was to investigate the binding and threading of polymer chains through the porphyrin cages of the 1:1 **Zn_2C_xDC**:DABCO sandwich complexes. The binding of polymers such as poly-tetrahydrofuran (polyTHF) derivatives in the cavities of single porphyrin cage compounds, e.g. **H_2SC** (Figure 2a), and their subsequent threading has been previously studied with the help of UV-Vis, fluorescence, and NMR spectroscopy, as well as with matrix-assisted laser desorption/ionization time of flight (MALDI-TOF) spectrometry.[8–12] In these studies, the THF polymers were equipped with a viologen (**V**) moiety, which was attached via a spacer to a 3,5-ditert-butylphenyl blocking group.[8–12] It was shown that a **V**-moiety, protected on both sides with this blocking group, is not able to bind in the cavity of **H_2SC**. This implies that the bulky 3,5-ditert-butyl group cannot be passed by **H_2SC**, and thus, in the case of the above described polymers, this host has to bind to the open side of the polymer and traverse the whole polymer chain in order to finally bind to the **V**-moiety. With the help of NMR spectroscopy it was found that solely 1:1 complexes between **H_2SC** and the blocked viologen-appended polyTHF derivatives were formed. And from the observed complexation-induced upfield shifts of the **V**-moieties, which are in line with the complexation-induced upfield shifts of **Me_2V** bound in the cavity of **H_2SC**, it was concluded that the viologen moieties of the polymers were bound in the cavity of **H_2SC** (Figure 2b).[8–10] MALDI-TOF analysis of the resulting complexes revealed an increase in mass of 1345 amu compared to the masses of the one-side blocked viologen-appended polyTHF derivatives in the absence of **H_2SC**, a difference that corresponds to the mass of the host molecule.[8] Additional studies were focused on determining the threading rates of **H_2SC** onto the blocked viologen-appended polyTHF derivatives. It was found that at millimolar concentrations the threading process occurred too fast to be measured by NMR spectroscopy. Therefore, fluorescence studies were performed because these can be carried out at much lower concentrations, at which the threading rate is lower, and because the **V**-moiety is able to quench the fluorescence emission of the porphyrin once it binds in the cavity of the host.[8,11,13,14] Hence, in order to study the

threading process, the decrease in fluorescence intensity of **H_2SC** was followed over time and it was found that it is a second order process, which depends on both the concentration of **H_2SC** and that of the polymer.[8] When the reciprocal concentration of **H_2SC** (1/[**H_2SC**]) was plotted versus time, straight lines were obtained up to at least 50% of quenching. From these graphs, the apparent rate constants for the threading (k_{on}) of a polymer at a fixed concentration could be derived, as well as the difference in free energies between the uncomplexed components and the transition state ($\Delta G^{\ddagger}_{on}$). The rate constants appeared to depend on the length of the polymer chain, in the sense that longer chain lengths decreased the threading rate. The polymer chains need to attain a conformation in which they are extended before **H_2SC** can traverse them, and this stretching is related to a barrier of entropic origin.[8] The threading of the one-side blocked viologen-appended polyTHF derivatives was also studied for the zinc derivative **ZnSC**. Threading of **ZnSC** onto these polymers turned to be a second order process as well, however, with a lower rate constant than found for the threading of **H_2SC**.[9] This lower rate constant was proposed to originate from the partial blocking of the cavity of **ZnSC** by the coordination of a MeCN solvent molecule to the zinc center at the inside of the host molecule. Upon the addition of an axial ligand, such as *t*-butyl pyridine, which coordinates to the zinc center at the outside of the cage molecule, the coordinated MeCN molecule at the inside was released and faster threading rates were observed. When the cavity of **ZnSC** was blocked by the much stronger binding ligand pyridine, which also binds at the inside of the cage molecule, no threading was observed. In order to study the threading of polymers through a double 2:1 **ZnSC**:DABCO cage complex, a tetra-hydroxy functionalized porphyrin cage compound (**$Zn(OH)_4SC$**, see Figure 2a) was employed, because intermolecular hydrogen bonding interactions between the hydroxy groups on top of the porphyrin cage ensured the formation of 2:1 **$Zn(OH)_4SC$**:DABCO sandwich complexes already at dilute concentrations.[12] The threading of polymers through this sandwich complex also exhibited second order kinetics and it was found that 2:1:1 and 2:1:2 **$Zn(OH)_4SC$**:DABCO:polymer complexes were formed simultaneously. The relatively slow threading rates that were measured and the observed enhanced binding constants between **$Zn(OH)_4SC$** and the viologen moieties when DABCO was present, suggested that the binding of the **V**-moiety influences the binding of DABCO via allosteric interactions and therefore communication between the cavities could be present. The addition of a second equivalent of polymer to a preformed 2:1:1 **$Zn(OH)_4SC$**:DABCO:polymer complex resulted in a very low threading rate. This phenomenon was attributed to the blocking of the second cavity of the complex as a result of the threading of the end of the polymer chain bound in the first cavity through the second cavity via a looping mechanism. The latter looping is caused by an effective molarity effect (Figure 2c).

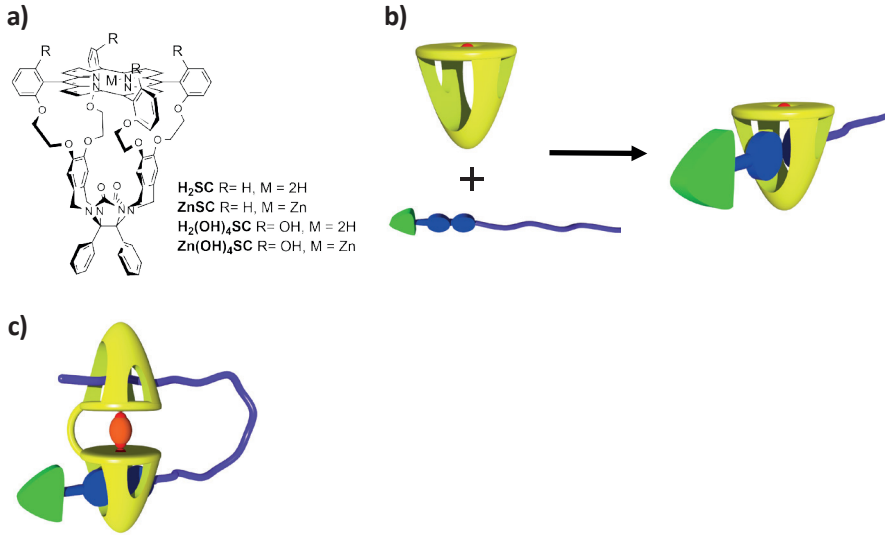

Figure 2 *a) Chemical structures of single porphyrin cage (**H$_2$SC**), its zinc derivative (**ZnSC**), single tetrahydroxy porphyrin cage (**H$_2$(OH)$_4$SC**), and its zinc derivative (**Zn(OH)$_4$SC**). b) Schematic representation of the complexation of a polyTHF molecule (purple), end-capped with a **V** binding station (blue) attached to a bulky blocking group (green), to **H$_2$SC** (yellow). c) Similarly, for a **Zn(OH)$_4$SC** dimer (blue) coordinated to DABCO (red) in which the second cavity is blocked by the end of the polymer chain (yellow) bound in the first cavity.*

The aim of the work presented in this chapter is to further investigate the threading properties of one-side blocked viologen-appended polyTHF derivatives onto double zinc porphyrin cages, in this case not held together by additional hydrogen bonding interactions, but by a single covalent linker, i.e. the 1:1 **Zn$_2$C$_x$DC**:DABCO sandwich complexes discussed in the previous chapters. The threading behavior was studied with the help of fluorescence spectroscopy supported by MALDI-TOF measurements.

5.2. Results and discussion

5.2.1 Synthesis of a series of blocked viologen-appended polyTHF compounds

Blocked viologen-appended polyTHF compounds were synthesized via an adapted literature procedure and purified by several consecutive size exclusion columns to obtain a narrow weight distribution (Figure 3a).[8] The properties of polymer compounds **P1** to **P3** are reported in Table 1. The double blocked viologen (**dbV**, Figure 3b), which cannot be traversed by the cavity of porphyrin cage compounds, was synthesized according to a literature procedure.[8]

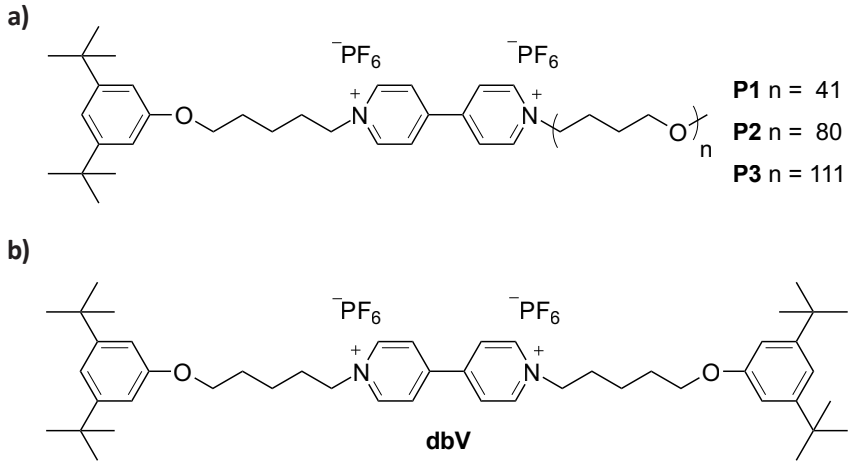

Figure 3 *Chemical structures of (a) polymer compounds **P1**-**P3** and (b) double blocked viologen (**dbV**) in which a **V**-moiety is blocked on both sides by a 3,5-ditert-butylphenyl blocking group, which cannot be traversed by the cavity of porphyrin cage compounds.*

Table 1 Number average weight (M_n), molecular weight (M_w), degree of polymerization (n), polymer length (L_n) and polydispersity index (PDI) of polymer compounds **P1**-**P3**.

Polymer (P#)	M_n (g/mol)[1]	M_w (g/mol)[1]	n	L_n (nm)[2]	PDI[1]
P1	3271	3445	41	25	1.05
P2	6064	6358	80	50	1.05
P3	8310	8687	111	69	1.05

[1] Determined by MALDI-TOF spectrometry. [2] $L_n = 0.62DP_n$ (length of 1 monomer unit).[8]

5.2.2 Threading of polymers through the 1:1 Zn2CxDC:DABCO sandwich complex: fluorescence studies

5.2.2.1 Experimental design

In order to study the threading kinetics of **P1**-**P3** through the cavities of the 1:1 **Zn$_2$C$_x$DC**:DABCO sandwich complexes, either one equivalent of polymer was added to a sandwich complex followed by a second equivalent (subsequent addition), or two equivalents of polymer were added at once (instantaneous addition, Figure 4a). The decay in fluorescence intensity was followed over time until a constant fluorescence value was reached, and a MALDI-TOF spectrum was measured from a sample of the resulting solution. The normalized fluorescence intensity is correlated to the concentration of free 1:1 **Zn$_2$C$_x$DC**:DABCO complex, as was found before in the

studies on the related **H_2SC** and **ZnSC** compounds.[8] Plotting 1/[free 1:1 **Zn_2C_xDC**:DABCO complex] against time results in a straight line with a slope that equals the apparent rate constant of the threading process (k_{on} in M^{-1} s^{-1}, Figure 4b). It was hypothesized that when the whole polymer chain is traversed and **V**-moieties are bound in both cavities of the 1:1 **Zn_2C_xDC**:DABCO sandwich complex, complete fluorescence quenching occurs. When one equivalent of **P1**-**P3** is added to the 1:1 **Zn_2C_xDC**:DABCO sandwich complex, maximally 50% of fluorescence quenching is

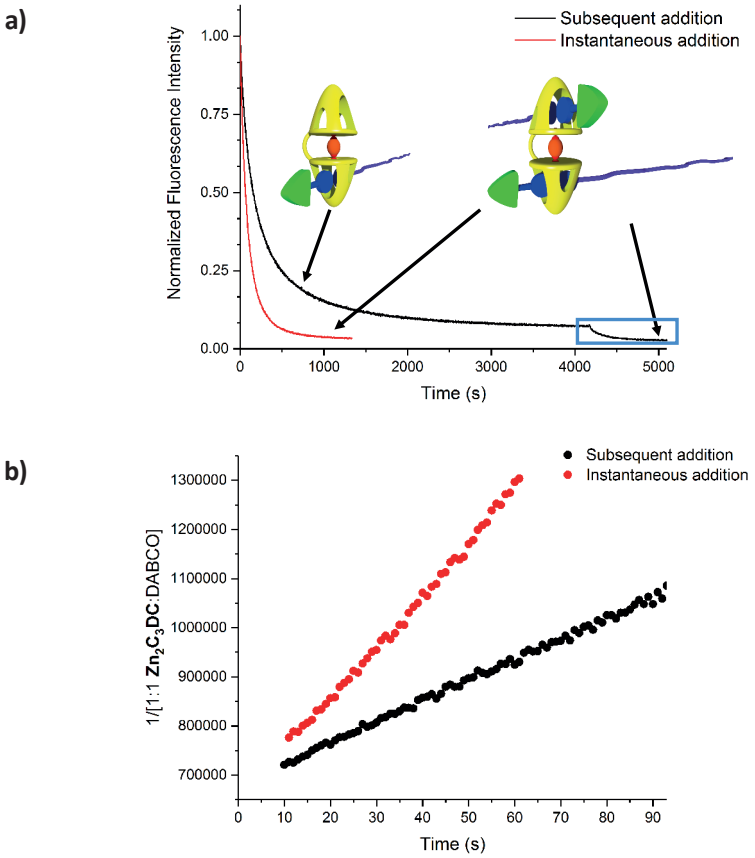

Figure 4 *a) Normalized fluorescence intensities of the 1:1* ***Zn_2C_3DC***:DABCO *sandwich complex measured over time after the subsequent (black line) and the instantaneous (red line) addition of two equivalents of* ***P3****. Schematic representations of the formed 1:1:1 and 1:1:2* ***Zn_2C_3DC***:DABCO:***P3*** *complexes are shown. The addition of the second equivalent* ***P3*** *in the subsequent addition experiment is indicated by the blue box and the black arrow. b) Second-order plots of the rate data shown in a); black curve: experiment in which the 1:1* ***Zn_2C_3DC***:DABCO *sandwich complex is complexed to the first added equivalent of* ***P3****, red curve: experiment in which this sandwich complex is complexed to two simultaneously added equivalents of* ***P3****.*

expected, at least in principle, because the quenching level of the porphyrins is usually directly proportional to the percentage of bound **V**-moieties (see, however, Chapter 4 and the following section for a deviation from this rule). Also, the addition of one equivalent of **P1**-**P3** is expected to result in a statistical distribution of polymeric guests bound in the cavities of the available hosts when no allosteric or other cooperative interactions are present between the two cavities of the sandwich complexes. In that case, the statistical distribution is expected to lead to the formation of 25%, 50%, and 25% of the 1:1:0, 1:1:1, and 1:1:2 **Zn_2C_xDC**:DABCO:(**P1**-**P3**) complexes, respectively. From the experiments in which **P1**-**P3** were added to the 1:1 **Zn_2C_xDC**:DABCO sandwich complexes (for an example see Figure 4a), it can be concluded that the 1:1 **Zn_2C_xDC**:DABCO sandwich complexes can traverse each of the polymers **P1**-**P3** and eventually bind to the **V**-moiety, because fluorescence quenching of the porphyrin was observed in all cases.

5.2.2.2 Percentage of quenching upon complexation of P1-P3 in the cavities of the 1:1 Zn2CxDC:DABCO sandwich complexes

When the **V**-moiety reaches the porphyrin cavities of the sandwich complexes, quenching of the porphyrin fluorescence emission is observed (Figure 4a). The amounts of quenching appeared to be dependent on how many equivalents of polymer were added. The results for the subsequent additions of **P1**-**P3** of are reported in Tables 2 and 3 and those for the instantaneous additions of these polymers in Table 4. When one equivalent of **P1**-**P3** was added, the amount of fluorescence quenching was on average 90.7 ± 5.5% for all the 1:1 **Zn_2C_xDC**:DABCO sandwich complexes. This may tentatively indicate that the **V**-moiety is bound by all the porphyrin cages in a similar fashion. Although this quenching result is not in line with the hypothesis mentioned in the previous section, i.e. quenching is directly proportional to the percentage of **V**-moieties bound in the cavities of the porphyrin sandwich complexes, it is similar to the results obtained for the addition of one equivalent of **Me_2V** to the 1:1 **Zn_2C_xDC**:DABCO sandwich complexes (92.6 ± 3.3%, see Chapter 4) within the error of the measurement (2σ). Apparently, similar to what was observed for **Me_2V**, the complexation of a **V**-moiety in one porphyrin cavity of the sandwich complex also significantly quenches the fluorescence of the other, nearby porphyrin cavity. The observation that the amount of quenching is over 90% and not 50%, as was expected, indicates that no linear relationship between the concentration of free sandwich complex and the amount of unbound cavities of the sandwich complex exists. This deviation also indicates that the calculation of k_{on} from the fluorescence spectra is less straightforward than in the case of the **H_2SC** compounds, which contain only one cavity. Another complication may be that the two cavities of the **Zn_2C_xDC** compounds can both thread simultaneously onto the same polymer chain. Hence, there is a possibility that a statistical mixture of 1:1 and 1:2 **Zn_2C_xDC**:(**P1**-**P3**) complexes is formed, and that a certain amount of **Zn_2C_xDC** remains uncomplexed

(see also Chapter 4). If complexes are formed in which the two cavities of the **Zn_2C_xDC** compound are threaded onto the same single polymer chain, the fluorescence intensity is supposed to be relatively high since one cavity is not available for binding and polymer chains remain unbound. In that case the same fluorescence quenching as observed for a 1:1:1 **Zn_2C_xDC**:DABCO:(**P1**-**P3**) complex can be expected, since in both cases only one cavity is occupied by a **V**-moiety. Unfortunately, since the amount of quenching in the presence of one equivalent of polymer is already over 90%, and since there is no linear relationship between the concentration of free cavities and the amount of bound polymer, it cannot be determined if and to what extent the two cavities of the 1:1 **Zn_2C_xDC**:DABCO sandwich complexes thread onto the same polymer chain.

In the series of experiments in which the two equivalents of polymer were added subsequently, the second addition was carried out when the fluorescence intensity after the first addition had achieved a constant value after an initial decrease (Figure 4a, blue box). This second addition led to an additional decrease in the fluorescence intensity of on average 6% resulting in an overall quenching value of 96.2 ± 2.8%. The binding of two equivalents of **Me_2V** in the 1:1 **Zn_2C_xDC**:DABCO sandwich complexes resulted in a fluorescence quenching of 97.6 ± 0.85% (see Chapter 4), which is the same as the value above within 2σ. It may tentatively be concluded, therefore, that the further decrease of the fluorescence intensity upon addition of the second equivalent of **P1**-**P3** to the 1:1:1 **Zn_2C_xDC**:DABCO:(**P1**-**P3**) complex is the result of the binding of the **V**-moiety of the second polymer in the empty cavity of the 1:1:1 **Zn_2C_x-DC**:DABCO(**P1**-**P3**) complex. When two equivalents of polymer were added instantaneously to the 1:1 **Zn_2C_xDC**:DABCO sandwich complexes, the same amount of quenching , i.e. 96.0 ± 2.3% (within 2σ) was obtained as when the two equivalents of polymer were added subsequently, which suggests that the binding modes of the **V**-moieties in the sandwich complex are similar or the same. For none of the three 1:1 **Zn_2C_xDC**:DABCO sandwich complexes a significant difference in quenching behavior was observed as a result of the difference in spacer length between the two cages of the compounds, neither for the subsequent nor for the instantaneous addition of the two equivalents of polymer (see Tables 2, 3 and 4).

In order to confirm the formation of the 1:1:1 and 1:1:2 **Zn_2C_xDC**:DABCO:(**P1**-**P3**) complexes, samples were taken from all the solutions of the fluorescence measurements and subjected to MALDI-TOF spectrometry. In the presence of one equivalent of **P1**-**P3** it may be expected that only 1:1:1 **Zn_2C_xDC**:DABCO:(**P1**-**P3**) complexes are observed. Likewise, in the presence of two equivalents of polymer it is expected that the masses of the 1:1:2 **Zn_2C_xDC**:DABCO:(**P1**-**P3**) complexes are visible. Table 5 presents the molecular masses (g/mol) of the expected complexes calculated using the mean molecular weight from the mass distribution of the polymer. Figure 5 shows the MALDI-TOF spectra of the samples in which one or two equivalents of **P3** were added subsequently or instantaneously to the 1:1

Table 2 Amount of quenching (in %) of the fluorescence emission of the 1:1 **Zn_2C_xDC**:DABCO sandwich complexes after the addition of one equivalent of polymers **P1**, **P2** or **P3** in a solvent mixture of chloroform and MeCN (1:1, (v/v)). The error in the percentages of quenching are reported as two times the standard deviation over the threefold measurement.

1:1 Zn_2C_xDC:DABCO	P1	P2	P3
Zn_2C_3DC:DABCO	89.8 ± 5.2	94.0 ± 0.8	91.4 ±1.8
Zn_2C_5DC:DABCO	89.1 ± 3.7	91.1 ± 1.1	84.5 ± 1.9
$Zn_2C_{11}DC$:DABCO	65.4 ± 2.8[a]	92.3 ± 0.6	93.0 ± 1.4
Average	89.5 ± 4.4[b]	92.5 ± 2.4	89.6 ± 7.4

[a] This may be an erroneous value because the polymer solution was slightly yellow/green, indicating that the **V**-moiety might have been reduced to some extent, which will then result in a different binding constant and amount of quenching.[15] [b] Average value in which the complexation of **P1** into the **$Zn_2C_{11}DC$**:DABCO sandwich complex was not taken into account.

Table 3 Amount of quenching (in %) of the fluorescence emission of the 1:1:1 **Zn_2C_xDC**:DABCO:(**P1**-**P3**) sandwich complexes after the addition of one equivalent of polymers **P1**, **P2** or **P3** in the solvent mixture of chloroform and MeCN (1:1, (v/v)). The error in the percentages of quenching are reported as two times the standard deviation over the threefold measurement.

1:1:1 Zn_2C_xDC:DABCO:P#	P1	P2	P3
Zn_2C_3DC:DABCO:**P#**	95.9 ± 0.7	96.5 ± 0.1	97.0 ± 0.7
Zn_2C_5DC:DABCO:**P#**	96.5 ± 0.6	96.4 ± 0.4	96.5 ± 0.2
$Zn_2C_{11}DC$:DABCO:**P#**	92.4 ± 0.8	96.9 ± 0.3	97.7 ± 0.2
Average	94.9 ± 3.6	96.6 ± 0.4	97.1 ± 1.1

Table 4 Amount of quenching (in %) of the fluorescence emission of the 1:1 **Zn_2C_xDC**:DABCO sandwich complexes upon the direct addition of two equivalents of polymers **P1**, **P2** or **P3** in the solvent mixture of chloroform and MeCN (1:1, (v/v)). The error in the percentages of quenching are reported as two times the standard deviation over the threefold measurement.

1:1 Zn_2C_xDC:DABCO	P1	P2	P3
Zn_2C_3DC:DABCO	96.2 ± 0.9	96.4 ± 0.4	96.3 ± 0.5
Zn_2C_5DC:DABCO	96.2 ± 0.1	95.6 ± 0.2	96.0 ± 0.3
$Zn_2C_{11}DC$:DABCO	93.0 ± 0.6	97.1 ± 0.2	97.2 ± 0.1
Average	95.1 ± 3.0	96.4 ± 1.2	96.5 ± 1.0

Zn_2C_5DC:DABCO complex. All spectra show distributions around 12 000 g/mol, which is around the expected mass for the complex with one equivalent **P3**. Upon addition of two equivalents of **P3** no intensity is observed around 19636 g/mol, the theoretical mass for a two equivalent complex. These spectra are also representative for those obtained for the other sandwich complexes and polymers. Thus, the experiments revealed that the masses of the 1:1:2 **Zn_2C_xDC**:DABCO:(**P1**-**P3**) complexes were generally not observed by MALDI-TOF (see Table 5 and Figure 5 yellow box). This does not necessarily mean, however, that these complexes are not present in solution. Whether an ion is created and desorbed from the sample holder in MALDI-TOF experiments is highly dependent on the nature of the used matrix, the type of sample, the laser power, and/or the acceleration voltage. For all the **Zn_2C_xDC** compounds and polymers, it appeared to be difficult to obtain reproducible mass spectra with an adequate signal to noise ratio at a laser power intensity < 50%. When more equivalents of the polymer were present, or when the polymer chains were longer, the signal to noise ratio decreased rapidly and it was extremely difficult to obtain reproducible results. When the **V**-moieties of **P1**-**P3** are bound inside the cavities of the 1:1 **Zn_2C_xDC**:DABCO complexes, their charges will be shielded and as a result the complexes need to be ionized before they can be detected. Figure 5 (panel 1+1 eq) shows that when a new equivalent of polymer is added to the 1:1:1 **Zn_2C_5D-C**:DABCO:**P3** complex, peaks corresponding to the free polymer and to the 1:1:1 **Zn_2C_5DC**:DABCO:**P3** complex become visible, but not peaks corresponding to the 1:1:2 **Zn_2C_5DC**:DABCO:**P3** complex. The most likely reason for the lack of the latter peaks is that this complex is hard to ionize and to detect for the reasons mentioned above. If free polymer **P3** is present in solution, this viologen containing species may be ionized easier than the complexes, because it is smaller and has a charge that is not shielded by a cage molecule. As a result, it may ionize and desorb more rapidly from the sample-holder. It may thus be detected while the complex is not. Another, albeit less probable, explanation for the observation of free polymer might be that fragmentation of the complex occurs in the mass spectrometer due to the used high laser power. However, in that case also fragmented species of lower molecular weights would have been observed, which was not the case. Unspecific, weak binding of the second polymer at the outside instead at the inside of the 1:1:1 **Zn_2C_5DC**:DABCO:**P3** complex may be considered, but this is rather unlikely since the amount of fluorescence quenching (97%) is very high, indicating that the viologen moieties of both polymers must bind inside the cavities of the 1:1 **Zn_2C_5DC**:DABCO sandwich complex. To further confirm the binding stoichiometries of the complexes, extensive 1D and 2D NMR studies at low temperatures (see Chapter 4) should be conducted, but this was not possible because of time constraints in the current project.

Table 5 Expected masses (g/mol) of the 1:1 **Zn_2C_xDC**:DABCO sandwich complexes in the presence of one or two equivalents of polymers **P1**, **P2**, and **P3**, based on the M_n values of the respective polymers and the molecular weights of the **Zn_2C_xDC** compounds without DABCO. Values in bold are actually observed in the MALDI-TOF spectra.

1:1 Zn_2C_xDC:DABCO	P1 (1 eq, g/mol)	P1 (2 eq, g/mol)	P2 (1 eq, g/mol)	P2 (2 eq, g/mol)	P3 (1 eq, g/mol)	P3 (2 eq, g/mol)
Zn_2C_3DC:DABCO	**6250**	9530	**9052**	15116	**11298**	19608
Zn_2C_5DC:DABCO	**6287**	9558	**9080**	15144	**11326**	19636
Zn_2C_{11}DC:DABCO	**6371**	9642	**9164**	15228	**11410**	19720

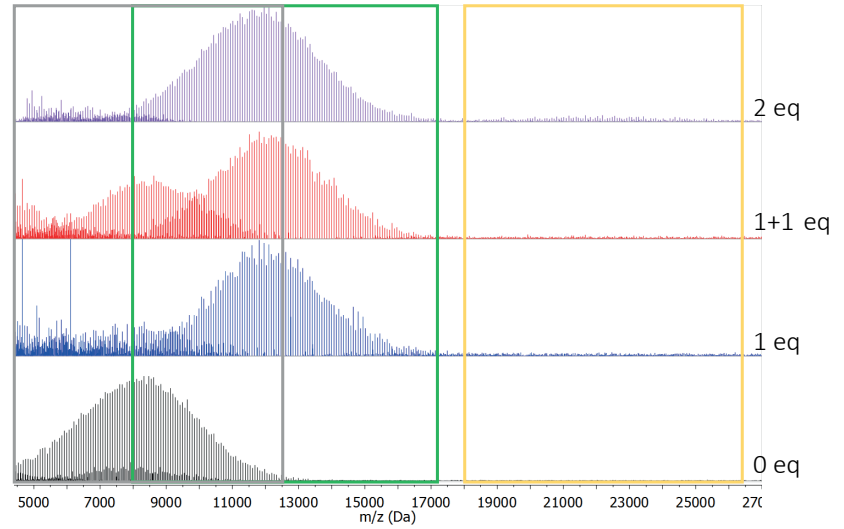

Figure 5 *MALDI-TOF spectra of uncomplexed **P3** (black spectrum) and the spectra of samples in which **P3** was added stepwise (blue and red spectra) and instantaneously (purple spectrum) to the 1:1 **Zn_2C_5DC**:DABCO sandwich complex. The region from 4400 to 27000 Dalton with intensities between 15000 to 25000 are shown for the different spectra. The regions where the masses of **P3**, the 1:1:1, and the 1:1:2 **Zn_2C_5DC**:DABCO:**P3** complexes are supposed to be present are depicted by the grey, green, and yellow boxes, respectively.*

5.2.2.3 Threading of polymers through the 1:1 Zn2CxDC:DABCO sandwich complexes: threading rates as a function of spacer and polymer length

In order to obtain a better understanding of the threading process and to investigate how complex formation occurs, the threading-on rate constants k_{on} and the corresponding free energies of activation $\Delta G^{\ddagger}_{on}$ for the various combinations of

sandwich complexes and polymers were determined by fluorescence spectroscopy, as indicated in section 5.2.2.1. Upon the addition of one or two equivalents of **P1**-**P3** to the 1:1 **Zn_2C_xDC**:DABCO sandwich complexes a second order threading process takes place because two particles, i.e. sandwich complex and polymer, are involved. Plots of 1/[1:1 **Zn_2C_xDC**:DABCO sandwich complex] versus time will then yield straight lines. It is expected that the k_{on}-values decrease upon an increase in polymer length, as was observed before in threading studies of the **SC** compounds.[8]

For both the instantaneous and the subsequent additions of **P1-P3** to the 1:1 **Zn_2C_xDC**:DABCO sandwich complexes plots of 1/[1:1 **Zn_2C_xDC**:DABCO sandwich complex] against time indeed gave straight lines in all cases (Figure 6). Furthermore, as expected, for all combinations of sandwich complexes and polymers the rate of threading became slower upon increasing polymer length.[9]

The second order plots for the threading reactions in which two equivalents of polymer were added to the sandwich complexes had steeper slopes than those in which only one equivalent of polymer was added (Figure 6), indicating a faster threading process in the former case. This can be rationalized because k_{on} is dependent on the concentration of polymer and when this concentration increases by a factor two, it is expected that the k_{on} also increases by this factor. Interestingly, however, the values in Tables 6 and 7 reveal that for the threading of two equivalents of polymer in all cases k_{on} increases by significantly more than a factor of two.

The slower threading rate for a longer polymer is governed by several factors. First, an initial energy barrier has to be overcome for binding the first atoms of the polymer chain inside one of the cavities of a 1:1 **Zn_2C_xDC**:DABCO sandwich complex (see Figure 7a and Chapter 1).[8,10] In order to be able to do so, the polymer needs to

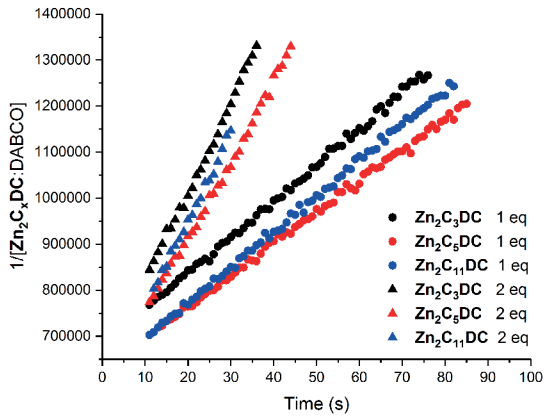

Figure 6 *Second order plots for the complexation of the 1:1* ***Zn_2C_xDC****:DABCO sandwich complexes with one (circles) or two (triangles) equivalents of* ***P2****.*

Table 6 Threading k_{on} -values (in M^{-1} s^{-1}) for the complexation of the 1:1 **Zn_2C_xDC**:DABCO sandwich complexes with one equivalent of polymer **P1**, **P2**, or **P3** in the solvent mixture chloroform and MeCN (1:1, (v/v)). The k_{on} -values are reported with an error of two times the standard deviation over the threefold measurement.

1:1 ZnC_xDC:DABCO	P1	P2	P3
Zn_2C_3DC:DABCO	$1.39 \times 10^4 \pm 1.66 \times 10^3$	$7.52 \times 10^3 \pm 6.14 \times 10^2$	$3.97 \times 10^3 \pm 3.79 \times 10^2$
Zn_2C_5DC:DABCO	$1.21 \times 10^4 \pm 1.35 \times 10^3$	$6.52 \times 10^3 \pm 3.67 \times 10^2$	$3.44 \times 10^3 \pm 2.96 \times 10^2$
$Zn_2C_{11}DC$:DABCO	$9.19 \times 10^3 \pm 4.92 \times 10^2$	$7.61 \times 10^3 \pm 3.46 \times 10^2$	$4.76 \times 10^3 \pm 4.19 \times 10^2$

Table 7 Threading k_{on} -values (in M^{-1} s^{-1}) for the complexation of the 1:1 **Zn_2C_xDC**:DABCO sandwich complexes with two equivalents of instantaneously added polymer **P1**, **P2**, or **P3** in the solvent mixture chloroform and MeCN (1:1, (v/v)). The k_{on} -values are reported with an error of two times the standard deviation over the threefold measurement.

1:1 ZnC_xDC:DABCO	P1	P2	P3
Zn_2C_3DC:DABCO	$4.00 \times 10^4 \pm 1.36 \times 10^3$	$1.88 \times 10^4 \pm 9.72 \times 10^2$	$1.05 \times 10^4 \pm 5.93 \times 10^2$
Zn_2C_5DC:DABCO	$3.58 \times 10^4 \pm 1.53 \times 10^3$	$1.67 \times 10^4 \pm 7.25 \times 10^2$	$9.46 \times 10^3 \pm 3.87 \times 10^2$
$Zn_2C_{11}DC$:DABCO	$3.46 \times 10^4 \pm 9.72 \times 10^2$	$1.96 \times 10^4 \pm 1.05 \times 10^3$	$1.21 \times 10^4 \pm 5.44 \times 10^2$

adopt the correct conformation, which is achieved by stretching the chain terminus, which roughly corresponds to a length of 5 atoms.[10] The subsequent movement of the cage complex along the polymer chain occurs via a series of randomly directed 'hopping' steps from one energy minimum to the next, until eventually the viologen-moiety is reached and threading is complete (Figure 7a). The number of these energy minima increases when the polymer length becomes longer. Furthermore, a longer chain decreases the chance to reach the viologen-moiety, because at each energy minimum the cage can either move towards this moiety or away from it. As a result, the threading speed decreases when the polymer chain is longer. Also, when the polymer chain is longer, its terminus will have a lower chance to find the cavity through which it has to thread, because this chain has more degrees of freedom than a smaller chain (Figure 7b, left). However, it has been shown for **SC** compounds that the viologen-moiety first binds weakly to the outside of the cavity of the host compound, as a result of which the polymer resides in close proximity of the porphyrin-cage compound, leading to an effective molarity (EM) effect that may favor threading (Figure 7b, right).[10] This effective molarity effect becomes smaller when the chain length increases. The intramolecular threading pathway, in which the polymer chain first binds to the outside of the cavity with a binding constant of K_a,

(Figure 7b, right) is only more favorable than an intermolecular threading pathway (Figure 7b, left) when K_a*EM > 1.[10] For **H_2SC** this K_a was determined to be 40 M^{-1}, and therefore polymer chains which are shorter than 40 atoms benefit from this EM effect while longer chains do not.[10] Since the cavities of the 1:1 **Zn_2C_xDC**:DABCO sandwich complexes are similar to the cavity of **H_2SC**, it is expected that the threading behavior is governed by the same factors. However, in comparison with the **SC** compounds the **Zn_2C_xDC**:DABCO sandwich complexes have an additional cavity and additional functional groups, i.e. the triazoles. This can give rise to different and more complex binding behavior of the viologen moieties of the polymers to the 1:1 **Zn_2C_xDC**:DABCO sandwich complexes. Once the viologen-moiety is bound at some place on the outside of the sandwich complex, the end of the polymer chain can thread through the cavity it is associated with, or through the second cavity of the same molecule. The threading through either cavity will result in the same 1:1:1 **Zn_2C_xDC**:DABCO:(**P1**-**P3**)complex. Another possibility is that the end of an already threaded polymer will subsequently thread through the remaining empty cavity, also as a result of an EM effect. This will lead to a situation in which both cavities will be

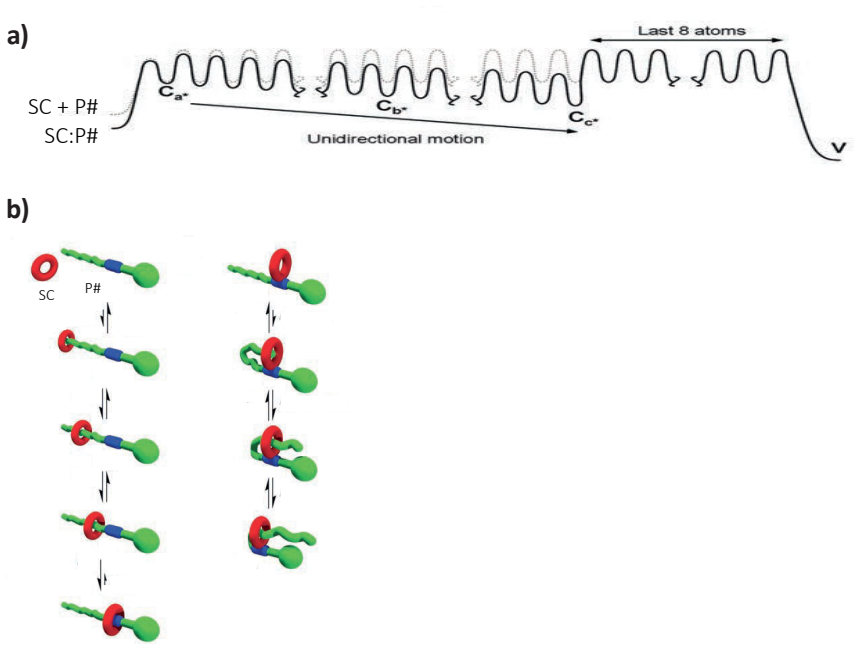

Figure 7 *Schematic representation of the energy landscapes and mechanisms of the threading process of one-side blocked viologen derivatives functionalized with polymer chains of different lengths. In (a) the consecutive hopping mechanism is depicted and in (b) the possible threading mechanisms: (left) intermolecular threading, (right) intramolecular threading in which the viologen moiety first complexes to the outside of the cage compound and then threads.[10]*

occupied by a polymer chain, but only one cavity is occupied by a viologen-moiety that quenches the porphyrin fluorescence. For the threading of a second polymer through the 1:1:1 **Zn_2C_xDC**:DABCO:(**P1**-**P3**) complex, the polymer chain already present inside the second cavity first has to de-thread before the next polymer chain and viologen-moiety can be bound. All different complexes will experience their own EM effects, which in turn will influence the respective k_{on}-values of the various threading events. Therefore, it can be envisaged that the observed differences between the k_{on}-values for the threading of one and two equivalents of **P1**-**P3** deviate from the expected factor two, when the concentration of **P1**-**P3** is varied by this factor. Instead, the observed rate constants in all cases increase by a larger number,

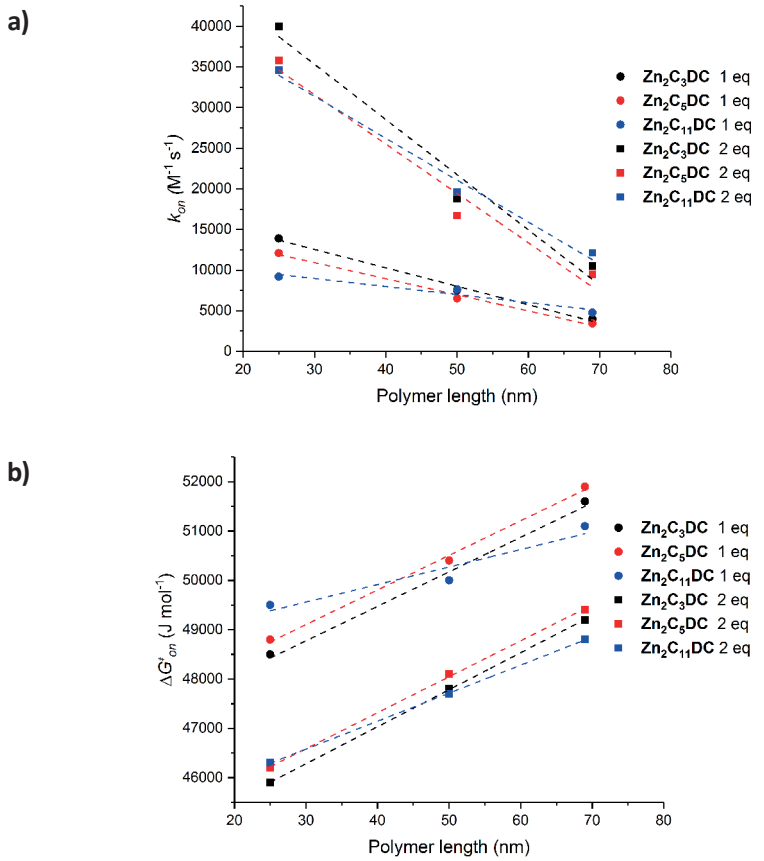

Figure 8 *Measured k_{on}-values (a) and $\Delta G^{\ddagger}_{on}$-values (b) for the threading of 1:1 **Zn_2C_xDC**:DABCO sandwich complexes onto polymers **P1**-**P3**. The data is plotted against polymer length for the threading of one (circles) or two (squares) equivalents of polymer. The linear fits are represented by the dotted lines.*

i.e. circa 2.5 times for the **Zn_2C_5DC**:DABCO and **Zn_2C_{11}DC**:DABCO sandwich complexes, and 2.9 to 3.8 times for the **Zn_2C_3DC**:DABCO sandwich complexes, depending on the polymer length.

For each of the polymers, the differences in k_{on}-values and the directly related $\Delta G^{\ddagger}_{on}$-values (Tables 8 and 9) measured for the different zinc double cage compounds are small and often within 2σ. It is concluded, therefore, that these values are not dependent on the spacer length between the two cavities. This can be rationalized by the fact that when a DABCO ligand is bound between the zinc porphyrins, the distances between these porphyrins are all around 7 Å (see Chapter 3).

In Figure 8, the $\Delta G^{\ddagger}_{on}$-values are plotted versus the polymer length. For **SC** compounds it was found that an increase in polymer length leads to an increase in $\Delta G^{\ddagger}_{on}$-value. The initial binding event of the polymer chain largely determines this $\Delta G^{\ddagger}_{on}$-value.[8,10] It is related to the above-mentioned entron effect, which in turn is dependent on the EM and the length of the polymer chain, together determining the chance that the end of the polymer chain and the cavity reside at a close distance. Thus, when the polymer chain is longer, the chance that its terminus is able to 'find' the cavity of the **SC** compound is smaller due to the ability of the chain to adopt a larger variety of orientations, lowering the EM.[10] As was stated above, the EM is governed by the binding of the viologen-moiety at the outside of the cavity, creating a loop when the end of the polymer chain binds inside the cavity (Figure 7b, right). And for **SC** this process was found to be favorable for the threading of polymer chains with lengths up to 40 atoms.[10] After the cage compound has traversed the polymer and has reached the last (8) atoms of the chain before forming a complex with the viologen-moiety, the loop has become so small that dissociation from the outside of the cage occurs (Figure 7a and b, right). For the 1:1 **Zn_2C_xDC**:DABCO sandwich complexes, the binding affinity of the viologen-moiety to the outside of the cavities may be different from that to the outside of the cavities of the **SC** compounds. Furthermore, when the viologen-moiety is associated to the outside of one of the cages of a sandwich complex, threading of the polymer chain may also occur through the cage to which it is not associated, which may have an effect on the mechanism by which the viologen dissociates from the outside of the cage at the end of the threading process. However, this increase in complexity of the threading mechanism it not expected to have an impact on the general trend that $\Delta G^{\ddagger}_{on}$ increases upon increasing the polymer length. For the **Zn_2C_3DC**:DABCO, **Zn_2C_5DC**:DABCO, and **Zn_2C_{11}DC**:DABCO sandwich complexes the slopes of the plots of $\Delta G^{\ddagger}_{on}$ versus polymer chain length correspond to threading-on energies of 69.9, 70.1, and 35.5 J mol^{-1} nm^{-1} for the threading process in which one equivalent of **P1**-**P3** is added, and 75.1, 72.9, and 52.8 J mol^{-1} nm^{-1} for the addition of two equivalents of **P1**-**P3** (Figure 8b). The slopes of the two plots of the **Zn_2C_{11}DC**:DABCO sandwich complex are less steep than those measured for the other two **Zn_2C_xDC**:DABCO sandwich complexes, indicating that the energy penalty for threading a polymer through the former

Table 8 $\Delta G^{\ddagger}_{on}$-values (in $J.mol^{-1}$) for the complexation of 1:1 **Zn_2C_xDC**:DABCO sandwich complexes with one equivalent of polymer **P1**, **P2**, or **P3** in the solvent mixture chloroform and MeCN (1:1, (v/v)). The $\Delta G^{\ddagger}_{on}$-values are reported with an error of two times the standard deviation over the threefold measurement.

$\Delta G^{\ddagger}_{on}$ (J mol^{-1})	P1	P2	P3
Zn_2C_3DC:DABCO	$4.85 \times 10^4 \pm 2.86 \times 10^2$	$5.00 \times 10^4 \pm 2.01 \times 10^2$	$5.16 \times 10^4 \pm 1.88 \times 10^2$
Zn_2C_5DC:DABCO	$4.88 \times 10^4 \pm 2.69 \times 10^2$	$5.04 \times 10^4 \pm 1.36 \times 10^2$	$5.19 \times 10^4 \pm 1.72 \times 10^2$
Zn_2C_{11}DC:DABCO	$4.95 \times 10^4 \pm 1.31 \times 10^2$	$5.00 \times 10^4 \pm 1.12 \times 10^2$	$5.11 \times 10^4 \pm 1.73 \times 10^2$

Table 9 $\Delta G^{\ddagger}_{on}$-values (in $J.mol^{-1}$) for the complexation of 1:1 **Zn_2C_xDC**:DABCO sandwich complexes with two equivalents of polymer **P1**, **P2**, or **P3**) in the solvent mixture chloroform and MeCN (1:1, (v/v)). The $\Delta G^{\ddagger}_{on}$-values are reported with an error of two times the standard deviation over the threefold measurement.

$\Delta G^{\ddagger}_{on}$ (J mol^{-1})	P1	P2	P3
Zn_2C_3DC:DABCO	$4.59 \times 10^4 \pm 8.33 \times 10^1$	$4.78 \times 10^4 \pm 1.26 \times 10^2$	$4.92 \times 10^4 \pm 1.13 \times 10^2$
Zn_2C_5DC:DABCO	$4.62 \times 10^4 \pm 1.04 \times 10^2$	$4.81 \times 10^4 \pm 1.07 \times 10^2$	$4.94 \times 10^4 \pm 8.09 \times 10^1$
Zn_2C_{11}DC:DABCO	$4.63 \times 10^4 \pm 6.82 \times 10^1$	$4.77 \times 10^4 \pm 1.31 \times 10^2$	$4.88 \times 10^4 \pm 8.96 \times 10^1$

complex is lower than that through the latter complexes. In comparison to the other **Zn_2C_xDC**:DABCO sandwich complexes, the **Zn_2C_{11}DC**:DABCO sandwich complex has more degrees of conformational freedom. The long C_{11} spacer may allow increased translational and rotational freedom within the sandwich complex, thereby enabling a conformation in which the distance and the angle between the porphyrin planes is optimal for the coordination of the DABCO ligand. Furthermore, such a higher degree of conformational freedom might enable a more optimal binding of the viologen moiety of a polymer to the outside of the porphyrin-cage compound, increasing the EM effect. Finally, an increase in conformational freedom may favor the entron effect in which the first atoms of the terminus of the polymer chain are bound in one of the cavities. All these factors may contribute to a more favorable threading of the polymers through the 1:1 **Zn_2C_{11}DC**:DABCO sandwich complex compared to the other sandwich complexes.

5.2.2.4 *Effect of a di-blocked viologen compound on the fluorescence properties of the 1:1 Zn2CxDC:DABCO sandwich complexes*

In a separate series of experiments the effect of the addition of a di-blocked viologen compound (**dbV**, see Figure 3) to the 1:1 **Zn_2C_xDC**:DABCO sandwich complexes on the quenching of the porphyrin fluorescence was studied. These studies with **dbV** served as reference measurements, because the blocking groups at both sides of the viologen-moiety cannot pass through the cavities of the complexes, preventing the latter moiety to bind inside the cavity and quench the fluorescence of the porphyrin.[8–10] When **dbV** was added to solutions of the afore-mentioned sandwich complexes in a solvent mixture of chloroform and MeCN (1:1, (v/v)), around 25 to 30 equivalents per 1:1 **Zn_2C_xDC**:DABCO sandwich complex were needed to almost fully quench the fluorescence emission of the porphyrins at a concentration of 1.5 µM (Figure 9). This relatively large quenching compared to that of the **SC** compounds indicates that **dbV** must have a fairly strong interaction with the **Zn_2C_xDC**:DABCO sandwich complexes. When the titration curves of the sandwich complexes with **dbV** are compared to those with **Me_2V**, it can nevertheless be concluded that the binding of **dbV** is still significantly weaker than that of **Me_2V**, because the latter guest effectuates an almost complete quenching after the addition of already one equivalent of compound (Figure 9). It was attempted to fit the data points of the titration curves to standard 1:1 and 1:2 host-guest binding models, but these fits resulted in significant deviations making that no reliable binding constants could be calculated. Apparently, the binding behavior of the sandwich complexes is more complex than that of the **SC** compounds. It was shown previously with the help of ^{1}H-NMR studies that **dbV** interacts relatively weakly with the outside of the cages of the **SC** compounds. The strength of this interaction (K_a = 40 M^{-1}), must be significantly lower than that exerted by **dbV** on the 1:1 **Zn_2C_xDC**:DABCO sandwich complexes, based on the above-mentioned fluorescence quenching behavior.[10] Compound **dbV** may display similar weak interactions with the outside of the 1:1 **Zn_2C_xDC**:DABCO sandwich complexes, but at more and also at different sites, e.g. the space between the porphyrin planes, where it may interact with the DABCO ligand, or with the spacer molecules, particularly the triazole groups. Although a binding constant for the complexation of **dbV** with the 1:1 **Zn_2C_xDC**:DABCO sandwich complexes could not be determined, it is clear from the titration data that this interaction cannot be neglected. For **SC** compounds, the binding of a viologen moiety to the outside of the cage molecules leads to a more favorable intramolecular threading pathway for polymers with chain lengths up to 40 atoms as a result of effective molarity effects (see above). It can be expected that when the binding of the viologen moiety to the outside of the cavity gets stronger, the intramolecular pathway will become beneficial for longer polymer chains as well.[11] Taking the number of atoms of **P1**-**P3** are taken into account, all three polymers, including **P1** since this polymer possesses circa 40 atoms, which is the upper limit for the **SC** compounds, will benefit from the intramolecular pathway.

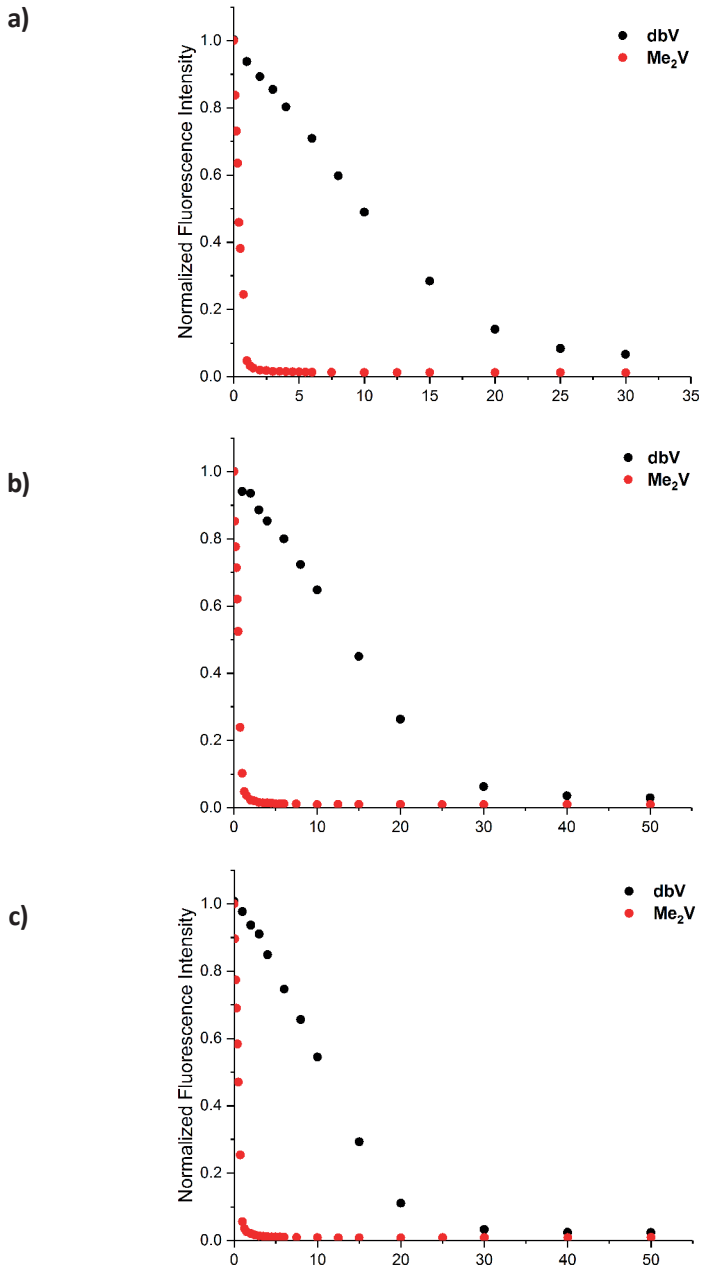

Figure 9 *Titration curves for the addition of **dbV** and (for comparison) **Me_2V** to the 1:1 **Zn_2C_3DC**:DABCO (a), **Zn_2C_5DC**:DABCO (b), and **$Zn_2C_{11}DC$**:DABCO (c) sandwich complexes. The normalized fluorescence intensity is plotted as a function of the number of equivalents of viologen derivative. Medium is a solvent mixture of chloroform and MeCN (1:1, (v/v)).*

Although a relatively strong interaction between **dbV** and the 1:1 **Zn_2C_xDC**:DABCO sandwich complexes is present, it still holds that the blocking groups of the viologen-moiety cannot be passed by the cavities of the latter complexes, otherwise the addition of one equivalent of **dbV** would have led to nearly complete quenching. Given the results presented in this section and the fact that the addition of one equivalent of **P1-P3** leads to > 90% quenching of the porphyrin fluorescence, it can be concluded that the 1:1 **Zn_2C_xDC**:DABCO sandwich complexes, just like the **SC** compounds, must traverse the whole polymer chains before the viologen-moieties can be complexed in their cavities. This threading process most likely also includes an intramolecular looping mechanism, as we reported before for the **SC** porphyrin cages.

5.3. Conclusion

The threading of polyTHF chains of different lengths equipped with a viologen (**V**) thermodynamic trap through the cavities of 1:1 **Zn_2C_xDC**:DABCO sandwich complexes was investigated by fluorescence spectroscopy. The 1:1 **Zn_2C_xDC**:DABCO sandwich complexes can traverse polymers with lengths up to circa 69 nm and reach the viologen-moieties, resulting in the quenching of the fluorescence emission of the porphyrins. Based on the percentage of quenching that occurs upon association to the viologen-moieties, it was concluded that 1:1:1 and probably also 1:1:2 **Zn_2C_xDC**:DABCO:polymer complexes are formed and that the viologen-moiety binds in a similar fashion as **Me_2V** to the 1:1 **Zn_2C_xDC**:DABCO sandwich complexes. No differences in the amounts of quenching were found when the two equivalents of polymer were added subsequently or instantaneously. All the 1:1:1 **Zn_2C_xDC**:DABCO:polymer complexes were visible by MALDI-TOF spectrometry, while the 1:1:2 **Zn_2C_xDC**:DABCO:polymer complexes could not be detected. The threading processes of the various combinations of polymers and sandwich complexes followed second order kinetics and by plotting 1/[1:1 **Zn_2C_xDC**:DABCO sandwich complex] versus time, the apparent threading rate constants (k_{on}) and the free energies of activation for threading ($\Delta G^{\ddagger}_{on}$) could be determined. It was found that when the polymer length increases, the rate of threading decreases, and that the overall k_{on} and $\Delta G^{\ddagger}_{on}$ do not greatly depend on the length of the spacer between the two cages of the sandwich complexes. Threading of the polymers through the 1:1 **$Zn_2C_{11}DC$**:DABCO sandwich complex turned out to be associated with a lower $\Delta G^{\ddagger}_{on}$ per nm than the threading through the other sandwich complexes, which is attributed to the presence of larger degrees of freedom in the former complex as a result of its large spacer length. Our experiments revealed that the mechanism of threading of polymer chains through the cavities of 1:1 **Zn_2C_xDC**:DABCO sandwich complexes is significantly more complex than the threading of polymers through the cavities of the previously studied **SC**

compounds. The following differences were noticed: (*i*) the viologen-moieties of the polymers associate stronger and probably also in a different way to the outside of the **Zn_2C_xDC**:DABCO sandwich complexes when compared to the **SC** compounds; (*ii*) a larger variety of types of cage-polymer complexes can be formed, e.g. 1:1:1 **Zn_2C_xDC**:DABCO:polymer complexes in which the viologen-moieties of the polymer chains are bound in the first cavity while the attached poly-THF chains thread through the second cavity; (*iii*) for the **Zn_2C_xDC**:DABCO sandwich complexes the quenching of the porphyrin fluorescence by the binding of the viologen-moieties of the polymers is not linearly related to the number of occupied cavities. For future studies, it may be useful to replace the viologen-moieties in the polymers by a different thermodynamic trap, making that quenching of the fluorescence intensity can occur at distances shorter than 7 Å. In this way the quenching of the fluorescence of only one porphyrin cage upon polymer complexation can be detected and the threading process be better followed and analyzed.

5.4. Experimental

All chemicals were commercially obtained and used without further purification unless stated otherwise. MeCN was distilled under argon from calcium chloride. THF was distilled under nitrogen from potassium, and chloroform (anhydrous, contains amylenes as stabilizers, ≥99%) was filtered over potassium carbonate under argon before use. DABCO was sublimated at 60-70 ^{0}C under vacuum prior to use. For size exclusion chromatography Biorad Biobeads (SX-1) were used.

^{1}H and ^{13}C-NMR spectra were recorded on a Bruker Avance III 400 MHz or 500 MHz spectrometer at 25˚C unless stated otherwise. Chemical shifts are reported in parts per million (ppm) relative to tetramethylsilane (TMS) as the internal reference. NMR data are presented as follows: chemical shift (∂) in ppm, multiplicity (s = singlet, bs = broad singlet, d = doublet, t = triplet, q=quartet, td = triplet of doublets, m = multiplet and/or multiple resonances), integration, assignment and coupling constant (J) in hertz (Hz). All NMR signals were assigned on the basis of ^{1}H, ^{13}C-NMR, COSY, ROESY, HSQC and HMBC experiments. Phase and baseline corrections were applied to all ^{1}H-NMR and ^{13}C spectra. The numbering of the protons used in the assignments is depicted in Figure 10. MALDI-TOF measurements were carried out on a Bruker Microflex LRF MALDI-TOF system using dithranol in chloroform (1 mg/mL) as the matrix. UV-Vis spectra were recorded with the program UV Probe on a Shimadzu UV 1800 spectrometer in a quartz cuvette with 1 cm path length and 3.8 mL total volume. The solvent was used as the baseline for the spectra. Fluorescence spectra were recorded with Labsolutions RF on a Shimadzu RF-5301PC Spectrofluorophotometer in a fluorescence cuvette with 1 cm path length and 3.5 mL total volume. The solution was excited at the maximum wavelength determined by UV-Vis. The

fluorescence intensity as a function of time was followed by using the time drive application of the software at the wavelength of maximum intensity determined by the fluorescence spectrum of the host. Compounds **dbV** and 1-(5-(3,5-di-tert-butyl-phenoxy)pentyl)-4,4'-bipyridin-1-ium hexafluorophosphate were synthesized according to literature procedures.[8]

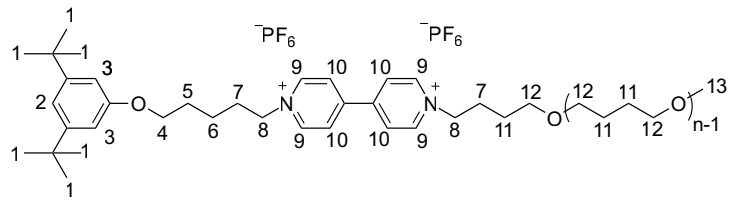

Figure 10 *Proton numbering for the viologen-appended polyTHF chains* ***P1*** *(n = 41),* ***P2*** *= (n = 80) and* ***P3*** *(n = 111), as used for the NMR analyses.*

5.4.1 Synthesis of the viologen-capped THF polymers

General procedure

To an oven-dried Schlenk flask, freshly distilled tetrahydrofuran (40 mL) was added under an argon atmosphere. The polymerization reaction was initiated by adding methyl trifluoromethanesulfonate (58 µL, 0.512 mmol). After stirring for x minutes, 1-(5-(3,5-di-tert-butylphenoxy)pentyl)-4,4'-bipyridin-1-ium hexafluorophosphate (0.35 g, 0.61 mmol) was added. The reaction mixture was stirred overnight at r.t. and the solvent was evaporated. The residue was then dissolved in chloroform/MeCN (7:1, (v/v)), a sat. aq. NH_4PF_6 solution (25 mL) was added and the resulting mixture was stirred for 2 h at r.t.. The water layer was washed with chloroform/MeCN (7:1, (v/v), 3 x 10 mL) and chloroform (3 x 20 mL). The combined organic layers were washed with water, dried over Na_2SO_4, filtered, and evaporated to dryness. Several consecutive size exclusion columns using THF as the eluent yielded the product as a white solid.

P1

Polymerization time x = 21 minutes, Yield: 262 mg, 15%.
^{1}H-NMR ($CDCl_3$:CD_3CN (1:1, (v/v)), 500 MHz): ð 8.94 (dd, 4H, Ar*H*-**9**, *J* = 2.2, 7.1 Hz), 8.41 (dd, 4H, Ar*H*-**10**, *J* = 3.1, 6.9 Hz), 7.01 (t, 1H, Ar*H*-**2**, *J* = 1.7 Hz), 6.73 (d, 2H, Ar*H*-**3**, *J* = 1.7 Hz), 4.71-4.64 (m, 4H, C*H*$_2$-**8**), 4.00 (t, 2H, C*H*$_2$-**4**, *J* = 6.2 Hz), 3.46-3.30 (m, 164H, C*H*$_2$-**12**), 3.29 (s, 3H, C*H*$_3$-**13**), 2.17-2.08 (m, 4H, C*H*$_2$-**7**), 1.90-1.82 (m, 2H, C*H*$_2$-**5**), 1.67-1.49 (m, 166 H, C*H*$_2$-**6,11**), 1.30 (s, 18H, C*H*$_3$-**1**). MALDI-TOF; M_n: 3271 g/mol, n = 41, PDI = 1.05.

P2

Polymerization time x = 40 minutes, Yield: 216 mg, 6.8%.
^{1}H-NMR ($CDCl_3$:CD_3CN (1:1, (v/v)), 500 MHz): ð 8.94 (dd, 4H, Ar*H*-**9**, *J* = 2.1, 7.1 Hz), 8.41 (dd, 4H, Ar*H*-**10**, *J* = 3.2, 6.9 Hz), 7.03 (t, 1H, Ar*H*-**2**, *J* = 1.7 Hz), 6.73 (d, 2H, Ar*H*-**3**, *J* = 1.7 Hz), 4.72-4.65 (m, 4H, C*H*$_2$-**8**), 4.01 (t, 2H, C*H*$_2$-**4**, *J* = 6.2 Hz), 3.46-3.31 (m, 320H, C*H*$_2$-**12**), 3.29 (s, 3H, C*H*$_3$-**13**), 2.18-2.07 (m, 4H, C*H*$_2$-**7**), 1.91-1.84 (m, 2H, C*H*$_2$-**5**), 1.75-1.40 (m, 322 H, C*H*$_2$-**6,11**), 1.31 (s, 18H, C*H*$_3$-**1**). MALDI-TOF; M_n: 6064 g/mol, n = 80, PDI = 1.05.

P3

Polymerization time x = 63 minutes, Yield: 438 mg, 10%.
^{1}H-NMR ($CDCl_3$:CD_3CN (1:1, (v/v)), 500 MHz): ð 8.94 (dd, 4H, Ar*H*-**9**, *J* = 2.0, 7.0 Hz), 8.41 (dd, 4H, Ar*H*-**10**, *J* = 3.3, 6.8 Hz), 7.03 (t, 1H, Ar*H*-**2**, *J* = 1.7 Hz), 6.73 (d, 2H, Ar*H*-**3**, *J* = 1.7 Hz), 4.73-4.65 (m, 4H, C*H*$_2$-**8**), 4.01 (t, 2H, C*H*$_2$-**4**, *J* = 6.2 1Hz), 3.47-3.30 (m, 444H, C*H*$_2$-**12**), 3.29 (s, 3H, C*H*$_3$-**13**), 2.18-2.09 (m, 4H, C*H*$_2$-**7**), 1.90-1.82 (m, 2H, C*H*$_2$-**5**), 1.75-1.50 (m, 446H, C*H*$_2$-**6,11**), 1.31 (s, 18H, C*H*$_3$-**1**). MALDI-TOF; M_n: 8310 g/mol, n = 111, PDI = 1.05.

5.4.2 Threading protocols

All threading measurements were carried out in threefold. The 1:1 solvent mixtures were prepared by weighing the desired amounts of both solvents into a closed Erlenmeyer flask. After thorough mixing of the solvents, the density of the solvent mixture was determined from the weight increase of a 50 mL volumetric flask.

A host stock solution was prepared by quantitatively weighing a certain amount of the host (between 1 and 2 mg), which was dissolved in 10 mL solvent or solvent mixture (HostStock). The HostStock was diluted to 1.5 µM (10 mL) and the appropriate amount of a DABCO stock solution (100 µL, 6.45 x10^{-3} M (**Zn_2C_3DC**), 7.65 x10^{-3} M (**Zn_2C_5DC**) and, 9.45 x10^{-3} M (**Zn_2C_{11}DC**)) was added ensuring that the maximum amount of 1:1 **Zn_2C_xDC**:DABCO sandwich complex was present in solution. Polymer and **dbV** solutions (300 µM) were made by weighing 2.13 mg (**P1**, 2 mL), 1.1 mg (**P2**, 1 mL), 2.58 mg (**P3**, 1 mL), and 1.49 mg (**dbV**, 5 mL). The volumes of solvent mixtures required for the host and **dbV** solutions were weighed on an analytical balance and the additions of the solvent mixtures required for the polymer solutions and the addition of the polymer solutions to the host solutions were carried out with Gilson pipets (up to a volume of 1000 µL).

The Soret band of the 1:1 **Zn_2C_xDC**:DABCO sandwich complexes in solution (2.0 mL) were excited and the resulting fluorescence was monitored as a function of time at the highest emission peaks. When the fluorescence signals had reached a constant intensity, the desired polymer solutions (10 µL for one equivalent and 20 µL for two equivalents) were added. The cuvette was shaken vigorously and placed back into the fluorescence spectrophotometer. The spike in the fluorescence emission resulting

from this action was removed before analysis of the spectra. After the fluorescence intensity had reached a constant value, either a sample of 10 µL was taken for MALDI-TOF analysis and another equivalent of polymer solution was added, or the measurement was stopped. The fluorescence data were normalized and analyzed by assuming that the first part of the equilibration process, up to 50% of the total conversion, can be described by a simple second order rate equation (1), in which A is the **Zn_2C_xDC**:DABCO complex, B is the polymer and C is the **Zn_2C_xDC**:DABCO:polymer complex.

$$A + B \rightarrow C \quad (1)$$

Because $[A]_0 = [B]_0$, the rate equation simplifies to equation (2), in which $[A]_0$ and $[B]_0$ are the concentrations in M of the **Zn_2C_xDC**:DABCO complex and polymer, respectively.

$$2A \rightarrow C \quad (2)$$

By integrating equation (2), the integrated rate equation (3) is obtained, in which k_{on} is the apparent rate constant of threading in M^{-1} s^{-1} and t is the time in s.

$$[A]^{-1} = k_{on}t \quad (3)$$

By plotting 1/[**Zn_2C_xDC**:DABCO] against time, a linear plot is obtained with a slope equal to k_{on}, which can be calculated using the least square method.

5.5 References

(1) Zhirnov, V.; Zadegan, R. M.; Sandhu, G. S.; Church, G. M.; Hughes, W. L. Nucleic Acid Memory. *Nat. Mater.* **2016**, *15* (4), 366–370.

(2) Lutz, J.-F. Coding Macromolecules: Inputting Information in Polymers Using Monomer-Based Alphabets. *Macromolecules* **2015**, *48* (14), 4759–4767.

(3) Mutlu, H.; Lutz, J.-F. Reading Polymers: Sequencing of Natural and Synthetic Macromolecules. *Angew. Chem. Int. Ed.* **2014**, *53* (48), 13010–13019.

(4) Goldman, N.; Bertone, P.; Chen, S.; Dessimoz, C.; LeProust, E. M.; Sipos, B.; Birney, E. Towards Practical, High-Capacity, Low-Maintenance Information Storage in Synthesized DNA. *Nature* **2013**, *494* (7435), 77–80.

(5) Church, G. M.; Gao, Y.; Kosuri, S. Next-Generation Digital Information Storage in DNA. *Science* **2012**, *337* (6102), 1628.

(6) Colquhoun, H.; Lutz, J.-F. Information-Containing Macromolecules. *Nat. Chem.* **2014**, *6* (6), 455–456.

(7) *See Chapter 2 of This Thesis*.

(8) Coumans, R. G. E.; Elemans, J. A. A. W.; Nolte, R. J. M.; Rowan, A. E. Processive Enzyme Mimic: Kinetics and Thermodynamics of the Threading and Sliding Process. *Proc. Natl. Acad. Sci. U. S. A.* **2006**, *103* (52), 19647–19651.

(9) Hidalgo Ramos, P.; Coumans, R. G. E.; Deutman, A. B. C.; Smits, J. M. M.; de Gelder, R.; Elemans, J. A. A. W.; Nolte, R. J. M.; Rowan, A. E. Processive Rotaxane Systems. Studies on the Mechanism and Control of the Threading Process. *J. Am. Chem. Soc.* **2007**, *129* (17), 5699–5702.

(10) Deutman, A. B. C.; Monnereau, C.; Elemans, J. A. A. W.; Ercolani, G.; Nolte, R. J. M.; Rowan, A. E. Mechanism of Threading a Polymer Through a Macrocyclic Ring. *Science* **2008**, *322* (5908), 1668–1671.

(11) Deutman, A. B. C.; Cantekin, S.; Elemans, J. A. A. W.; Rowan, A. E.; Nolte, R. J. M. Designing Processive Catalytic Systems. Threading Polymers through a Flexible Macrocycle Ring. *J. Am. Chem. Soc.* **2014**, *136* (25), 9165–9172.

(12) Cantekin, S.; Markvoort, A. J.; Elemans, J. A. A. W.; Rowan, A. E.; Nolte, R. J. M. Allosterically Controlled Threading of Polymers through Macrocyclic Dimers. *J. Am. Chem. Soc.* **2015**, *137* (11), 3915–3923.

(13) Deutman, A. B. C.; Monnereau, C.; Moalin, M.; Coumans, R. G. E.; Veling, N.; Coenen, M.; Smits, J. M. M.; de Gelder, R.; Elemans, J. A. A. W.; Ercolani, G.; et al. Squaring Cooperative Binding Circles. *Proc. Natl. Acad. Sci. U. S. A.* **2009**, *106* (26), 10471–10476.

(14) Thordarson, P.; Coumans, R. G. E.; Elemans, J. A. A. W.; Thomassen, P. J.; Visser, J.; Rowan, A. E.; Nolte, R. J. M. Allosterically Driven Multicomponent Assembly. *Angew. Chem. Int. Ed.* **2004**, *43* (36), 4755–4759.

(15) Aristov, N.; Habekost, A. Electrochromism of Methylviologen (Paraquat). *World J. Chem. Educ.* **2015**, *3* (4), 82–86.

6

Summary and outlook

6.1. Recapitulation of the aim of the project

As was explained in the previous chapters, data storage is an emerging research field given the fact that it is expected that the global digital archive will contain 3×10^{24} bits by 2040.[1] Also, Moore's law, which predicts that the performance of chip devices including the ones needed for data storage will double every 18 months, cannot be sustained due to technological barriers.[2–4] This combination gives rise to the need for new methods to deposit and process data. A new trend is to store data in natural and synthetic polymers and this is an appealing approach, because it allows high-density information storage. Recently, Goldman *et al.* and Church *et al.* have reported the storage of non-biological data, e.g. the 154 sonnets of Shakespeare, in DNA, while they were also able to successfully recover the original files with high fidelity.[5,6] They employed the polymerase chain reaction (PCR), to make multiple copies of their DNA files containing the afore-mentioned information.[7,8] Despite the many advantages of employing a natural system for the storage of data, natural polymers such as DNA are often less robust to environmental changes and they can be used only in a narrow temperature range and in water as the solvent.[9] Therefore, the storage of information into synthetic polymers is more desirable since they are easier to handle and can make use of the binary code, which is already common practice in all-day computing.[10,11] Until now only a few examples of information storage in synthetic polymers have been published and all reported procedures make use of encoded polymers prepared by step-by-step synthesis protocols.[12–18] The aim of the work described in this thesis was to follow a new approach, i.e. to design and construct a catalytic 'machine' that can thread onto a polymer chain and write information on it in the form of chemical functions, while moving along it. Such writing of a code onto an already existing synthetic polymer would be more efficient than an encoding process, in which the information is incorporated into the polymer chain by a step-by-step synthesis procedure.

The design of this catalytic 'machine' is based on the key features exhibited by the DNA-polymerases, i.e. a catalytic part and a ring that keeps the catalyst attached to the polymer chain (together forming a so-called 'processive catalyst'). In our case this natural design was translated into a ring-shaped cage compound (**H_2SC**) containing a catalytically active metal complex, i.e. a porphyrin molecule. The cage compound is a diphenylglycoluril clip to which a porphyrin 'roof' is attached. In a previous study it has been shown that the manganese derivative of this porphyrin cage compound (**MnSC**) can thread onto a polybutadiene substrate and convert all its double bonds into epoxide functions in a randomly processive fashion.[19–21] If a formed epoxide is defined as a 1 and an unreacted double bond as a 0, then binary information can in principle be written and stored with the help of this catalytic system. However, to enable targeted data storage, the porphyrin cage compound should also harbor structural characteristics that enable the control of the location

at which the catalytic epoxidation reaction takes place, i.e. an 'instruction' unit. It was decided, therefore, to extend the porphyrin cage compound **MnSC** with a second, so-called 'instruction' cage, in which a 'promotor' guest molecule can be bound, leading to the 'double porphyrin cage' compound (**H_4C_xDC**, Figure 1). The idea was that this second porphyrin cage, which is attached to the first one via a covalent linker, can influence the catalytic reaction that takes place in the latter cage via allosteric interactions. To this end, a ditopic ligand should connect the two porphyrins via metal-ligand coordination. When subsequently a promotor molecule binds in the instruction cage, information may be transferred, via de ligand, to the catalytic cage. In this way the catalytic process may be switched from an 'off'- to an 'on'-state, and *vice versa*. It has previously been shown that ditopic ligands, such as 1,4-diazabicyclo[2.2.2]octane (DABCO), can fulfill this function and affect via allosteric interactions the binding of a *N,N*'-dimethylviologen dihexafluorophosphate (**Me_2V**) guest inside the cavity.[22,23] It was decided, therefore, to select DABCO as the ditopic ligand to facilitate the coordination bond and **Me_2V** as the promotor molecule to

a)

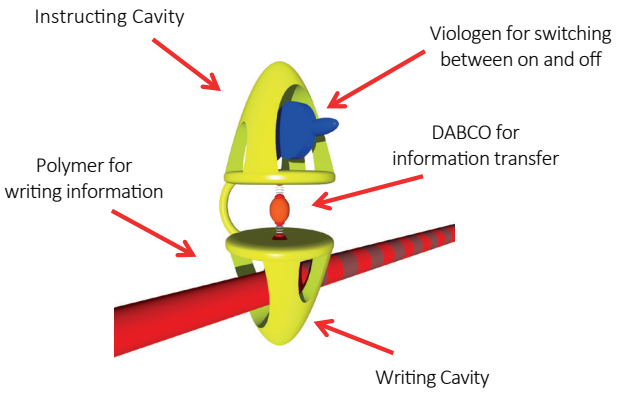

b)

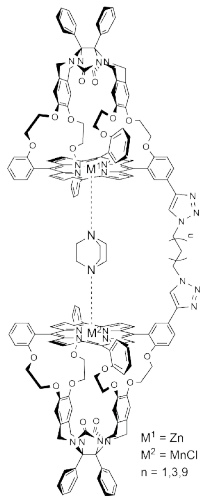

Figure 1 *a) Schematic representation of a double porphyrin cage compound consisting of two molecular cages capped with a porphyrin roof that are covalently linked (yellow). The instructing cage contains a zinc center and the writing cage a manganese center. The binding of a ditopic ligand such as DABCO (orange) in between the two porphyrins should allow the transfer of information from the instructing cage to the writing cage, thus enabling the possibility of influencing the catalytic reaction. The binding of a viologen guest (blue) inside the instructing cage may influence the binding of DABCO to the manganese center that performs a catalytic reaction on a polymer (red), via a series of allosteric interactions. b) Chemical structure of the zinc-manganese double porphyrin cage compounds with spacer lengths of 3, 5 or 11 carbon atoms, binding DABCO as ditopic axial ligand.*

influence the catalytic reaction. In this thesis, the synthetic efforts to covalently link two porphyrin cage compounds and the studies of their behavior upon the binding of DABCO, **Me_2V**, and polymer chains have been described.

6.2. Summary and discussion of the results

We embarked on the project by first synthesizing a series of three double porphyrin cage compounds (Chapter 2). Using 'click'-chemistry, two mono-functionalized porphyrin cage compounds were linked together by a single alkyl chain of different length. These mono-substituted porphyrin cage compounds were initially prepared from a porphyrin that was mono-functionalized via statistical synthesis methods. As this did not yield a pure product, a newly developed multistep synthesis procedure was employed to give three double porphyrin cages, each with an alkyl spacer of different length, i.e. 3, 5, and 11 carbon atoms (**H_4C_XDC**, in which x is 3, 5 or 11), between the two porphyrins. The structures of these double porphyrin cages were fully characterized by NMR, which revealed that each of them consisted of mixtures of two diastereoisomers. These diastereoisomers may exhibit different binding behavior towards guests and/or ligands. Therefore, it may be of interest to separate them in the future, e.g. by column chromatography. NMR studies on the zinc double porphyrin cages (**Zn_2C_xDC**) revealed that the triazole functions, present in the linkers can coordinate intermolecularly to the zinc centers in the porphyrins, leading to lower solubility of the complexes, which may complicate the complexation of guests and ligands. Therefore, in the future design of double porphyrin cage compounds, the use of linkers without coordinating functions is worth considering. Furthermore, the *meso*-phenyl bromide-functionality of the starting porphyrin cage compound may be replaced by an azide and combined with a spacer that is terminated on one side with an alkyne for coupling and on the other side again with an azide that can be coupled to a second porphyrin cage compound containing an alkyne function. This will enable the modular and selective coupling of different porphyrin cage compounds, e.g. a zinc and a manganese one to yield a double cage compound with an 'instructing' and a 'writing' cavity.

Before the double porphyrin cage compounds can be employed for the storage of data in synthetic polymers, the formation of 1:1 sandwich complexes between the ditopic axial ligand DABCO and the double cage compounds needed to be investigated. The formation of these 1:1 **Zn_2C_xDC**:DABCO sandwich complexes, in which one DABCO molecule is bound in between the two zinc porphyrin planes, is essential because it may enable information transfer between the two cavities through allosteric interactions. The formation of such 1:1 **Zn_2C_xDC**:DABCO sandwich complexes and additionally also 1:2 open **Zn_2C_xDC**:DABCO complexes, in which each zinc porphyrin is bound to a DABCO molecule, was demonstrated in chloroform and

in a solvent mixture of chloroform and acetonitrile (MeCN, 1:1, (v/v)) (Chapter 3). **Zn_2C_3DC** formed the strongest 1:1 sandwich complex with DABCO, while the differences in binding strengths of DABCO with the other **Zn_2C_xDC** hosts were rather small. The association constants of the 1:2 open complexes were found to be circa 3 orders of magnitude lower than those of the 1:1 sandwich complexes. With the help of variable temperature ^{1}H NMR studies in a solvent mixture of $CDCl_3$ and acetonitrile-d_3 (1:1, (v/v)), the formation of the above-mentioned complexes was confirmed. Surprisingly, when dichloromethane was employed as the solvent, a solvolysis reaction, in which DABCO acted as a nucleophilic reagent, interfered with the formation of well-defined 1:1 **Zn_2C_xDC**:DABCO sandwich complexes. Although dichloromethane had been employed before in catalysis reactions using manganese porphyrins, it cannot be used when DABCO is employed as axial ligand. Therefore, either another solvent or another bidendate ligand needs to be chosen in order to be able to apply the double porphyrin compounds as catalysts in the future. An alternative ditopic ligand could be pyrazine (Figure 2), which is a rigid molecule and is expected to show lower reactivity towards dichloromethane because its nitrogen atoms are less nucleophilic. Its size is comparable to DABCO, and molecular modeling showed that it can bind in a similar sandwich-like fashion as DABCO to the zinc centers of the **Zn_2C_xDC** compounds. A disadvantage may be that this ligand can also bind inside the cavity of the **Zn_2C_xDC** compounds, and thereby compete with and/or hinder the binding of the promotor molecule and the polymeric substrate. Also, 4,4'-bipyridine (bipy, Figure 2) may be considered as a potential axial ligand, although this compound may not have the optimal geometry for coordination to **Zn_2C_xDC** compounds with short linkers. Instead of replacing the axial ligand, also the solvent in which the catalytic epoxidation reactions are conducted can be changed to a solvent that does not react with DABCO but still dissolves the double porphyrin cage compounds. Examples of such solvents are 1,2-dichloroethane, 1,1,3-trichloroethane, chlorobenzene, or toluene. However, catalysis experiments in dichloromethane may still be possible if the strong ditopic coordination of the DABCO ligand in a zinc double porphyrin cage sandwich complex would protect the ligand for reaction with the solvent. In that case, information transfer may still be successful, but whether such a stabilization effect will work over longer periods of time requires further investigation.

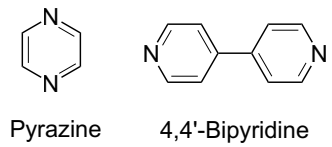

Figure 2 *Chemical structures of pyrazine and 4,4'-bipyridine (bipy).*

In chloroform as a solvent some unusual behavior was observed in the formation of complexes between DABCO and the **Zn_2C_xDC** compounds (Chapter 3). In the UV-vis spectra, hardly any changes in the absorbance of the Soret band originating from the free **Zn_2C_xDC** compounds were visible during the addition of approximately the first five equivalents of DABCO, indicating an inability of this ligand to coordinate to the zinc centers. After this initial delay, changes did occur, but the experimental titration curves deviated from the theoretically predicted curves for a standard 1:2 binding model. Since this deviation was not observed in other solvents such as dichloromethane or a mixture of chloroform and acetonitrile, a modified binding model, which includes the association of *n* molecules of DABCO to alternative binding sites on the cage compounds, fitted the experimentally determined titration curves better than the standard 1:2 binding model.

Since the formation of 1:1 **Zn_2C_xDC**:DABCO sandwich complexes was confirmed to take place in a solvent mixture of chloroform and MeCN (1:1, (v/v)), the next step to accomplish information transfer was to investigate the binding of 'promotor' guest molecules, i.e. viologen (**Me_2V**) molecules. This study was performed by following the quenching of the porphyrin molecules in the sandwich complexes by **Me_2V** as a function of time. In the proposed system to write data onto polymer chains, such a promotor should bind in one of the cavities of the sandwich complex and influence the catalytic reaction in the second cavity, e.g. by turning it into an 'off' or 'on'-state, and *vice versa* (Chapter 4). The complexation of already one equivalent of **Me_2V** guest was capable of quenching more than 90% of the total porphyrin fluorescence of the double cage compounds in the sandwich complexes, which is remarkable. This high degree of quenching was explained by the fact that both porphyrins of the sandwich complex are within quenching distance when a **Me_2V** guest is bound in one of its two cavities. Upon hosting **Me_2V** guests in the sandwich complexes, the DABCO ligands remained bound between the two porphyrin planes, and binding of **Me_2V** in one of the two cavities was shown to affect the coordination of DABCO to the porphyrin zinc centers as shown by a shift in the Soret band of the porphyrins. The 1:1 and 1:2 host-guest binding constants between **Me_2V** and the 1:1 **Zn_2C_xDC**:DABCO sandwich complexes were found to be independent of the length of the spacer between the two cages of the sandwich complexes. The binding constants between **Me_2V** and these 1:1 **Zn_2C_xDC**:DABCO sandwich complexes were found to be higher than those between **Me_2V** and the open **Zn_2C_xDC** compounds; all the complexes showed highly negative cooperativities for the binding of the two **Me_2V** guests. This negative cooperativity was stronger in the 1:1 **Zn_2C_xDC**:DABCO sandwich complexes than in the open **Zn_2C_xDC** compounds in the absence of DABCO. In the latter **Zn_2C_xDC** compounds, the negative cooperativity might be explained by steric hindrance and charge repulsion between the two bound **Me_2V** guests. For the 1:1 **Zn_2C_xDC**:DABCO sandwich complexes, the negative cooperativity is probably a result of allosteric effects mediated by the DABCO ligand coordinated between the two zinc

porphyrins, implying that some form of information transfer is present between the two cavities of the double cage compounds. Variable temperature ^{1}H-NMR studies on the 1:1 **Zn_2C_3DC**:DABCO sandwich complex confirmed that upon the addition of **Me_2V** DABCO remains bound in between the porphyrins of this sandwich complex. The binding of two equivalents of **Me_2V** to this complex gives rise to multiple sets of proton resonances of the guest, which originate from the binding of **Me_2V** in the different diastereoisomeric forms of the double cage compound. Since it was found that the binding of one equivalent of **Me_2V** already quenches over 90% of the porphyrin fluorescence, it is advised to employ in future studies another guest as promotor molecule because this strong quenching effect severely complicates the binding and threading studies. The ideal promotor should have strong interactions with the double porphyrin cage compounds to ensure nearly full occupation of one of its cavities at already a low number of equivalents of the guest, and show a linear relationship between the amount of bound guest and the quenching of the fluorescence. A molecule that might fulfill this function is 1-methyl-4-phenylpyridinium (**MMP$^+$**, Figure 3). Its size is roughly the same as that of **Me_2V**, and therefore it is expected to fit in the cavity. Another option might a viologen molecule functionalized with alcohol groups: **$(EtOH)_2$V** (Figure 3). Previous studies have shown that this molecule binds inside the cavity of porphyrin cages, albeit in a different orientation, i.e. a parallel one with respect to the porphyrin plane (see Chapter 1). This alternative guest is known, to induce larger shifts in the Soret band of the porphyrin upon binding than **Me_2V**, and this may allow the use of UV-Vis instead of fluorescence spectroscopy for the host-guest binding studies.

In subsequent studies (Chapter 5), the threading of polytetrahydrofuran (polyTHF) chains, equipped on one side with a blocking group and a viologen moiety as binding station, through the cavities of a porphyrin sandwich complex was investigated. It was shown that all three 1:1 **Zn_2C_xDC**:DABCO sandwich complexes can traverse polymer chains with lengths up to 69 nm, and that their viologen moieties bind in a similar fashion as **Me_2V** to these complexes. MALDI-TOF spectrometry confirmed the formation of the 1:1:1, but not of the 1:1:2 **Zn_2C_xDC**:DABCO:polyTHF complexes. The latter might be due to the fact that these complexes do not efficiently ionize in the MALDI-TOF spectrometer. It was demonstrated that an

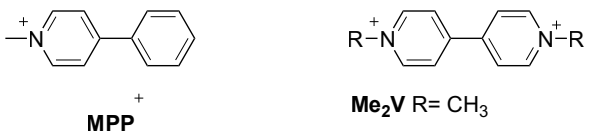

Figure 3 *Chemical structures of* ***MPP$^+$***, ***Me_2V*** *and* ***$(EtOH)_2$V***.

increase in polymer length decreased the threading rate, while there is no significant dependence of this rate or the free energy of activation for threading on the spacer length between the porphyrins in the double porphyrin cage compounds. To further elucidate the threading mechanism, in future studies the viologen moiety might be replaced by another binding station, preferably one that shows a linear relationship between fluorescence quenching and the percentage of the guest moiety that is bound in a cavity (as was suggested above for the binding of simple **Me_2V** guests), or a binding station that allows the use of another technique such as UV-Vis spectroscopy. Since in the present studies no polymers with alkene moieties were used, the investigation of the threading of polybutadiene chains will be of interest for future catalysis studies. However, before doing this it is advised to first investigate if catalytic epoxidation of small substrates, e.g. *cis*-stilbene and *trans*-stilbene, by double cage sandwich complexes with one zinc and one manganese center is possible and can be influenced by the binding of a promotor molecule.

6.3. Outlook

When double porphyrin cage compounds are to be employed to store data on synthetic polymers, several challenges remain. This section will discuss some possible improvements to be considered to enable the bulk storage of data onto synthetic polymers in the future.

6.3.1. Synthesis

To employ double porphyrin cage compounds on a large scale, their synthesis needs to be scaled up to comply with the future demand. However, the current synthesis route involves a step-wise construction of the porphyrin and requires several extensive, column-based purification steps to yield a pure compound. Such an elaborate synthesis route will not be cost and time efficient. To eliminate several synthesis steps, a double porphyrin cage compound might be constructed from a di-substituted porphyrin which is covalently linked via two oppositely oriented meso-phenyl rings. The construction of such a porphyrin is expected to be easier because the required functional bromine groups can be implemented in one single condensation reaction of a bromo-functionalized dipyrromethane derivative with o-anisaldehyde (Figure 4). A disadvantage might be, however, that during the coupling of the resulting bis-functionalized porphyrin cages to yield porphyrin double cage compounds, polymers are formed, complicating the purification process. This problem may be circumvented by carrying out the coupling reactions under high dilution conditions. The linking of the porphyrin cages by two spacers may limit their conformational freedom with respect to each other, which in turn may have an impact on the allosteric binding properties of these compounds, which is of interest to investigate.

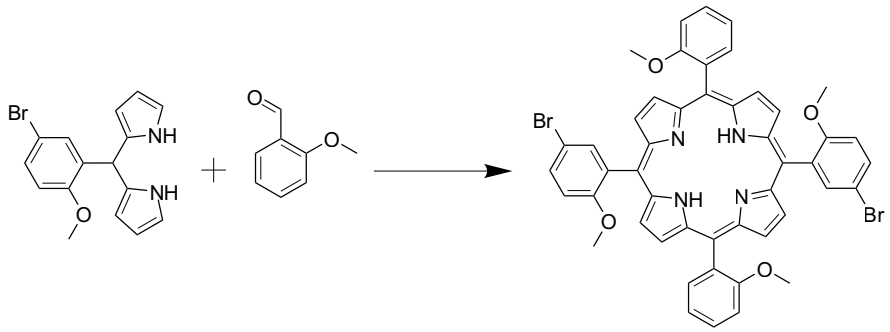

Figure 4 *Reaction scheme to from a bis-bromo substituted porphyrin.*

6.3.2 Ditopic ligands

In this research, DABCO was employed as the ditopic ligand, which enabled the transfer of allosteric interactions between the two zinc porphyrins of the double cage compounds. Although DABCO binds with high association constants, it might not be the most ideal ditopic ligand due to its reactivity with dichloromethane and its possible complex, non-covalent interactions with chloroform, as was shown in Chapter 3. As alternatives, pyrazine and/or bipy may be employed as ditopic ligands (see above). In the case of bipy, it is expected that complexes with less favorable coordination geometries will be formed with the double cage zinc porphyrin compounds, if the spacers are relatively short. Extension of the spacer lengths may solve this problem. Also ditopic ligands that contain other hetero-atoms such as sulfur or oxygen may be considered.

6.3.3 Promotors

It is the intention of the information transfer system based on double cage compounds that the writing of information in the form of epoxides on a polymer chain can be switched 'on' or 'off', and *vice versa,* by the binding of a single promotor molecule in one of the cavities of the compounds. **Me_2V** was shown to bind with high binding constants in the cavities of the double porphyrin compounds, but the formed host-guest complexes are always in dynamic equilibrium with their free components. To ensure that the promotor molecule is always in close proximity of the instructing cavity, it may be included in a ring-shaped thread that is interlocked in the instructing cavity to form a catenane (Figure 5). In previous studies it has already been shown that it is possible to form catenanes from porphyrin cage compounds via a metathesis reaction.[24,25] Instead of **Me_2V**, also **MMP^+** (Figure 3) may be employed as a promotor moiety, because it is expected to bind in the cavity with a high binding constant and it can be incorporated easily in a catenane ring. If in the future the double porphyrin cage compounds are to function as advanced catalytic writing machines, the catenane

should be able to switch between different states and thus should contain at least two different functional groups. One method to achieve this is to attach **Me_2V** or **MMP^+** moieties to chiral centers and enable switching between host-guest complexes of different chirality, which via allosteric interactions through the coordinated DABCO ligand might induce enantioselectivity in the epoxidation reactions that take place in the second cavity. The binding of the different chiral moieties is expected to induce slightly different conformational changes in the cavities of the double porphyrin cage compounds. The promotor moieties in the catenane need to be switchable, e.g. between the binding of one or the other promotor moiety or no promotor in the cavity of the double cage compound. Such a switching may be accomplished by light when the promotor moiety is also combined with a diazo group (Figure 6), which is known to be switchable from the *trans* to the *cis*-isomer state upon irradiation with light.[26–29] It is expected that when the diazo group exists as the *trans*-isomer, the promotor can still be bound inside the cavity, whereas in the case of the *cis*-isomer,

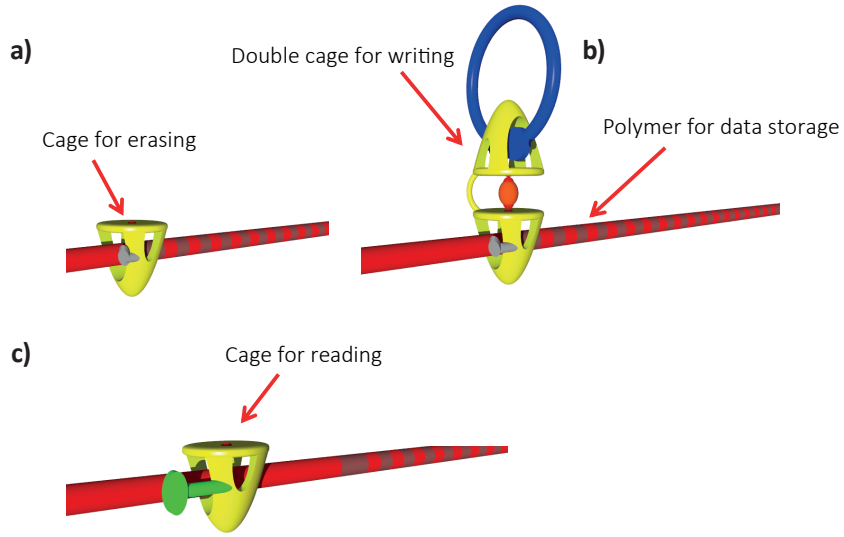

Figure 5 *Blueprint of an advanced catalytic writing machine based on separate porphyrin cage compounds (yellow), which can thread onto a synthetic polymer (red) on which information can be stored. The process can start with a porphyrin cage that contains an 'erasing cavity' with a rhenium metal center, to erase all information present on the synthetic polymer (a). This is followed by the activity of a double cage compound for the writing of information, containing a 'writing cavity' with a manganese center in the porphyrin and a catenane ring (blue, b). This 'writing cavity' binds a DABCO ligand (orange) and contains a ratchet for unidirectional movement (grey). It also includes an instruction cage with a binding station for e.g. a viologen moiety in the catenane ring, which can be switched by external stimuli, e.g. light or redox chemistry. Then, finally the advanced system also requires a porphyrin cage compound with a (FRET) sensor (green) for the reading of information that is present on the polymer chain (c).*

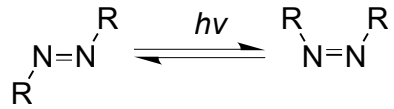

Figure 6 *Isomerization under the influence of light of a trans to cis-diazo compound, with R being any alkyl or aryl substituent.*

binding will be hampered. Another method of switching between promotors in the catenane ring may be by means of redox chemistry, i.e. by influencing the binding affinity of a promotor moiety for the cavity by reducing or oxidizing it. However, one has to be careful to employ such redox chemistry, since it might interfere with the epoxidation catalysis that takes place in the writing cavity.

6.3.4 Threading

The threading of polymer chains through the cavity of double porphyrin cage compounds is essential for the subsequent process of writing data. Up till now, only the treading of polyTHF chains through the double porphyrin cage compounds has been carried out, but this should be extended to polybutadiene chains. Also the threading of polymer chains through one cavity in the presence of a promotor molecule in the second cavity is needed to investigate if possible allosteric interactions give rise to a different translocation rate of the chain. Ideally, the translocation of the polymer chain should be slowed down to match the rate of the epoxidation reaction.[20] It has been shown previously that an extended, more flexible porphyrin cage can wrap itself around the polymer chain, resulting in a slower movement along this chain.[20] Despite this decrease, the measured threading rate was still faster than the rate of epoxidation. To further slowdown the threading speed, the porphyrin cage compound can be equipped at one or both of its side walls with a handle to which substituents of adjustable size can be attached.[30] Via supramolecular interactions, these substituents may then interact with the polymer chain and slow down its translocation until it synchronizes with the rate of epoxidation (see grey handle in Figure 5b). At the same time, these handles may function as a 'ratchet' to enable unidirectional threading of the chain, which is needed to write data onto the polymer in a controlled sequence.

6.3.5 Catalysis

The double porphyrin cage compounds were designed to catalytically write information onto a synthetic polymer. However, so far no catalysis studies have been carried out. Therefore, it is of vital importance to investigate if the manganese double porphyrin cage compounds (**Mn_2C_xDC**) show similar catalytic behavior as the manganese single porphyrin cage compounds, both in the presence and in the absence of axial ligands. These studies can be carried out with small substrates, e.g.

cis-stilbene or *trans*-stilbene, and polymeric substrates like polybutadiene.[19,21,31] Next, the heterometallic zinc manganese double porphyrin cage compounds (**$ZnMnC_xDC$**) may be synthesized, which may be accomplished by reacting the **H_4C_xDC** compounds with one equivalent of manganese acetate, followed by a reaction with zinc acetate. However, by using this synthesis route probably a statistical mixture of double porphyrin cage compounds with 0, 1, and 2 manganese centers will be obtained. Such a mixture may be difficult to purify. As an alternative, the **$ZnMnC_xDC$** compounds may be obtained more efficiently via a modular coupling of single manganese and zinc porphyrin cage compounds, using the click method described in section 6.2 of this chapter. Subsequently, the catalytic properties of the **$ZnMnC_xDC$** compounds should be investigated, in particular under conditions in which both a DABCO ligand is present between the two porphyrins and a viologen promotor molecule in the cavity of the zinc porphyrin cage. In that case it is of interest to see if the bound promotor molecule can influence the catalytic reaction that takes place in the manganese cage, via allosteric interactions through the bridging DABCO ligand.

6.3.6 Advanced machines for storing data

In addition to the application of the double porphyrin cage compounds as molecular machines that can write data on synthetic polymers, it would also be of interest to see if this data can be read out and erased. With these additional abilities, the double porphyrin cage compounds might be employed as more advanced machines for storing data. In further studies, effective techniques for the reading out of data stored on the polymer need to be developed. To enable this read-out of data, an additional dye moiety, which has a donor-acceptor interaction with the porphyrin, can be attached to a porphyrin cage compound. Such a dye could be an Alexa-dye that forms a FRET (fluorescence resonance energy transfer) pair with a porphyrin in which e.g. a platinum, gold, zinc, or tin metal center is present (Figure 5c).[32,33] It is expected that parts of a polymer containing double bonds, or parts of a polymer containing epoxides, are accommodated in different geometries in the cavity of double porphyrin cage compounds. These different geometries might induce a change in the fluorescence behavior of the FRET pair, which can be the basis for the reading-out process.

To erase epoxides that are written on the synthetic polymer, the reverse catalytic reaction should be enabled. To convert an epoxide back to its double bond precursors, a rhenium porphyrin catalyst in the presence of a reductant, e.g. triphenylphosphite, might be used.[34–37] Such a rhenium catalyst can also be attached to a porphyrin cage compound containing an 'erasing' cavity, which can erase all the data on a synthetic polymer before it is newly encoded (Figure 5a).

Successful completion of all the above mentioned steps in the future would allow the production of a fully functioning data storage machine. Although this is a

futuristic picture and many challenges remain, the results presented in this thesis show the feasibility of some of the first basic steps required to develop such a storage machine based on double porphyrin cage compounds.

6.4 References

(1) Zhirnov, V.; Zadegan, R. M.; Sandhu, G. S.; Church, G. M.; Hughes, W. L. Nucleic Acid Memory. *Nat. Mater.* **2016**, *15* (4), 366–370.
(2) Moore, G. E. Cramming More Components onto Integrated Circuits. *Electronics* **1965**, *38* (8), 114–117.
(3) R. W. Keyes. Fundamental Limits of Silicon Technology. *Proc. IEEE* **2001**, *89* (3), 227–239.
(4) Markov, I. L. Limits on Fundamental Limits to Computation. *Nature* **2014**, *512*, 147.
(5) Goldman, N.; Bertone, P.; Chen, S.; Dessimoz, C.; LeProust, E. M.; Sipos, B.; Birney, E. Towards Practical, High-Capacity, Low-Maintenance Information Storage in Synthesized DNA. *Nature* **2013**, *494* (7435), 77–80.
(6) Church, G. M.; Gao, Y.; Kosuri, S. Next-Generation Digital Information Storage in DNA. *Science* **2012**, *337* (6102), 1628.
(7) van Dongen, S. F. M.; Clerx, J.; Nørgaard, K.; Bloemberg, T. G.; Cornelissen, J. J. L. M.; Trakselis, M. A.; Nelson, S. W.; Benkovic, S. J.; Rowan, A. E.; Nolte, R. J. M. A Clamp-like Biohybrid Catalyst for DNA Oxidation. *Nat. Chem.* **2013**, *5* (11), 945–951.
(8) Johnson, A.; O'Donnell, M. Cellular DNA Replicases: Components and Dynamics at the Replication Fork. *Annu. Rev. Biochem.* **2005**, *74* (1), 283–315.
(9) Colquhoun, H.; Lutz, J.-F. Information-Containing Macromolecules. *Nat Chem* **2014**, *6* (6), 455–456.
(10) Lutz, J.-F. Coding Macromolecules: Inputting Information in Polymers Using Monomer-Based Alphabets. *Macromolecules* **2015**, *48* (14), 4759–4767.
(11) Mutlu, H.; Lutz, J.-F. Reading Polymers: Sequencing of Natural and Synthetic Macromolecules. *Angew. Chem. Int. Ed.* **2014**, *53* (48), 13010–13019.
(12) Lutz, J.-F. Writing on Polymer Chains. *Acc. Chem. Res.* **2013**, *46* (11), 2696–2705.
(13) Niu, J.; Hili, R.; Liu, D. R. Enzyme-Free Translation of DNA into Sequence-Defined Synthetic Polymers Structurally Unrelated to Nucleic Acids. *Nat. Chem.* **2013**, *5* (4), 282–292.
(14) Roy, R. K.; Meszynska, A.; Laure, C.; Charles, L.; Verchin, C.; Lutz, J.-F. Design and Synthesis of Digitally Encoded Polymers That Can Be Decoded and Erased. *Nat. Commun.* **2015**, *6*, 7237.
(15) Al Ouahabi, A.; Charles, L.; Lutz, J.-F. Synthesis of Non-Natural Sequence-Encoded Polymers Using Phosphoramidite Chemistry. *J. Am. Chem. Soc.* **2015**, *137* (16), 5629–5635.
(16) Pfeifer, S.; Zarafshani, Z.; Badi, N.; Lutz, J.-F. Liquid-Phase Synthesis of Block Copolymers Containing Sequence-Ordered Segments. *J. Am. Chem. Soc.* **2009**, *131* (26), 9195–9197.
(17) Trinh, T. T.; Oswald, L.; Chan-Seng, D.; Charles, L.; Lutz, J.-F. Preparation of Information-Containing Macromolecules by Ligation of Dyad-Encoded Oligomers. *Chem. – Eur. J.* **2015**, *21* (34), 11961–11965.
(18) Martens, S.; Landuyt, A.; Espeel, P.; Devreese, B.; Dawyndt, P.; Du Prez, F. Multifunctional Sequence-Defined Macromolecules for Chemical Data Storage. *Nat. Commun.* **2018**, *9* (1), 4451.
(19) Thordarson, P.; Bijsterveld, E. J. A.; Rowan, A. E.; Nolte, R. J. M. Epoxidation of Polybutadiene by a Topologically Linked Catalyst. *Nature* **2003**, *424* (6951), 915–918.
(20) Coumans, R. G. E.; Elemans, J. A. A. W.; Nolte, R. J. M.; Rowan, A. E. Processive Enzyme Mimic: Kinetics and Thermodynamics of the Threading and Sliding Process. *Proc. Natl. Acad. Sci. U. S. A.* **2006**, *103* (52), 19647–19651.
(21) Monnereau, C.; Ramos, P. H.; Deutman, A. B. C.; Elemans, J. A. A. W.; Nolte, R. J. M.; Rowan, A. E. Porphyrin Macrocyclic Catalysts for the Processive Oxidation of Polymer Substrates. *J. Am. Chem. Soc.* **2010**, *132* (5), 1529–1531.
(22) Thordarson, P.; Bijsterveld, E. J. A.; Elemans, J. A. A. W.; Kasák, P.; Nolte, R. J. M.; Rowan, A. E. Highly Negative Homotropic Allosteric Binding of Viologens in a Double-Cavity Porphyrin. *J. Am. Chem. Soc.* **2003**, *125* (5), 1186–1187.
(23) Deutman, A. B. C.; Monnereau, C.; Moalin, M.; Coumans, R. G. E.; Veling, N.; Coenen, M.; Smits, J. M. M.; de Gelder, R.; Elemans, J. A. A. W.; Ercolani, G.; et al. Squaring Cooperative Binding Circles. *Proc. Natl. Acad. Sci. U. S. A.* **2009**, *106* (26), 10471–10476.
(24) Coumans, R. G. E.; Elemans, J. A. A. W.; Rowan, A. E.; Nolte, R. J. M. Interlocked Porphyrin Switches. *Chem. – Eur. J.* **2013**, *19* (24), 7758–7770.
(25) Coumans, R. G. E.; Elemans, J. A. A. W.; Thordarson, P.; Nolte, R. J. M.; Rowan, A. E. Synthesis of Porphyrin-Containing [3]Rotaxanes by Olefin Metathesis. *Angew. Chem. Int. Ed.* **2003**, *42* (6), 650–654.

(26) Samanta, S.; Beharry, A. A.; Sadovski, O.; McCormick, T. M.; Babalhavaeji, A.; Tropepe, V.; Woolley, G. A. Photoswitching Azo Compounds in Vivo with Red Light. *J. Am. Chem. Soc.* **2013**, *135* (26), 9777–9784.
(27) Coelho, P. J.; Castro, M. C. R.; Fonseca, A. M. C.; Raposo, M. M. M. Photoswitching in Azo Dyes Bearing Thienylpyrrole and Benzothiazole Heterocyclic Systems. *Dyes Pigments* **2012**, *92* (1), 745–748.
(28) Beharry, A. A.; Woolley, G. A. Azobenzene Photoswitches for Biomolecules. *Chem. Soc. Rev.* **2011**, *40* (8), 4422–4437.
(29) Mourot, A.; Kienzler, M. A.; Banghart, M. R.; Fehrentz, T.; Huber, F. M. E.; Stein, M.; Kramer, R. H.; Trauner, D. Tuning Photochromic Ion Channel Blockers. *ACS Chem. Neurosci.* **2011**, *2* (9), 536–543.
(30) Varghese, S.; Spierenburg, B.; Swartjes, A.; White, P. B.; Tinnemans, P.; Elemans, J. A. A. W.; Nolte, R. J. M. Direct Synthesis of Chiral Porphyrin Macrocyclic Receptors via Regioselective Nitration. *Org. Lett.* **2018**, *20* (13), 3719–3722.
(31) Elemans, J. A. A. W.; Bijsterveld, E. J. A.; Rowan, A. E.; Nolte, R. J. M. A Host–guest Epoxidation Catalyst with Enhanced Activity and Stability. *Chem. Commun.* **2000**, *24*, 2443–2444.
(32) Lee, A. J.; Ensign, A. A.; Krauss, T. D.; Bren, K. L. Zinc Porphyrin as a Donor for FRET in Zn(II)cytochrome c. *J. Am. Chem. Soc.* **2010**, *132* (6), 1752–1753.
(33) Finikova, O. S.; Chen, P.; Ou, Z.; Kadish, K. M.; Vinogradov, S. A. Dynamic Quenching of Porphyrin Triplet States by Two-Photon Absorbing Dyes: Towards Two-Photon-Enhanced Oxygen Nanosensors. *J. Photochem. Photobiol. Chem.* **2008**, *198* (1), 75–84.
(34) Nakagiri, T.; Murai, M.; Takai, K. Stereospecific Deoxygenation of Aliphatic Epoxides to Alkenes under Rhenium Catalysis. *Org. Lett.* **2015**, *17* (13), 3346–3349.
(35) Gable, K. P.; Brown, E. C. Rhenium-Catalyzed Epoxide Deoxygenation: Scope and Limitations. *Synlett* **2003**, *2003* (14), 2243–2245.
(36) Sousa, S. C. A.; Fernandes, A. C. Rhenium-Catalyzed Deoxygenation of Epoxides without Adding Any Reducing Agent. *Tetrahedron Lett.* **2011**, *52* (51), 6960–6962.
(37) Gable, K. P.; Brown, E. C. Efficient Catalytic Deoxygenation of Epoxides Using [Tris(3,5-Dimethylpyrazolyl)hydridoborato]rhenium Oxides. *Organometallics* **2000**, *19* (5), 944–946.

Summary

The amount of digital information that is produced nowadays increases exponentially. All this information has to be processed and stored, making that new methods for depositing and processing data have to be developed. One possible solution is to store data in natural and synthetic polymers, which is an appealing approach, because it allows for high-density information storage. The aim of the work described in this thesis was to design and construct a catalytic 'machine' that can thread onto a polymer chain and move along it while writing digital information on that chain in the form of chemical functions. The design of this catalytic 'machine' is based on the key features exhibited by the DNA-polymerases, i.e. a catalytic part and a ring that keeps the catalyst attached to the polymer chain. Together they form a so-called 'processive catalyst', i.e. a catalyst that can perform multiple rounds of catalysis without detaching from its substrate (usually a polymer). In our case this natural design was translated into a blueprint involving two synthetic cage molecules that are linked via an alkyl spacer containing 3, 5, and 11 carbon atoms (**H_4C_XDC**, in which x is 3, 5 or 11) and can influence each other's binding behavior in order to control the transfer of information. These cages are attached to a catalytically active metal complex, i.e. a porphyrin molecule. The cage compound is a diphenylglycoluril clip to which a porphyrin 'roof' is attached. It was envisioned to employ the ditopic axial ligand 1,4-diazabicyclo[2.2.2]octane (DABCO) to connect the two porphyrins via a metal-ligand coordination. When a *N,N*'-dimethylviologen dihexafluorophosphate (**Me_2V**) guest molecule is bound inside one of the cavities, the binding of a second guest molecule in the other cage might be influenced by allosteric interactions.

We embarked on this project by first synthesizing a series of three double porphyrin cage compounds (**Chapter 2**) using 'click'-chemistry. The produced structures were fully characterized by NMR, which showed that each of them consisted of mixtures of two diastereoisomers.

Before the double porphyrin cage compounds can be employed as catalysts for the storage of data in synthetic polymers, the formation of 1:1 sandwich complexes between the ditopic axial ligand DABCO and the double cage compounds needed to be investigated. The formation of these 1:1 **Zn_2C_xDC**:DABCO sandwich complexes is essential because it may enable the transfer of information between the two cavities through allosteric interactions. **Chapter 3** describes the formation of the 1:1 **Zn_2C_xDC**:DABCO sandwich complexes in dichloromethane, chloroform, and in a solvent mixture of chloroform and acetonitrile (1:1, (v/v)). **Zn_2C_3DC** was found to form the strongest 1:1 sandwich complex with DABCO, while the differences in binding strengths of DABCO with the other **Zn_2C_xDC** hosts were smaller and rather similar. Surprisingly, when dichloromethane was employed as the solvent, a solvolysis

reaction took place, in which DABCO acted as a nucleophilic reagent. This reaction interfered with the formation of the well-defined 1:1 **Zn_2C_xDC**:DABCO sandwich complexes. In chloroform, unusual behavior was observed indicating the initial inability of the ligand to coordinate to the zinc centers. Since this deviation behavior was not observed in other solvents, a modified binding model, which includes the association of *n* molecules of DABCO to alternative binding sites on the cage compounds, was proposed.

The next step towards the construction of a catalytic machine that can write information was to investigate the effect of binding of a 'promotor' viologen (**Me_2V**) molecule to the 1:1 **Zn_2C_xDC**:DABCO sandwich complexes. This study was performed by following the quenching of the fluorescence of the porphyrin molecules in the sandwich complexes as function of the number of equivalents of **Me_2V** (**Chapter 4**). In the proposed system such a promotor should bind in one of the cavities of the sandwich complex and influence the catalytic reaction in the second cavity, e.g. by turning it into an 'off' or 'on'-state, and *vice versa*. The complexation of already one equivalent of **Me_2V** guest was found to quench more than 90% of the total porphyrin fluorescence, which was explained by the fact that both porphyrins of the sandwich complex are within quenching distance when a **Me_2V** guest is bound in one of its two cavities. The 1:1 and 1:2 host-guest binding constants between **Me_2V** and the 1:1 **Zn_2C_xDC**:DABCO sandwich complexes were found to be high and independent of the length of the spacer between the two cages of the sandwich complexes. They were found to be higher than those of the complexes between **Me_2V** and the open **Zn_2C_xDC** compounds. All these systems showed highly negative cooperativities for the binding of the two **Me_2V** guests. This negative cooperativity was explained by steric hindrance and charge repulsion between the two bound **Me_2V** guests. It could also be the result of allosteric effects mediated by the DABCO ligand coordinated between the two zinc porphyrins, implying that some form of information transfer occurred between the two cavities of the double cage compounds.

In subsequent studies (**Chapter 5**), the threading of the 1:1 **Zn_2C_xDC**:DABCO sandwich complexes onto polytetrahydrofuran (polyTHF) chains was studied. These polymer chains were open on one side and contained a blocking group on the other side. Close to this blocked side a viologen moiety as binding station was located. The process of threading was followed by recording the fluorescence of the porphyrin as a function of time. This fluorescence is quenched when the cage complex traverses the polymer chain and reaches the viologen moiety. It was shown that all three 1:1 **Zn_2C_xDC**:DABCO sandwich complexes can traverse polymer chains up to lengths of 69 nm. Furthermore, it was found that the viologen moieties in the polymers bind in a similar fashion to these complexes as **Me_2V**. It was demonstrated that an increase in polymer length decreases the threading rate, while there was no significant

dependence of this rate or the free energy of activation for threading on the spacer length between the porphyrins in the double porphyrin cage compounds.

In the last chapter of the thesis (**Chapter 6**) the future perspectives and challenges for the production of a fully functioning machine that can write data on a polymer chain are discussed.

Samenvatting

De hoeveelheid informatie, die tegenwoordig wordt geproduceerd, is enorm en neemt exponentieel toe. Al deze informatie moet worden verwerkt en opgeslagen en dit maakt dat er nieuwe methodes nodig zijn om dit te realiseren. Een mogelijk nieuwe methode is het opslaan van data op natuurlijke of synthetische polymeren. Dit is een aantrekkelijke aanpak omdat hiermee veel gegevens op een kleine hoeveelheid materiaal kunnen worden samengebracht. Het doel van het onderzoek dat in dit proefschrift wordt beschreven, is het ontwerpen en synthetiseren van een katalytische 'machine' die zich over een polymere keten kan voortbewegen en informatie kan schrijven op deze keten in de vorm van chemische functionaliteiten. Het ontwerp van deze machine is gebaseerd op de essentiële functies van het enzym DNA-polymerase, dat een katalytisch deel bevat en een ring die dat katalytische deel aan de polymere keten bindt. Tezamen vormen ze een zogenaamde 'processieve katalysator', d.w.z. een katalysator die meerdere katalytische cycli kan doorlopen zonder zich van zijn substraat los te maken. In dit proefschrift is het natuurlijke ontwerp vertaald naar een synthetisch molecuul, dat twee kooien met een katalytisch actief metaalcomplex bevat, welke met elkaar zijn verbonden door middel van een keten van 3, 5 of 11 koolstofatomen (**H_4C_XDC**, waarin x is 3, 5 of 11). De kooi bestaat uit een diphenylglycoluril mand met een metaalporfyrine 'dak'. Het doel was om de metaalcentra van de twee porfyrines met elkaar te verbinden door middel van een ditopisch-ligand, te weten de verbinding 1,4-diazabicyclo[2.2.2]octaan (DABCO). Door daarnaast een gast, *N,N*'-dimethylviologeen dihexafluorofosfaat (**Me_2V**), in een van de holtes te binden kan mogelijkerwijs het bindingsgedrag van de tweede holte worden beïnvloed, een proces dat allostere interactie wordt genoemd.

In het eerste stadium van het project werd een serie van drie dubbele porfyrine-kooien gesynthetiseerd die door middel van 'click' chemie aan elkaar werden verknoopt (**Hoofdstuk 2**). Deze verbindingen werden volledig gekarakteriseerd met behulp van NMR spectroscopie. Hierbij werd vastgesteld dat elk van de dubbele porfyrine-kooien bestond uit een mengsel van twee diastereo-isomeren.

Voordat de dubbele porfyrine-kooien kunnen worden gebruikt als katalysatoren voor de opslag van data op synthetische polymeren, moest de vorming van 1:1 dubbelgevouwen complexen tussen het bidentaat-ligand DABCO en de dubbele zinkporfyrine kooien worden onderzocht. De vorming van deze 1:1 **Zn_2C_xDC**:DABCO dubbelgevouwen complexen is essentieel omdat hiermee de overdracht van informatie tussen de twee holte-moleculen mogelijk wordt door middel van allostere interacties. **Hoofdstuk 3** beschrijft de vorming van deze complexen in chloroform en in een mengsel van chloroform en acetonitril (1:1, (v/v)). Het 1:1 dubbelgevouwen complex met de sterkste DABCO-binding werd gevormd door de verbinding **Zn_2C_3DC**,

waarbij de complexen van DABCO met de andere **Zn_2C_xDC** moleculen lagere, maar ongeveer dezelfde bindingsterkten vertoonden. Wanneer dichloormethaan als oplosmiddel werd gebruikt, werd de vorming van goed gedefinieerde 1:1 **Zn_2C_xDC**: DABCO dubbelgevouwen complexen verassend genoeg belemmerd door een reactie van DABCO met het oplosmiddel (solvolyse-reactie). In chloroform werd ongebruikelijk bindingsgedrag waargenomen, waarbij de DABCO ligand niet onmiddellijk coördineerde aan de zinkcentra. Aangezien deze afwijking niet werd waargenomen in andere oplosmiddelen, werd er een gemodificeerd bindingsmodel voorgesteld, waarbij *n* moleculen DABCO eerst op andere plaatsen op de dubbele porfyrine-complexen binden.

De volgende stap om informatieoverdracht mogelijk te maken, is het binden van een 'promotor' viologeen (**Me_2V**) molecuul in een van de holtes van de complexen. Dit proces werd onderzocht met behulp van fluorescentiespectroscopie, waarbij de uitdoving (quenching) van de fluorescente van de porfyrine-moleculen door **Me_2V** werd gevolgd als functie van de hoeveelheid viologeen moleculen (**Hoofstuk 4**). In het in de toekomst te construeren katalytische systeem zou **Me_2V** als promotor moeten functioneren en binden in een van de holtes van het dubbelgevouwen complex om daarmee de katalytische reactie in de andere holte te beïnvloeden, bijvoorbeeld door deze reactie van de 'aan' naar de 'uit' stand te schakelen en omgekeerd. Verrassend genoeg bleek de binding van reeds één equivalent **Me_2V** de fluorescentie van het porfyrine voor meer dan 90% uit te doven. Dit werd verklaard door aan te nemen dat beide porfyrines in het dubbelgevouwen complex zich binnen de quenching-afstand van een **Me_2V** gast bevinden, als deze gebonden is in een van de twee holtes. De bindingsconstanten van de 1:1 en 1:2 complexen tussen **Me_2V** en de 1:1 **Zn_2C_xDC**:DABCO dubbelgevouwen complexen waren erg hoog en onafhankelijk van de spacer-lengte tussen de twee holtemoleculen. Zij waren ook hoger dan de bindingsconstanten van de complexen tussen **Me_2V** en de open **Zn_2C_xDC** moleculen. Alle complexen vertoonden een sterk negatieve coöperativiteit voor de binding van **Me_2V** gastmoleculen. Deze negatieve coöperativiteit kan een gevolg zijn van sterische hindering en ladingsafstoting tussen de twee gebonden **Me_2V** gasten. Het zou ook het gevolg kunnen zijn van allostere effecten onder invloed van de DABCO-ligand, die coördineert tussen de twee zinkcentra in de porfyrines. De laatste verklaring zou impliceren dat er een vorm van informatieoverdracht tussen de twee holtes van de dubbele porfyrine-kooienplaats vindt.

In een vervolgstudie (**Hoofdstuk 5**) werd het rijgen (threading) van de holtemoleculen aan polytetrahydrofuran (polyTHF) ketens van verschillende lentes onderzocht. Deze polymeerketens waren aan een kant open en aan de andere kant afgeschermd door een sterisch omvangrijke groep. Deze laatste groep was gelegen naast een viologeen-molecuul, dat als bindingsplaats voor de 1:1 dubbelgevouwen complexen fungeerde.

Het rijgen kan derhalve alleen plaatsvinden via de open kant van het polymeer en het proces kan worden gevolgd door de afname van de fluorescentie te meten als functie van de tijd. Deze fluorescentie-afname is een gevolg van het feit dat de 1:1 dubbel-gevouwen complexen binden aan de viologeenmoleculen. Alle drie de 1:1 **Zn_2C_xDC**: DABCO dubbelgevouwen complexen bleken aan de polymeerketens te binden en hierlangs te kunnen lopen. De langste polymeerketen had een lengte van 69 nm. Het viologeen-gedeelte van de polymeren bleek op een soortgelijke manier te binden in de holtemoleculen als **Me_2V** zelf. Er werd gevonden dat als het polymeer langer is, de snelheid van het rijgen lager is, waarbij de vrije activering voor het rijgen niet significant afhankelijk was van de lengte van de spacer tussen de porfyrines in de dubbelgevouwen complexen.

In het laatste hoofdstuk van het proefschrift (**Hoofdstuk 6**) worden de toekomstper-spectieven en uitdagingen voor de constructie van een volledig functionerende machine voor het schrijven van informatie op synthetische polymeren bediscussieerd.

Dankwoord

Fairy tales, as G. K. Chesterton once pointed out, are not true. They are more than true. Not because they tell us that dragons exist, but because they tell us that dragons can be defeated. – Neil Gaiman

Aan het begin van een promotie begin je met een wit vel waar langzaam de lijnen die uiteindelijk een kleurplaat beslaan, op worden getekend. Gedurende het onderzoek worden steeds meer stukken van de kleurplaat vormgegeven, op elkaar aangesloten en uiteindelijk ook ingekleurd. Totdat uiteindelijk ieder hoofdstuk zijn vorm heeft gekregen en de kleurplaat compleet af is. Het eindproduct, is het proefschrift wat je nu in je handen houdt. Zo'n kleurplaat ontwerp je niet alleen en door de invulling te delen met wat gastartiesten wordt het een heus kunstwerk.

Allereerst, Roeland en Alan, bedankt dat jullie mij de kans hebben gegeven om mijn eigen kleurplaat te maken. Alan, als ik met jou een meeting had gehad, dan zou ik daarna een kleurplaat van 10 pagina's kunnen maken met alle wilde ideeën die ter sprake kwamen. Halverwege mijn PhD heb je een baan in Australië geaccepteerd en ik wens je daarmee alle succes van de wereld.

Roeland, dankjewel voor de vele suggesties tijdens het onderzoek en het schrijven van dit manuscript. Ik heb bij jou altijd veel vrijheid en ook verantwoordelijkheid in/voor mijn onderzoek ervaren waardoor ik het zelf heb kunnen vormgeven. Dit was een uitdaging die ik met veel plezier ben aangegaan.

Hans (Dr. Bernard), na mijn bachelor ben ik wat later met mijn masterstage bij jou begonnen en dit was eigenlijk het begin van een mooie samenwerking die we hebben voortgezet tijdens de PhD. Ik waardeer vooral dat je bij jou ook kan aankloppen voor niet-werk-gerelateerde zaken en dat er altijd tijd is voor een geintje waardoor de sfeer er altijd goed in zat, iets wat ik minstens zo belangrijk vind als productiviteit, want ze gaan hand in hand. Gewapend met de verkleedkist voor de kerstfoto (toen dat nog mocht…), of met een pot Bicarb voor het bicarb-schuiven voor de lab-Olympics (volgens mij staan de strepen nog steeds op de vloer) of gewoon humor achter de zuurkast/het bureau, het heeft veel momenten opgeleverd om aan terug te denken! Daarnaast heb je mijn manuscript minutieus gecorrigeerd, het zou niet hetzelfde zijn zonder die correcties, dank daarvoor.

Ik wil ook graag de leden van de manuscriptcommissie bedanken voor het lezen en beoordelen van mijn proefschrift: Prof. dr. Floris Rutjes, Prof. dr. Joost Reek en Dr. Peter Korevaar, bedankt!

De gast-kunstenaars waren mijn studenten of te wel de Gruppo Stout! Dit begon met Mathijs (Surfer-dude) als eerste student. Mathijs, jij kwam bij mij stage lopen toen ik net zelf twee maanden bezig was met m'n PhD en er dus eigenlijk nog helemaal niks was. We hadden al wat routes uitgeprobeerd en alleen nog maar niet scheidbare rotzooi gekregen. Toch ben je de uitdaging aangegaan en heb je samen met Theo en mij jezelf in de synthese vastgebeten. Toen we eenmaal een paar mg in handen hadden van de eerste dubbele clip, was deze wereldvoorraad van jou en heb jij daaraan de eerste bindingstudies gedaan. Tijdens je stage heb je mij continue uitgedaagd en me gemotiveerd om verder te denken. Het was ontzettend fijn om mijn onderzoek met jou te kunnen delen en om jou als sparringpartner te hebben (en of course, je POV-ray skills zijn legendary voor mij)!

Fabian (Fabioooooo) jij bent de tweede student die de uitdaging aan ging om bij mij stage te lopen. Ik ken jou als een ontzettend harde en gedisciplineerde werker waarbij je kapsel een tijd in fase heeft gelopen met dat van Luuk. Tijdens de synthese van de dubbele clip heb jij het voor elkaar gekregen om twee keer dezelfde blaf te reproduceren (hulde!) waarna je ook twee keer de volledige zuurkast kon poetsen! Ook heb je gewerkt aan katalytische studies, met jawel, DABCO als axiaal ligand in DCM. Daar hebben we interessante inzichten uitgehaald maar het heeft helaas niet dit boekje gehaald, al kunnen we ze nu wel beter verklaren.

Jeroen (Cap'tain Blackleg) en Eline (Miss Cocktail), de twee studenten die samen begonnen zijn aan een bachelorstage bij mij en de ballen hebben gehad om deze voort te zetten met een masterstage, hulde! Jeroen, jij wilde je graag in een stuk synthese vastbijten en dat heeft er voor gezorgd dat we nu geen last meer hebben van ongewenste zouten en dat de acetyleen koppeling/ontscherming een heel stuk soepeler gaat! Voor je masterstage wou je iets meer dan synthese, iets meer meten en vooral ook iets meer programmeren, wat er in is uitgemond dat je eigenlijk bij allerlei projecten de losse eindjes hebt opgepakt. Hiervoor ben ik je erg dankbaar. Ook heeft je werk aan de dubbele porfs ons de nodige inzichten gegeven. Daarnaast kan ik je humor, geduld, fotoskills (thanks voor de foto's van mn konijntjes!) en vooral ook je muzieksmaak waarderen, want als bijna de enige van mijn studenten, delen wij dezelfde geweldige muzieksmaak!

Eline, jij werd aan mij gekoppeld door Alan want hij dacht dat wij wel goed samen zouden kunnen werken en ik denk dat dit zeker waar is! Tijdens je bachelor heb je de eerste threading experimenten uitgevoerd en heb je de dubbele porf en meegenomen naar Cambridge. Via de skype hadden we een verslaaaaag van de daaaaag en is de "aanslag" op Stephen Hawking mislukt. Voor je masterstage wilde je de dubbele clip zelf maken en daarna bindingstudies meten. We hebben gemeten totdat we een ons wogen, daar op het practicum. Met 4 UV-Vis spectrofotometers en 1 fluorescentie

spectrofotometer in gebruik, hebben we die titraties er met hoge efficiëntie doorheen terwijl we weddenschappen maakten over welke verkiezingsposter het eerste naar beneden zou mieteren en af en toe werd de frustratie met de knuppel losgelaten. Ik vond het super leuk om je te begeleiden en je te zien groeien, je vragen te horen stellen waarop je eigenlijk geen antwoord wilde hebben, maar vooral om met je bepaalde zaken te relativeren!

Joëlle, jij hebt je bachelorstage bij mij gelopen, waarbij we tot diep in de nacht diffusie met de NMR hebben gemeten en veel van je experimenten zijn terug te vinden in deze thesis. Het geheel hebben we afgesloten met een super congres in Seoul, waarbij we op sleeptouw zijn genomen door locals en daardoor terecht kwamen in een tent, ergens in een kelder, waar we super goede kip hebben gegeten. Toch een betere ervaring dan de Mac niet?

Ingrid (Bruut Kalf), jou kende ik al voordat je stage kwam lopen, je bent een super leuke toevoeging van de groep geweest. Ook al staat niks van je onderzoek in mijn boekje, het was een genot om je op het lab te begeleiden. Daarnaast ben je een goede motivatie geweest om tijdens het schrijven van het proefschrift op tijd naar de uni te komen, ik schrijven en jij leren. Ik ken maar weinig mensen die zo zijn als jij, zo lekker onbeschaamd, eerlijk en oprecht, je bent een schatje!

Bram, jij was een beetje mijn adoptie-student aangezien je niet aan mijn project werkte maar wel op hetzelfde lab stond. Wel altijd gezellig, hardwerkend en als vanzelfsprekend onderdeel van de Gruppo Stout.

Onderdeel van het begeleiden van de Gruppo Stout was in mijn geval ook het hebben van creabea-avondjes (waar creaties met een droogtijd van xx cm per dag, die het daglicht niet kunnen verdragen, zijn gemaakt…), Disney avonden, escaperooms uitvogelen, Sinterklaas vieren, de Efteling onveilig maken en vooral sushi eten (waarbij het toch verbazingwekkend is dat we elke keer weer terug mogen komen…)! Laten we deze activiteiten erin houden!

Gedurende de tijd op de afdeling sta je niet alleen in het lab, bedankt voor alle gezelligheid tijdens de pauzes, alle foute en net-over-de-top opmerkingen en de goede adviezen. Dus Femke (thanks voor de hulp bij de synthese en de goede gesprekken), Joris, Daniël (Schreeuwlelijk), Stijn, Onno, Anika (altijd goed om met je te gaan kickfitten!), Arjan, Zaskia, Niels, Bart (Bril), Dennis, Roy, Johan, Luuk (Poedel), Mo, Roel, Tim, Pascale, Toine, Anne (een van de leukste toevoegingen tijdens het schrijven!), Wessel, Luc, Daan, Huub, Jeroen, Marc, Max, Wesley en iedereen uit vleugel 8, bedankt voor alle hulp/afleiding!

Zonder ondersteunend personeel loopt een PhD gigantisch in de soep. Paula, Desiree, Paul Schlebos (The Dancing Destroyer, altijd leuk om bij je langs te komen), Ad, Peter van Dijk, Peter van Galen, Helene en Jan, bedankt voor alle hulp in de afgelopen jaren! Dan natuurlijk niet te vergeten Theo en Paul. Theo, in de eerste maanden heb ik jou 'ingelijfd' in mijn onderzoek en het was super leuk/leerzaam om met je samen te werken (ik ken weinig mensen met meer ervaring op het lab dan jij!). Je hebt een essentiële bijdrage geleverd aan het onderzoek en ik vind het dan ook heel leuk dat je mijn paranimf wilt zijn!

Paul, during my second year, you started working at the RU. Your presence gave my research a boost, let's face it: NMR is a super cool technique. But way more important, you became one of my closest friends. You have grown tremendously since I met you and I am glad to call you my friend. I am looking forward to more tasty BBQs&cider, relaxing evenings and awesome karaoke nights!

Tom (Tommie) en Luuk, zonder de apparatuur van het practicum, had ik nooit alle metingen kunnen doen in mijn laatste jaar, ontzettend veel dank daarvoor! Maar niet alleen voor dat, ook voor de praatjes en suggesties en natuurlijk voor het eten 'op zaal'!

Meneer van Weerd, de eerste keer dat ik je sprak was hoogst onaangenaam. Je fameuze woorden kan ik mij nog goed heugen: 'Stout!, De inhoud van je praatje was erg goed, maar je had de uitstraling van een zak aardappelen…'. Ik ben blij dat dit is uitgemond in een mooie vriendschap, waarin mij de waarde van het woordje NEE goed is bijgebracht.

Wester, jij bent de afgelopen jaren mijn zwemmaatje geweest. Eerst lekker zwemmen, dan samen eten en dan op slakkentempo series kijken op Netflix. Ik waardeer je positieve kijk op het leven, je authentieke lach, je schilder & dichtkunst, waarvan de captain Gorgeous bundel een absoluut hoogtepunt is dat mijn boekenkast siert. Thanks voor het wachten op mij als experimenten toch net iets langer duurden en voor alle gezwommen baantjes!

Sommige vrienden gaan (of blijven) in het buitenland wonen, maar dat maakt het contact niet minder aangenaam, hoogstens anders. Laurens, Kess, Stephanie en Donata, fijn dat we contact hebben gehouden. Kess, ik vond de vele g-chat gesprekken over van alles en nog wat erg fijn! Ook lekker dat we elkaar zo goed begrijpen en kunnen helpen met een paar berichtjes! Steef, dat wij met skypen de 8 uur kunnen aantikken, zegt, denk ik, genoeg! Er is altijd meer dan zat om over te praten en ik kijk altijd uit naar de periodes dat jij weer in NL bent! Laurens, nu ben je weer in NL maar niet echt dichterbij (Leeuwarden is niet om de hoek) maar altijd goed om bij te

kletsen. Donata, although we don't speak that often, you always have super pragmatical advise and I wish you all the best in CA!

Ellen, ik kan met recht zeggen dat jij een van de leukste 'bijproducten' uit m'n PhD bent, want hoe raar kan het lopen! Vanaf het begin hebben we een goede klik gehad, laten we vooral niet stoppen met bellen, sauna bezoekjes en al helemaal niet met dansen!

Sandra, Vero en Jori, mijn festival & concert-maatjes! Elke keer weer kijk ik uit naar de dagen van Wacken, om even in een hele andere setting lekker compleet mezelf te zijn. Ik ben blij dat ik dit met jullie kan doen! Sandra (in je uppie naar een concert gaan kan resulteren in een hele leuke vriendschap), heerlijk hoe jij in het leven staat: lol hebben en gaan met die banaan, niks is te gek! Vero, jij bent een lekker uitgesproken persoonlijkheid, blijf vooral wie je bent. Jori, m'n 'persoonlijke' muziekencyclopedie, wie had gedacht dat een match in zo'n leuke vriendschap zou uitmonden?!?! Door jou kan ik nooit meer hetzelfde naar een concert luisteren en laten we vooral nog een keertje Nijmegen op z'n kop zetten!

Al die tijd heb ik heerlijk gewoond op de Diepenbrockstraat. Ik wil mijn buren (Annemiek, Erik & Akira, Henriette, Jo en Ria) bedanken voor het in de gaten houden van m'n huisje, het voeren van m'n konijntjes gedurende vakanties en vooral voor de kleine gezellige gesprekjes en wandelingen.

Elke donderdagavond had ik een punt van rust: Edelsmeden. Daar heb ik geleerd dat er tijdens elk proces iets mis gaat, maar dat dit altijd is op te lossen en het eindresultaat altijd mooi is. Ik heb genoten van de geweldige positieve sfeer die er was tijdens de lessen: alles is mogelijk en we helpen elkaar. Wilma, Brigitte, Adri, Sandra, Marielle, Julliette en Kaisa, fijn dat jullie deze sfeer neerzetten. En blijf vooral die mooie dingen maken!

Dan zijn er ook nog mensen te bedanken die niet in één categorie samen te vatten zijn: Anja, vriendinnen sinds de middelbare school, altijd nog in voor even gekke acties en vol met de wonderbaarlijkste verhalen, gewoonweg top! Aukje, ook jou ken ik al een hele tijd (samen huppelen schept een band), samen naar de sauna gaan is altijd goed. Femke R., je hebt altijd een verfrissende kijk op zaken. Robin, super dat we elkaar weer tegen gekomen zijn met een weekend. We vinden vast een datum om te meeten. Jan-Willem, je prikt mij al een aantal jaren met naaldjes en het is altijd goed om te horen dat ik vooruit ga op meerdere vlakken. Verder het LEEF-festival, altijd leuk en goed om die ene dag in het jaar in een hele andere omgeving te zijn, vol met positiviteit en een geweldige sfeer, keep up the good work!

Sinds enige tijd ben ik werkzaam bij Zuyd Hogeschool. Ik heb hier een hele diverse en leuke baan gevonden met ontzettend leuke collega's, hierdoor voelt het als thuis! Evelien, wie had gedacht dat twee mensen die op dezelfde dag beginnen met een baan, zo'n goede klik konden hebben. Ik zeg surfen in Portugal was super vet en op naar nog meer concerten/festivals! En spelletjes spelen is fijn, op naar meer spelletje-savondjes met Tim, Elena, Charlotte, Bram en Kirsten! Sis, bedankt voor de hulp met de samenvatting. Met een nieuwe woonplaats komen ook nieuwe vrienden en een leuk huis, Agnes, Barbara, Petra, Perla, Niko, Ale, Tia, Elli, Sophie, en Dani, op naar nieuwe avonturen!

Dianne, halverwege mijn PhD heb ik bij jou aangeklopt voor hulp en wat heb ik veel aan jou gehad! Met je praktische tips en goede motto's (De beste keuze is de keuze voor jezelf!) ben ik heelhuids uit m'n PhD gekomen. Je inzichten en confronterende spiegels hebben mij telkens een stapje verder geholpen, om mezelf te begrijpen, en daar pluk ik dagelijks de vruchten van. Het is mede jouw verdienste dat het nu heel goed met mij gaat en ik vind het ook super dat je mijn paranimf wilt zijn, om zo ook samen het laatste stukje af te maken! Je bent een topper!

Dan nog zo'n topper is Ivonne, dankjewel voor alle hulp en begeleiding. De begeleiding van de afgelopen tijd is wel wat anders dan het uitleggen van middelbare school Natuurkunde. Je hebt meer gedaan voor mij dan dat ik ooit in woorden kan onder kan brengen, het is mede ook jouw verdienste dat er hier nu een boekje ligt!

Dit boekje is opgedragen aan Oma en Snuf. De mensen die mij een beetje kennen, weten hoeveel ze voor mij betekenen. Oma, bij jou kon ik altijd mezelf zijn, je maakte dat ik me speciaal voelde omdat je altijd alle aandacht voor mij had en ongelofelijk veel liefde uitstraalde. Ik bewonder je doorzettingsvermogen en ik vind het ontzettend jammer dat je niet meer het einde van mijn promotie kan meemaken maar dit boekje is mede voor jou! Snuf, jij was mijn maatje door dik en dun, maakte thuis echt thuis en doordat jij zo ontzettend kon genieten van alles (en dan vooral net dat ene plekje met zon) was je ook een goede reminder voor mij om af en toe ook de tijd te nemen om te genieten! Nu jij er niet meer bent, zet Doera, zoals alleen zij dat kan, de boel op stelten. Gaan waar je niet mag komen en mijn grenzen uittesten maar stiekem ben je een schatje!

Lieve Ancella (Sisters from head to foot) en Wouter (Thanks voor de usb-boot, hij heeft veel 'chemische' data vervoerd), al jaren wonen we aan de andere kant van het land en hebben we daar een heel eigen leven, maar weet ik dat ik altijd bij jullie kan aan kloppen als er wat is en dat is fijn!

Lieve papa en mama, dankjewel dat jullie me altijd hebben gestimuleerd om m'n best te doen, het maximale uit mezelf te halen, me hebben geleerd om zelfstandig na te denken en een eigen mening te vormen, waar je vervolgens ook voor mag gaan staan. Jullie onvoorwaardelijke vertrouwen, steun, interesse en enthousiasme hebben me altijd verder geholpen. Bedankt dat ik altijd een thuis heb om bij thuis te komen (of om naar toe te bellen)!

Uiteindelijk heb ik mijn persoonlijke draak, deze promotie inclusief proefschrift verslagen en ik wil iedereen die daar op de een of andere manier aan bij heeft gedragen heel hartelijk bedanken. Zonder jullie was de weg een stuk minder aangenaam geweest! Dus bedankt!

Kathleen

List of publications

Synthesis of double porphyrin cage compounds and the formation of sandwich complexes with a ditopic ligand - *Manuscript in preparation*

K. Stout, T. Peters, M. F. J. Mabesoone, F. Visschers, E. M. Meijer, J. van den Berg, J-R. Klop, S. Cantekin, P. B. White, P. T. Tinnemans, J. A. A. W Elemans, A. E. Rowan, and R. J. M Nolte

Allosteric binding of viologen guests in double zinc porphyrin cage complexes
- *Manuscript in preparation*

K. Stout, M. F. J. Mabesoone, J-R. Klop, P. B. White, J. A. A. W Elemans, A. E. Rowan and R. J. M Nolte

Threading of polymer chains through zinc double porphyrin cage compounds
- *Manuscript in preparation*

K. Stout, T. Peters, P. B. White, J. A. A. W Elemans, A. E. Rowan and R. J. M Nolte

Publications from previous work

The Trisubstituted-Triazole Approach to Extended Functional Naphthalocyanines

M. Juríček, K. Stout, P. H. J. Kouwer, A. E. Rowan. *J. Porphyr. Phthalocyanines* **2011**, *15* (9-10), 898–907

Fusing Triazoles: Toward Extending Aromaticity

M. Juríček, K. Stout, P. H. J. Kouwer, A. E. Rowan. *Org. Lett.* **2011**, *13* (13), 3494–3497

Curriculum vitae

Kathleen Stout werd geboren op 1 Augustus 1988 te Ede, Nederland. Na het behalen van haar VWO-diploma in 2006 aan Het Streek, is ze scheikunde gaan studeren aan de Radboud Universiteit Nijmegen (2006-2013). Haar hoofdvakstage was getiteld: Stereo- and Substrate-Selectivity of Catalytic Manganese Porphyrin Trimers, en die voerde zij uit bij de afdeling Molecular Materials onder begeleiding van Dr. Hans Elemans en Prof. dr. Alan Rowan. Deze stage werd gevolgd door een stage van 6 maanden bij IBM Almaden Research Center (San Jose, United States of America) onder de supervisie van Joe Sly op het onderwerp; Star Polymers: Origin and Functional Materials. Na het behalen van haar Master-diploma (*cum laude*), starte zij in 2013 met haar PhD in de vakgroepen Molecular Materials en Molecular Nanotechnology van Prof. dr. Alan Rowan en Prof. dr. Roeland Nolte, respectievelijk. De resultaten van haar onderzoek zijn in dit proefschrift beschreven. Sinds mei 2018 is zij werkzaam als docent/onderzoeker bij Zuyd Hogeschool (Heerlen).

Kathleen Stout was born on the first of August 1988 in Ede, the Netherlands. After obtaining her VWO in 2006 at Het Streek, she studied Chemistry at Radboud University Nijmegen (2006-2013). Her master thesis, carried out in the department Molecular Materials under supervision of Dr. Hans Elemans and Prof. dr. Alan Rowan, was titled: Stereo- and Substrate-Selectivity of Catalytic Manganese Porphyrin Trimers. Her master program was completed with an internship of 6 months at IBM Almaden Research Center (San Jose, United States of America) under the supervision of Joe Sly on the subject: Star Polymers: Origin and Functional Materials. After obtaining her master degree (*cum laude*), she started with her PhD research in the groups of Prof. dr. Alan Rowan (Molecular Materials) and Prof. dr. Roeland Nolte (Molecular Nanotechnology). The results of this PhD research are presented in this thesis. From May 2018 on, she is working as a teacher/researcher at Zuyd University of Applied Sciences (Heerlen, the Netherlands).